Investigation of the Function and Regulation of ABC Transporters

Begum Gokcen Akkaya

A thesis presented for the degree of

Doctor of Philosophy

August 2014

Membrane Transport Biology Group

Centre for Cutaneous Research

Blizard Institute

Queen Mary University of London

‘Deniz’ koydum adını

Kederi bende saklı

ABSTRACT

ATP-Binding-Cassette (ABC) transporters are primary active pumps that typically couple the binding and hydrolysis of ATP to the translocation of compounds across cellular membranes. Some, like ABCB1, ABCC1 and ABCC3, are polyspecific and can efflux clinically important drugs which may contribute to their therapeutic failure.

In this study I have investigated (1) the mechanism of ABC transporter function, (2) studied the potential for regulation by ubiquitin ligases (both using ABCB1 as a model), and (3) tested the involvement of ABCC1 and ABCC3 in autocrine signalling in cancer. (1) In 1966, Jardetzky *et. al* [1] proposed that membrane pumps function by exposing their ligand-binding pocket alternately on different sides of the membrane. For ABC transporters, this coupling of the aspect and affinity of the ligand-binding cavities of the two transmembrane domains (TMDs) to the ATP catalytic cycle of the two nucleotide-binding domains (NBDs) is fundamental to the transport mechanism but is poorly understood at the molecular level. Structure data suggest signals are transduced through intracellular loops of the TMDs which slot into grooves on the top surface of the NBDs. At the base of these grooves is the Q-loop. By analysing the function of Q-loop mutants in combination with ligand binding cavity mutants I have discovered that the Q-loops are crucial to the transport cycle and that they are required to couple ligand binding to conformational changes at the NBDs necessary to drive the transporter into an inward closed state.

(2) ABCB1 is known to be a key component of chemical barrier separating the circulation from the cerebrospinal fluid. It has also been reported to transport β-amyloid across the lumenal membrane and into the circulation. Loss of ABCB1 from the barrier with age has therefore been suggested to play a role in Alzheimer's Disease. The ubiquitin ligase Nedd4-1 has been implicated in the post-translational regulation of ABCB1 abundance in cells. Here, I report that ABCB1 can be ubiquitinated by Nedd4-1 in vitro and identify the residues modified (by mass spectrometry).

(3) Lysophosphatidylinositol (LPI) is an autocrine metabolite produced by cancer cells that binds to the G-protein coupled transmembrane receptor GPR55 on the surface of cells. Stimulation of GPR55 activates a signalling cascade that induces proliferation and metastases of the cancer cells. How LPI is released from the cells was not known. In this study I show that ABCC1 and ABCC3, which are known to be expressed in ovarian and pancreatic cancers, can transport LPI into inside-out vesicles suggesting a new role for these "drug resistance" transporters in cancer biology.

Declaration of own work

I, Begum Gokcen Akkaya, confirm that the research included within this thesis is my own work or that where it has been carried out in collaboration with, or supported by others, that this is duly acknowledged below and my contribution indicated. Previously published material has been acknowledged in the text and a list of references is given.

I attest that I have exercised reasonable care to ensure that the work is original, and does not to the best of my knowledge break any UK law, infringe any third party's copyright or other Intellectual Property Right, or contain any confidential material. I accept that the College has the right to use plagiarism detection software to check the electronic version of the thesis. I confirm that this thesis has not been previously submitted for the award of a degree by this or any other university.

Begum Gokcen Akkaya
PhD Student
19.08.2014

Acknowledgements

First of all, I would like to thank the best ever supervisor in the world, Kenneth J. Linton, for his invaluable supervision from the first to the last day of my PhD study. I would also like to thank all the past and present group members of Membrane Transport Biology Group for their help and advice and also for making the lab such a pleasant place to work in.

Finally, I would like to thank my mum and dad for their support throughout my life and most of all I would like to thank my beloved husband who is my *genius*. And one last big thanks to the rest of my family, and especially my parent-in-laws, and friends who were always there when I needed.

Table of Contents

List of Figures

List of Tables

Chapter One

1. Introduction

1.1. Transport ATPases

Transport ATPases comprise four distinct classes; P-, F- & V-type and ABC transporters [2]. The history of transport ATPases reach back to 1957 with the discovery of the P-type Na^+/K^+ ATPase [3]. The P-type ATPases are a large group of ion and lipid pumps which are vital for life. The P-type ATPases, also known as E1-E2 ATPases, are named from the covalent phosphorylated intermediate in their reaction cycle which makes this class distinct from the other transport ATPases [4]. The reason they are also described as E1-E2 ATPases is because they all appear to switch between two different conformations, denoted by E1 and E2. In E1, the pump has high affinity for the exported substrate and low affinity for the imported substrate and *vice versa* in E2. The prominent examples of P-type ATPases are; Na^+/K^+-ATPase, H^+-ATPase, H^+/K^+ ATPase, Ca^{2+} ATPase [5].

The F-type ATPases (also called F_oF_1 ATPases) are found in bacteria, chloroplasts and in the inner mitochondrial membrane in eukaryotes and do not generally function as ATPases but mainly as ATP synthases. They synthesize ATP in the electron transport chain reaction in eukaryotes. The F_o domain is embedded in the membrane and F_1 domain is the soluble portion [6]. Proton flux across the membrane is necessary to drive the synthesis of ATP from ADP by F-type ATPases. ATP synthesis by F-type ATPases can be reversed and, especially in bacteria, ATP hydrolysis can be performed to provide a proton gradient.

The V-type ATPases are found in intracellular vacuoles and lysosomes of eukaryotic cells and these ATPases are named in reference to vacuolar localization but can also be found in the plasma membrane of prokaryotes and eukaryotic cells. The V-type ATPases are proton pumps and they play a variety of roles in pH homeostasis and proton-coupled transport.

They comprise 14 protein subunits arranged in two domains, the V0 and the V1 domain. The V0 domain is the membrane embedded domain which is responsible for proton translocation across the membrane, whereas the V1 domain is the cytoplasmic domain which is responsible for ATP hydrolysis [7].

The ATP-binding cassette (ABC) transporters were first coined in 1991 to describe this superfamily's most conserved feature, the ATP binding domains [8]. The ABC transporters transport a wide range of ligands that are important for cellular functions. The transport direction of ABC transporters varies from bacteria to humans. In bacteria, there are both importers and exporters whereas there appear to be only exporters in humans.

1.2. ATP-binding cassette (ABC) Transporter Proteins

The first characterized ABC transporters were binding protein dependent transporters of *E. coli* [9, 10]. Bacteria have both importer and exporter ABC transporters. All species of bacteria use a large number of ABC transporters to obtain essential nutrients and to efflux metabolic products and toxins [8]. The bacterial ABC transporter research is important for humans because some of the ABC transporters in bacteria can function to form resistance against antibiotics. For example, the ABC transporter MsrA causes erythromycin resistance of *Staphylococcus* [11].

In humans, only the ABC exporter class is found [12]. There are 49 human ABC transporter genes encoding 42-44 ABC transporter complexes. Phylogenetic analysis has allowed the human ABC gene superfamily to be divided into seven subfamilies, entitled A to G [13]. The typical ABC transporter contains two Nucleotide Binding Domains (NBD) which are highly conserved across the superfamily and two Transmembrane Domains (TMD) which are not necessarily conserved throughout the superfamily; but all of the human TMDs are related. Distinct from the other classes, most of the ABCC class ABC transporters have a third additional transmembrane domain at the amino terminus (TMD0) [14]. There are also half-transporters which only contain one NBD and one TMD and they need to form dimers to function [12]. Some 'half-transporters' form heterodimers to function, which is why the gene count for ABC transporters is greater than the transporter number.

Some of the human ABC exporters are very specific for particular ligands but some are poly-specific for multiple ligands and those generally protect the body from exotoxins and can therefore cause resistance to multiple therapeutic drugs.

1.3. Multidrug Resistance

Multidrug resistance (MDR) is referred to as the resistance of pathogenic microorganisms against distinct antimicrobials and also the resistance of tumour cells against antineoplastic drugs in humans. MDR in tumour cells can be an ATP dependant mechanism which is due to the overexpression of certain types of ABC transporter proteins. In 1973, Dano *et al.* demonstrated the active efflux of daunomycin from MDR tumor cells [15]. Further studies on MDR provided the discovery of ABCB1 in 1976 [16], the first described ABC protein in humans. ABCB1 causes resistance against a wide range of drugs. In 1992, ABCC1 was

discovered in a small cell lung carcinoma cell line which was resistant to anthracyclines [17] and ABCC2, another ABCC class MDR protein, was identified in 1995 while searching for the hereditary defect of the hepatobiliary excretion of anionic conjugates by transport-deficient mutant rat hepatocytes [18]. ABCC3 which has common ligands with ABCC1 was described in 1997, together with ABCC4 and ABCC5 by a search of the human expressed sequence tag database [19]. ABCC1, ABCC2 and ABCC3 have an extra N-terminal transmembrane domain (TMD0) which is specific to ABCC class proteins. Another ABC MDR protein was also described by the search of the human expressed sequence tag database in 1996 and its gene was mapped to Chr4q22 [20]. This protein was described in 1998 in an anthracycline-resistant human breast cancer cell line and is a half-transporter with a single NBD at the N-terminus followed by a single TMD which is today known as ABCG2 [21]. From these MDR proteins, ABCB1, ABCC1 and ABCC3 will be discussed in this thesis (Please see Table 1.1 for ABC MDR proteins).

Human ABC Transporter Family Multidrug Resistance Proteins			
Nomenclature	Common Alias	Domain sequence	References
ABCB1	P-glycoprotein, MDR1	TMD-NBD-TMD-NBD	[22, 23]
ABCC1	MRP1	TMD-TMD-NBD-TMD-NBD	[17, 24, 25]
ABCC2	MRP2	TMD-TMD-NBD-TMD-NBD	[26]
ABCC3	MRP3	TMD-TMD-NBD-TMD-NBD	[27]
ABCC4	MRP4	TMD-NBD-TMD-NBD	[28]
ABCC5	MRP5	TMD-NBD-TMD-NBD	[29]
ABCG2	BCRP, MXR, ABCP	NBD-TMD	[12]

Table 1.1: Multidrug resistance ABC transporters and their domain sequences.

1.4. ABCB1

Currently, four full transporters including ABCB1 and seven half transporters have been identified in the ABCB transporter class which is the only human ABC transporter class to have both types of transporters [13].

1.4.1. Introduction to ABCB1

The function of ABCB1 (P-glycoprotein), the main subject of this thesis, was first described by Dano *et al.* in 1973 by the discovery of active export of daunomycin by drug resistant Ehrlich ascites tumor cells. These cells were resistant to anthracyclines and also some other chemotherapeutic agents such as vinca alkaloids [15]. Later, in 1976, Juliano and Ling identified a 170 kDa protein in drug-resistant Chinese hamster ovary cell membranes and termed it P-glycoprotein (phosphoglycoprotein) [16]. In 1982, Debenham *et al.* suggested that P-glycoprotein was correlated to the multidrug resistance phenotype of mouse L cells [30] and in 1986, P-glycoprotein was shown to be the product of the multidrug resistance (*MDR1*) gene (later to be renamed ABCB1) [22, 23].

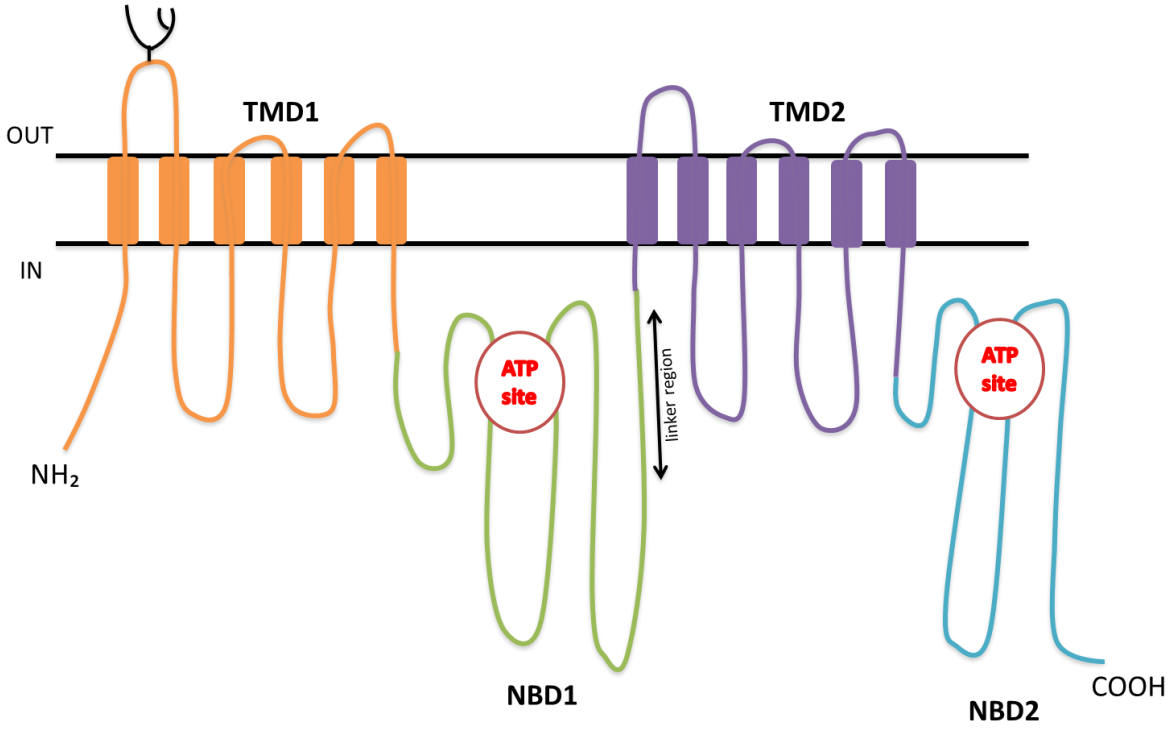

Figure 1.1: ABCB1 2D model. ABCB1 consists of two halves, each comprising one NBD and one TMD, connected by a linker region. In the first extracellular loop, ABCB1 has three N-glycosylation residues.

The *ABCB1 (MDR1)* gene is located on Chromosome 7q21.12 and has 29 exons, 27 of which are coding. The ABCB1 product is 1280 amino acids long and consists of four domains: two TMDs and two NBDs, arranged as two homologous halves connected by a short, phosphorylated, linker region. Each half has one TMD followed by one NBD (Figure 1.1 and Figure 1.2).

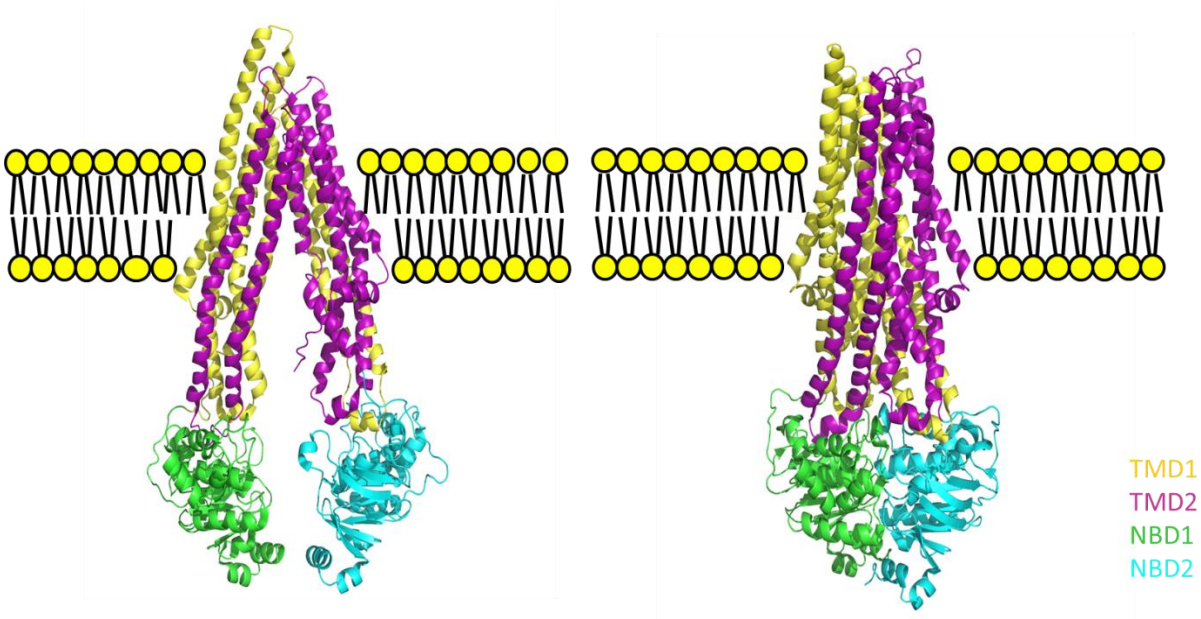

Figure 1.2: ABCB1 homologue mouse Abcb1a in an inwardly open state (left hand side, pdb ID 3G60), ABCB1 homologue *S. aureus* Sav1866 in outwardly closed (nucleotide (ADP) bound) conformation (right hand side, pdb ID 2HYD).

1.4.2. Regulation of ABCB1

1.4.2.a. Transcriptional Level

The ABCB1 gene has 11 different transcripts, 10 of which are alternatively spliced mRNAs and 1 is the unspliced form. From these 11 mRNAs, 2 were shown to be expressed at the protein level producing 1280 and 1216 amino acid proteins. Both of the two protein encoding mRNAs have 29 exons and they differ from each other by truncation of the 5' end or the 3' end, various splicing of 3 exons and/or splicing or retention of one intron. The mRNA encoding the full length protein (1280 amino acids) (hereafter referred to as 'the first mRNA') has 2 exons in the 5' end region before the common exons start whereas the mRNA encoding the 1216 amino acid protein (hereafter referred to as 'the second mRNA') has 3. The reason for this is the second intron of the second mRNA is not spliced and is conserved within the second exon of the first mRNA. Other than this, the 7th exon of the

first mRNA is spliced in the second mRNA forming the 7th intron of the second mRNA and 29th exons of each mRNA are different than each other (Figure 1.3) (http://www.ncbi.nlm.nih.gov/IEB/Research/Acembly/av.cgi?db=human&term=ABCB1&submit=Go, accessed on 15.08.2014).

Figure 1.3: Comparison of two ABCB1 expressing mRNAs. The full-length, 1280 amino acid protein synthesizing mRNA (upper figure) has same number of exons as the 1216 amino acid synthesizing mRNA (lower figure).

Research on ABCB1 regulation has shown that hypomethylation of CpG sites in the promoter region of *ABCB1* gene is important for its expression. Demethylating agent 5-azadeoxycytidine (5aC) activated the *ABCB1* promoter to allow detection of mRNA levels [31, 32]. The two most likely ways that DNA methylation can affect the transcription levels of genes are direct physical prevention of transcription proteins binding to the DNA or the attraction of methyl-CpG-binding domain proteins which can then attract additional proteins to the site, such as histone deacetylases that can modify histones and form heterochromation. It has been established that methyl-CpG binding protein 2 (MeCP2) is involved in methylation-dependent silencing of human *ABCB1* [33]. In the repressed state the *ABCB1* promoter is embedded in chromatin enriched with MeCP2 and deacetylated histone. Histone deacetylase inhibitor trichostatin A (TSA) induces significant acetylation of histones H3 and H4 but did not activate transcription. However, 5aC induced DNA demethylation leads to the release of MeCP2, promoter acetylation, and partial relief of repression. *ABCB1* expression is significantly increased following combined 5aC and TSA

treatments [33]. These data suggest that both methylation of DNA and acetylation of histones have roles in *ABCB1* regulation with the former being more important than the latter. Another study has suggested that ABCB1 expression is strongly regulated via mRNA stability [34]. Up-regulation of *ABCB1* mediated by mRNA stability does not appear to result in immediate protein expression but requires prolonged drug exposure. However, a further study has demonstrated that *ABCB1* up-regulation is regulated by transcriptional activation in a very low level ABCB1 expressing acute T-cell leukemia cell line; CEM-Bcl2 and also in the high level ABCB1 expressing colon carcinoma cell line; SW620 [35]. In the CEM-Bcl2 cells *ABCB1* is also regulated by mRNA stability.

Pregnane X receptor (PXR), which is also known as steroid and xenobiotic sensing nuclear receptor (SXR), is a transcriptional regulator of the cytochrome P450 gene *CYP3A4* which is important in the metabolism of xenobiotics. PXR binds to the response element of the *CYP3A4* promoter as a heterodimer with retinoid X receptor (RXR) to induce *CYP3A4* activation and it is activated by several ligands including dexamethasone and paclitaxel [36]. It has recently been found that PXR can also regulate ABCB1 [37]. This common transcriptional regulator in the *CYP3A4* and *ABCB1* regulation systems supports the potential coordination of two xenobiotic handling systems (metabolism and efflux). *ABCB1* has also been shown to be regulated by vitamin D response elements (VDREs) located between -7880 and -7810 basepairs upstream of the promoter region, providing binding sites for vitamin D receptor (VDR)/retinoid X receptor α (RXRα) heterodimers. In a 1α, 25-dihydroxyvitamin D_3 mediated manner, VDR/RXRα binding to VDREs has been shown to induce ABCB1 expression [38]. A forkhead transcription factor, FOXO3a which binds to the

proximal promoter region of *ABCB1* was later shown to induce ABCB1 expression in K562 leukemic cells at protein, mRNA and gene promoter levels [39].

1.4.2.b. Post-translational Level

i. Glycosylation

In eukaryotes and archaea, N-Linked glycosylation usually occurs at asparagine (Asn) residues in Asn-X-Ser/Thr sequons where X cannot be proline (Pro) [40]. ABCB1 has ten putative N-glycosylation sites, only three of which are extracellular. The three extracellular sites, the only ones that will be exposed to glycosyltransferases in the E.R. lumen, reside in the first extracellular loop at asparagine residues 91, 94, and 99 and all three are glycosylated [41]. N-glycosylation has been shown to have no role in the transport function of ABCB1, because glutamine substitutions of the relevant asparagines have no impact on ligand transport. However, N-glycosylation has an effect on the protein, either improving ABCB1 trafficking to membrane or stabilizing it [41]. Later, it has been suggested that unglycosylated ABCB1 results in a fraction of the protein being improperly folded and degraded by the proteasome although the protein expressed at the cell surface remains functional [42]. Another study supported these findings via inhibition of glycosylation by tunicamycin, which inhibits the addition of N-linked oligosaccharide chains in the E.R., and which was shown to increase ubiquitination and turnover of ABCB1 [43].

ii. Phosphorylation

ABCB1 is phosphorylated at serines (Ser) 661, 667, 671, 675 and 683, all of which reside in the linker region [44]. The linker region of ABCB1 is 75 amino acids long and connects the two homologous halves of the protein. Deletion of this central core has no effect on ABCB1 expression levels but the protein is no longer functional [45]. Ser661, Ser667 and Ser671 can be phosphorylated by protein kinase C (PKC) and Ser667, Ser671 and Ser683 can be phosphorylated by cyclic AMP dependent protein kinase (protein kinase A, PKA) [46]. Previously, by using protein kinase C inhibitors like staurosporine and calphostin C that inhibit ABCB1 phosphorylation, ABCB1 ligands were observed to accumulate inside the cells. These results suggested that phosphorylation has a role in ABCB1 function [47, 48]. However, Germann *et al.* and Goodfellow *et al*., in 1996 found that phosphorylation might not be important for ABCB1 transport function. They substituted the phosphorylated five serine residues with alanine or aspartic acid residues and showed that non-phosphorylatable ABCB1 is still fully functional and that the presence of neutral or charged residues in these positions had no effect on function [49, 50]. The limitation of this study is in the selection of wild-type or mutant ABCB1 expressing cell lines with long chemotherapeutic agent exposure. In 1999, Castro *et al.* showed that protein kinase C inhibitors that interfere with ABCB1 function compete with transport ligands to bind and inhibit ABCB1 function [51]. The role of phosphorylation and why phosphorylation is condensed in the linker region is unclear but it was suggested that phosphorylation might affect ABCB1 half-life or substrate specificity but further study revealed phosphorylation has no role in protein half-life via the ubiquitination-proteasome degradation pathway [43].

iii. Ubiquitination

ABCB1 has a half-life of 14 to 17 hours and is considered as a relatively stable protein, at least in the four different human and hamster multidrug resistant cell lines used [52]. ABCB1 is subject to ubiquitination-proteasomal degradation that does not involve the lysosome in ABCB1 turnover [43]. Ubiquitin is a small 8.5 kDa protein (76 amino acids long) found in almost all tissues in eukaryotic organisms [53]. The linkage is formed between the carboxyl group of the C-terminal glycine (Gly76) in ubiquitin and the ε-amino group of lysine in the substrate protein [54]. Ubiquitination of a protein can trigger the 26S proteasome degradation cascade or endocytosis of the protein. Ubiquitination requires three types of enzymes; the ubiquitin activating enzyme E1, the ubiquitin-conjugating enzyme E2 and an ubiquitin E3 ligase which catalyses the binding of ubiquitin to the target protein [55]. ABCB1 is shown to interact with the E3 ligase FBXO15, by co-immunoprecipitation and siRNA knock-down studies in human colorectal cancer cells HCT-15 and SW620 [56]. Ubiquitination of ABCB1 by the E3 ligase Nedd4-1 was tested in the course of my study and is reported in chapter 4 of this thesis.

1.4.3. Structure of ABCB1

1.4.3.a. The Nucleotide Binding Domain Structure and Its Relevance to ATP Catalysis

The NBDs show extensive amino acid sequence similarity throughout the ABC superfamily. Each NBD has two subdomains termed the core subdomain and the α-helical subdomain. The protein fold of the core subdomain is similar to the equivalent domains of other transport ATPases and includes highly conserved motifs called the Walker A and Walker B

motifs found in many ATPases and also the A-, D-, Q- and H- loops that are unique to ABC transporters. Also unique to ABC transporters, is the ABC signature motif which is a feature of the α-helical subdomain. Two ATP molecules bind between the two NBDs in an arrangement referred as the 'ATP sandwich dimer' (Figure 1.4) [57]. This dimer forms two ATP binding pockets between the Walker A, Walker B, Q- and H- loops of one NBD and the D-loop and ABC signature motif of the other NBD [58, 59]. A complex communication web is formed between these motifs and the bound ATPs, some parts of which remain to be elucidated [60, 61]. From the high resolution structures of bacterial NBDs, it is evident that the Walker A and Walker B motifs make the most significant contacts to the bound nucleotides. The glutamate residue in the Walker B motif is also known as the catalytic carboxylate and it is located near the γ phosphate of the ATP molecule. Single mutations of the Walker B glutamate residues (i.e. replacing the glutamate in either NBD1 or NBD2) inactivate the protein. The A-loop (also known as the stacking aromatic) stacks with the adenine ring of the nucleotide [62]. The D-loop of one NBD is hydrogen bonded to the peptide backbone of the Walker A motif of the second and provides a coordinating residue that interacts with the γ phosphate of ATP through a water molecule or through the divalent cation which is important for hydrolysis [63, 64]. The Q-loop has also been shown to interact with ATP attacking water molecule [63] though it is later contradicted [65, 66]. The Q-loop links the core subdomain and the α-helical subdomain of the NBDs, and also lines the base of a groove into which intracellular loops of the TMDs insert. This interaction is likely to be important for the conformational changes required for ligand transport and the structural data on isolated NBDs in the apo and ATP-bound forms suggest that the Q-loop acts like a flexible hinge. To bind nucleotide in the ATP sandwich dimer conformation, the α-helical subdomains are proposed to rotate around the Q-loops to contact nucleotide

that is bound by the core subdomain of the apposed NBD [60]. This is likely to be coupled to conformational changes of the TMDs to couple ligand binding to distinct NBD conformations and *vice versa,* but this needs to be investigated further and it is the subject of chapter 3 of this thesis.

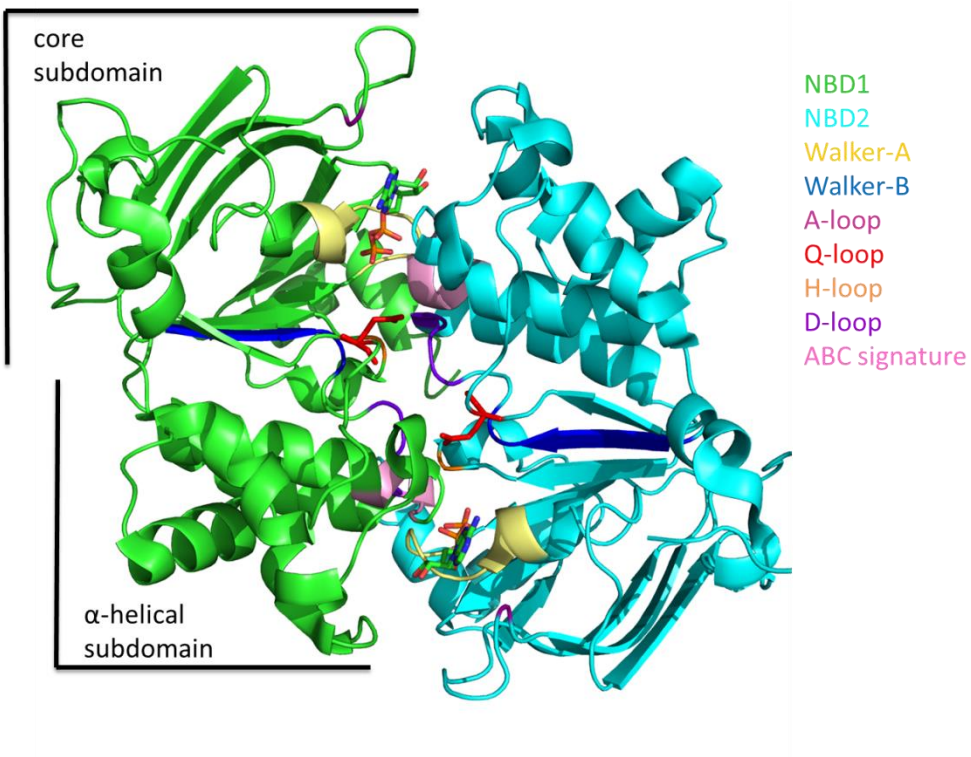

Figure 1.4: 'ATP sandwich dimer' showing the conserved motifs converging at the NBD-NBD interface. A model of the human ABCB1 homologue Sav1866 structure (pdb ID 2HYD) is viewed from above with the TMDs hidden for clarity. Well-conserved residues of the NBDs are indicated in different colors. Nucleotide (2x ADP) bound at the interface of the two NBDs are shown in stick format.

1.4.3.b. The Transmembrane Domains

The TMDs are not necessarily homologous in all ABC transporters although all of the human ABC transporters are likely to have a common ancestral TMD. The TMDs are often important in ligand selection of a particular ABC transporter. ABCB1 has been described as a 'hydrophobic vacuum cleaner' in 1990 because it transports a wide range of hydrophobic and amphipathic ligands, effluxing them directly from the lipid bilayer [67]. The TMDs of ABCB1 form the transport ligand binding site(s) [68]. As mentioned above, ABCB1 comprises two homologous halves, each with one TMD and one NBD. When *ABCB1* was first cloned and sequenced, its internal duplication was suggested to be important in giving rise to two distinct ligand binding sites (one per TMD) thereby increasing the range of transported ligands [69]. However, biochemical and structural data suggest that the situation is more complicated [68, 70-72]. By X-ray crystallography, Aller *et al*. (2009) showed that the ABCB1 homologue, mouse Abcb1a, can bind two ligands (actually stereoisomeric inhibitors of the transporter, QZ59-RRR and QZ59-SSS) at the same time but at the interface formed between the two TMDs. QZ59-RRR was found to bind to a central site and QZ59-SSS bound to two different sites (both of which overlap with the QZ59-RRR binding site) of a large ligand binding cavity formed by the TMDs [70]. The transported ligands of the ABCB1 vary greatly in size and for the small ligands to bind to this large cavity and induce the transport cycle, a cholesterol fill-in model has been proposed. In this model, which also explains the dependency of ABCB1 on cholesterol, cholesterol occupies the empty space in the ligand binding cavity of ABCB1 when small ligands bind [73].

Each ABCB1 TMD has 6 transmembrane helices which extend from the membrane into the cytoplasm. The TMDs cross the membrane as two bundles of transmembrane helices

(TMH); each bundle comprises helices from both TMDs. The TMDs are thought to change conformation in order to bind and transport ligand and this movement is coupled to ATP binding and hydrolysis. In the crystal structure model of mouse Abcb1a which is nucleotide-free and in an inwardly open conformation, TMH 1, 2, 3 and 6 of TMD1 cross the membrane in association with TMH 10 and 11 of TMD2, and the remaining helices of TMD1, TMH 4 and 5, cross the membrane with TMH 7, 8, 9 and 12 of TMD2 (Figure 1.5). In the nucleotide bound, inwardly-closed *S. aureus* Sav1866 structure (an ABCB1 homologue), TMH 1 and 2 of TMD1 cross the membrane with TMH 9, 10, 11 and 12 of TMD2, while TMD2 TMH 7 and 8 cross with TMH 3, 4, 5 and 6 of TMD1 (Figure 1.6). Thus assuming that, these two structures represent different intermediates in the transport cycle, two TMH from one TMD and four TMH from the other, form a helical bundle, and the TMH content of the bundles changes during the transport cycle.

a.

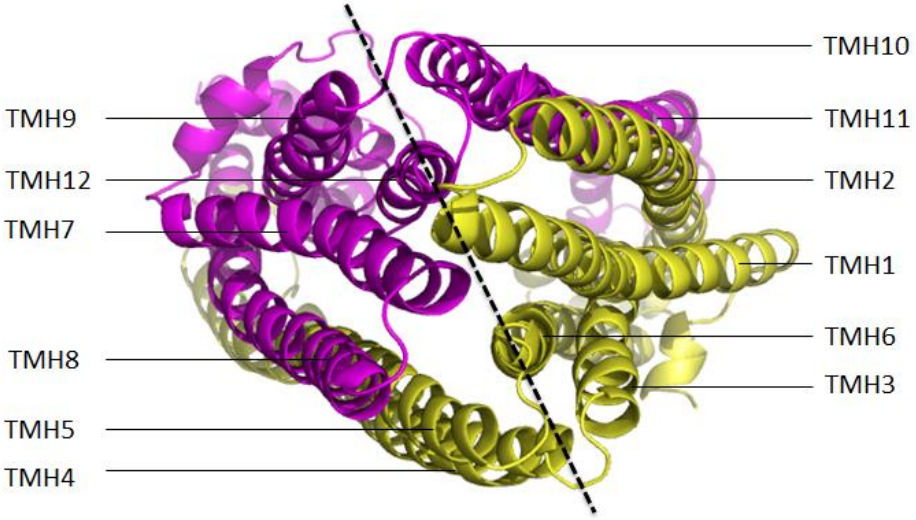

b.

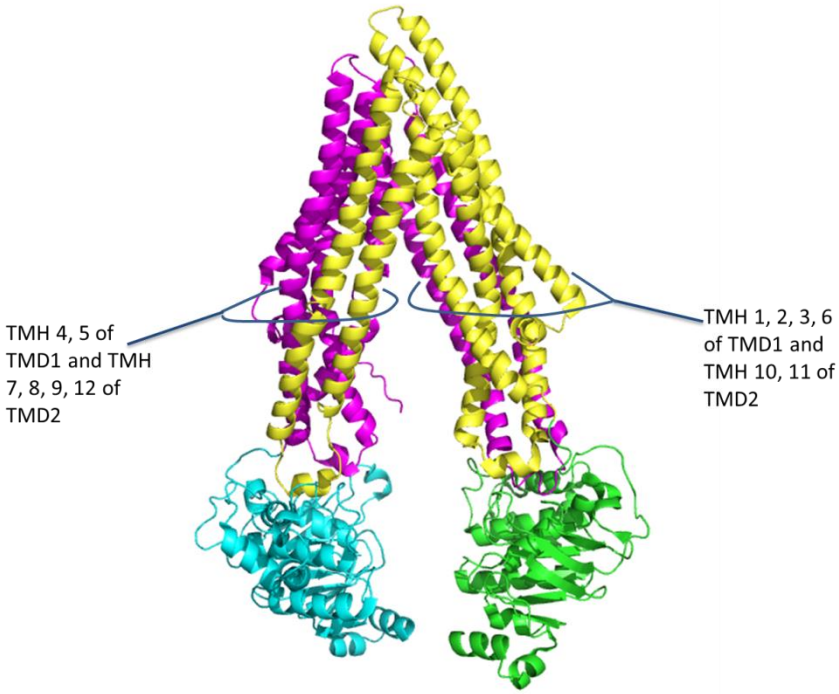

Figure 1.5: ABCB1 homologue mouse Abcb1a (pdb ID 3G60); top down view (a. NBDs are removed for clarity) and side view (b.) TMD1; yellow, TMD2; magenta, NBD1; green, NBD2; cyan. TMH 1, 2, 3 and 6 of TMD1 cross the membrane with TMH 10 and 11 of TMD2. TMH 7, 8, 9, 12 of TMD2 cross the membrane with TMH 4 and 5 of TMD1.

a.

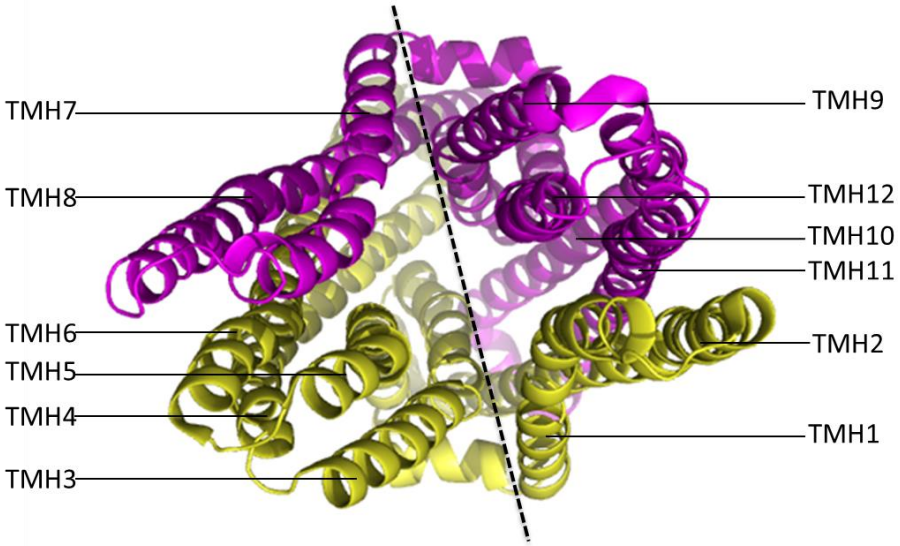

b.

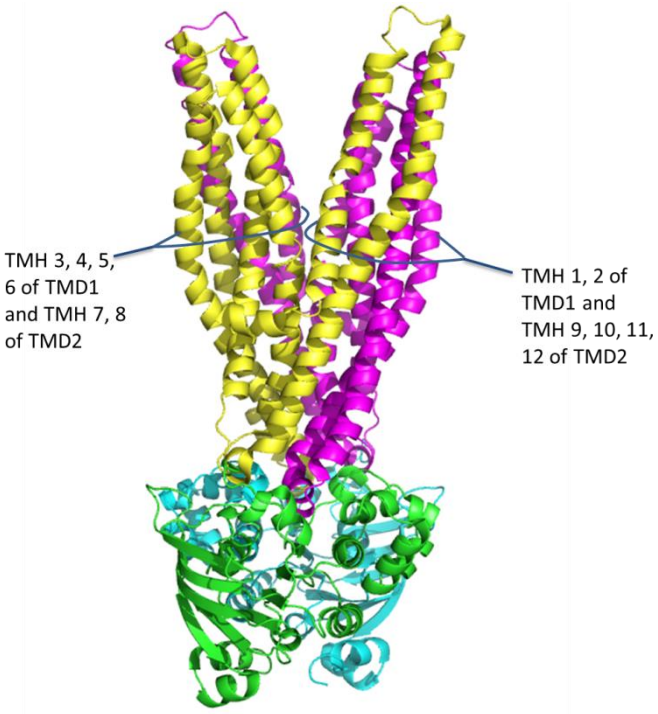

Figure 1.6: ABCB1 homologue *S. aureus* Sav1866 (pdb ID 2HYD); top-down view (a. NBDs are removed for clarity) and side view (b.) TMD1; yellow, TMD2; magenta, NBD1; green, NBD2; cyan. TMH 1 and 2 of TMD1 cross the membrane with TMH 9, 10, 11 and 12 of TMD2. TMH 7 and 8 of TMD2 cross the membrane with TMH 3, 4, 5 and 6 of TMD1.

1.4.4. ABCB1 Transport Mechanism

1.4.4.a. Interdomain Communication

Communication between the TMDs and NBDs is suggested by the X-ray structure data [57] to be mediated by the four, long, intracellular loops of the TMDs. The first two intracellular loops (ICL); ICL1 and ICL2 belong to the first TMD and ICL3 and ICL4 extend from the second TMD. The first intracellular loops of both TMDs (ICL1 and ICL3) contact the NBDs directly below the TMD (NBD1 and NBD2, respectively) whereas the second ICLs of each TMD cross over to contact the apposed NBDs (Figure 1.7). Thus ICL4 from TMD2 sits in the groove on the top surface of NBD1 alongside ICL1 from TMD1, and the second ICL of TMD1 (ICL2) interacts in a similar manner on the top surface of NBD2 alongside ICL3 of TMD2. Importantly, the Q-loop motifs of the NBDs are at the base of the grooves occupied by ICL2 and ICL4 (the latter is shown on Figure 1.7) [74].

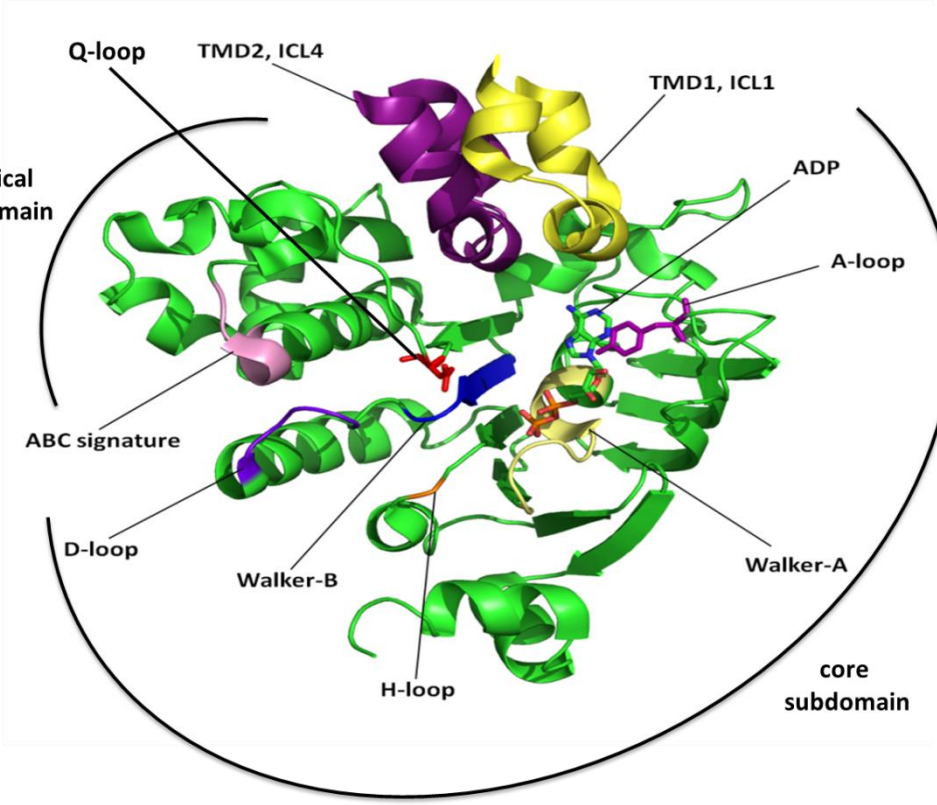

Figure 1.7: Human ABCB1 homologue *S. aureus* Sav1866 (pdb ID 2HYD) showing the conformational relationship between the Q-loop in NBD1 and intracellular loop 4 (ICL4) of TMD2. Interface view of NBD1 from NBD2. During conformational changes ICL4 of TMD2 should sit in the groove formed in NBD1 between the α-helical and the core subdomains which are linked by the Q-loop. The side chain of the glutamine of Q-loop is shown in red stick. Other motifs are indicated. ADP is also in stick format.

Using molecular dynamics simulations, Becker *et al.* (2009) have suggested two different possible NBD to TMD communication pathways [75]. The first potential communication pathway starts from the adenine ring of the nucleotide which is in contact with the NBD stacking aromatic residue of the A-loop. From the aromatic residues of NBD1 the signal would be conducted to ICL1 of TMD1 and then to ICL4 of TMD2 (the pathway would flow through ICL3 of TMD2 and ICL2 of TMD1 when initiated from the aromatic residue of NBD2). The second possible pathway starts from the ATP phosphates and from there, the signal communicates directly with the Q-loop motif of the same core subdomain, or via the Q-loop of the apposed NBD via the ABC signature motif of the apposed NBD. From the

NBD1 or NBD2 Q-loop, the energy would flow through ICL4 of TMD2 or ICL2 of TMD1, respectively [75]. The same group also suggests that the Q-loop is important for triggering signal transduction from the NBDs following dissociation of nucleotide [76]. These molecular modelling studies need to be tested by biochemical studies. Signal transduction pathways within ABCB1 are explored in chapter 3 of this thesis.

1.4.4.b. ATP Catalysis, NBD: TMD Signal Transduction and the Transport Cycle

Exactly when and how ATP binding and hydrolysis is coupled to ligand transport is still debated. Among the different transport cycle models, the 'ATP switch model' arguably fits best to the biochemical and structural data [77]. In this model, ABCB1 has a low affinity for ATP and a high affinity for ligand binding in its basal state (Figure 1.8). Ligand binds to the high affinity ligand binding cavity of the inwardly-open transporter from the inner leaflet of the membrane [75] and triggers the transport cycle. Ligand binding to the TMDs must trigger signal transduction to the NBDs, otherwise ATP binding and hydrolysis would occur independently from ligand transport and ABCB1 would perform futile ATP hydrolysis cycles [78]. Utilization of fluorescent nucleotide derivatives has shown that ligand binding increases the affinity of nucleotides to the transporter up to 4 fold [79]. In the ATP switch model the next step is the nucleotide binding which in this model considered the power stroke of the transport cycle. By binding nucleotide, the NBDs change conformation and form the inwardly-closed dimer state, the ATP sandwich dimer [58, 61]. The study of Martin *et al.* has shown that binding of ATP analogues results in a decreased affinity for transport ligand which suggests that binding of the nucleotide rather than its hydrolysis is enough for the transporter to export its ligands [80]. Vanadate (Vi) trapping and subsequent cross

linking of 8-azido-ADP to the protein has shown that ABCB1 displays low affinity for vinblastine when 8-azido-ADP and Vi are bound to mimic the post hydrolytic state, but the high-affinity ligand binding is restored upon dissociation of phosphate [81]. Disulphide cross-linking between transmembrane helices has also shown that ATP binding results in ABCB1 conformational change and its subsequent hydrolysis and dissociation resulted in further distinct conformational changes presumably to reset the transporter back to its basal state [82]. Nevertheless, it is theoretically possible that different power strokes may result in transport of different ligands and the three steps in ATP catalysis (ATP binding, hydrolysis and ADP/Pi release), may reconfigure the binding sites for different ligands at different stages.

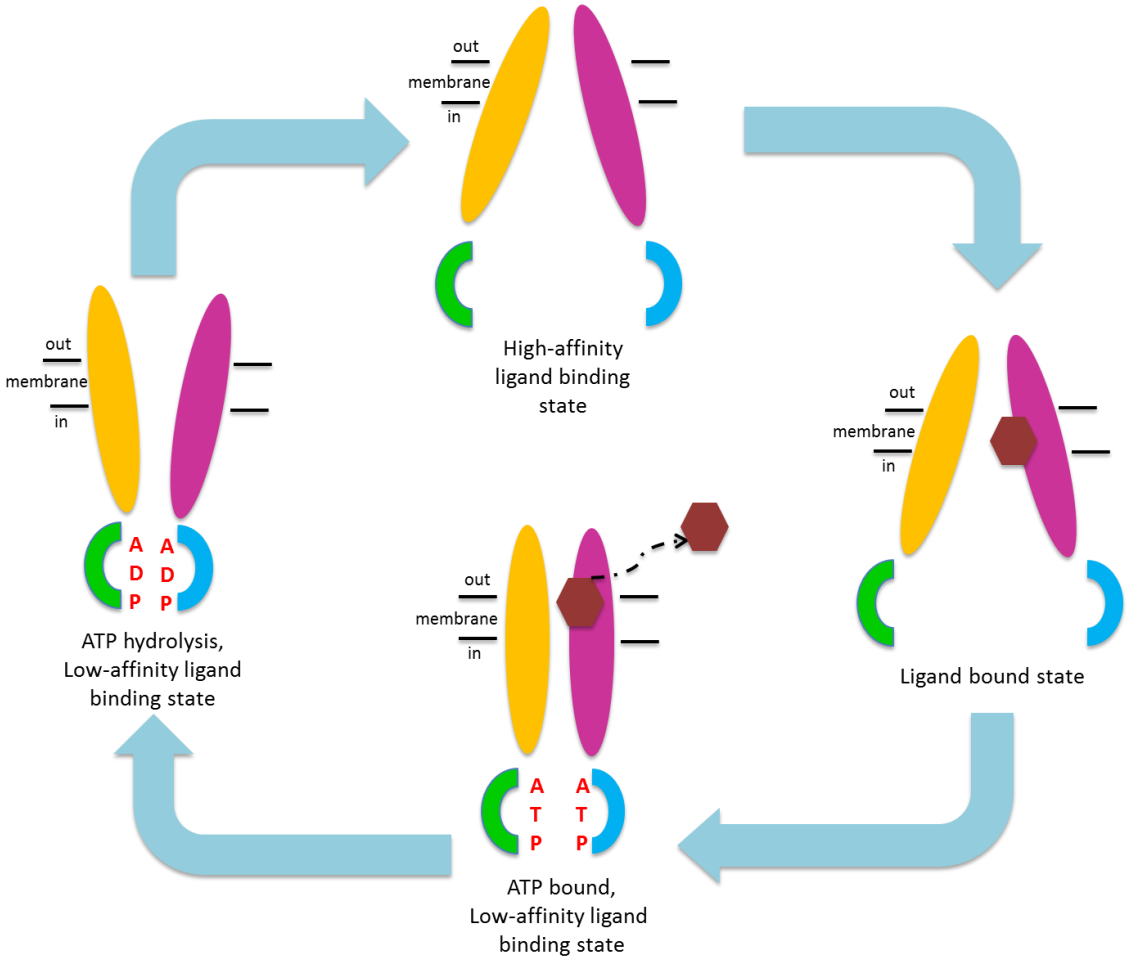

Figure 1.8: Cartoon of the ATP switch model. ABCB1 is in a high-affinity ligand binding state in its basal state (top). When the ligand binds (right), it turns into a high-affinity nucleotide binding state and binds two molecules of ATP which results in conformational change and ligand dissociation (bottom). Nucleotide hydrolysis and product (Pi then ADP) release returns the protein back to its inwardly open basal state. Orange elliptical shape represents TMD1 and purple elliptical shape represents TMD2, green shape represents NBD1 and cyan shape represents NBD2 and dark red hexagon symbolizes transport ligand.

Today, there is clear evidence that the closed dimer conformation adopted by the NBDs induces conformational changes in the TMDs that result in ligand export [82-85] but there is still little evidence to show how ATP hydrolysis is triggered. There might be communication from the TMDs to the NBDs after ligand dissociation to induce catalysis or another possibility is the autohydrolysis of the nucleotides following formation of the ATP sandwich dimer. Even though the details of the ATP catalysis is not known, hydrolysis itself does not appear to be sufficient to restore the basal state of the transporter [86]. The observation that vanadate can replace Pi and can trap the protein in the ADP bound state, suggests that Pi dissociates before ADP. The ADP-vanadate trapped conformation retains a low affinity for ligand [87], therefore only after Pi and ADP dissociate sequentially, is the protein likely to return to the inwardly open basal state and restore the high-affinity ligand binding cavity.

1.4.5. Functions of ABCB1

ABCB1 is widely expressed on many cell types, but is particularly abundant in the adrenal gland and especially in the adrenal cortex (http://biogps.org/#goto=genereport&id=5243, accessed on 15.08.2014). Other expression sites include the apical membranes of epithelial cells of liver, intestine and kidney [88]. ABCB1 is also found on barrier-function sites like the blood-brain barrier [89], the blood-testis barrier [90], the blood-inner ear barrier [91] and the maternal-foetal barrier [92] forming a protective shield against drugs and exotoxins. Its function can also be detrimental by inducing multidrug resistance against chemotherapeutic agents [12]. Other than multidrug resistance there is no known pathological condition related to altered ABCB1 expression or function [13].

1.4.5.a. Transported Ligands

ABCB1 is a multidrug transporter protein which deserves its 'Hydrophobic Vacuum Cleaner' description [93]. ABCB1 can transport a wide range of ligands, which are generally nonpolar, amphipathic compounds, including anticancer drugs, antibiotics, steroids, linear and cyclic peptides (Table 1.2).

ABCB1 Transport Ligands, Inducers and Inhibitors		
Transported Ligands	Inducers of Expression	Inhibitors of Transport
Anticancer Agents		
Actinomycin D		
Daunorubicin	Daunorubicin	
Doxorubicin	Doxorubicin	
Etoposide	Etoposide	
Paclitaxel		
Teniposide		
Vinblastine	Vinblastine	Vinblastine
Antihypertensive agents		
Diltiazem	Diltiazem	Diltiazem
Losartan		
Anti-arrhythmics		
Digoxin		
Verapamil	Verapamil	Verapamil
Antimicrobial agents		
Erythromycin	Erythromycin	Erythromycin
Itraconazole		Itraconazole
Ketoconazole		Ketoconazole
Levofloxacin		
Rifampicin	Rifampicin	
Anti- HIV agents		
Indinavir	Indinavir	
Anticonvulsants		
Phenobarbital	Phenobarbital	
Phenytoin	Phenytoin	
Anti-emetics		
Ondansetron		
H_2 antagonists		
Cimetidine		
Immunosuppressants		
Cyclosporine	Cyclosporine	Cyclosporine
Tacrolimus	Tacrolimus	Tacrolimus
Valspodar		Valspodar
Neuroleptics		
Chloropromazine		Chloropromazine
Steroid hormones		
Aldosterone		
Cortisol		Cortisol
Dexamethasone	Dexamethasone	
		Progesterone
Phospholipid Messenger		
Platelet-activating Factor (PAF)		

Table 1.2: Selected ABCB1 transport ligands, inducers of ABCB1 expression and inhibitors of transport (References; [94-96]).

1.4.5.b. Physiologic Role

i. Lipid Signalling and Transport of Platelet Activating Factor

Platelet activating factor (PAF, acetyl-glyceryl-ether-phosphorylcholine) is an important signal transmitter, as a mediator and activator of inflammation, allergic response, thrombosis, angiogenesis and potentially metastasis. It is synthesized in two ways; by a *de novo* pathway or by cleavage from a membrane phospholipid precursor. The cleavage pathway is the most common source and is thought to be the primary source of PAF under pathological conditions while the *de novo* pathway is used to maintain PAF levels during normal physiologic conditions. Using phosphatidylcholine as a starting material, phospholipase A2 (PLA2) removes a fatty acid, most commonly arachidonic acid, from the sn-2 position [97]. Removal of arachidonic acid from phosphatidylcholine produces the intermediate lysophosphatidylcholine. Addition of an acetyl group to the sn-2 position carbon atom of this intermediate by an acetyltransferase produces PAF [98].

The PLA2s are a diverse family with different regulation and substrate specificities [99]. The group IVA cytosolic PLA2 (cPLA2α) is calcium-dependent and selective for arachidonic acid, so it is activated during transient intracellular calcium rise to produce arachidonic acid and lysophosphatidylcholine, and consequently PAF, rapidly and in large quantities. On the other hand, the group VI calcium-independent PLA2s (iPLA2) which are secreted, hydrolyse sn-2 fatty acids slowly and continuously result in PAF generation [99]. Three different groups of PLA2 have been shown to induce PAF synthesis. Group V secreted PLA2 (sPLA2) which has been shown to be activated by VEGF [100], a secreted PLA2; iPLA2 which is thrombin-stimulated [101] and the cytosolic PLA2 (cPLA2α) which has been shown to synthesize PAF and arachidonic acid in neutrophils [102].

ABCB1 has been shown to transport PAF from a mesangial cell line which expresses endogenous ABCB1 [103] and an epithelial cell line which is transfected with a plasmid encoding the ABCB1 gene [104]. Numerous studies have demonstrated that PAF is secreted from cancer cells [105-107] although opposing results exist [108]. A more recent study showed that the PAF receptor is important in UVB mediated skin cancer, in which inflammation is an important factor in tumorigenesis [109]. Like ABCB1, PAF and G protein-coupled PAF receptor (PAFR) are also found in most cell types but especially in myeloid cells, in contrast ABCB1 is more abundant on lymphoid cells. Within the lymphocyte class, PAF level is more prominent in B cells whereas ABCB1 is expressed better on T cells and natural killer cells (http://biogps.org/#goto=genereport&id=5243 accessed on 15.08.2014, http://biogps.org/#goto=genereport&id=5724 accessed on 15.08.2014). Although ABCB1 can transport PAF, the differential abundance on different cell types suggests a more complicated relationship that is not understood.

Lysophosphatidylinositol (LPI) is one of the products of phosphatidylinositol hydrolysis by cytosolic PLA2 and transport of LPI is analysed in chapter 5 of this thesis. Like PAF, LPI is also a cytokine, and also a product formed during arachidonic acid synthesis. It is exported from prostate and ovarian cancer cells and recognised by protein coupled receptor GPR55 through which it functions as part of an autocrine loop important in tumorigenesis [110].

ii. Abundance in Adrenal Gland

ABCB1 is most abundant in the adrenal gland, especially in the adrenal cortex. In 1992, it was revealed that ABCB1 can transport cortisol, dexamethasone and aldosterone. Progesterone can also interact with ABCB1 but inhibits its function [111].

In the mouse, there are two ABCB1 homologues; Abcb1a and Abcb1b. *Abcb1a* mRNA is more prominent in the intestine, liver, brain, testis and *Abcb1b* mRNA is more prominent in the adrenal gland, placenta, ovarium and uterus and in the other tissues both *Abcb1a* and *Abcb1b* mRNAs are similarly prominent [112]. Mice lacking both *Abcb1a* and *Abcb1b* show no signs of disease, are normally viable and fertile under physiologic conditions [113]. Recently however, the role of glucocorticoids under stress conditions has been studied in the *Abcb1a/1b* knock-out mice [114]. Behavioural tests to quantify the fight or flight response times were performed and *Abcb1a/1b* double knock-out mice were shown to respond slower than wild-type mice. Corticosterone injection resulted in significant reductions of immobility of the knock-out mice under stress conditions. It was also shown that corticosterone concentrations were lower in knock-out mice under both naïve and stress conditions and glucocorticoid receptor expression in brain tissue was increased [114]. These results suggest that ABCB1 might have a role in the hypothalamic-pituitary adrenal feedback axis under stress conditions in mice.

iii. Barrier- function

As mentioned above, ABCB1 is found on barrier-function sites of the body, like the blood-brain barrier [89], the blood-testis barrier [90], the blood-inner ear barrier [91] and the maternal-foetal barrier [92]. The presence of ABCB1 in the luminal membrane of the vascular endothelial cells is thought to protect the body against xenobiotic entry and accumulation.

In *Abcb1a* knock-out mice, the sensitivity of orally administered drugs and accumulation of ABCB1 ligands in the brain tissue increased [115]. However, when *Abcb1a* is knocked out, Abcb1b expression levels can increase. Abcb1b levels were studied in both female and male mice, demonstrating very low or no expression of Abcb1b in the male kidney whereas the female kidney has a prominent Abcb1b expression. As a result of the *Abcb1a* knock-out, in both sexes, Abcb1b levels increased and also became more prominent in male kidney [115]. As Abcb1b is prominent in the adrenal gland and more prominent in female mice, it may also have a role under stress conditions during development *in utero*. ABCB1 is expressed on the syncytiotrophoblasts of the human placenta and its expression levels decrease with advanced gestation [116, 117]. The highest expression levels exist in the first trimester and decrease with the increase of progesterone and decrease of β-human chorionic gonadotropin (β-hCG) [117]. These findings have raised the question of whether ABCB1 is important in protecting the foetus from excess maternal corticosteroids under stress conditions [116].

1.4.5.c. Multidrug Resistance in Cancer Cells

ABCB1 has been shown to cause multidrug resistance in many different cancers. A meta-analysis study showed that ABCB1 expression in breast cancer cells is associated with a poor response to chemotherapy [118]. A clinical study which examined 73 ovarian cancer patient samples at stage 3 of the International Federation of Obstetricians and Gynaecologists (FIGO) staging system, prior to and after chemotherapy, concluded that ABCB1 expression is a marker for chemotherapy resistance and a poor prognosis in ovarian cancer [119]. In a retrospective study, detectable levels of ABCB1 were correlated with

poor prognosis in children with soft tissue sarcoma [120]. Another study which examined lymphoblasts from bone marrow or peripheral blood samples of 352 newly diagnosed acute myeloid leukemia (AML) patients showed that high ABCB1 expression and AML resistant to chemotheraphy were highly related [121]. Trials to inhibit ABCB1 function in cancer patients have almost always failed to date due to side effects causing high toxicity largely because the inhibitors used were not particularly specific for ABCB1 but also inhibit cytochrome P450; CYP3A4 [122]. As a result of cytochrome P450 inhibition, pharmacokinetics of the co-administered therapeutic drugs alter significantly.

1.5 ABCC1 and ABCC3:

A new field of multidrug resistance research began when a non-ABCB1-mediated multidrug resistance was discovered in the doxorubicin-selected small cell lung cancer cell line, H69AR [17]. This new finding raised the possibility that other ABC drug transporters might exist and indeed, additional drug transporters were identified as ABCC subfamily members. The ABCC subfamily contains 13 full transporters with a wide functional spectrum from ion diffusion to multidrug resistance. ABCC1 and ABCC3 transport glutathione conjugates and/or other organic anions [13]. ABCC1 and ABCC3 are mostly localized to the basolateral membrane in polarized cells and activities of both ABCC1 and ABCC3 have been shown to result in multidrug resistance *in vitro* [123, 124].

1.5.1. Introduction to ABCC1 and ABCC3

ABCC1 was first discovered on a small cell lung carcinoma cell line called H69AR which is resistant to anthracyclines and which does not overexpress ABCB1 [17]. The predicted molecular weight of ABCC1 is between 170 to 190 kDa and it is encoded on chromosome 16p13.1. Sequencing of *ABCC1* resulted in its classification with CFTR (ABCC7) which encodes a channel protein rather than an active transporter [125]. Despite classified in a different subfamily than ABCB1, ABCC1 works in a similar fashion. ABCC1 can export a different but overlapping range of ligands which may be glucuronidated, sulphated, or ligands which are co-transported with glutathione [126]. *ABCC3* was first cloned in 1997 [19] . It is a 170 kDa protein, encoded on Chr 17q21.33 and has 31 exons. Like ABCC1, ABCC3 is also overexpressed in various cancer cells and cause multidrug resistance [127, 128].

1.5.2. Structure of ABCC1 and ABCC3

ABCC1 has two NBDs which are less similar to each other than many of the other ABC proteins but they function in a similar fashion and are likely form the ATP-sandwich dimer to bind and hydrolyse ATP [129]. Specific to some C subclass ABC proteins, ABCC1 has an extra N-terminal transmembrane domain (TMD0) which is predicted to contain 5 transmembrane helices (Figure 1.9).

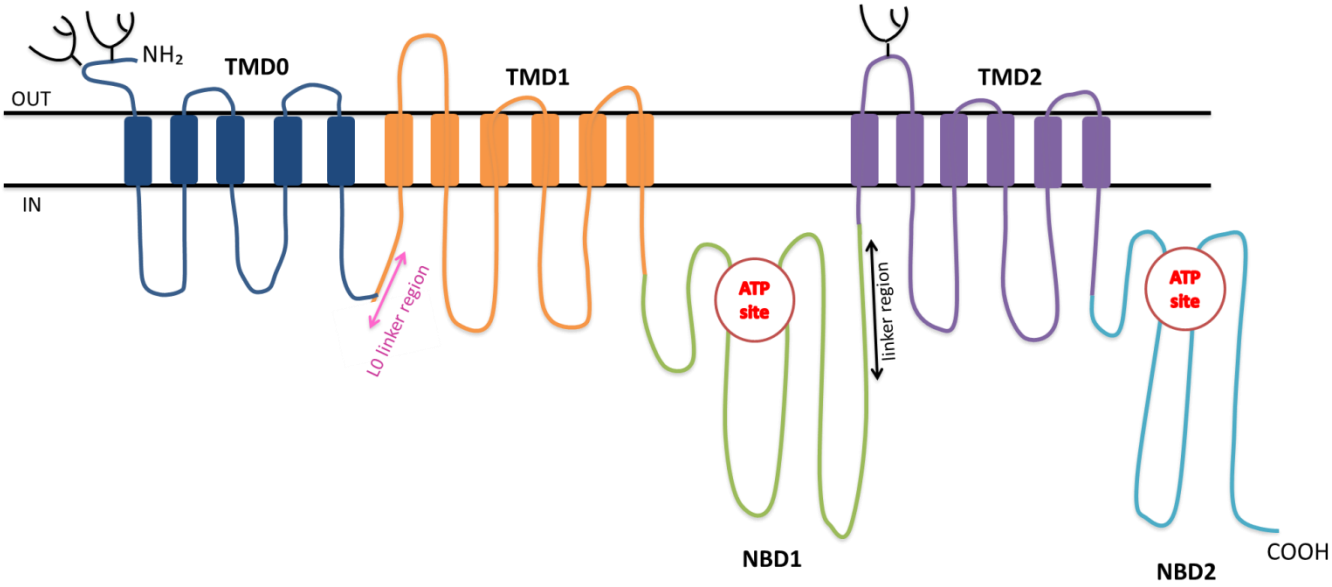

Figure 1.9: Predicted 2D structure model of ABCC1 with the 5 TMH topology of TMD0 [130]. N-glycosylation sites are predicted to exist on the first extracellular loops of TMD0 and TMD2. The pink arrow indicates the L0 linker region which is located between TMD0 and TMD1 and the black arrow indicates the second linker region which is between NBD1 and TMD2.

N-linked glycosylation inhibition studies with tunicamycin showed that ABCC1 was glycosylated [131]. Later, N-linked glycosylation of the amino-terminal first 32 amino acids was supported by epitope insertion studies. In Muller *et al*. study, two of the inserted FLAG epitopes in extracellular loops of the TMD0 or TMD2 were only accessible upon removal of N-glycosylation sites (N to Q mutations at positions 17, 23, and 1006, respectively) [132]. Surprisingly, an IgG1 monoclonal antibody (IU2H10) generated against the amino terminus (amino acids between 8th and 17th residues), presumed to be extracellular, could not access its epitope when the cells were not permeabilized, suggesting a new structural model for the amino terminus of ABCC1 [133]. The same study has also suggested a 31 amino acid β-strand structure in the amino terminus of the protein, which will need a β-turn to form a U-shape. Prediction algorithms for β-turns suggests that Asp13, Pro14, Leu15, and Trp16 residues may form this potential β-turn [134]. Another study has also suggested that the

amino terminus forms a U-shaped structure with the bottom of the U-shape facing cytoplasm and both ends residing in the extracellular space [135]. This was determined by inserting a hemagglutinin (HA) epitope at the carboxyl end of the amino terminus which resulted in a protein that is more resistant to vinblastine, adriamycin, colchicine and VP-16. As a result, they suggested that the U-shaped fold may plug a putative gate-access channel in wild-type ABCC1 and that the HA epitope may have forced the gate to open and allow the protein to transport anticancer drugs more efficiently. Deletion of the entire 32 amino acids of the amino terminus resulted in higher multidrug resistance than that conferred by wild-type ABCC1.

A 25 Å resolution crystal structure of ABCC1 has shown ABCC1 in homodimers [136]. This may be an artefact of crystallization, however another study also showed that ABCC1 can exist as homodimers using biochemical methods such as gel filtration chromatography, perfluoro-octanoic acid polyacrylamide gel electrophoresis (PFO-PAGE), non-denaturing PAGE, chemical cross-linking, co-immunoprecipitation and sucrose density gradient sedimentation [137]. The same study has also suggested that the dimerization domain is likely to exist in the first 281 amino terminal amino acids. However, a derivative of ABCC1 in which the entire TMD0 region (the amino-terminal 204 amino acids) has been deleted, is still functional whereas the protein lacking TMD0 and the loop between the TMD0 and TMD1 (the amino-terminal 281 amino acids) is not [137]. This suggests that the loop linking TMD0 to the TMD1 is an important region of the protein but whether or not it is relevant to dimerization remains to be determined.

ABCC1 is also post-translationally modified with several phosphorylation and ubiquitination sites and one acetylation site (lysine residue 498) as shown by proteomic-discovery mode mass spectrometry (http://www.phosphosite.org/proteinAction.do?id=8736&showAllSites=true, accessed on 15.08.2014).

ABCC3 is also an ABCC subfamily protein with an extra N-terminal transmembrane domain (TMD0). It has the highest sequence identity to ABCC1 within ABCC subfamily proteins (58% amino acid identity) [27]. It has three predicted N-glycosylation sites two on the possible first extracellular loop of the TMD0 and the other on the first extracellular loop of TMD2. The predicted 2D membrane topology is similar to the predicted membrane topology model of ABCC1 (Figure 1.9).

1.5.3. Function of ABCC1 and ABCC3

As a multidrug resistance protein ABCC1 can transport a wide range of ligands. The first described ligand of ABCC1 was Leukotriene C_4 (LTC_4) [24] which is an eicosanoid important in inflammation. However, *ABCC1* double knock-out mice (*ABCC1* (-/-)) studies has shown that ABCC1 is not essential because these mice are vital and fertile and develop no pathology under physiologic conditions but they had a decreased inflammatory response [138]. Expression of ABCC1 was later shown to be important in dendritic cell trafficking from skin to lymph nodes and the migration can be restored by exogenously added LTC_4 and LTD_4 [139].

ABCC1 is widely expressed in the human body (http://biogps.org/#goto=genereport&id=4363, accessed on 15.08.2014) and like ABCB1 it is also expressed in the blood-tissue barriers like the maternal-foetal barrier, the blood-CSF barrier and the blood-inner ear barrier and knocking out *ABCC1* results in xenobiotic accumulation in these sanctuary sites of the body [140-143].

Glutathione can stimulate the transport of some ABCC1 ligands with which it can be co-transported or it can also be transported itself as glutathione disulphide [144, 145]. An extremely diverse range of glutathione, glucuronide and sulphate conjugates of xenobiotics have been shown to be transported by ABCC1 in subsequent years [126].

A pathophysiological role for ABCC1 has been suggested for some cancers where it was shown that ABCC1 expression was increased in small cell and non-small cell lung cancer specimens after chemotherapy [146]. ABCC1 also may have a role in early-stage breast cancer in which its expression correlates with shorter relapse-free survival times and decreased overall survival in patients treated with cyclophosphamide, methotrexate, and fluorouracil (CMF chemotherapy) [147].

ABCC3 is also widely expressed in the human body but it has a prominent expression in adrenal gland and cortex (like ABCB1) and is also highly expressed in colon and pancreas (http://biogps.org/#goto=genereport&id=8714, accessed on 15.08.2014). ABCC3 transports a wide range of ligands and it shares some ligands with ABCC1, for example; LTC_4 and estradiol-17-β-D-glucuronide, but glutathione is not transported by ABCC3 and glutathione conjugates are poorly transported [148, 149].

Previously, it was thought that ABCC3 is highly expressed in the liver but immunohistochemistry of frozen sections has revealed that in healthy liver, there are only modest levels of ABCC3, especially in the basolateral membranes of cholangiocytes and hepatocytes surrounding the portal tracts [27]. Studies demonstrating up-regulation of *ABCC3* mRNA levels, but curiously not protein levels, in the liver during cholestatic conditions suggest that ABCC3 is important in the cholehepatic circulation of bile salts [150-152]. During cholestasis, bile salts start to accumulate in the hepatocytes which might be the triggering mechanism that switches on efflux of bile salts back into the portal vein across the basolateral membrane by ABCC3.

In relation to cancer, *ABCC3* mRNA has been shown to be upregulated in pancreatic carcinoma and was correlated with tumor grading [127]. It is also associated with a poor outcome in childhood acute lymphoblastic leukemia (ALL) [128].

The putative role of both ABCC1 and ABCC3 in an autocrine loop important in cancer proliferation and metastasis is studied and discussed further in chapter 5.

1.5.4. Ligands of ABCC1 and ABCC3

ABCC1 and ABCC3 are both organic anion transporters and they transport a wide variety of overlapping ligands, please see the selected ligands in Table1.3.

ABCC1 Transport Ligands	**ABCC3 Transport Ligands**
Antineoplastic Drugs	
Doxorubicin	Doxorubicin
Daunorubicin	Daunorubicin
Etoposide	Etoposide
Vincristine	Vincristine
Vinblastine	Vinblastine
Methotrexate	Methotrexate
	Cisplatin
	Paclitaxel
Antiviral Drugs	
Ritonavir	
Metalloids	
Sodium Arsenite	
Sodium Arsenate	
Toxins	
Aflatoxin B_1	
Folates	
Folic acid	Folic acid
Peptides	
Glutathione	
Endogenous Eicosanoids and Hormones	
Leukotriene C_4 (glutathione conjugated)	Leukotriene C_4
Estradiol-17-β-D-glucuronide	Estradiol-17-β-D-glucuronide
Estrone 3-sulfate	Estrone 3-sulfate
Prostaglandin (glutathione conjugated)	
	Taurocholate

Table 1.3: Selected transport ligands of ABCC1 [126] and ABCC3 [153-155].

Chapter Two

2. Materials and Methods

2.1. Bacterial culture

XL10-Gold® Ultracompetent *E.coli* cells:

Tetracycline and chloramphenicol resistant XL-Gold strain has the following genotype; Tetr D (mcrA) 183 D(mcrCB-hsdSMR-mrr)173 endA1 supE44 thi-1 recA1 gyrA96 relA1 lac Hte [F¢ proAB lacI qZDM15 Tn10 (Tetr) Amy Camr].

2.1.1. S.O.C. medium

After plasmid transformation into XL10-Gold® Ultracompetent *E.coli* cells, they were grown in S.O.C. medium to help survival of transformed bacteria. Super Optimal Broth with Catabolite repression (S.O.C.) is Super Optimal Broth (S.O.B.) medium with added glucose, obtained by adding 2% (w/v) tryptone, 0.5% (w/v) yeast extract, 10 mM NaCl, 2.5 mM KCl, 10 mM $MgCl_2$, 10mM $MgSO_4$ and 20mM glucose in 1000 mL dH_2O.

2.1.2. LB medium

Lysogeny broth (LB) medium consists of 1% (w/v) NaCl, 1% (w/v) tryptone, 0.5% (w/v) yeast extract (Fisher Scientific Ltd, UK; BPE1427-500). 20 g LB powder resuspended in 1000 ml dH_2O and autoclaved at 121°C for one 15 minute cycle. The medium was allowed to cool below 55°C before 100 µg/ ml ampicillin (Sigma-Aldrich, UK) was added.

2.1.3. LB agar plates

1.5% (w/v) bactoagar (BD Biosciences, UK) was added into LB medium prior to autoclaving to make LB agar plates. Before pouring the agar into plates, it was cooled below 55°C and 100 µg/ ml ampicillin (Sigma-Aldrich, UK) was added. Plates were stored up to one month.

2.1.4. Culture Conditions

Bacterial cultures were grown overnight at 37°C, shaking at 220 rpm. For large-scale cultures, a starter culture of 5 ml was grown for at least 5 hours before inoculation into a larger culture.

2.2. Insect cell culture

2.2.1. Insect cells; Sf21 and Hi5

The Sf21 insect cell line isolated from ovarian tissue of the fall army worm, *Spodoptera frugiperda* embryos, was cultured in suspension and in T75 flasks with TC-100 medium (Gibco, UK) or Sf-900™ II SFM medium (Gibco, UK) at 27°C. The High Five insect cell line originating from *Trichoplusia ni* embryonic tissue was grown in EX-CELL® 405 serum-free medium (Sigma-Aldrich, UK) again at 27°C.

2.2.2. Media and reagents

Sf-900™ II SFM and TC-100 insect cell media were purchased from Gibco. EX-CELL® 405 serum-free medium was purchased from Sigma. Penicillin-streptomycin solution and foetal calf serum (FCS) were purchased from Invitrogen.

2.2.3. Culture conditions

Penicillin-Streptomycin Solution was added to all insect cell tissue culture media to a final concentration of 100 units/ml penicillin G, and 100µg/ml streptomycin sulphate. In addition, TC-100 was supplemented with 10% FCS, unless otherwise stated. All manipulations were performed in a sterile environment, with disposable plasticware and glassware reserved specifically for the purpose.

All suspension cultures of insect cells were grown in round-bottom glass flasks at 27°C, shaking at 120 rpm. All monolayer insect cell cultures were grown in non-vented T75 flasks (BD biosciences, UK) at 27°C.

2.2.4. Insect cell co-transfection

Sf21 cells were co-transfected using *flash*BAC (Oxford Expression Technologies, UK) or ProFold™-ER1 (AB vector, UK) as instructed by the manufacturer. $1.5x10^6$ cells were plated onto a 35 mm tissue culture dish (BD Biosciences,UK) in TC-100 medium.

For each co-transfection with *flash*BAC, the following reagents were mixed:

100 ng *flash*BAC DNA

500 ng transfer plasmid (pBacPAK9-based vector)

5 µl Lipofectin® transfection reagent (Invitrogen, UK)

1 ml TC-100 without serum or antibiotics

The solution was mixed and incubated for 30 minutes at room temperature. The culture medium was then aspirated and washed twice with TC-100 medium without serum or antibiotics and then the transfection mixture was carefully added to the insect cell monolayer. Each dish was then incubated for 5 hours at 27°C in a sealed box containing a layer of paper wetted with 10mM EDTA. Following this, 1ml TC-100 (with 10% FCS and antibiotics) was added to each dish and the dishes were placed back inside the sealed box which was incubated at 27°C for 120 hours in total.

The protocol for ProFold™-ER1 co-transfection was the same as for *flash*BAC except, 200 ng ProFold™-ER1 DNA was substituted for 100 ng *flash*BAC DNA.

Following incubation, the medium was aseptically transferred into 5 ml bijou containers and retained as cotransfected (Co-T) baculovirus.

2.2.5. Amplification of baculovirus

The rationale for baculoviral amplification is to infect insect cells with low ratio of baculovirus (multiplicity of infection; MOI) to allow cell growth and duplication to continue while multiple cycles of viral infection and release occur. The steps are similar for both *flash*BAC and ProFold™-ER1.

2.2.6. Amplification of Co-T baculovirus to intermediate stock

A suspension culture containing 25 ml Sf21 cells at a density of $2x10^6$ cells/ ml in Sf-900™ II SFM media was infected with 0.5 ml Co-T baculovirus. The cells were incubated overnight, before dilution with 25 ml fresh Sf-900™ II SFM media. After 5 days, the cells were removed by centrifugation at 500 *g* for 10 minutes (Hettich rotanta 46R), and the supernatant was stored at 4°C as 'intermediate stock' baculovirus. At this stage the virus titre was calculated by plaque assay.

2.2.7. Amplification of intermediate stock to working stock

A suspension culture containing 100ml Sf21 cells in Sf-900™ II SFM media at a density of $2x10^6$ cells/ ml (in total $2x10^8$ cells) was infected at a MOI of 0.1 with intermediate stock baculovirus. The cells were incubated overnight, before dilution with 100ml fresh Sf-900™ II SFM. After 5 days, the cells were removed by centrifugation at 500 *g* for 10 minutes (Hettich rotanta 46R), and the supernatant was stored at 4°C as 'working stock' baculovirus.

2.2.8. Plaque assay to quantify viral load of recombinant baculovirus

For each baculovirus, 35mm tissue culture dishes (BD Biosciences,UK) were seeded with $1x10^6$ Sf21 cells in TC-100 medium with 10% FCS, and left to adhere on a flat surface. While the cells were settling, a series of dilutions were prepared using intermediate baculovirus stocks (10^4, 10^5, 10^6 dilutions) to a final volume of 1 ml in TC-100. The culture medium was aspirated from the dishes, and 100 µl of each dilution was added. The cells were incubated for 45 minutes at room temperature, and during this step, 4% low melting point agarose

(LMP agarose; Sigma-Aldrich, UK) was melted in a microwave oven and placed in a 37°C water bath. The TC-100 medium was also preheated to 37°C in a water bath prior to the next step.

The 4% LMP agarose was diluted to 1% using the prewarmed TC-100. The medium covering the Sf21 monolayer was aspirated and each dish was layered with 1.5 ml 1% LMP agarose in TC-100 media. The dishes were placed on a flat surface and incubated at room temperature till the agarose solidified. Following this, 2 ml TC-100 with 10% FCS was added onto the agarose layer and the dishes were placed inside a sealed box containing a layer of paper wetted with 10mM EDTA, and incubated at 27°C for 72 hours. Later, a solution containing 0.03% neutral red (Sigma-Aldrich, UK) in PBS was added to each dish (2.5 ml) after aspirating the overlaying media and incubated for 3 hours. The dye on the surface of the agarose plug was then aspirated and the dishes were inverted and left overnight in the dark at room temperature. The neutral red stains live cells, allowing the visualisation of virus-induced 'plaques' of lysed or dying cells as clear regions of the monolayer.

To estimate the titre of each viral intermediate stock, the plaque numbers on each dish were counted. The titre (in plaque forming units/ml; pfu/ml) is equal to the plaque count multiplied by the dilution factor.

2.2.9. Large-scale infection for protein production

A suspension culture containing 100 ml Sf21 serum-free cells at a density of $2x10^6$ cells/ ml (in total $2x10^8$ cells) in Sf-900™ II SFM media or 100 ml Hi5 cells at a density of $1x10^6$ cells/ ml (in total $1x10^8$ cells) in EX-CELL® 405 serum-free medium was infected with working stock baculovirus. The volume of virus added was calculated from western blot results of infection ratios of incremental volumes of viruses to insect cells. The cells were incubated overnight, before being diluted with fresh Sf-900™ II SFM or EX-CELL® 405 serum-free media to a volume of 200 ml in total. The cells were harvested after a total of 72 hours following initial infection.

2.3. Mammalian cell culture

2.3.1. HEK293T mammalian cells

Transformation of cultures of human embryonic kidney cells with sheared adenovirus 5 DNA resulted in HEK 293 cells [156]. A variant of this cell line, HEK293T cell line, in addition contains SV40 large T antigen allowing for the amplification of transfected plasmids containing the SV40 origin of replication. HEK293T cells were obtained from Imperial Cancer Research Fund, cell production unit.

2.3.2. Media and reagents

HEK293T cells were grown in Dulbecco's modified Eagle's medium (DMEM) with glutamax (Invitrogen, UK) supplemented with 10% foetal bovine serum (FBS) (Sigma-Aldrich, UK). Cells were detached from the plasticware using TrypLe Express (Invitrogen, UK).

2.3.3. Culture conditions

HEK293T cells were grown in T75 vented flasks (VWR, UK) in 10% FBS supplemented DMEM and incubated in 5% CO_2 incubator at 37°C. Cells were passaged every 3-4 days in 1/20 dilution. All studies were performed under sterile conditions.

2.3.4. Transfection reagents

25kDa polyethyleneimine (PEI; Sigma-Aldrich, UK) solution (45 mg PEI dissolved in 8 ml H_2O corrected to pH 7.2 with dilute HCl) was used to transfect HEK293T cells.

2.3.5. Transfection conditions

For transfections in a T25 vented tissue culture flask (BD Biosciences, UK), HEK293T cell monolayers were grown to 70% confluency. Polyethyleneimine (PEI)–DNA complexes: 10 µg DNA and 2 µl 5% glucose were mixed with 3 µl 25 kDa PEI solution in a total volume of 20 µl (topped up with sterile dH_2O). The complexes were diluted in 5 ml DMEM with FBS and added to the cell monolayer. The cells were either harvested after 48 hours and reseeded into 8-well chamber slides (Millipore, UK) for microscopy experiments and/or harvested 72 hour post-transfection with TrypLE Express (0.5ml) and 4.5 ml DMEM with FBS for transport assays. T75 vented flasks (BD Biosciences, UK) were used for membrane

vesicle preparations. Transfection conditions were the same with cell number and transfection reagents tripled.

2.4. Plasmids

For mammalian cell transfection with ABCB1 expression, twelve histidine (12-His) tagged wild-type or mutant ABCB1 cDNA encoded by the pCI-neo mammalian expression vector (Promega, WI, USA) was used (Figure 2.1) [157].

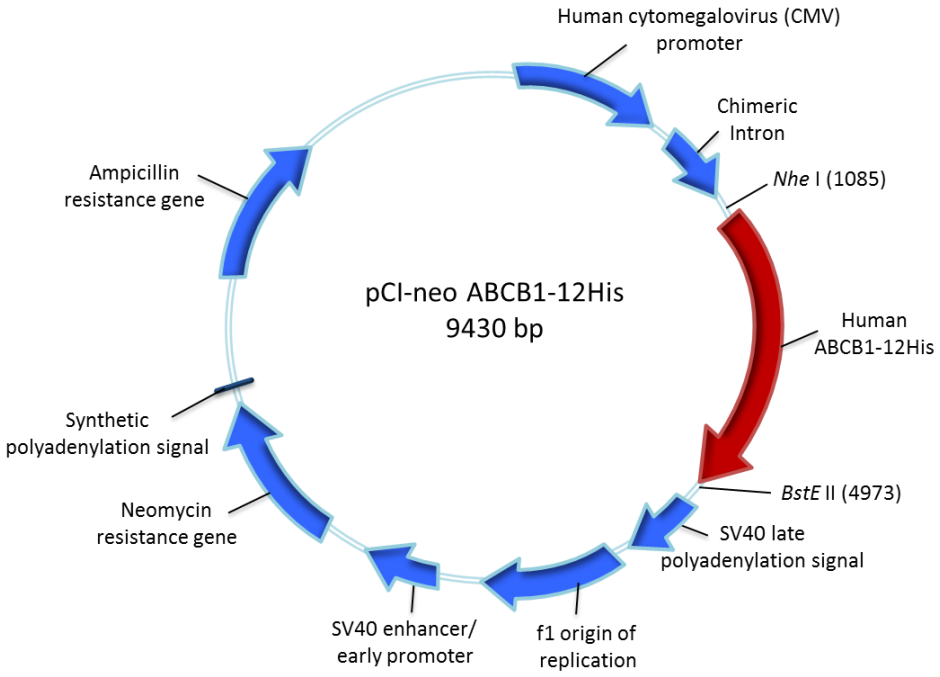

Figure 2.1: Mammalian cell transfection vector; ABCB1-12His cDNA inserted pCI-neo.

Wild-type ABCC1 or ABCC3 cDNA expressed from pcDNA3.1 vectors were kind gifts from Prof. Susan Cole Lab (The Cancer Research Institute, Queen's University, Canada)[158, 159].

For baculoviral infections of insect cells, pBacPAK9 vector encoding 12-histidine tagged wild-type ABCB1 cDNA was used (Figure 2.2) (Please see section 2.8.).

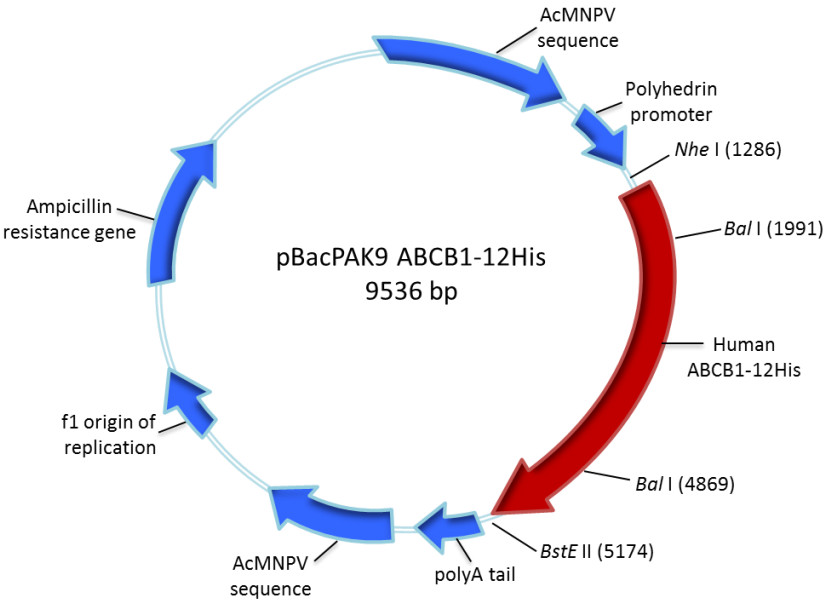

Figure 2.2: Wild-type ABCB1 encoding pBacPAK9 vector for protein expression in insect cell lines.

2.5. Primer list

The primers for Q-loop or ligand binding cavity mutants were designed and introduced by Dr. Zolnerciks (Linton lab, personal communication). The primers for single Walker B mutant introduction into Q132R/Q1118A mutant, were designed and introduced by myself and the lists of all primers can be found in the related chapters. Oligonucleotide-directed mutations were introduced into wild-type ABCB1 expressing pCI-neo vector by QuickChange II XL site directed mutagenesis kit (Agilent Technologies, UK) described in section 2.7.

2.6. Isolation of plasmid DNA from E.coli cells

2.6.1. Small scale

Small-scale plasmid DNA preparations were generated using the GenElute HP Plasmid Miniprep Kit as described by the manufacturer (Sigma-Aldrich, UK). Bacterial cells from a 5 ml overnight culture were harvested by centrifugation for 1 min at 12,000 *g* (EBA 12, Hettich; Germany). The cell pellet was then resuspended in 200 µl Resuspension Solution with 100 µg/ ml RNase A. Lysis Buffer (200µl) was then added and the solution was mixed by 3-4 times inversion. The alkalinity of the Lysis Buffer causes the denaturation of the nucleic acids and protein within the lysate. After 3-5 minutes incubation at room temperature, Neutralization Buffer (350 µl) was added, causing the aggregation of insoluble genomic DNA and high molecular weight RNA, and the precipitation of protein-SDS (sodium dodecyl sulphate) complexes. The lysate was then centrifuged for 10 minutes at 12,000 *g*. GenElute HP Miniprep Binding Columns were prepared by adding 500 µl Column Preparation Solution and centrifuging for 1 min at 12,000 *g*. The supernatant from the cell lysate was then added to the column and the supernatant was passed through the columns by centrifugation at 12,000 *g* for 1 min. The columns were washed by adding Wash Solution (500 µl) and centrifuged for 1min at 12,000 *g*. Then, the columns were centrifuged as before in order to remove any traces of Wash Solution. Plasmid DNA was eluted by adding 100 µl Elution Solution (10 mM Tris-HCl, pH 8.0, 1 mM EDTA) to the column and centrifuged for 1min at 12,000 *g*.

2.6.2. Large scale

Large-scale bacterial cultures were inoculated from a starter culture with a dilution factor of 1/500 to 1/1000. The Plasmid Mega Kit (Qiagen, UK) was used to generate DNA from large scale cultures as described by the manufacturer. 500 ml overnight culture was harvested by centrifugation for 15 minutes at 6000 rpm, 4°C in a Sorvall RC-5B centrifuge (Fiberlite* F12-6x500 LEX Rotor; Sorvall LLC, DE, USA). The cell pellet was resuspended in 50 ml Resuspension Solution (Buffer P1 - Resuspension Buffer; 50mM Tris-Cl, pH 8.0, 10mM EDTA, 100ug/mL RNase A), then 50ml Lysis Buffer (Buffer P2 - Lysis Buffer; 200 mM NaOH, 1% SDS) was added before mixing by inversion and incubating for 5 minutes at room temperature. Following addition of 50 ml Neutralization Buffer (Buffer P3 - Neutralization Buffer; 3.0 M potassium acetate, pH 5.5), the solution was then mixed by 4-6 times inversion, and incubated on ice for 30 minutes. The resulting lysate was cleared by centrifugation for 40 minutes at 20,000 *g*, 4°C. During the centrifugation, a QIAGEN-tip 2500 equilibrated by applying 35 ml Column Equilibration Buffer (Buffer QBT; 750 mM NaCl, 50 mM MOPS, pH 7.0, 15% isopropanol, 0.15% Triton X-100), and allowed the column to empty by gravity flow. The cleared supernatant was poured onto the column, then washed with 200ml Wash Buffer (Buffer QC - Wash Buffer; 1.0 M NaCl, 50 mM MOPS, pH 7.0, 15% isopropanol) before the DNA was eluted using 35ml Elution Buffer (Buffer QF-Elution Buffer; 1.25 M NaCl, 50 mM Tris-HCl, 15% isopropanol, pH 8.5). Room-temperature isopropanol (24.5ml) was added to the elute and the DNA precipitate was pelleted by centrifugation for 30min at 15,000 *g*, 4°C in a Sorvall RC-5B centrifuge (SS-34 rotor). The pellet was washed using 70% ethanol (7ml), centrifuged for 10 minutes at 15,000 *g*,

4°C,then air-dried, and resuspended in 500µl TE buffer (10 mM Tris•Cl, pH 8.0; 1 mM EDTA).

2.7. Site directed mutagenesis

Mutations were introduced into a plasmid encoding human ABCB1 with a C-terminal twelve histidine tag (pCIneo-wtABCB1-12His) by QuikChange II XL site-directed mutagenesis kit (Agilent Technologies, UK) using oligonucleotides in the primer lists (Table 3.1 and Table 3.3).

The QuikChange II XL site-directed mutagenesis method is performed using PfuUltra high-fidelity (HF) DNA polymerase. The template DNA is PCR amplified using a pair of mutagenic primers, each complementary to opposite strands of the vector, extended during temperature cycling by PfuUltra HF DNA polymerase to generate the mutant strands. Thermal cycling reactions were set up in the thin walled PCR tubes (Sigma-Aldrich, UK). Each reaction was set up as listed in Table 2.1 and cycled using the parameters outlined in Table 2.2.

QuickChange Reaction	Volume (µl)
Reaction Buffer (10x)	5 µl
dsDNA template	1 µl (10 ng)
Primer #1	1 µl (125 ng)
Primer #2	1 µl (125 ng)
dNTP mix	1 µl
QuikSolution	3 µl
ddH_2O	To 50 µl final volume
Pfu Turbo DNA Polymerase	1 µl

Table 2.1: Protocol for the QuickChange II XL site-directed mutagenesis kit (Agilent Technologies, UK). This protocol was used to introduce the required mutations into pCI-neo wild-type ABCB1 vector. Reaction Buffer (1x): 200 mM Tris-HCl (pH 8.8), 20 mM $MgSO_4$, 100 mM KCl, 100 mM $(NH_4)_2SO_4$, 1% Triton X-100, 1 mg/ml nuclease freebovine serum albumin (BSA).

Time (sec)	Temperature (°C)	No. of Cycles	Cycles
60	95	1	Denaturation
50	95	18	Amplification
50	60		
600	68		
420	68	1	Extension

Table 2.2: PCR programme used to mutagenize pCI-neo wild-type ABCB1 vector.

Following PCR amplification, endonuclease digestion of methylated and hemi-methylated DNA is carried out using *Dpn* I endonuclease (target sequence: 5′-Gm^6ATC-3′). Since the template plasmid DNA is generated using dam^+ *E.coli* strain, whereas PCR-synthesised DNA is unmethylated, the template is susceptible to *Dpn* I digestion. Thus only the newly synthesised DNA is transformed into XL-10 Gold *E.coli*.

2.8. Subcloning

The wild-type ABCB1-12-His cDNA encoded by the pCI-neo mammalian expression vector (Promega, UK) was subcloned into pBacPAK9 vector using the *Nhe*I and *BstE*II (New England Biolabs, UK) restriction enzyme sites at the 5'- and 3'-ends of the gene.

DNA ligases catalyse the formation of a phosphodiester bond between the 3' hydroxyl and 5' phosphate of adjacent DNA residues. The DNA ligase from bacteriophage T4 is the ligase most-commonly used in laboratories. T4 ligase can ligate cohesive (sticky) ends or blunt ends of DNAs. Ligations in this thesis were carried out using T4 DNA ligase (400U) in ligation buffer (50 mM Tris-HCl pH 7.5, 10 mM $MgCl_2$, 1mM ATP, 10 mM dithiothreitol) overnight at 16°C.

2.9. Agarose gel electrophoresis of DNA

1% agarose gels were prepared by melting the necessary amount of agarose powder (DNA grade; Invitrogen, UK) in Tris base, acetic acid and EDTA (TAE) buffer (40 mM Tris-acetate, 1 mM EDTA), by heating in a microwave until clear. The melted solution was cooled before ethidium bromide (0.5 µg/ ml) or GelRed™ Nucleic Acid Gel Stain (10,000X in Water; VWR, UK) was added and poured into a gel tray (Owl Seperation Systems, Thermo Fisher Scientific, MA, USA) to allow solidification. Prior to loading into the gel, the samples were mixed with $1/6^{th}$ volume of Gel Loading Dye, Orange (6X stock; 2.5% Ficoll®-400,11 mM EDTA, 3.3 mM Tris-HCl, 0.017% SDS, 0.15% Orange G, pH 8.0, at 25°C; NEB, UK). The DNA fragments were separated by electrophoresis at 100 V. The DNA fragments were visualised

by a UV transilluminator and images were recorded with The MultiImage® Light Cabinet (Alpha Innotech Corporation, CA, USA).

2.10. Isolation of DNA from agarose gels

Desired DNA fragments were excised from agarose gel with a clean blade taking care to minimise the amount of gel around the DNA. The DNA fragments were isolated from the gel using GenElute™ Gel Extraction system (Sigma-Aldrich, UK). Briefly, the gel slice was weighed and incubated at 50-60°C for 10 minutes with three gel volumes (w/v) of Gel Solubilisation Buffer was added. During incubation, the GenElute Binding Column G was prepared by adding 500 µl of the Column Preparation Solution and centrifuged at 12,000 *g* for 1 minute. After the gel was solubilised, one gel volume (w/v) of 100% isopropanol was added, mixed until homogenous and loaded onto the column and centrifuged at 12,000 *g* for 1 minute. The column was washed by adding 700 µl wash solution and centrifuged for 1 min. The DNA was eluted from the column by the addition of 50 µl pre-warmed Elution Buffer (10 mM Tris-HCl, pH 8.5), and centrifugation for 1 min at 12,000 *g*.

2.11. Determination of DNA yield and quality

DNA yield in nucleic acid preparations was determined by measuring absorbance using the NanoDrop® Spectrophotometer ND-1000 V3.5 (Thermo Fisher Scientific, MA, USA). Estimation of the purity of the plasmid DNA was carried out by measuring the ratio of OD_{260}/OD_{280} or OD_{260}/OD_{230}. An absorbance ratio of ~ 1.8 at 260 and 280 nm is accepted as 'pure' DNA and an absorbance ratio in the range of 1.8-2.2 is accepted as pure at 260 and 230 nm. If the ratio is lower in either case, this may indicate the presence of contaminants.

2.12. DNA sequencing

2.12.1. Automated DNA sequencing

Automated DNA sequencing was out-sourced and performed by Source Bioscience LifeSciences, UK.

2.12.2. In-house sequencing

In-house sequencing was performed by using BigDye® Terminator v3.1 Cycle Sequencing (Invitrogen, UK).

2.12.2.a. cycle sequencing on plasmid DNA

Each reaction mixture was prepared by mixing; 1 µl oligonucleotide (3.2 pmol/ µl), 2 µl BigDye Sequencing Buffer, 250 ng DNA template, 0.5 µl Ready Reaction Premix and dH_2O to a final volume of 10 µl. Cycle sequencing was performed with RoboCycler® Gradient 40 Thermal Cycler (Stratagene, CA, USA) which saves temperature ramping time with four blocks set to different desired temperatures. The cycles set for plasmid DNA sequencing starts with one cycle of 1 minute at 96 °C and continued with 25 cycles of 30 sec at 96°C, 15 sec at 50°, 4 minutes at 60°C. After the cycling is complete, the samples were kept at 4°C in the robocycler.

2.12.2.b. ethanol/ EDTA precipitation of DNA

Prior to electrophoresis, to remove unincorporated dye terminators which can obscure data, ethanol/EDTA precipitation of DNA was performed.

The amplified products in 10 µl volumes were centrifuged briefly, before sequential addition of 2.5 µl 125mM EDTA (Sigma-Aldrich, UK) and 30 µl 100% ethanol (Sigma-Aldrich, UK). The tubes were mixed by 4 times inversion, incubated at room temperature for 15 minutes and centrifuged for 10 minutes at 17,000 *g*, 4°C (Heraus Fresco 17; Thermo Fisher Scientific, MA, USA). The supernatant was discarded and the samples were air-dried for 30 minutes in the dark. After 30 minutes, the samples were resuspended in 10 µl Hi-Di™ Formamide (Applied Biosystems, UK) and loaded into MicroAmp® Optical 96-Well Reaction Plate (Invitrogen, UK).

2.12.2.c. sample electrophoresis

The samples were heated to 96°C for 5 minutes to denature DNA and then rapidly cooled for 1 minute by placing the 96-well plate on ice. Automated sample electrophoresis and sequencing analyses were performed with ABI Prism® 4-capillary 3130xl Genetic Analyzer (Applied Biosystems, UK). The sequencing protocol 'sequencing_600bp_POP7' and the analysis protocol '3130 POP7_BDTU3-KB_DENOVO_V.5.2' were selected.

2.12.2.d. sequencing data analyses

Sequencing data analyses were performed using MacVector with Assembly (version 11.1.0).

2.13. Isolation of whole-cell or membrane protein fraction

2.13.1. Insect cell monolayer culture and HEK293T whole-cell extracts

At the desired time point (72 hours for insect cells and 48 hours for HEK293T cells post infection/transfection), cell monolayers were washed three times with phosphate-buffered saline (PBS; Sigma-Aldrich, UK) and then lysed in an appropriate volume (500 µl for 30 mm dish and 1 ml for T25 flasks) of lysis buffer (2% sodium dodecyl sulphate in PBS supplemented with protease inhibitors (cOmplete, Mini, EDTA-free; Roche, UK) and 25 U/µl Benzonase® (Merck Millipore, DE, USA)). After 15 minutes of incubation on ice to allow the endonuclease to function, the samples were centrifuged in 1.5 ml eppendorf tubes (Eppendorf, UK) at 17,000 *g*, 4°C for 8 minutes to remove any insoluble material. The supernatants were either processed directly to western blotting or stored at -20 °C. For western blotting, 4X SDS gel loading buffer was added to a final concentration of 50 mM Tris-HCl, 100 mM dithiothreitol (DTT), 2% SDS (w/v), 0.1% bromophenol blue (v/v), 10% glycerol (v/v). The samples were incubated at 37°C for 15 minutes prior to loading.

2.13.2. Insect cell suspension culture membrane extracts

Sf21 or Hi5 cell suspension cultures (200 ml) were separated into four 50 ml centrifuge tubes (BD Biosciences, UK) 72 hours post-infection and centrifuged at 1000 *g* for 10 minutes (4°C; Hettich rotanta 46R). The supernatant was discarded and each of the cell pellets were washed with 5 ml lysis buffer (10 mM Tris pH 7.4, 250 mM sucrose, 0.2 µM CaCl2, 40 µM leupeptin, 2 mM benzamidine, 2 µM pepstatin A). The cells were centrifuged

as before and all four pellets were resuspended in a total of 16 ml lysis buffer. The cell suspension was homogenized on ice using an Ultra-Turrax T25 (IKA Labortechnik, Germany). The homogenizer was used, at full speed, for ten times in ten second bursts, with 30 second gaps between bursts. The homogenate was then centrifuged at 500 *g* for 10 minutes (4°C; Hettich rotanta 46R) to pellet any residual whole cells and large organelles. The crude membrane fraction was isolated from the resulting supernatant by ultracentrifugation in T865 rotor (Sorvall Discovery 90 Ultracentrifuge, Thermo Fisher Scientific, MA, USA) at 100,000 *g* for 1 hour, and was resuspended in 10 ml ice-cold resuspension buffer (10 mM Tris-HCl, pH 7.4, 250 mM sucrose, 10% glycerol, 40 µM leupeptin, 2 mM benzamidine, 2 µM pepstatin A). The membrane preparation was homogenized by repeatedly passing through a syringe with a 25G needle. Membrane preparations were stored at –80°C.

2.13.3. HEK293T membrane vesicle preparation

Monolayers of HEK293T cells were grown in T75 flasks were harvested at 48 hours post-transfection with 2 ml TrypLE Express (Invitrogen, UK) and diluted with 8 ml DMEM (supplemented with 10% FBS) for membrane vesicle preparation. The samples were centrifuged at 1000 *g* for 10 minutes (4°C; Hettich rotanta 46R). The supernatant was discarded and the cell pellets were washed with 10 ml of lysis buffer (10 mM Tris-HCl, 250 mM sucrose, 3 mM KCl, 0.25 mM MgCl2, pH 7.5, 40 µM leupeptin, 2 mM benzamidine, 2 µM pepstatin A) twice. The cells were centrifuged as before and all pellets were resuspended in 5 ml lysis buffer. The cell suspension was homogenized on ice with 60 propels using large clearance pestle of all-glass dounce tissue grinder (Sigma-Aldrich, UK). The homogenate was then centrifuged at 500 *g* for 10 minutes (4°C; Hettich rotanta 46R) to

pellet any residual whole cells and large organelles. The crude membrane fraction was isolated from the resulting supernatant by ultracentrifugation in T865 rotor (Sorvall Discovery 90 Ultracentrifuge, Thermo Fisher Scientific, MA, USA) at 100,000 *g* for 1 hour, and resuspended in 3 ml ice-cold resuspension buffer (50 mM Tris-HCl, 250 mM sucrose, pH 7.5, 40 µM leupeptin, 2 mM benzamidine, 2 µM pepstatin A). The membrane vesicles were made by repeatedly passing the resuspended homogenate through a syringe with a 27G needle. Membrane vesicles were stored at –80°C for up to two weeks.

2.14. Protein biochemistry

2.14.1. Protein quantitation

Protein concentration of samples was measured using the Bio-Rad DC Protein Assay (Bio-Rad, UK). The assay is based on the Lowry method [160] and was carried out according to the manufacturer's protocol. Samples were diluted where necessary, and complemented to a constant volume of 20 µl with dH2O. A range of bovine serum albumin (BSA; Sigma-Aldrich, UK) concentrations (0, 0.05, 0.1, 0.2, 0.3, 0.4, 0.5, 0.75 and 1 µg/ µl) were used to produce a standard curve and the concentrations of samples were analysed by Synergy™HT spectrophotometer (BioTek, VT, USA) at 750 nm.

2.14.2. ABCB1 purification

Insect cell membrane preparations were pelleted by centrifugation at 4°C, 100,000 g for 45 minutes (Sorvall Discovery 90 Ultracentrifuge, Thermo Fisher Scientific, MA, USA) and then solubilized at a concentration of 5 mg protein/ ml in solubilisation buffer. Solubilisation buffer was prepared by, first, mixing 1120 µl total E.coli lipid (100mg/ml in 3:1 v/v chloroform: methanol; Avanti Polar Lipids, AL, USA) and 280 µl cholesterol (100mg/ml in 3:1 v/v chloroform: methanol; Sigma-Aldrich, UK). The sample was mixed in a round-bottom glass tube and dried under N_2. The lipid film was then dried in a vacuum desiccator overnight. The lipid film was resuspended in a total volume of 35 ml in Buffer 1 (150 mM NaCl, 20 mM Tris, 1.5 mM $MgCl_2$, 20% glycerol (v/v), 40 µM leupeptin, 2 mM benzamidine, 1 µM pepstatin, pH 6.8) containing 2% n-Dodecyl β-D-maltoside (DDM; Merck Serono, UK) (w/v). 18 ml of the solubilisation buffer (72 mg total lipid (E.Coli lipid:cholesterol ratio is 4:1) resuspended in 150 mM NaCl, 20 mM Tris, 1.5 mM $MgCl_2$, 20% glycerol, 2% DDM buffer with protease inhibitors) was used to homogenize. Membrane preparations were solubilised by repeated extrusion cycles with a 25G needle, on ice. The insoluble fraction was pelleted by centrifugation at 4°C, 100,000 g for 30 minutes (Sorvall Discovery 90 Ultracentrifuge, Thermo Fisher Scientific, MA, USA). Ni-NTA Agarose (Qiagen, UK) was washed with dH_2O (2 ml of 50% slurry/ 100 mg protein) and pre-equilibrated in solubilisation buffer with 10 mM imidazole, at a volumetric ratio of 1:10 (packed resin: buffer). To prevent non-specific interactions between proteins and resin, imidazole was added to the soluble fraction at a final concentration of 10 mM. The solubilised protein and resin were incubated with continuous mixing for 1 hour at 4°C to ensure the binding of the 12-His-tagged ABCB1. After centrifugation at 500 g for 2 minutes, the non-bound proteins

were decanted (flow-through), and to remove non-specifically bound proteins the resin bed was washed four times with 20 bed volumes of ice-cold imidazole (washes 1-4; 40 mM, 80 mM, 100 mM, 120 mM imidazole), all in Buffer 2 (similar to Buffer 1 but at pH 8 and 0.1% DDM added). The resin was washed a final time with 20 bed volumes of Buffer 1 with 0.1% DDM, in the presence of 5 mM imidazole, to alter the pH for optimum elution (Elution 0). Bound protein was eluted in a further 3 washes in Buffer 1 with 0.1% DDM, in the presence of 500 mM imidazole (elutions 1-3).

2.14.3. Protein concentration

Amicon® Ultra-4 Centrifugal Filter Units (for proteins above 100 kDa; Merck Millipore, DE, USA) were used to concentrate purified ABCB1 protein, depending on the manufacturer's instructions. Briefly, 4 ml of sample was centrifuged at 4000 *g* for 15 minutes to obtain 35 µl of concentrated sample and subsequent centrifugation cycles with 4 ml of 10 mM Tris pH 7.4 were carried out to dilute the imidazole concentration within the sample.

2.14.4. Trichloroacetic acid (TCA) precipitation

Purified ABCB1 protein was concentrated by trichloroacetic acid (TCA) precipitation for quantification in SDS-PAGE gels. 0.15% sodium deoxycholate (0.1 volumes of sample volume (v/v)) was added to the protein sample and incubated at room temperature for 5 minutes. Following this, 0.1 (v/v) of room-temperature 72% trichloroacetic acid was added, mixed, and incubated for 10 minutes at room temperature. Protein was recovered by centrifugation at 17,000 *g* for 8 minutes (Heraus Fresco 17; Thermo Fisher Scientific, MA, USA). The supernatant was carefully removed and discarded, and the pellet resuspended in

15 µl resuspension buffer (4% SDS, 0.2 M Tris pH 7.4, 0.15 M NaOH). Samples were either directly loaded into SDS-PAGE gels or stored in -20°C for later analysis.

2.14.5. SDS-PAGE (sodium dodecyl sulphate polyacrylamide gel electrophoresis)

For separating proteins in SDS-polyacrylamide gels, Tris –glycine electrophoresis buffer (25 mM Tris base, 250 mM glycine, 0.1% SDS (w/v)) was used. The protein samples were loaded into vertical 1 mm thick polyacrylamide gels which were composed of two parts; stacking gel (4% acrylamide (v/v), 125 mM Tris pH 6.8, 0.1% SDS (w/v) and 1% ammonium persulfate (w/v) polymerised with 0.1% N,N,N',N'-tetramethylethylenediamine (TMED)) and resolving gel (7.5% acrylamide (v/v), 375 mM Tris pH 8.8, 0.1% SDS (w/v), 1% ammonium persulphate (w/v) polymerised with 0.08% TMED). Mini-PROTEAN® Electrophoresis System (Bio-Rad, UK) was used to perform protein separation in SDS-Polyacrylamide gels. Precision Plus Protein™ All Blue Standards (Bio-Rad, UK) was used to determine the molecular weight and the samples were run at 100V.

2.14.6. Colloidal blue staining

Protein visualisation following separation by SDS-PAGE was carried out by Colloidal Blue Staining (Invitrogen, UK), according to the manufacturer's instructions. Briefly, the SDS-PAGE gel was placed in a clean staining tray with colloidal blue solution (per gel: 20 ml Stainer A which contains ammonium sulfate and phosphoric acid, 5 ml Stainer B which contains Coomassie G-250, 20 ml 100% methanol, 55 ml dH_2O), and incubated for 3-12 hours at room temperature on a rocking platform. The gel was then washed several times

with dH_2O at room temperature, rocking, in order to de-stain and allow visualisation of the proteins. The visualisation process was performed by ODYSSEY® (LI-COR Biosciences, UK).

2.14.7. Western blot

Proteins separated by SDS-PAGE were electroblotted onto a polyvinylidene fluoride (PVDF) membrane (immobilon-P; Millipore, Billerica, MA), which was pre-soaked to 100% methanol for 1 minute. Electroblotting was carried out either overnight at 20V or at 100V for 1 hour in transfer buffer (25 mM Tris-HCl, 192 mM glycine, 20% methanol) with Mini-PROTEAN® wet-transfer system (Bio-Rad, UK). Following electroblotting, the PVDF membrane was incubated in blocking buffer (5% skimmed milk powder in PBS-T (0.2% Tween20 in PBS)) for 1 hour at room temperature on a rocking platform. The membrane was then incubated with 1 ml blocking buffer with primary antibody in 1:1000 dilution (ABCB1 primary antibody C219 (Cambridge Bioscience, UK), ABCC1 primary antibody QCRL1 (Alexis, UK), ABCC3 primary antibody C-18 (Santa Cruz, UK)) inside a heat-sealed bag overnight at 4°C on a rocking platform. The membrane was given three 10 minutes washes with PBS-T before incubation with anti-mouse (to detect ABCB1 and ABCC1 primary antibody) or anti-goat (to detect ABCC3 primary antibody) secondary antibody (Dako UK Ltd, UK), conjugated to horseradish peroxidase (HRP). The secondary antibodies were also diluted 1:1000 in 1 ml blocking buffer and the membrane was incubated with a secondary antibody in a heat-sealed bag for 1 hour at room temperature on a rocking platform. The membrane was given three 10 minutes washes in PBS-T before visualisation of the protein-bound HRP by enhanced chemiluminescence (ECL), as directed by the manufacturer (GE Healthcare, UK), together with Amersham Hyperfilm ECL (GE Healthcare, UK).

2.15. Flow cytometry

ABCB1 transport ligand Rhodamine123 was purchased from Sigma, BODIPY® FL-taxol, BODIPY® FL-verapamil and BODIPY® FL-vinblastine were purchased from Invitrogen. Each ABCB1 mutant and wild-type ABCB1 was assessed for function using end point drug accumulation assay. HEK293T cells expressing ABCB1 were incubated with BODIPY® FL-verapamil (0.8 µM; Invitrogen, UK), BODIPY® FL-taxol and BODIPY® FL-vinblastine (0.4 µM; Invitrogen, UK) or Rhodamine123 (5 µM; Sigma-Aldrich, UK) in DMEM/F12 (Invitrogen, UK) supplemented with 1% FBS for 30 minutes at 37°C before analysing with a FACScan or BD LSR II flow cytometer (Becton Dickinson, NJ, USA). BODIPY® FL conjugated to verapamil, vinblastine and taxol has an excitation and emission wavelength of 503 and 512 nm, respectively. Rhodamine123 excitation and emission wavelengths are 511 and 534 nm, respectively. The cells were gated for normal size and granularity from forward scatter (FSC), side scatter (SSC) channels. Data was collected for 50,000 normal cells. Drug accumulation was measured by using FL-1 (green, 515-545 nm) channel and antibody binding was assessed from FL-2 (red, 543-627 nm) channel. Flow cytometry data were acquired using CellQuest Pro Software (BD Biosciences, San Jose, CA) and analysed using FlowJo (Tree Star, OR, USA). As each population of transfected cells contain both transfected (ABCB1-expressing) and untransfected (ABCB1-negative) cells, and each subpopulation could be clearly distinguished on the basis of 4E3 (ABCB1 primary antibody, 1 µg of 4E3 antibody at 250 µg/ ml concentration was added to saturate all ABCB1 on $1x10^6$ cells; AbD Serotec, UK) and R-Phycoerythrin conjugated antibody (5 µg of polyclonal goat anti-mouse immunoglobulin at a concentration of 1 mg/ ml was used to saturate all 4E3 primary antibody, Dako UK Ltd, UK) binding, the untransfected subpopulation could be

used as an internal control for measuring drug accumulation. The optimal concentration of antibody, which was titrated by Dr. Zolnerciks, was important to label all the ABCB1 on the cell surface [157]. ABCB1 transport activity was therefore assessed as the fold difference in drug accumulation between the ABCB1 expressing and non-expressing cell populations within each population of transfected cells. UIC2-PE (Immunotech, Beckman Coulter, CZ, USA) binding was carried out due to the manufacturer's instructions; saturating amounts of UIC2-PE (25 µl from a concentration of 15 µg/ ml for $1x10^6$ cells) was added to double-Q-loop mutant and wild-type ABCB1 expressing cells to reveal their ligand binding state. The samples were incubated with the antibodies for 30 minutes at 4°C. At least three experiments were carried out for each mutant and different condition and statistical analyses were carried out using GraphPad PRISM® V5.0 software (Graphpad Software, CA, USA). Student's two-tailed t-test was used to analyse differences between means, whereas differences among means were analysed using one-way ANOVA followed by pairwise Student-Newman-Keuls post hoc testing. ABCC1 and ABCC3 calcein-AM (0.5 µM; Invitrogen, UK) transport data were acquired in a similar way, except no antibody was used for these experiments so only the FL-1 (green) channel was used.

2.16. Microscopy

For detection of ABCB1, primary antibody (4E3, AbD Serotec, UK) was directly conjugated to Alexa633 dye using the Mix-n-Stain (Biotium, CA, USA) according to the manufacturer's instructions (conjugation was carried out by Dr. Snippe, Linton lab, personal communication). Transfected HEK293T cells were split, 24 hours post-transfection, onto 8-well glass-chamber slides (Lab-Tek, Thermo Fisher Scientific, MA, USA). 48hrs post-transfection, the live cells were washed 3 times in DMEM/F12 medium (Invitrogen, UK) then incubated with the Alexa633-conjugated 4E3 antibody (1/100 dilution in DMEM/F12 medium) plus BODIPY®FL-verapamil (0.8 µM) or BODIPY®FL-vinblastine (0.4 µM) for 30 min at 37°C, 5% CO_2. The cells were washed a further 3 times, then imaged using a Zeiss LSM510 inverted confocal laser scanning microscope. Images were obtained using a plan-apochromat 63x oil objective with a numerical aperture of 1.4. For excitation of BODIPY® FL, the Argon laser (488 nm laser line) was used at a current of 6.1 Amp; for Alexa633 the HeNe laser (633 nm) was used. Emission was detected using the HFT UV/488/543/633 main dichroic beam splitter in combination with a band pass filter (BP 505-530) for BODIPY® FL or a NFT 545 secondary beam splitter and a long pass filter (LP650) for Alexa633. The pinhole was set at approximately 1 airy unit (AU). Operating in multitrack mode allowed for crosstalk-free imaging of the two dyes.

2.17. Transport of ^{3}H-Estradiol 17-β-D-glucuronide and ^{3}H-Lysophosphatidylinositol (LPI)

Tritium (^{3}H) labelled transport experiments were carried out in the radioactivity suite of the Blizard Institute (Barts and the London School of Medicine and Dentistry, UK). Membrane vesicles containing 60 µg of total protein prepared from HEK293T cells were incubated in a reaction mixture of 150 µl containing 10 mM ATP (Sigma-Aldrich, UK), 10 mM $MgCl_2$ (Sigma-Aldrich, UK), 100 µg/ml creatine kinase (Roche, UK), 10 µM creatine phosphate (Roche, UK), 400 nM estradiol 17-β-D-glucuronide (Sigma-Aldrich, UK) with 40 nCi ^{3}H-estradiol 17-β-D-glucuronide (Perkin Elmer, MA, USA) or lysophosphatidylinositol (cold-LPI amount depends on the quantity of cold-LPI already exists in the ^{3}H-LPI sample; Sigma-Aldrich, UK) with 0.5 nCi ^{3}H-lysophosphatidylinositol (Prof. Falasca, personal communication) including or excluding 100 µM vanadate (Sigma-Aldrich, UK) or 100 µM glutathione (Sigma-Aldrich, UK). The vesicles were incubated at 37°C for 15 minutes. The reaction was stopped by adding 1 ml of ice-cold transport buffer (50mM Tris-HCl, 250 mM sucrose, pH 7.5) and immediately filtered through cellulose nitrate filter discs (0.2µm pore size, 25mm diameter Whatman; Fisher, UK) using a 1225 Sampling Manifold (Millipore, UK) and washed 4 times with 3 ml of ice-cold transport buffer. The cellulose nitrate filter discs were recovered and placed into scintillation tubes with 5 ml of scintillation fluid Optiphase HiSafe 3 (Perkin Elmer, MA, USA).The radioactivity content of each sample was analysed in a Beckman LS 6000SC scintillation counter (Beckman Coulter, UK). Each experiment was performed in triplicates and at least three independent experiments were carried out.

Statistical analyses were performed by one-way ANOVA (analysis of variance) using GraphPad PRISM® V5.0 software (Graphpad Software, CA, USA).

2.18. Nedd4-1 ubiquitination

Nedd4-1 ubiquitination of purified ABCB1 was carried out by Dr. Sullivan. Briefly, ABCB1 (20 µg in 50 µl final volume of reaction solution) was mixed with 5 µg of methylated ubiquitin, 100 ng of ubiquitin-activating enzyme (E1, Boston Bichem, MA, USA), 100 ng of ubiquitin-conjugating enzyme (E2) and 20 µl of Nedd4-1 (the ubiquitin ligase (E3)) at a concentration of 500 ng/ µl in a reaction solution of 50 mM Tris pH 7.4, 10 mM ATP, 10 mM $MgCl_2$ and incubated at 37°C for 2 hours. As a control, methylated ubiquitin was not added to the reaction mixture of one ABCB1 sample. After two hours, the reaction was stopped by adding 50 µl of SDS sample buffer (4 gr SDS, 20 ml glycerol, 50 ml Buffer A (Tris 30.24 gr, SDS 2 gr, pH 6.8 in 1000 ml in dH_2O), 5 ml β-mercaptoethanol, 0.05%bromophenol blue (w/v) complemented to a total volume of 100 ml with dH_2O) and the samples were loaded onto 8% Precise™ tris- glycine gel (Thermo Fisher Scientific, UK). Electrophoresis was performed using a Mini-PROTEAN® Electrophoresis System (Bio-Rad, UK). Colloidal blue staining was performed as described in section 2.14.6.

2.19. Mass Spectrometry

Following electrophoresis and staining of purified wild-type ABCB1 after Nedd4-1 treatment with and without methylated ubiquitin, the protein was excised and placed in sealed 1.5 ml eppendorf tubes (Eppendorf, UK) and sent to the mass spectrometry analysis facility (Birmingham Science City Translational Medicine: Experimental Medicine Network of Excellence project, with support from Advantage West Midlands). Mass spectrometry was couriered by a Thermo Fisher Scientific LTQ Orbitrap Velos ETD mass spectrometer. Following excision from the tris-glycine gel, the protein was digested using trypsin, yielding peptide fragments of known size. The tryptic fragments were dissolved in 0.1% formic acid and injected onto the reverse-phase liquid chromatography (RPLC). Subsequently, Dionex Ultimate 3000 with a NCS pump (Thermo Fisher Scientific, Germany) is used to provide a 30 minutes linear gradient from 3.2% to 44% mobile phase B (acetonitrile (JT Baker, UK) with 0.1% formic acid (Sigma Aldrich, UK)) and a nanoflow of 350 nL/min. The spray voltage of 1.7 kV is applied to the triversa nanomate and the sample is dispersed into highly charged droplets. The transfer line temperature is 250°C and 0.3 psi nitrogen is used. This gas helps to direct the sample ions to the mass spectrometer. The nano-charged droplets diminish in size by solvent evaporation and at this point the ions are transferred to the gas phase and introduced to the mass spectrometer under high vacuum for analysis. Then the results were analysed with SearchGUI [161] and peptide-shaker [161, 162] programmes.

Chapter Three

3. Molecular Communication Pathways Between ABCB1 Domains

3.1. Introduction

The latest biochemical and pharmacological evidence suggests that ABCB1 has two ligand binding cavities and that they can be separated by mutagenesis [163]. Parveen *et al.* (2011) identified two glutamine residues (Q132 and Q773) in symmetric positions in TMH 2 and 8, respectively, which gate entry into the two ligand binding cavities (Figure 3.1). They hypothesized that mutating these glutamines into the positively charged arginines should repel positively-charged ligands and block entry into that cavity. As controls they replaced the glutamines with neutral alanine residues. They then determined the first order rate constants for efflux of fluorescent drugs in wild-type and mutant ABCB1s by flow cytometry. In the mutant with both residues replaced by arginine, Rhodamine123 efflux activity was absent but when the residues were substituted with alanine the transport activity was similar to the wild-type level, confirming their hypothesis. The single arginine mutations of Q132 and Q773 behaved differently, and Rhodamine123 transport was more affected by the Q773R mutation. They also measured IC50 values of propafenone analogs and also verapamil and vinblastine for inhibition of Rhodamine123 export. The IC50s of the three inhibitors were lower in the Q773R mutant than in the Q132R mutant suggesting that these drugs have a higher affinity for the Q132-lined cavity (i.e. the wild-type cavity of the Q773R mutant). As a result, they concluded that different drugs bind to symmetrical but divergent binding cavities within the TMDs of ABCB1 with different affinities [163].

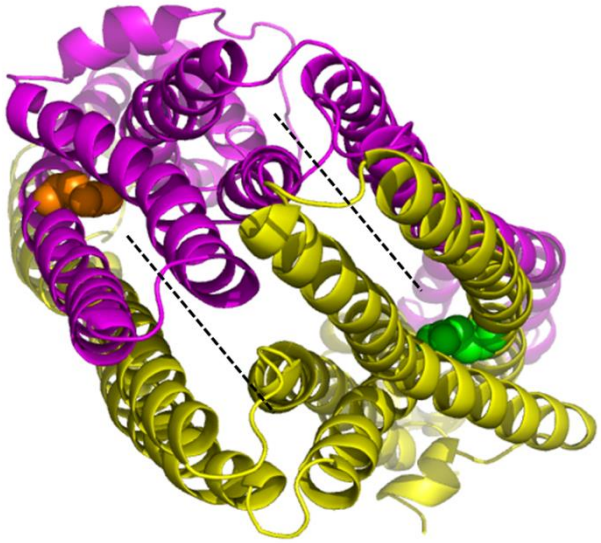

Figure 3.1: Human ABCB1 homologue mouse Abcb1a (pdb ID 3G60). Pharmacological labeling and modeling studies suggest the presence of two ligand binding cavities. This is a top down view of the membrane spanning helices showing, the prospective ligand binding cavities (dashed black lines) and the conserved glutamines (Q132 and Q773) that gate entry into the cavities which when mutated to arginine inhibit binding to the adjacent cavity by electrostatic repulsion [163]. TMD1, yellow; TMD2, purple.

The Q-loop glutamines of the NBDs have attracted attention as residues localized very near to the attacking water molecule required for ATP hydrolysis and also as highly conserved residues between ABC proteins (see discussion). A study of Q-loop mutants in which mouse Abcb1a (mouse homologue of ABCB1) was expressed in yeast *P. pastoris*, purified and reconstituted into proteoliposomes, suggested that the single mutants lost nearly all (between 90-98%) of their drug (verapamil, vinblastine and tetraphenylphosphonium)-stimulated ATPase activity and that alanine mutations were more affected than glutamate mutations [164]. In the study by Urbatsch *et al.*, cells expressing wild-type or mutant Abcb1a were disrupted with glass beads to make membranes and then solubilised using n-dodecyl β-D-maltoside (DDM). To purify the expressed proteins, Ni-affinity chromatography and Diethylaminoethyl (DEAE)-cellulose ion exchange chromatography were performed

and the purified protein was concentrated by pressure filtration. To reconstitute the activity, Abcb1a was incubated with 8 mM DTT and 1% (w/v) *Escherichia coli* lipids with a final ratio of 100/1 of lipid/protein and ATPase activity was measured by the method of Van Veldhoven and Mannaerts [165].

Dr. Zolnerciks (Linton lab, unpublished data), recently demonstrated that the purified Q-loop single mutants (Q475A, Q1118A) of human ABCB1 behave similarly to the mouse mutants and retain only 8-9% of drug-stimulated ATPase activity *in vitro* (Figure 3.2) The experimental design of this study involved human ABCB1 expression in insect cells, solubilisation of insect cell membranes by DDM and Ni-affinity chromatography for purification. The Chifflet method was used to measure the ATPase activity of purified and reconstituted wild-type or mutant ABCB1[166]. However, these data did not correlate with studies of ATP turnover in live cells. Verapamil-stimulated ATP turnover in live HEK293T cells expressing wild-type or mutant ABCB1 was determined using extracellular acidification rate (ECAR) measurements (Figure 3.3) [167] and compared to mock-transfected cells. The single Q-loop mutants appeared to retain 35-50% of wild-type ABCB1 drug-stimulated ATPase activity (Figure 3.4). ECAR data was applied to a kinetic model based upon a modified Michaelis-Menten equation; $V_s = \frac{K_1K_2V_0 + K_2V_1C_s + V_2C_s^{\,2}}{K_1K_2 + K_2C_s + C_s^{\,2}}$ (Cs; ECAR as a function of the drug concentration, V0; basal ECAR in the absence of drug, V1; maximum ECAR assuming only activation, V2; activity at infinite drug concentration, K1; drug concentration giving half-maximum activation, K2; drug concentration giving half-maximum reduction) in which verapamil stimulates the ATPase activity at low concentrations and inhibits at high concentrations [168]. The double Q-loop mutant (Q475A/Q1118A) showed no activity in either the *in vitro* or cellular ATPase measurements (data not shown).

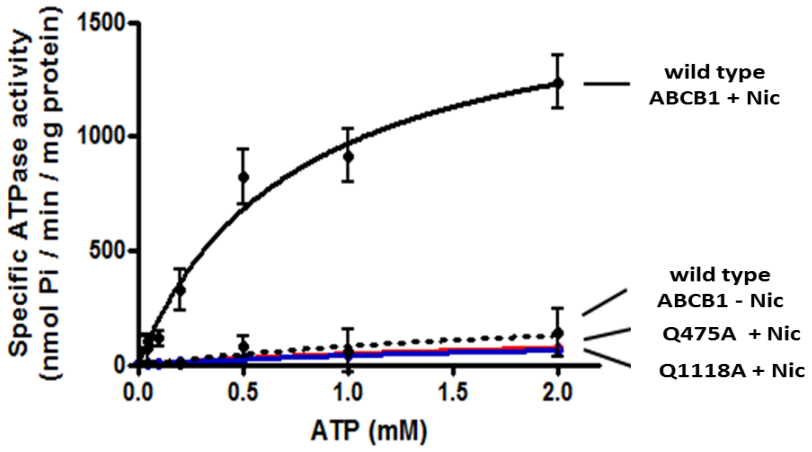

Figure 3.2: ***In vitro*** **ATPase activity of wild-type and single Q-loop mutants. Measurement of nicardipine-stimulated ATPase activity using purified NBD1-Q475A and NBD2-Q1118A mutant ABCB1 upon reconstitution into proteoliposomes reveals over 90% loss of nicardipine-stimulated activity (Vmax = 160 nmol Pi/min/mg and 140 nmol Pi/min/mg, respectively, versus 1.7 µmol Pi/min/mg for wild-type ABCB1). (Dr. Zolnerciks, personal communication)**

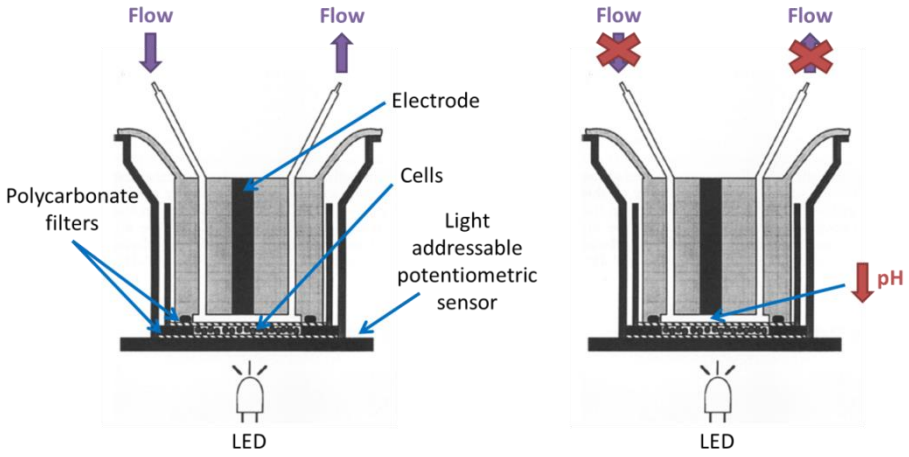

Figure 3.3: Measuring ECAR in live cells using a cytosensor microphysiometer [169]. Left panel shows HEK293T cells sandwiched between polycarbonate filters in a flow chamber. Unbuffered medium (± drug) is allowed to flow over cells. Right panel shows that when the flow of medium through chamber is stopped, a reduction in pH is measured due to excretion of acidic metabolites. The rate of pH change is dependent on cellular metabolism (ATP turnover).

A.

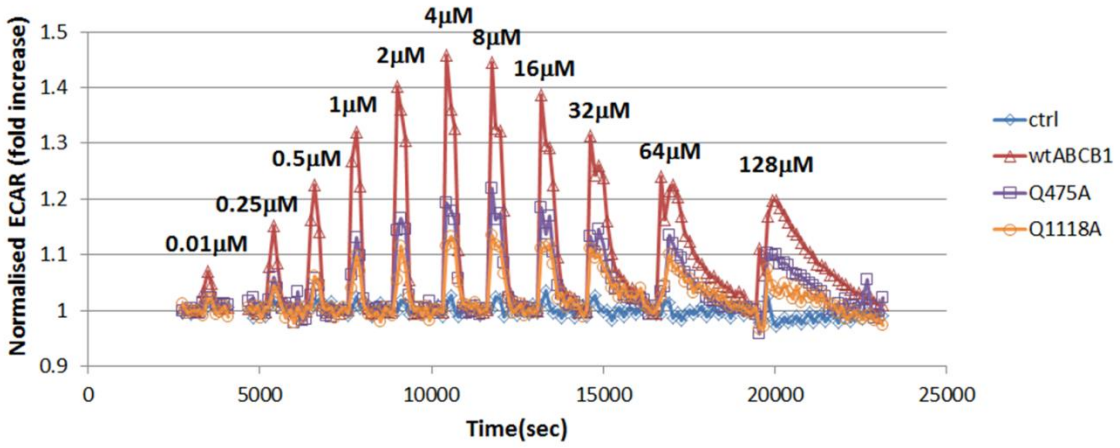

B.

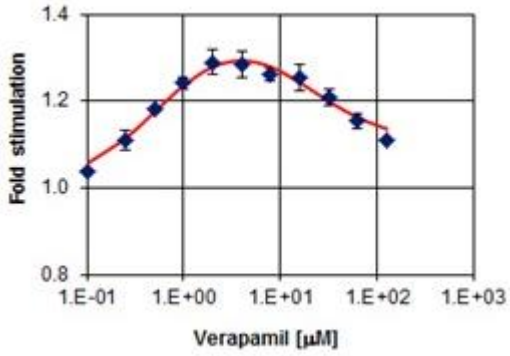

C.

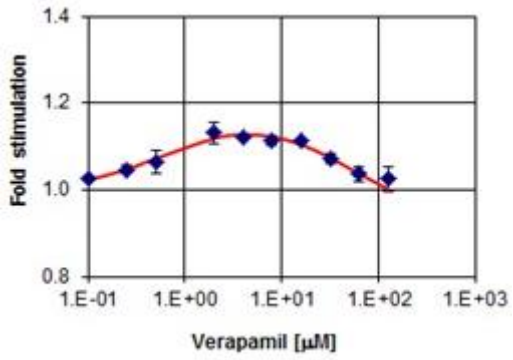

D.

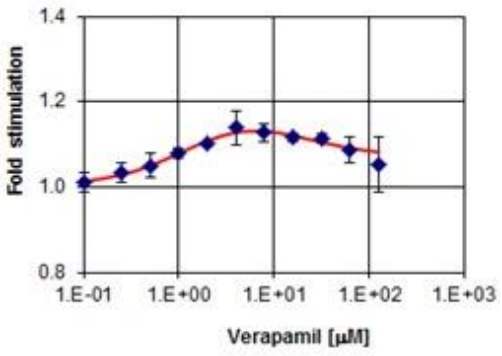

E.

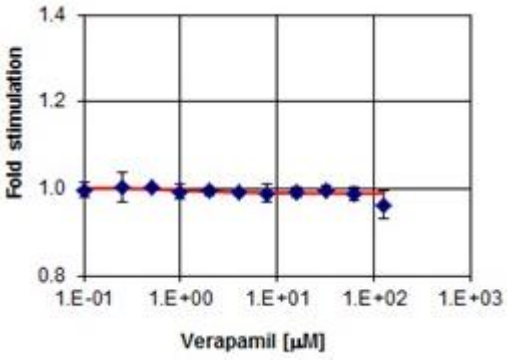

Figure 3.4: Verapamil-stimulated ATPase activity measurements of wild-type and mutant ABCB1 in live HEK293T cells. Verapamil-stimulated ATP turnover in live HEK293T cells expressing ABCB1 was determined using extracellular acidification rate (ECAR) measurements [167] and compared to mock transfected cells. (A) When examined in live cells, NBD1-Q475A and NBD2-Q1118A mutant ABCB1 exhibited 50% and 35% maximal verapamil-stimulated ATPase activity, respectively. Plots are shown as a function of time, with increasing verapamil concentration indicated above each experimental peak. (B-E)

Representative plots from a single experiment, performed in duplicate with error bars indicating standard deviation, are shown using cells expressing (B) wild-type, (C) NBD1-Q475A, (D) NBD2-Q1118A, and (E) Q475A/Q1118A ABCB1. The ATPase activity of single Q-loop mutants suggest that the loss of activity seen using purified protein (Figure 3.2) results from inactivation of the Q-loop mutants during the purification process. (Dr. Zolnerciks, personal communication)

ABCB1 modelling studies suggest the importance of the Q-loops in the communication cascades between the ATP catalytic domains and the ligand binding domains, and also between the two subdomains of the NBDs [75, 76]. The Q-loops sit at the base of the grooves occupied by the second intracellular loops of each TMD and because the double Q-loop mutant has no activity (drug transport or ATPase activity), it is hypothesized that the ligand binding cavities communicate with the NBDs through their Q-loops to influence the ATP binding and/or catalysis. The studies of Dr. Zolnerciks demonstrated that single Q-loop mutations are not inactive as suggested previously and that they may be capable of ligand transport.

3.2. Aims

- To test the drug transport functionality of the single Q-loop mutants.
- To investigate the coupling between the ligand binding cavities and the ATP catalytic sites.

3.3. Results

3.3.1. Generation, Combination and Expression of Gating Mutants with Q-loop Mutants

The codons for the ligand binding cavity mutations Q132R (NBD1) and Q773R (NBD2) were introduced into the cDNAs encoding the ABCB1 Q-loop mutant Q475A (NBD1) and Q1118A (NBD2) to investigate possible signal transduction pathways and determine the effect on transport activity. The introduced mutants are shown in Table 3.1, some of which contain introduced restriction endonuclease sites to allow screening by agarose gel electrophoresis. The sequencing data for a selected mutant is shown in Figure 3.5. The integrity of the whole wild-type and mutant ABCB1 coding regions were verified by careful inspection of the electropherograms.

	Mutation	Sequence
Ligand Binding Cavity Mutants	Q132A	5'-GGTTGCTGCTTACATCgcgGTTTCATTTTGGTGC-3'
	Wild-type	5'-GGTTGCTGCTTACATCCAGGTTTCATTTTGGTGC-3'
	Q132R	5'-GGTTGCTGCTTACATCcgaGTTTCATTTTGGTGC-3'
	Wild-type	5'-GGTTGCTGCTTACATCCAGGTTTCATTTTGGTGC-3'
	Q773A	5'-GGAATTATTTCTTTTATTACATTTTTCCTTgcgGGTTTCACATTTGGCAAAGCTGG-3'
	Wild-type	5'-GGAATTATTTCTTTTATTACATTTTTCCTTCAGGGTTTCACATTTGGCAAAGCTGG-3'
	Q773R	5'-GGAATTATTTCTTTTATTACATTTTTCCTTcgaGGTTTCACATTTGGCAAAGCTGG-3'
	Wild-type	5'-GGAATTATTTCTTTTATTACATTTTTCCTTCAGGGTTTCACATTTGGCAAAGCTGG-3'
Q-loop mutants	Q475A	5'-GGGAAATCATTGGTGTGGTGAGTgctGAGCCTGTATTGTTTGCCACCACG-3'
	Wild-type	5'-GGGAAATCATTGGTGTGGTGAGTCAGGAACCTGTATTGTTTGCCACCACG-3'
	Q1118A	5'-GGGCATCGTGTCCgcgGAGCCCATCCTGTTTG-3'
	Wild-type	5'-GGGCATCGTGTCCCAGGAGCCCATCCTGTTTG-3'
Walker B mutants	E556Q	5'-CCCCAAGATCCTCCTGCTTGATcagGCCACGTCAGCCTTGG-3'
	Wild-type	5'-CCCCAAGATCCTCCTGCTGGATGAGGCCACGTCAGCCTTGG-3'
	E1201Q	5'-CAGCCTCATATTTTGCTTCTTGATcagGCCACGTCAGCTCTGGATAC-3'
	Wild-type	5'-CAGCCTCATATTTTGCTTTTGGATGAAGCCACGTCAGCTCTGGATAC-3'

Table 3.1: The mutagenic oligonucleotides designed to introduce mutations of interest (Dr. Zolnerciks, personal communication). The mutations of Q-loop or ligand binding cavity residues were introduced into wild-type human ABCB1 cDNA and combined mutations were obtained by introducing ligand binding cavity mutations into the relevant Q-loop mutant cDNAs. The Walker B mutants were engineered for use as negative controls in each experiment performed. The silent nucleotide changes to introduce restriction endonuclease sites are underlined.

A.

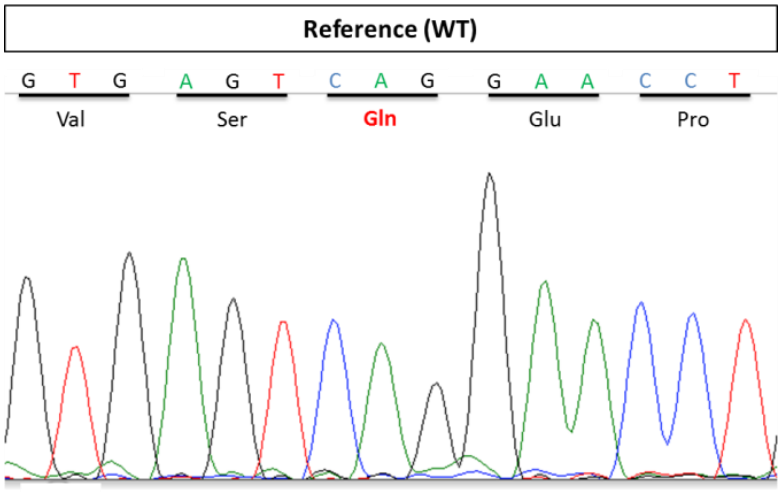

B.

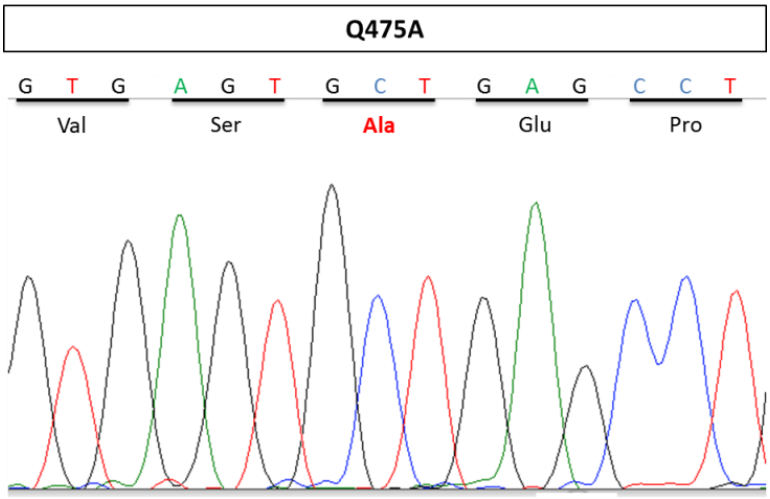

Figure 3.5: Electropherogram of DNA sequencing of wild-type ABCB1 (A) and the putative Q475A mutant (B). Glutamine (CAG) at position 475 in the amino acid sequence of wild-type ABCB1 has been replaced with alanine (GCT) following successful mutagenesis.

3.3.2. The Mammalian Expression Vector, pCI-neo

To express the wild-type and mutant ABCB1, a high throughput transient transfection system was chosen. The cDNA coding sequence for wild-type ABCB1 was previously introduced into the pCI-neo vector to generate the plasmid pABCB1-12His [157]. This vector was used to produce functional ABCB1 (with a twelve histidine tag at the carboxy terminus) in mammalian cells and was also used as a template for mutagenesis of the ABCB1 cDNA and expression of mutant ABCB1. The pCI-neo vector is bi-functional and contains an origin of replication and encodes β-lactamase to amplify the plasmid and confer ampicillin resistance in bacterial cells, respectively. The human cytomegalovirus (CMV) immediate-early enhancer/promoter ensures constitutive expression of the ABCB1 cDNA in mammalian cells. In addition, a chimeric intron is located downstream of the CMV enhancer/promoter. Studies have shown that the presence of such intronic sequences flanking a target gene can increase expression levels [170, 171]. The pCI-neo vector also contains an SV40 late polyadenylation signal downstream of the multiple cloning region. This feature is thought to enhance RNA stability and increase levels of translation [172, 173]. The plasmid also encodes a neomycin resistance gene for neomycin phosphotransferase which can be used to select stably-transfected cell lines, but was not used in this study (Figure 3.6).

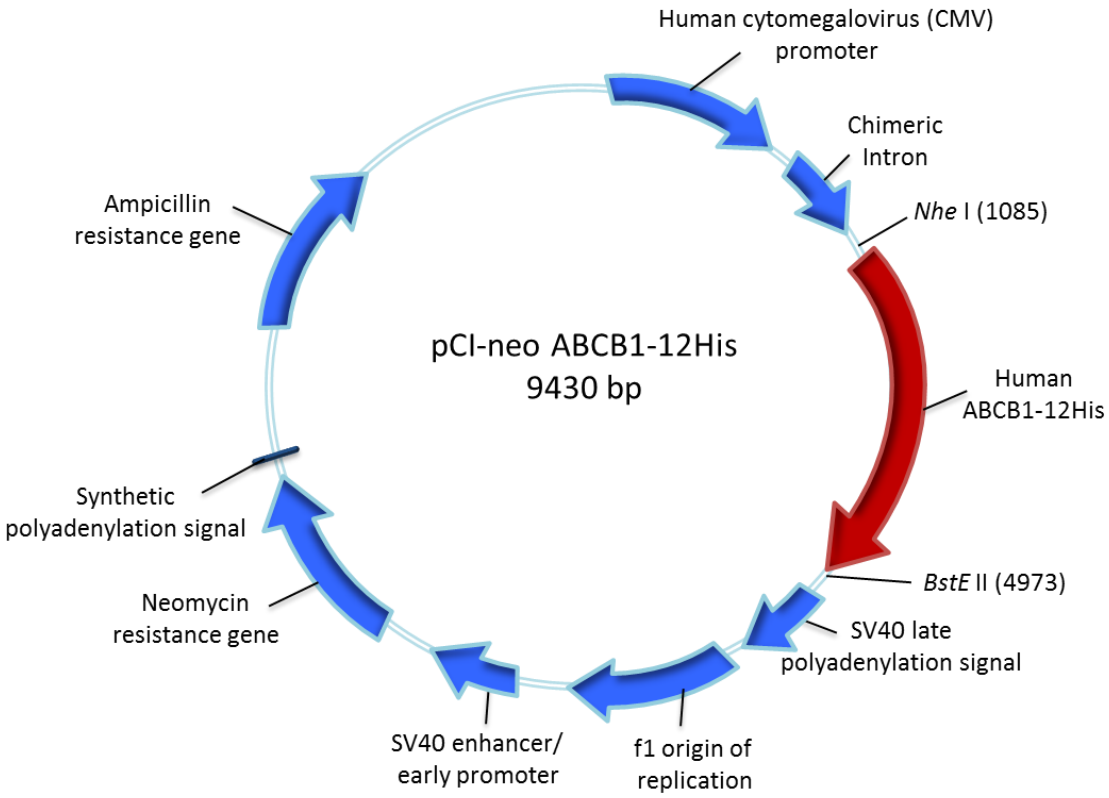

Figure 3.6: pABCB1-12His vector based on pCI-neo from Promega.

3.3.3. Polyethylenimine Transfection and Expression of ABCB1 In a Mammalian Cell Line

The branched polycation PEI was first identified as a transfection agent by Boussif and co-workers [174]. It generates a very high efficiency of transfection, considered to arise from the ability of DNA/PEI complexes within endosomes to avoid the degradative lysosomal pathway [175]. As a quick and inexpensive reagent, PEI was chosen as a suitable transfection reagent to introduce wild-type and mutant pABCB1-12His into cells. The human embryonic kidney (HEK293T) cell line was chosen to express human ABCB1. HEK293T cells do not endogenously express ABCB1 and stably express the SV40 large T antigen, allowing maximal expression from the pCI-neo vector.

3.3.4. Flow Cytometric Analysis

Flow cytometry uses a fluidics system which contains a central narrowing channel through which the cells pass. This channel is surrounded by an outer sheath that contains faster flowing fluid which forces cells within the narrowing channel into a capillary with single-line flow by hydrodynamic focusing. To identify an epitope of interest, different varieties of fluorochrome-conjugated antibodies can be used. Fluorochromes can also be covalently attached to drugs to measure their uptake by cells. Fluorochromes are essentially dyes which accept light energy at a given wave length and re-emit it with a longer wavelength but lower energy state.

3.3.5. Gating the Cells of Normal Size and Granularity

The experimental model requires the transiently-transfected cells to be viable to show the active export of the transport ligands by ABCB1. In this transport assay the cells were harvested, labelled with antibody to measure the abundance of ABCB1 on the cell surface, and incubated with the transport ligand. During this process some cells might die and these cells are excluded from the experimental measurements by gating only on cells with normal size and granularity using the forward and side scatter channels. This helps to differentiate live cells from dead or unhealthy, dying cells without affecting the experimental design and the transport activity of ABCB1. Figure 3.7 shows the gating process used.

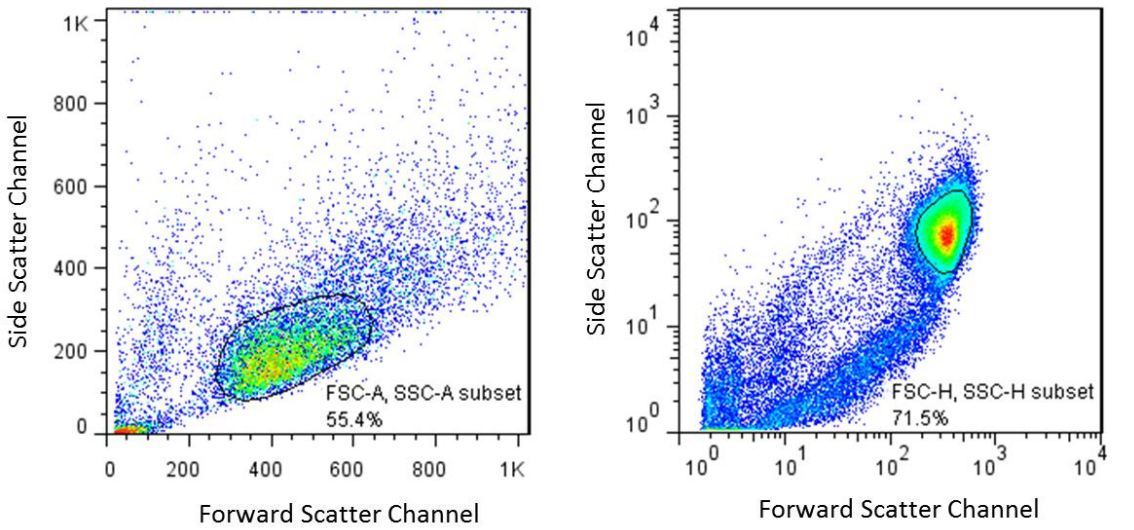

Figure 3.7: Gating viable cells in BD LSR II (left panel) and FACScan (right panel).

3.3.6. Gating the Cells of Interest That Express Equal Levels of ABCB1 on Cell Surface

PEI generates a very high efficiency of transfection of HEK293T cells (see section 3.3.3.), however there is always a population of untransfected cells. To measure the transport activity of cells expressing wild-type or mutant ABCB1, the untransfected cells are differentiated from the transfected population using R-phycoerythrin (R-PE) conjugated to an anti-ABCB1 antibody (4E3; FL-2 channel; Figure 3.8). Conditions were previously determined to ensure that the antibodies were in saturating quantities such that the higher level of the antibody bound to the cell surface, the higher the level of ABCB1 is expressed. Transient expression of wild-type or mutant ABCB1 results in a heterogeneous population of cells with potentially varying levels of surface expression, and the introduction of mutations in membrane proteins may affect the folding and trafficking of the protein.

As the expression levels of wild-type or mutant ABCB1 can affect end-point ligand accumulation within the cells, it is important to measure the expression levels. Saturating concentrations of primary (4E3) and secondary antibodies were titrated by Dr. Zolnerciks previously [157]. The mutants studied in this chapter have similar levels of surface protein expression, but the experiment is designed to allow gating on cell populations expressing equivalent levels of ABCB1 even in cases where the mean expression levels varied (so long as there is overlap in the level of expression). This is achieved by selecting level of expression in the antibody binding channel that is common to all the mutants and controls in the experiment (Figure 3.8). The primary mouse monoclonal antibody 4E3, which recognises an extracellular epitope of ABCB1, does not interfere with ABCB1 function [176]. When incubated with green fluorescent drug, cells that express wild-type ABCB1, fluoresce less in the FL-1 channel (all of the ABCB1 transport ligands used, emit fluorescence in FL-1 channel) because the transport ligands are pumped out of the cells by ABCB1.

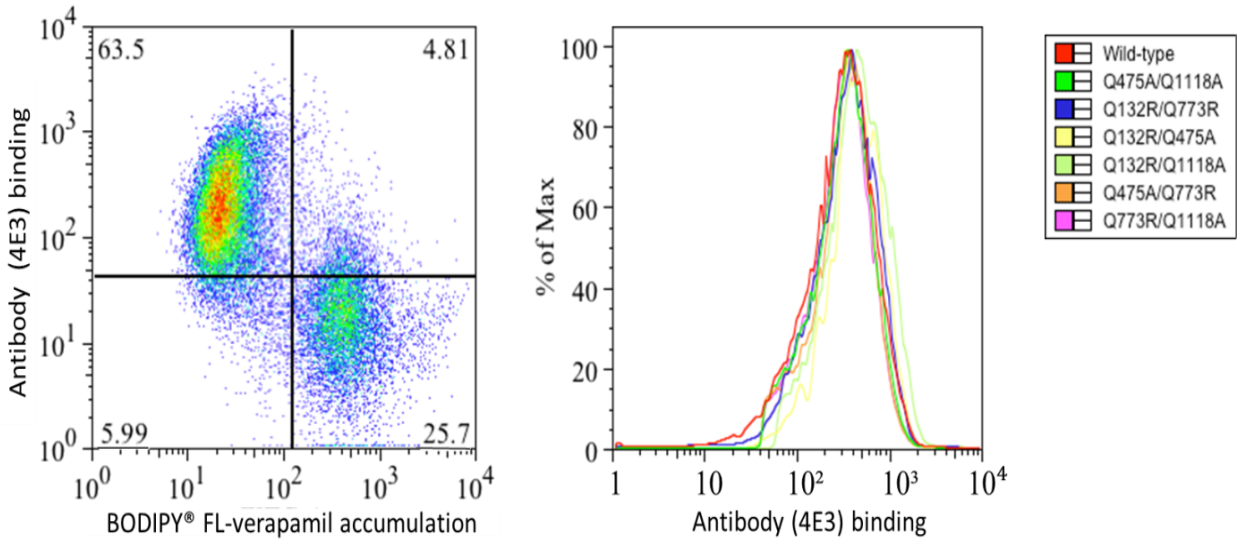

Figure 3.8: Differentiating between transfected and untransfected cells. The left panel dotplot in which each dot represents an individual cell, shows the two populations in the antibody binding (FL-2) and BODIPY® FL-verapamil accumulation (FL-1) channels. The antibody bound population in the upper left quadrant accumulated less drug, a characteristic of cells expressing wild-type ABCB1. The second population in the lower right quadrant is the untransfected population. The histogram on the right shows the antibody binding channel (FL-2), wild-type and double mutant ABCB1 used in this study express similar levels of surface protein.

3.3.7. Single Q-loop mutants, Q475A and Q1118A are capable of BODIPY® FL-verapamil transport

The verapamil-stimulated ATPase activity measurements of single Q-loop mutants recorded in cells (Figure 3.4, Dr. Zolnerciks) suggested that these mutants might be capable of ligand transport and to test this hypothesis transport activity measurements of single Q-loop mutants were performed.

Verapamil is an L-type calcium channel blocker. It is a transport ligand of ABCB1 and higher concentrations of verapamil have also been used to inhibit ABCB1 function. BODIPY® FL-verapamil is the fluorescent form of this drug which is covalently bound to BODIPY® FL (Figure 3.9). Cells transfected with pABCB1-12His were incubated with 0.8 µM BODIPY® FL-

verapamil in each independent experiment. The transport efficiency of wild-type and mutant ABCB1 expressing cells was measured by flow cytometry in a two-colour experiment in which the ABCB1 expression level on the plasma membrane was measured in the FL-2 channel (R-PE conjugated 4E3 antibody) in parallel with the quantification of BODIPY® FL-verapamil accumulation (measured in the FL-1 channel).

The activity of wild-type and mutant ABCB1 was calculated by measuring mean values of BODIPY® FL-verapamil accumulation in the untransfected and transfected populations within the same sample and calculating the fold difference in BODIPY® FL-verapamil accumulation in these two populations. One-way ANOVA followed by pairwise Student-Newman-Keuls post hoc testing was used to measure the significance of the differences among means of BODIPY® FL-verapamil accumulation in wild-type and mutant ABCB1 expressing cells. The verapamil transport activity of the single Q-loop mutants was not significantly different to the wild-type protein but the double Q-loop mutant had no activity (Figure 3.10). Each experiment includes, as negative controls, the inactive single Walker B mutants, E556Q and E1201Q which are unable to hydrolyse ATP. The inactivity of the double Q-loop mutant implies that the Q-loops are important for function, but the activity of the single mutants demonstrates that there is redundancy in the molecular mechanism. Intriguingly, in all of the experiments Q475A/Q1118A showed an apparent increase in BODIPY® FL-verapamil accumulation with a fold difference compared to the untransfected cells of less than one (the reason for this is described in section 3.3.14.).

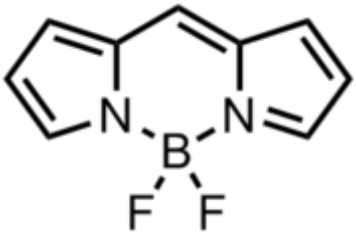

Figure 3.9: BODIPY (boron-dipyrromethene) structure.

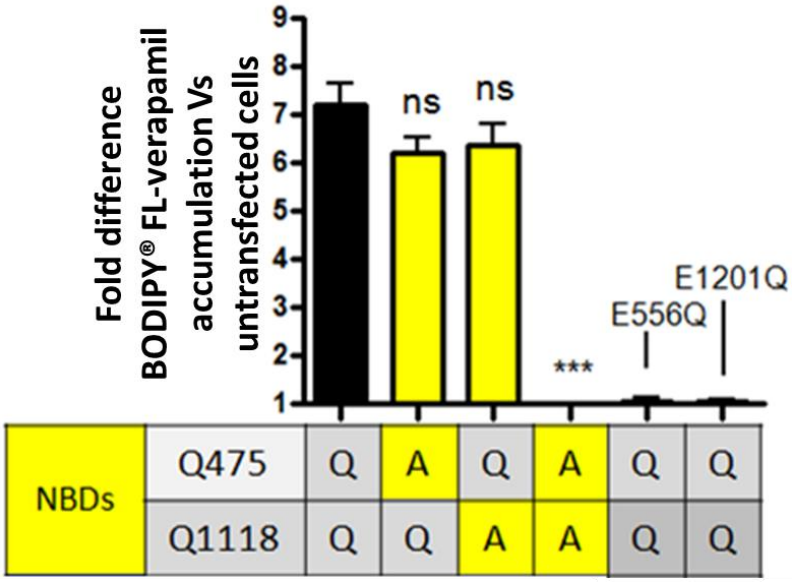

Figure 3.10: BODIPY® FL-verapamil transport activity of wild-type (black bar) and Q-loop mutant ABCB1. Flow cytometry data showing the fold reduction in BODIPY® FL-verapamil accumulation in wild-type and mutant ABCB1 expressing cells compared to untransfected cells. Single Q-loop mutants are fully active but the Q475A/Q1118A double mutant is significantly impaired. Inactive single Walker B mutants (E556Q and E1201Q) were included as negative controls. p values calculated with respect to wild-type activity; n≥4, *** p<0.001, ns p>0.05.

3.3.8. Single Ligand Binding Cavity Mutants are Functional whereas the Double Mutant has diminished BODIPY® FL-verapamil Transport Activity

The ligand binding cavity mutants previously described by Parveen *et al.* (see section 3.1.) were combined with the Q-loop mutants to reveal possible signal transduction pathways between the ligand binding cavities of the TMDs and the Q-loops of the NBDs. The ligand binding cavity Q132 and Q773 alanine mutants (Q132A, Q773A, Q132A/Q773A), introduced as controls, had no effect or very little effect on BODIPY® FL-verapamil transport activity, indicating that the wild-type glutamines are not critical for BODIPY® FL-verapamil transport (Figure 3.11). The Q132R mutant showed a decrease in BODIPY® FL-verapamil export while the Q773R mutant was not significantly different to the wild-type, indicating that BODIPY® FL-verapamil has a higher tendency to be effluxed from the Q132-lined ligand binding cavity (Figure 3.12). The transport activity of double Q132R/Q773R mutant was reduced by 50%. The remaining 50% transport activity might be indicative of a third binding site for BODIPY® FL-verapamil or, perhaps, the positive charge on the verapamil was partially masked by the BODIPY® FL moiety.

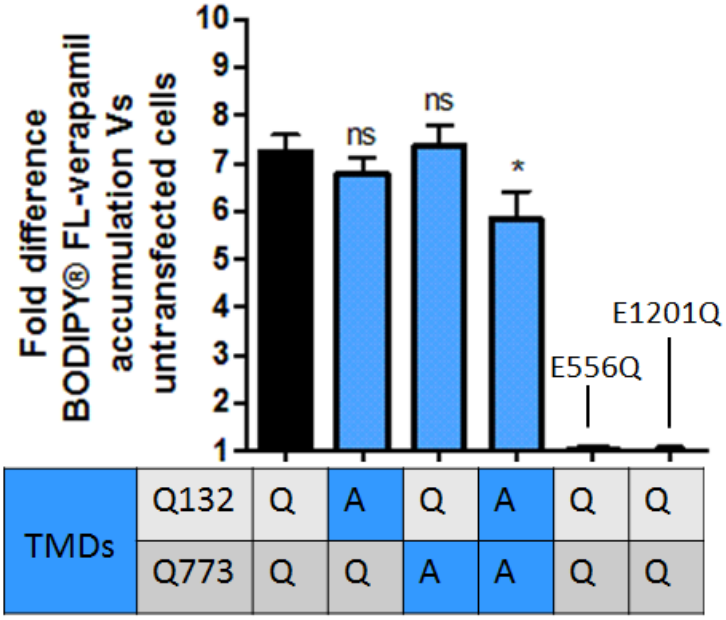

Figure 3.11: BODIPY® FL-verapamil transport activity of wild-type (black bar) and ligand binding cavity mutants (light blue bars). Flow cytometry data showing the fold reduction in BODIPY® FL-verapamil accumulation in cells expressing wild-type or ligand binding cavity mutant ABCB1 compared to untransfected cells. The activities of single Q132A or Q773A mutants are not significantly different to the wild-type protein and the Q132A/Q773A mutant has little impact on transport activity. Inactive single Walker B mutants (E556Q and E1201Q) were included as negative controls. p values calculated with respect to wild-type activity; n≥4, * p<0.05, ns p>0.05.

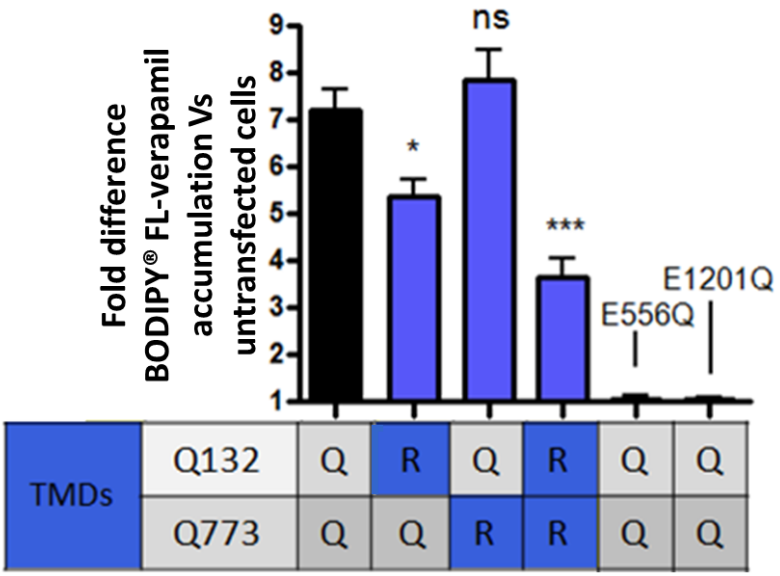

Figure 3.12: BODIPY® FL-verapamil transport activity of wild-type (black bar) and ligand binding cavity mutants of ABCB1. Flow cytometry data showing the fold reduction in BODIPY® FL-verapamil accumulation in wild-type and mutant ABCB1 expressing cells compared to untransfected cells. The Q773R mutant is fully active while the Q132R mutant has reduced activity similar to the previous report by Parveen *et al.* [163]. The double mutant has further diminished activity. Inactive single Walker B mutants (E556Q and E1201Q) were included as negative controls. p values calculated with respect to wild-type activity; n≥4, *** p<0.001, * p<0.05, ns p>0.05.

3.3.9. The Q773-lined Ligand Binding Cavity Communicates Primarily With the First NBD Q-loop To Efflux BODIPY® FL-verapamil

The combination of ligand binding cavity Q132R and Q773R mutants with the single Q-loop mutants indicated a signal transduction pathway between the NBDs and the TMDs for BODIPY® FL-verapamil transport. When the Q132 residue was mutated to arginine and combined with the first NBD Q-loop mutant, the transport activity of the double mutant was diminished by 65% whereas combination of Q132R with the second NBD Q-loop mutant had no effect on activity (Figure 3.13). This indicates that the wild-type Q773-lined cavity of these mutants communicates only via the first NBD Q-loop and not the second

NBD Q-loop during BODIPY® FL-verapamil transport. In contrast, the Q132-lined ligand binding cavity appears to require both Q-loops because both the Q475A/Q773R and Q773R/Q1118A mutants have greatly diminished activity and are not significantly different to each other.

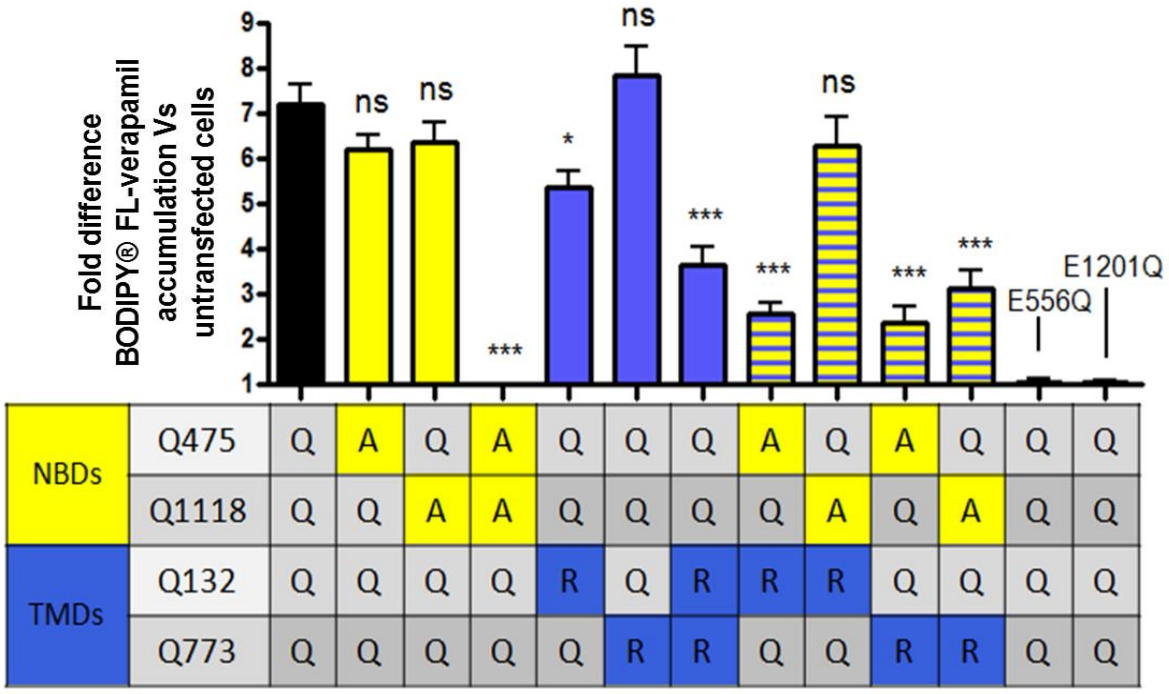

Figure 3.13: BODIPY® FL-verapamil Transport. Black bar, wild-type ABCB1; yellow bars, Q-loop mutants; blue bars, ligand binding cavity mutants; blue and yellow striated bars, Q-loop and ligand binding cavity combined mutants. p values calculated with respect to wild-type activity; n≥4, *** p<0.001, * p<0.05, ns p>0.05.

3.3.10. Does the transporter interact with different transport ligands in the same way?

Different classes of ABCB1 transport ligands were selected to test whether the signal transduction pathways differ for different transport ligands. To achieve this aim, two additional positively charged ligands were studied; Rhodamine123 and BODIPY® FL-vinblastine, and also the neutral BODIPY® FL-taxol (Table3.2).

Transport Ligands	MW	Role	Classification	Charge at pH 7.4
Rhodamine123	380.83	mitochondria tracer	Xanthene	66.4% positive
BODIPY® FL-verapamil	769.177	L-type Ca^{+2} channel blocker	Phenethylamine	99.5% positive
BODIPY® FL-vinblastine	1043.02	mitotic inhibitor (inhibitor of microtubule assembly)	Vinca Alkaloid	99.5% positive
BODIPY® FL-taxol	1024	mitotic inhibitor (microtubule stabilizer)	Taxoid	99.5% neutral

Table 3.2: Features of selected ABCB1 transport ligands. Charge at pH 7.4 was acquired with JChem and Marvin Software (ChemAxon, MA, USA).

3.3.11. Rhodamine123 Transport Is From the Q773-lined Cavity and Requires Both Q-loops

Rhodamine123 is a cationic dye normally used to label mitochondria in living cells and it is an ABCB1 transport ligand. In the Parveen *et al.* study which first described the Q132R and the Q773R mutants, Rhodamine123 was used as the ligand for real time efflux assays; they also measured apparent transport activity of other transport ligands by competitive inhibition of Rhodamine123 transport [163].

In the end point assay used herein, wild-type ABCB1 was able to reduce accumulation of Rhodamine123 by 15 fold compared to untransfected cells and the ligand binding cavity Q132 and Q773 alanine mutants (Q132A, Q773A, Q132A/Q773A), introduced as controls, had no effect on Rhodamine123 transport activity, indicating that the wild-type glutamines

have no direct involvement in Rhodamine123 transport, as demonstrated previously by Parveen *et al.*(Figure 3.14).

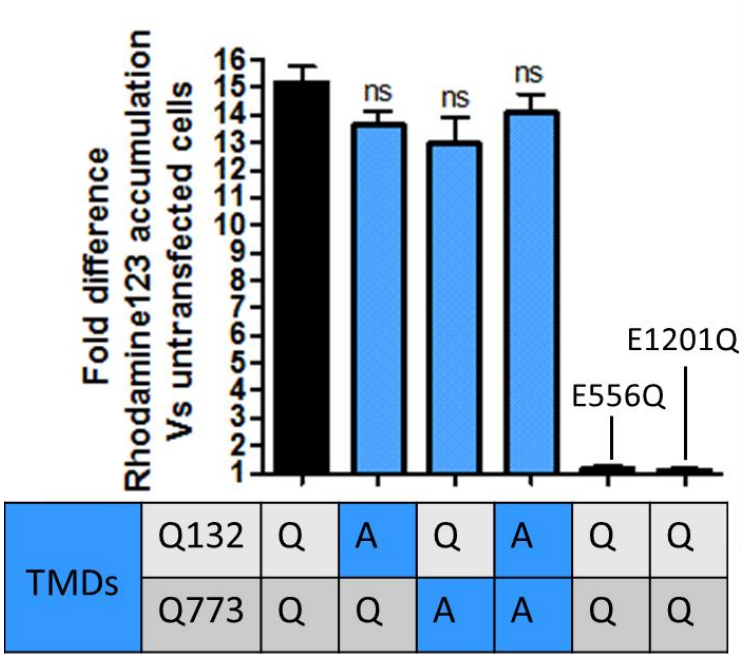

Figure 3.14: Rhodamine123 transport activity of wild-type (black bar) and ligand binding cavity mutants (light blue bars). Flow cytometry data showing the fold reduction in Rhodamine123 accumulation in cells expressing wild-type or ligand binding cavity mutants of ABCB1 compared to untransfected cells. The Q132A, Q773A or Q132A/Q773A mutants are not significantly different from the wild-type Rhodamine123 transport activity. Inactive single Walker B mutants (E556Q and E1201Q) were included as negative controls. p values calculated with respect to wild-type activity; n=3, ns p>0.05.

The double binding cavity mutant with arginines introduced instead of the wild-type glutamines (Q132R/Q773R) had a large effect on transport activity permitting only a 2-fold reduction in Rhodamine123 accumulation that is not statistically different by one-way ANOVA analysis from the inactive Walker B mutants, indicating that the positively-charged arginines can effectively repel Rhodamine123 from the ligand binding cavities. The transport activity of the Q132R mutant decreased Rhodamine123 accumulation to 14 fold preserving 93% of the wild-type protein function, while the Q773R mutant was significantly

impaired and only able to reduce Rhodamine123 accumulation to 5-fold compared to untransfected cells. This suggests that Rhodamine123 binds to and is efficiently effluxed from the Q773-lined cavity with comparatively little transported via the Q132 cavity. These data from the ligand binding cavity mutants are consistent with the earlier results of Parveen *et al.* [163] (Figure 3.14). The single Q-loop mutants (Q475A and Q1118A) had significantly reduced transport activity but still supported a 5 to 6 fold decrease in Rhodamine123 accumulation, while the double Q-loop mutant was inactive (Figure 3.15).

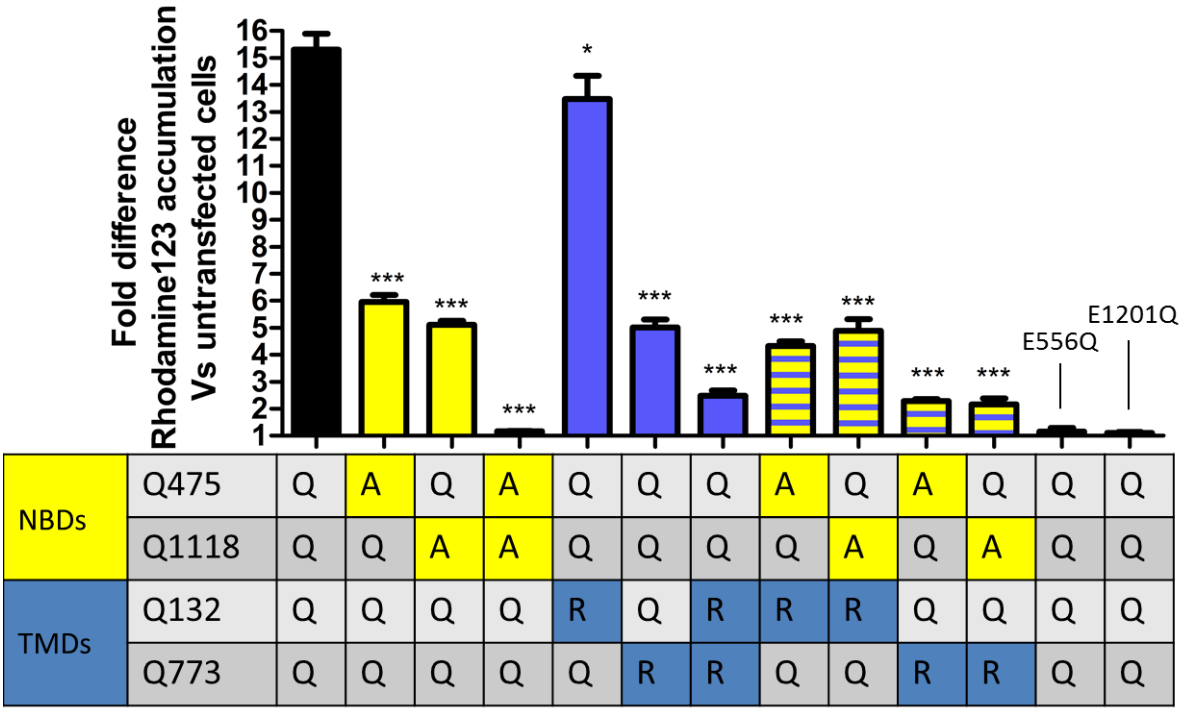

NBDs	Q475	Q	A	Q	A	Q	Q	Q	A	Q	A	Q	Q	Q
	Q1118	Q	Q	A	A	Q	Q	Q	Q	A	Q	A	Q	Q
TMDs	Q132	Q	Q	Q	Q	R	Q	R	R	R	Q	Q	Q	Q
	Q773	Q	Q	Q	Q	Q	R	R	Q	Q	R	R	Q	Q

Figure 3.15: Rhodamine123 Transport. Black bar, wild-type ABCB1; yellow bars, Q-loop mutants; blue bars, ligand binding cavity mutants; blue and yellow striated bars, combined Q-loop and ligand binding cavity mutants. p values calculated with respect to wild-type activity; n=3, *** p<0.001, * p<0.05.

The effect on Rhodamine123 transport activity was similar when single Q-loop mutations were combined with either of the two ligand binding cavity mutation, suggesting that both Q-loops are required to complete the Rhodamine123 export cycle.

3.3.12. BODIPY® FL-vinblastine Transport Requires Both Q-loops

Vinblastine is a vinca alkaloid which inhibits microtubule assembly in the mitotic spindle. It is used as an antineoplastic agent and is transported by ABCB1. Like BODIPY® FL-verapamil, it is conjugated to BODIPY® FL fluorescent moiety for use in this study.

The ligand binding cavity Q132 and Q773 alanine mutants (Q132A, Q773A, and Q132A/Q773A), introduced as controls, had no or very little effect on BODIPY® FL-vinblastine transport activity, indicating again that the wild-type glutamines have little direct involvement in BODIPY® FL-vinblastine transport (Figure 3.16). Cells expressing the ligand binding cavity mutants, Q132R or Q773R, have 50% of BODIPY® FL-vinblastine transport activity of the wild-type ABCB1. However, there is no further reduction in activity when both mutants were combined (Q132R/Q773R) and as single Q-loop mutants are unable to transport BODIPY® FL-vinblastine any further investigation of the signal/energy transduction pathway was precluded (Figure 3.17).

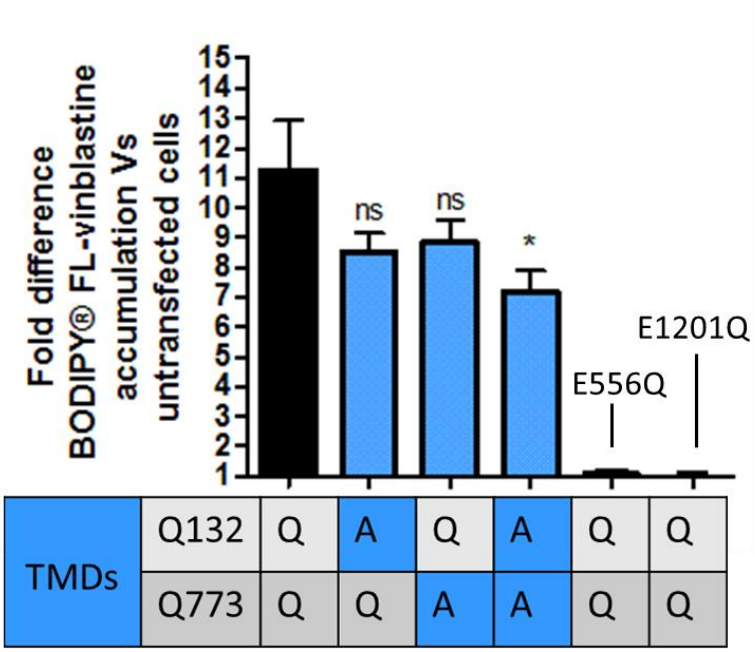

Figure 3.16: BODIPY® FL-vinblastine transport activity of wild-type (black bar) and ligand binding cavity mutants (light blue bars). Flow cytometry data showing the fold reduction in BODIPY® FL-vinblastine accumulation in cells expressing wild-type or ligand binding cavity mutants of ABCB1 compared to untransfected cells. The activities of single Q132A or Q773A mutants are not significantly different to the wild-type protein and the Q132A/Q773A mutant only just reaches significance. Inactive single Walker B mutants (E556Q and E1201Q) were included as negative controls. p values calculated with respect to wild-type activity; n=3, * $p<0.05$, ns $p>0.05$.

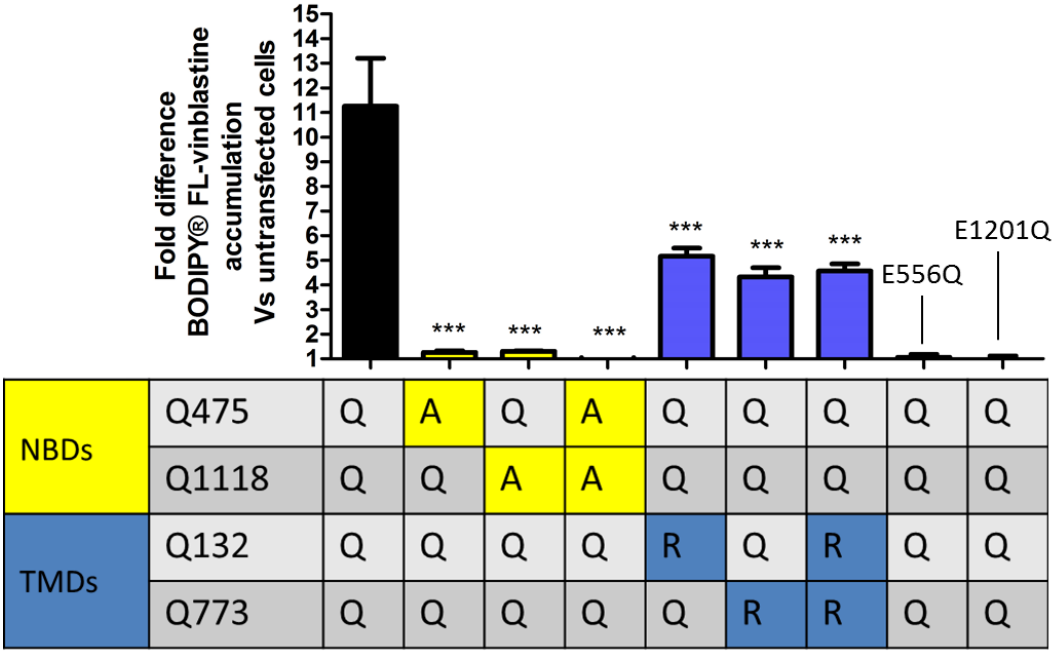

Figure 3.17: BODIPY® FL-vinblastine Transport. Black bar, wild-type ABCB1; yellow bars, Q-loop mutants; blue bars, ligand binding cavity mutants. p values calculated with respect to wild-type activity; n=3, *** p<0.001.

BODIPY® FL-vinblastine transport assays suggest that both Q-loops of ABCB1 are vital for BODIPY® FL-vinblastine export because each single Q-loop mutant is unable to efflux the BODIPY® FL-vinblastine and is not significantly different to the inactive Walker B mutants (E556Q and E1201Q) (Figure 3.17). Similar to the observations made with BODIPY® FL-verapamil, cells expressing the double Q-loop mutant appeared to accumulate more BODIPY® FL-vinblastine than untransfected cells (see below).

3.3.13. Arginines Introduced into the Ligand Binding Cavities are Unable to Prevent BODIPY® FL-taxol Transport

Paclitaxel (Taxol) is a mitotic inhibitor which inhibits the disassembly of microtubules. It is used as an antineoplastic agent and it is also a transport ligand for ABCB1. Taxol is conjugated with BODIPY® FL to form the fluorescent BODIPY® FL-taxol for use in flow cytometry.

BODIPY® FL-taxol is different in one important feature from the other ABCB1 transport substrates selected that it is neutral. It is a high molecular weight compound of similar size to vinblastine (vinblastine has a molecular weight of 810.9 g/mol and paclitaxel has a molecular weight of 853.9 g/mol).

Mutant ABCB1 showed a new pattern of transport for BODIPY® FL-taxol. The single Q-loop mutants reduced BODIPY® FL-taxol efflux from cells, as compared to the wild-type protein, and the second NBD Q-loop mutant (Q1118A) affects function more than the Q475A mutant. The double Q-loop mutant showed no transport activity again indicative of the importance of the Q-loops for the mechanism of ABCB1. The ligand binding cavity single and double arginine mutants were found to have much less impact on BODIPY® FL-taxol transport although the activities of the single and double mutants were significantly different to the wild-type transporter. The lack of inhibition observed for the double binding cavity mutant Q132R/Q773R was probably due to the neutral charge of BODIPY® FL-taxol, and precluded further investigation of the signal/energy transduction pathways for this drug (Figure 3.18).

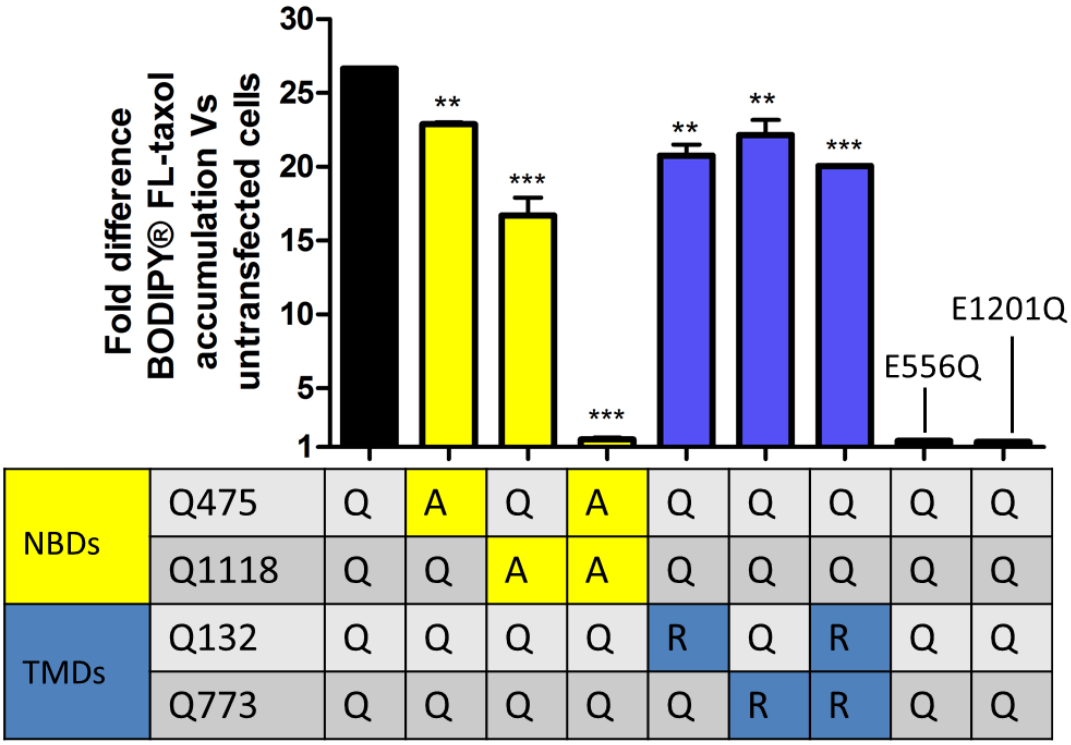

NBDs	Q475	Q	A	Q	A	Q	Q	Q	Q	Q
	Q1118	Q	Q	A	A	Q	Q	Q	Q	Q
TMDs	Q132	Q	Q	Q	Q	R	Q	R	Q	Q
	Q773	Q	Q	Q	Q	Q	R	R	Q	Q

Figure 3.18: BODIPY® FL-taxol Transport. Black bar, wild-type ABCB1; yellow bars, Q-loop mutants; blue bars, ligand binding cavity mutants. p values calculated with respect to wild-type activity; n=3, *** p<0.001, ** p<0.01.

3.3.14. Cells expressing the Q475A/Q1118A Mutant Accumulate More BODIPY® FL-verapamil and BODIPY® FL-vinblastine

As reported in related sections, the double Q-loop mutant was unable to efflux Rhodamine123, BODIPY® FL-verapamil, BODIPY® FL-vinblastine and BODIPY® FL-taxol and it appeared that cells expressing this mutant accumulated more BODIPY® FL-verapamil and BODIPY® FL-vinblastine than mock transfected cells. Dot plots showing the fluorescence of individual cells for ABCB1 expression levels and for BODIPY® FL-verapamil accumulation are shown in Figure 3.19. Cells that express more double Q-loop mutant accumulate more drug. The mean fold differences in BODIPY® FL-verapamil and BODIPY® FL-vinblastine accumulation between untransfected and transfected cells are shown in Figure 3.20. This

increase in ligand accumulation is less obvious but still apparent when cells were loaded with 10 µM of BODIPY® FL-verapamil (Figure 3.21). BODIPY® FL-verapamil accumulation in cells expressing the double Q-loop mutant can be obscured when non-competitive inhibitor elacridar (GF120918; 1 µM) [177] or cyclosporin A (100 µM) which is a transport ligand of ABCB1 and a competitive inhibitor at higher concentrations, are co-administered possibly due to the inhibition of BODIPY® FL-verapamil interaction with the transporter (Figure 3.22). The increase in accumulation of BODIPY® FL-verapamil or BODIPY® FL-vinblastine could be due to either the import of these drugs into the cell by the double Q-loop mutant, or because drugs bind to the mutant transporter but do not dissociate and the mutant protein therefore provides extra binding sites for the drugs in the membrane.

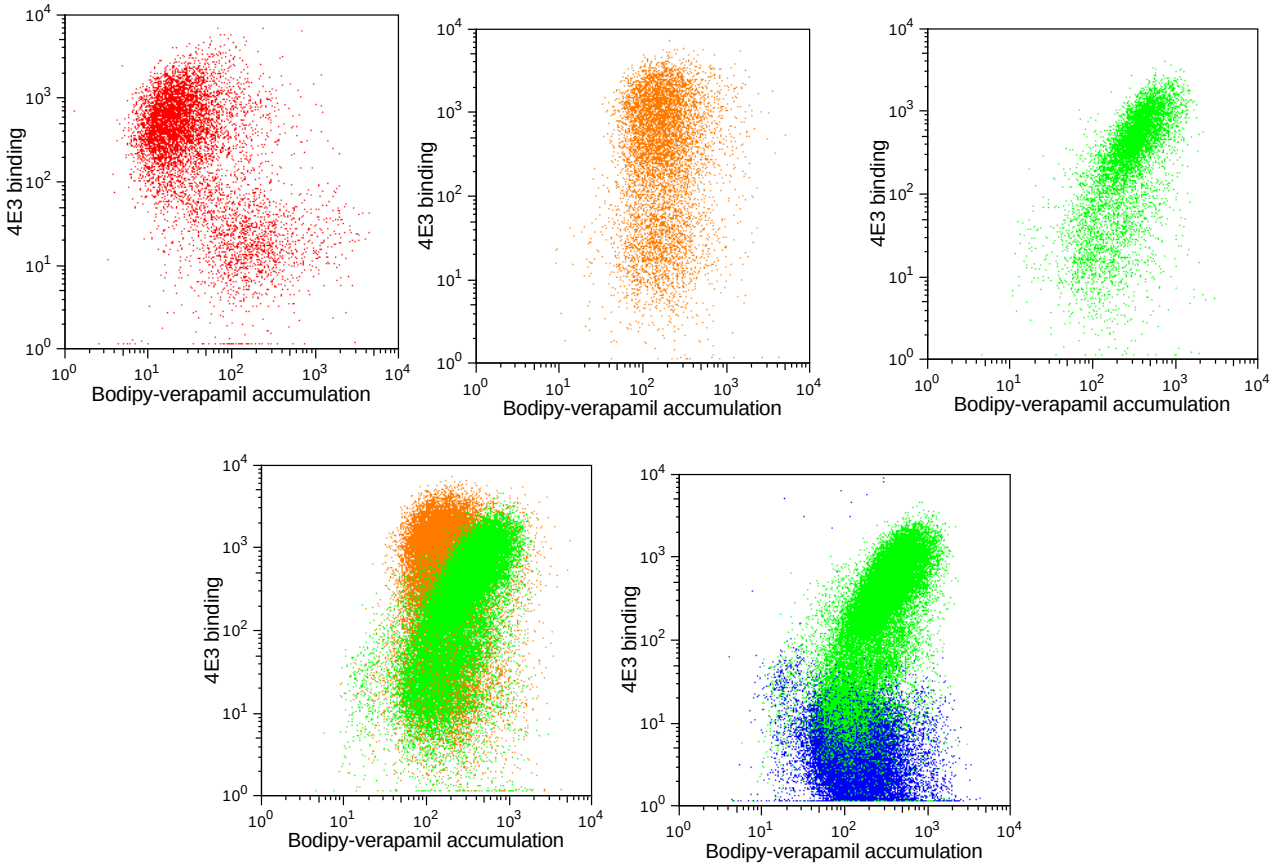

Figure 3.19: The double Q-loop mutant Q475A/Q1118A accumulates more BODIPY® FL-verapamil than mock transfected cells. Dot blot from two-colour flow cytometry experiments show the relationship between ABCB1 surface expression (4E3 labelling) and BODIPY® FL-verapamil accumulation. Each dot represents an individual cell. In the population of cells (red, top left panel) that was transiently-transfected with plasmid encoding wild-type ABCB1, increased surface labelling with 4E3 (and so increased ABCB1 expression) correlates with decreased accumulation of BODIPY® FL-verapamil (the group to the bottom right of the plot are non-transfected cells within the population). Cells expressing the catalytically inactive Walker B mutant E1201Q (gold, top centre panel) accumulate BODIPY® FL-verapamil to the same level as mock transfected (or non-expressing cells within the E1201Q transfection experiment). In contrast cells expressing the double Q-loop mutant Q475A/Q1118A (green, top right panel) accumulate more BODIPY® FL-verapamil than cells expressing the E1201Q mutant, and the level of accumulation goes up with increasing expression of Q475A/Q1118A. Direct comparison of the level of BODIPY® FL-verapamil accumulation of cells expressing Q475A/Q1118A, with mock transfected cells (blue) and cells expressing E1201Q is given in the overlay plots to the bottom left and bottom right, respectively.

A.

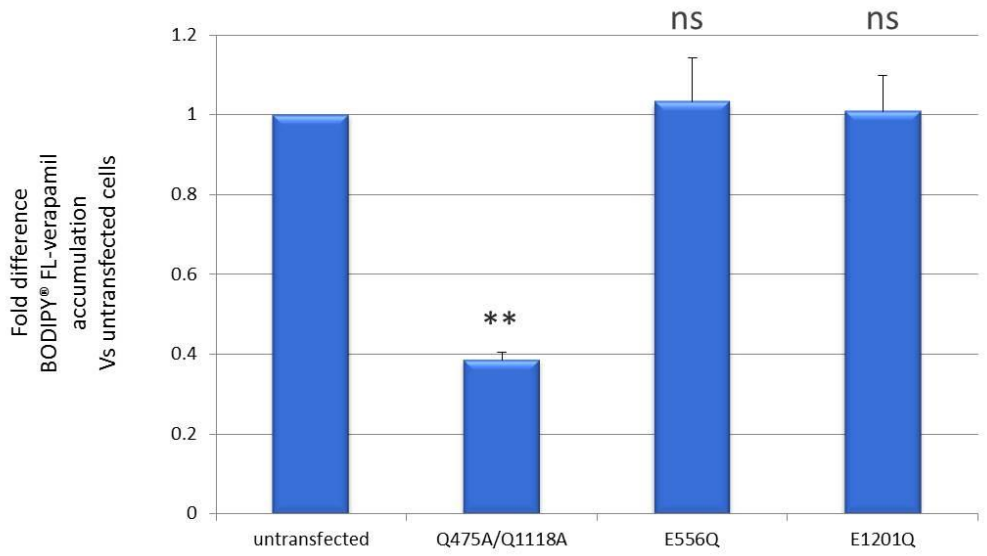

B.

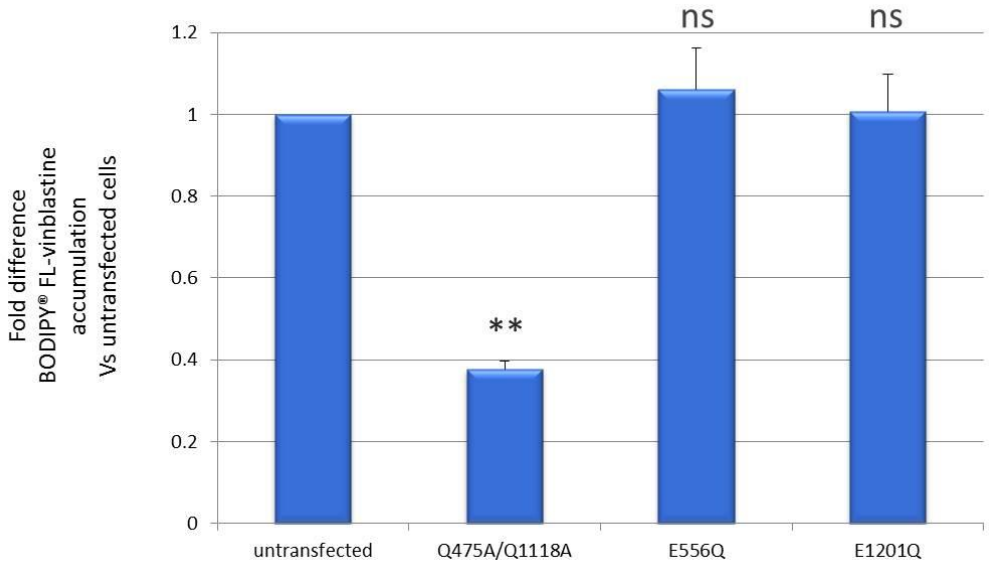

Figure 3.20: (A) BODIPY® FL-verapamil transport (B) BODIPY® FL-vinblastine transport. The x-axes indicate the different ABCB1 mutants expressed. The y-axes indicate the fold difference in drug accumulation between the transfected and the untransfected cells within each sample. The fold difference of Q475A/Q1118A mutant as compared to untransfected cells gives a value ~0.4 which means the cells expressing the Q475A/Q1118A mutant accumulate more drug than untransfected cells. p values calculated with respect to drug accumulation in untransfected HEK293T cells; n=6 for BODIPY® FL-verapamil transport data and n=3 for BODIPY® FL-vinblastine transport data , ** p<0.01, ns p>0.05.

A.

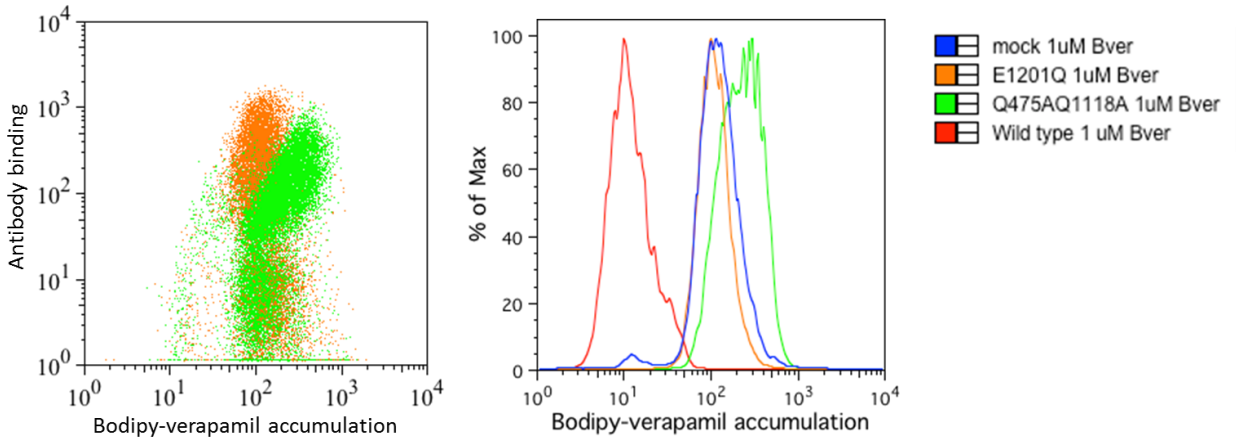

B.

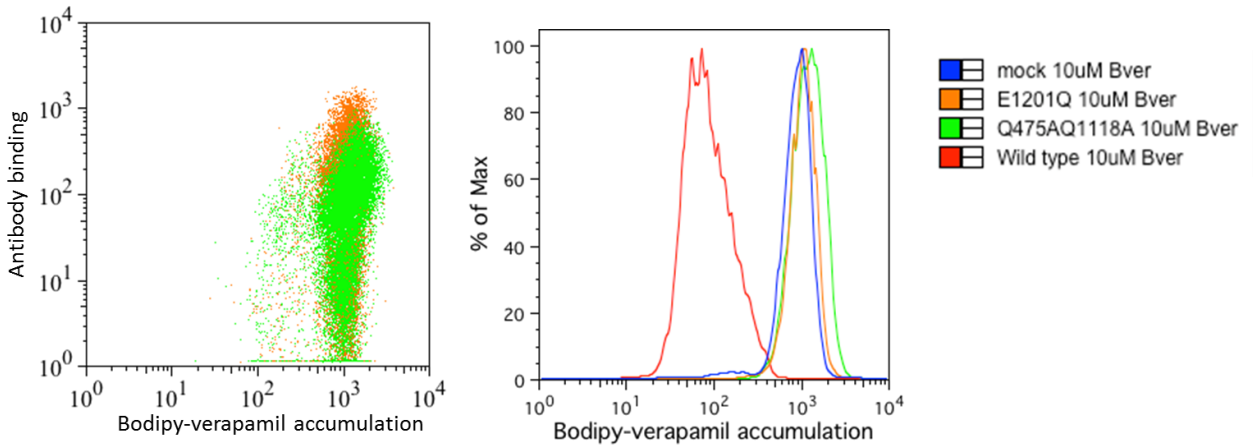

Figure 3.21: The increase in BODIPY® FL-verapamil accumulation in cells expressing Q475A/Q1118A is less apparent when 10 µM BODIPY® FL-verapamil is used. A. 1 µM BODIPY® FL-verapamil. B. 10 µM BODIPY® FL-verapamil.

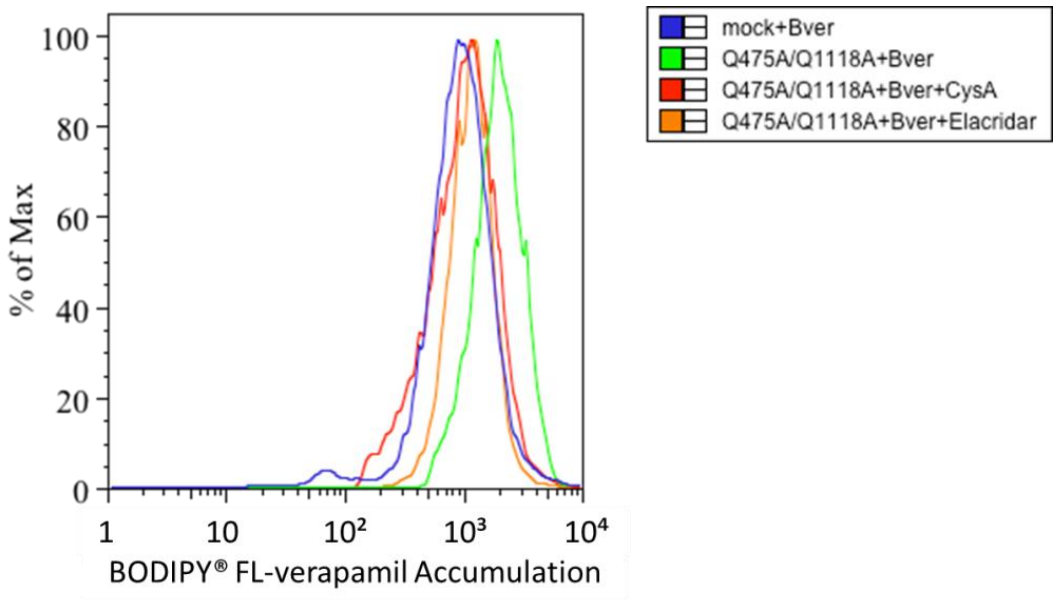

Figure 3.22: ABCB1 inhibitors Cyclosporin A (100 µM) and Elacridar (1 µM) can inhibit the increased BODIPY® FL-verapamil (0.8 µM) accumulation pattern observed when cells express the Q475A/Q1118A mutant ABCB1. BODIPY® FL-verapamil accumulation in cells expressing the Q475A/Q1118A mutant in the absence of inhibitor (green), and in the presence of the competitive inhibitor Cyclosporin A (orange) or noncompetitive inhibitor, Elacridar (red), as compared to mock cells (blue).

3.3.15. Can Single Q-loop Mutants Short Circuit in the Transport Cycle?

The retention of wild-type levels of BODIPY® FL-verapamil efflux activity by the single Q-loop mutants despite at least a 50% reduction in ATP hydrolysis activity (Dr. Zolnerciks, Dr. Linton, unpublished data, Figure 3.4) and because transport of BODIPY® FL-verapamil from the Q773-lined ligand binding cavity only requires the Q475 Q-loop motif, might suggest a change in stoichiometry and that single Q-loop mutants may power the transport cycle by hydrolysing just one ATP, as depicted by the short-circuit in Figure 3.23. It has been suggested previously that ABCB1 may hydrolyse only one ATP to return to the basal state [178]. If this is the mechanism used by single Q-loop mutants, they might be insensitive to mutation of one of the Walker B catalytic glutamates which normally results in an inactive

protein. To investigate this, single Walker B mutants (E556Q and E1201Q) were introduced into Q132R/Q1118A mutant (Table 3.3). These mutants only have the NBD1 Q-loop vital for the transport of BODIPY® FL-verapamil from the Q773-lined cavity, and one or other of the Walker B catalytic glutamates. Transport assays showed a significant decrease in activity of both triple mutants; Q132R/E556Q/Q1118A and Q132R/Q1118A/E1201Q, compared to the original Q132R/Q1118A mutant, however the transport activity of the Q132R/Q1118A/E1201Q mutant showed a subtle increase over the Walker B, E1201Q mutant. The difference was significant according to two-tailed Student's t-test (Figure 3.24) and suggests partial rescue of the Walker B mutant. However, the increase in activity is much less than might be expected if the transport mechanism had been short-circuited to no longer require hydrolysis of the ATP in the E1201 pocket. Alternatively, it is possible that the Walker B glutamate is involved in a further step in the mechanism other than ATP catalysis.

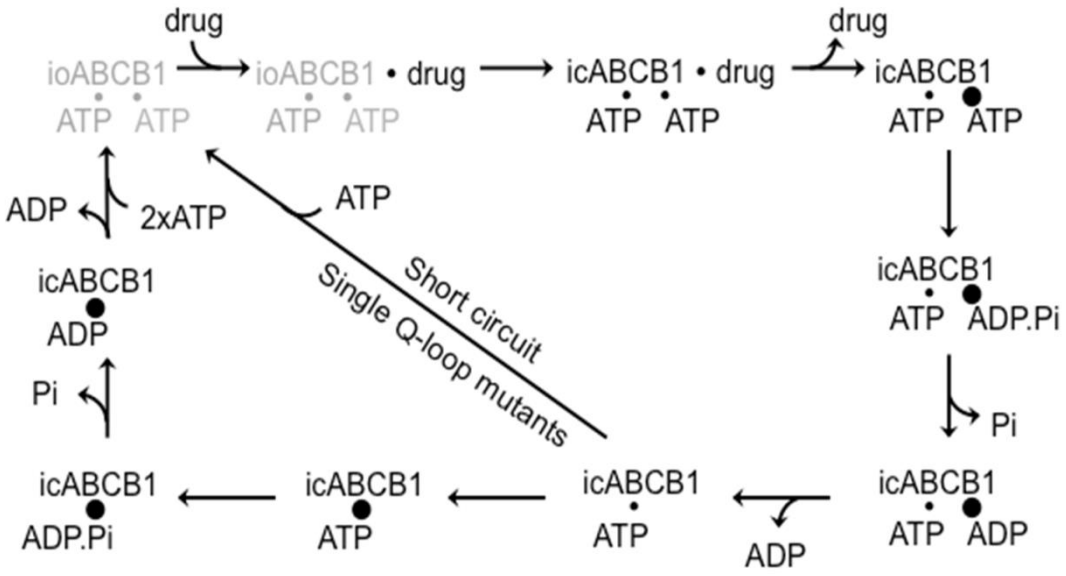

Figure 3.23: Possible scheme for the transport cycle of ABCB1. Inward-open (io) ABCB1 binds drug which, communicating through the Q-loops via the coupling helices, allows closure of the two NBDs around two molecules of ATP. The ATPs may already be bound to the F1-core subdomains of the NBDs, but the conformation of the coupling helices prevents closure of the NBD:NBD interface in the absence of drug. The drug-dependent and ATP-dependent inward-closed (ic) conformation of ABCB1 causes a conformational change in the TMDs which results in release of drug, and also occludes one of the ATPs committing it for hydrolysis. Dr. Zolnerciks' ECAR data imply that both ATPs are hydrolysed in concert in the wild-type transporter, but there may be circumstances, for example when drug is only bound to the Q773-lined cavity, or in the absence of one of the Q-loop glutamines, when the transporter short circuits and commits only one ATP to hydrolyse and loses the other from the non-occluded pocket.

Walker B mutants	E556Q	5'-AAGATCCTCCTGCTGGATcagGCCACGTCAGCCTTGGC-3'
	Wild-type	5'-AAGATCCTCCTGCTGGATGAGGCCACGTCAGCCTTGGC-3'
	E1201Q	5'-CCTCATATTTTGCTTTTGGATcaaGCCACGTCAGCTCTGGAT-3'
	Wild-type	5'-CCTCATATTTTGCTTTTGGATGAAGCCACGTCAGCTCTGGAT-3'

Table 3.3: Oligonucleotides designed to introduce Walker B mutants into the plasmid encoding the Q132R/Q1118A mutant.

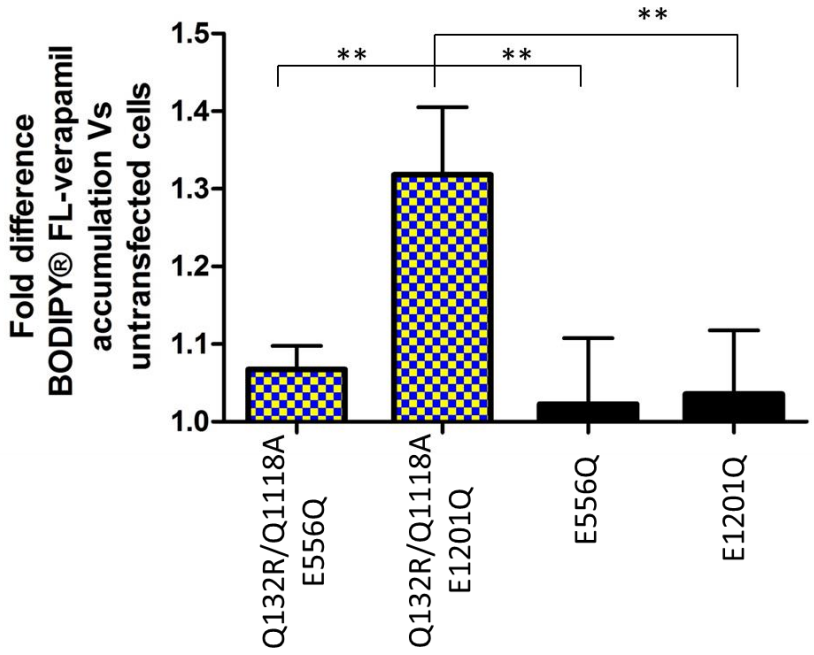

Figure 3.24: BODIPY® FL-verapamil transport activity of the Q132R/Q1118A/E1201Q mutant is significantly different from the single Walker B mutant E1201Q according to two-tailed Student's t-test. p values calculated with respect to Q132R/Q1118A/E1201Q mutant activity; n=3, ** p<0.01.

3.3.16. UIC2 Antibody Binding Suggests Q475A/Q1118A is Trapped in the 'Basal State'

Mouse monoclonal UIC2 antibody was first described in 1992 to recognize a moiety on the first extracellular loop of ABCB1 [179]. In the study by Mechetner *et al.*, UIC2 antibody inhibited the transport of drugs from mouse BALB/c 3T3 cells transiently expressing ABCB1 and increased their cytotoxicity, whereas no effect was detectable with other anti-ABCB1 antibodies. It was shown that UIC2 reactivity with ABCB1 was increased by the addition of ABCB1 transport ligands or ATP-depleting agents and also by mutation of the Walker A motif lysine residues [180]. Mutation of the Walker A motif lysine residues to methionine had previously been shown to prevent ATP binding [181]. This suggested that the UIC2 epitope is obscured in the ATP bound form of ABCB1, which equates to the inwardly-closed nucleotide bound conformation as observed in the crystal structure of the ABCB1 homologue Sav1866 [57]. The addition of transport ligands to the wild-type ABCB1 is thought to drive the transporter through the transport cycle and this increases UIC2 binding because it involves conformational change to the inwardly-open conformation [180].

3.3.16.a. Titration and Use of the UIC2 Antibody

The UIC2 antibody was titrated to saturate all wild-type or mutant ABCB1 on cell surface. Cells were transfected with pABCB1-12HIs, as described in section 2.3.5., and after harvesting the cells were aliquoted into eight fractions, each containing 1x 10^6 cells. These fractions were then labelled with 0, 0.5, 2.5, 5, 12.5, 25, 50, 100 µl of UIC2 antibody which was conjugated to phycoerythrin (PE) (stock UIC2 supplied by Immunotech was at a

concentration of 15 µg/ ml) in the presence of 0.8 µM BODIPY® FL-verapamil to drive ABCB1 through the transport cycle. The cells were incubated for 30 minutes at 37^{O}C, then washed and the fluorescence associated with the cells was measured by flow cytometry. Fluorescence from antibody bound non-specifically to untransfected cells was subtracted from the fluorescence associated with from ABCB1-expressing cells to reveal the specific binding of UIC2 antibody. From this data, it was concluded that 0.375 µg of UIC2 per 1x10^{6} cells was sufficient to saturate the ABCB1 on the surface of cells, as any increase above this level resulted in a minimal increase in fluorescence (Figure 3.25).

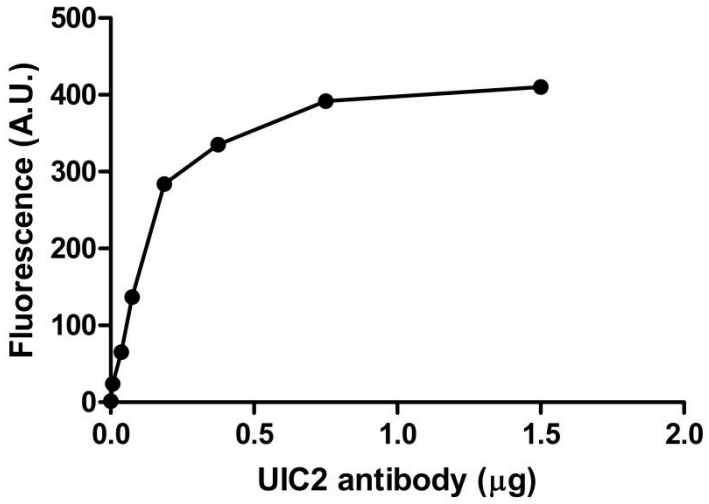

Figure 3.25: Titration of UIC2 antibody binding to HEK293T cells expressing wild-type ABCB1. 1x10^{6} cells transfected with p-ABCB1-12His were labelled with UIC2 antibody conjugated to PE for 30 minutes at 37°C in the presence of 0.8 µM BODIPY® FL-verapamil. After washing, UIC2 binding was determined by flow cytometry and specific UIC2 binding was calculated by subtracting corresponding FL-2 fluorescence values from untransfected cells labelled in the same manner.

To investigate the conformation of the Q475A/Q1118A mutant, the conformation-specific antibody UIC2 was used. HEK293T cells were transfected transiently to express either the wild-type ABCB1, the single or double Q-loop mutants or the NBD2 Walker B mutant (E1201Q). The cells were labelled with 4E3 antibody to measure the total amount of ABCB1 on the cell surface (Figure 3.26A). This showed that all mutants express to a similar level as the wild-type protein. The BODIPY® FL-verapamil transport activities of single Q-loop mutants (Q475A and Q1118A) are similar to wild-type protein, and the NBD2 Walker B mutant (E1201Q) was unable to transport the drug. As before, the double Q-loop mutant accumulates more drug than mock transfected cells or cells expressing the NBD2 Walker B mutant (Figure 3.26B). UIC2 binding was significantly higher in the Q475A/Q1118A expressing cells (Figure 3.26C), while the NBD2 Walker B mutant bound less UIC2 than wild-type ABCB1. The simplest interpretation of this data is that a larger fraction of double Q-loop mutant is in the inwardly-open conformation with a high-affinity for UIC2, while the Walker B single mutant which has previously been shown to be trapped in the ATP-bound conformation [182] has a low-affinity for UIC2.

A

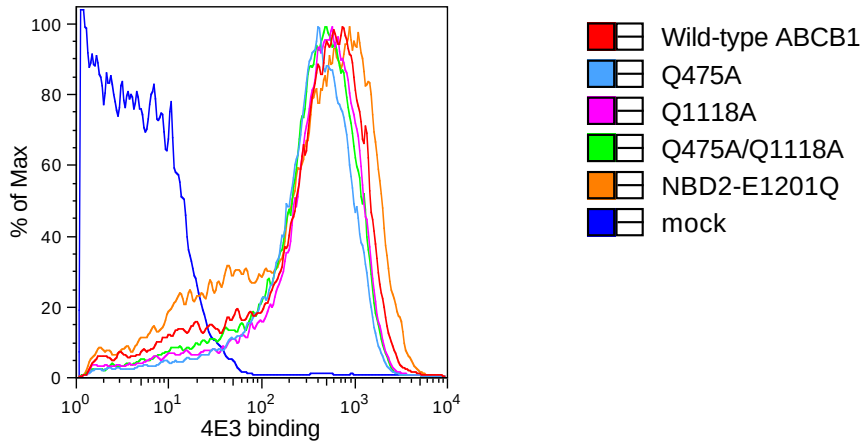

B

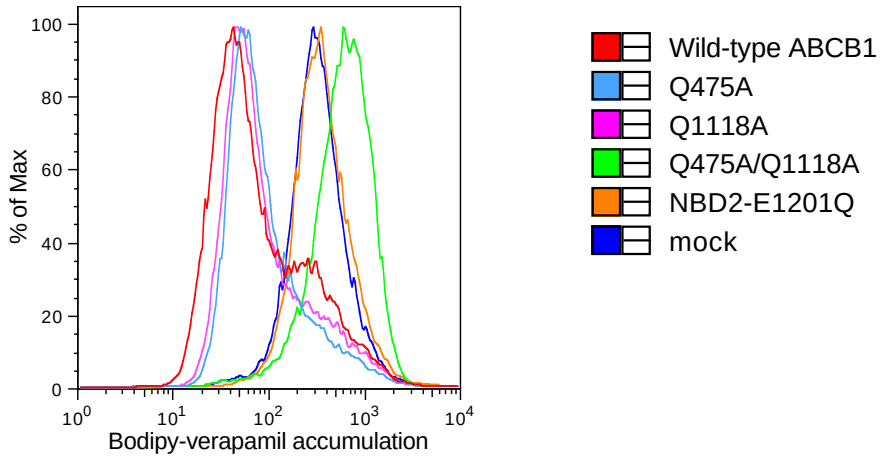

C

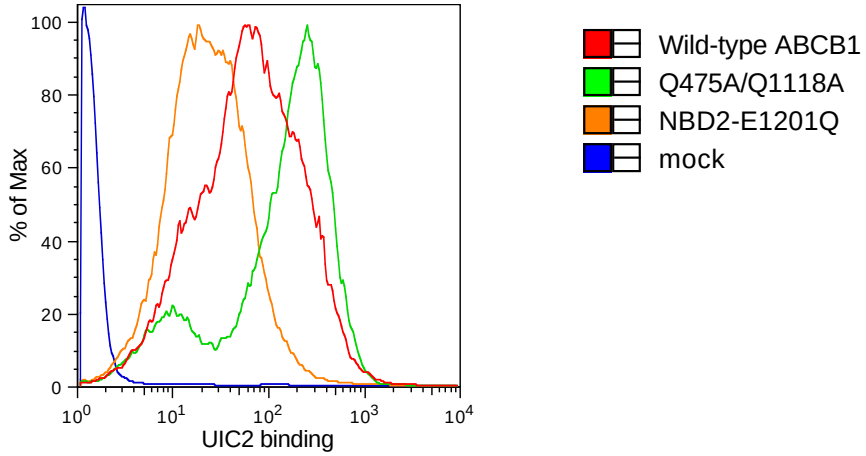

Figure 3.26: Conformation-specific UIC2 antibody differentiates the conformations of the wild-type, Walker B and double Q-loop mutant. (A) HEK293T cells expressing wild-type ABCB1, Q-loop mutants NBD1-Q475A, NBD2-Q1118A and Q475A/Q1118A, and the Walker B mutant E1201Q, together with mock transfected cells were labelled with the ABCB1-specific antibody 4E3. (B) The effect of the wild-type and mutant ABCB1 on BODIPY® FL-verapamil accumulation. (C) Labelling of HEK293T cells expressing wild-type ABCB1, the double Q-loop mutant Q475A/Q1118A, the Walker B mutant E1201Q, and mock transfected cells with the conformation-sensitive ABCB1 antibody UIC2.

3.3.17. Confocal Microscopy Shows Drug Bound to the Q475A/Q1118A Mutant in the Membrane and Confirms the Inward-open Conformation of This Mutant

Confocal microscopy was invented by Marvin Minsky in 1955, based on the main idea of rejection of the out-of focus light [183]. It uses a point-by-point image construction by focusing on a point of light in the specimen and this avoids most of the unwanted scattered light from indeterminate points when the entire specimen is illuminated. Additionally, the returning rays from the visualised point of the specimen pass through a second pinhole before detection ensuring that only light from the focal point is measured which is why the pinhole size is critical. These two systems; a first pinhole to illuminate a single point and a second before the detector that eliminates the out of focus light, is why the microscope is referred as 'confocal'. The focussed light rays are then collected by a photomultiplier and the image is gradually constructed.

Confocal microscopy was performed to determine whether the Q475A/Q1118A mutant binds drug, or binds and internalises drug. Cells expressing the Q475A/Q1118A mutant were found to accumulate BODIPY®FL-verapamil or BODIPY®FL-vinblastine in the plasma membrane where it co-localises with the signal from the ABCB1-specific antibody 4E3 (Figure 3.27 and Figure 3.28, respectively). Consistent with the UIC2 binding data, this implies the double Q-loop mutant ABCB1 binds BODIPY® FL-verapamil or BODIPY®FL-vinblastine but is unable to progress in the transport cycle, and so is trapped in the inward-open conformation which has a high affinity for drug. Consistent with this interpretation, neither BODIPY® FL-verapamil nor BODIPY®FL-vinblastine could be visualised bound to the Walker B E1201Q mutant, supporting the conclusion drawn from the UIC2 binding

experiments that the single Walker B mutant is trapped in the ATP-bound inwardly-closed conformation which would be expected to have a low affinity for drug.

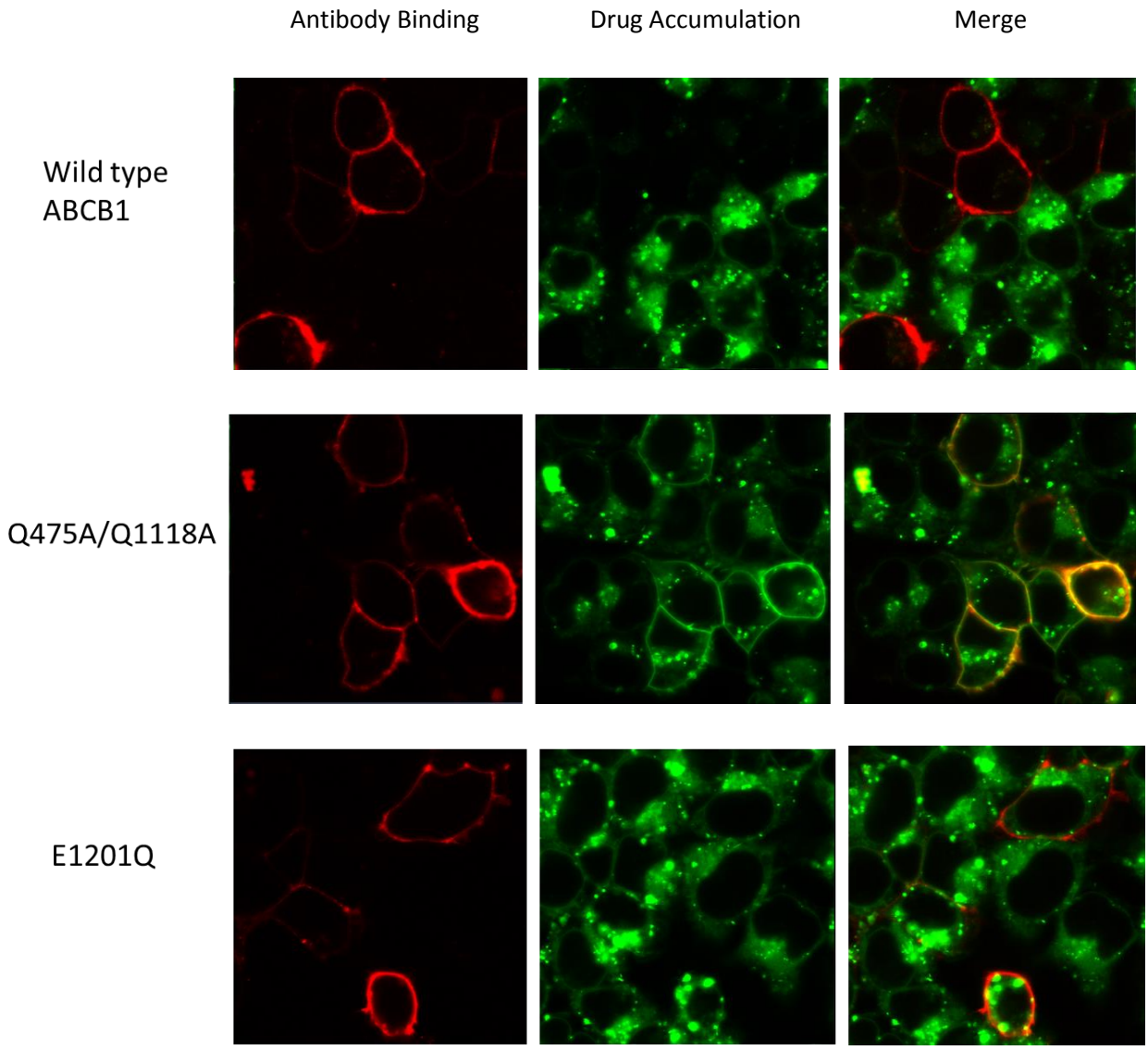

Figure 3.27: Transiently-transfected HEK293T cells were used to investigate the subcellular location of accumulated drug. The red-fluorescence reports ABCB1 antibody binding (4E3), and green fluorescence is BODIPY®FL-verapamil accumulation. The right hand panel shows the merged image of red and green fluorescence. Wild type ABCB1 is highly active and exports BODIPY®FL-verapamil out of the cell such that very little, if any, drug accumulation can be seen in the cell or cell membrane. The Q475A/Q1118A double Q-loop mutant binds drug and the merged image shows drug accumulation in the plasma membrane overlapping with the bound antibody. In contrast, the Walker B mutant (E1201Q) looks similar to untransfected cells and has no detectable drug in the plasma membrane.

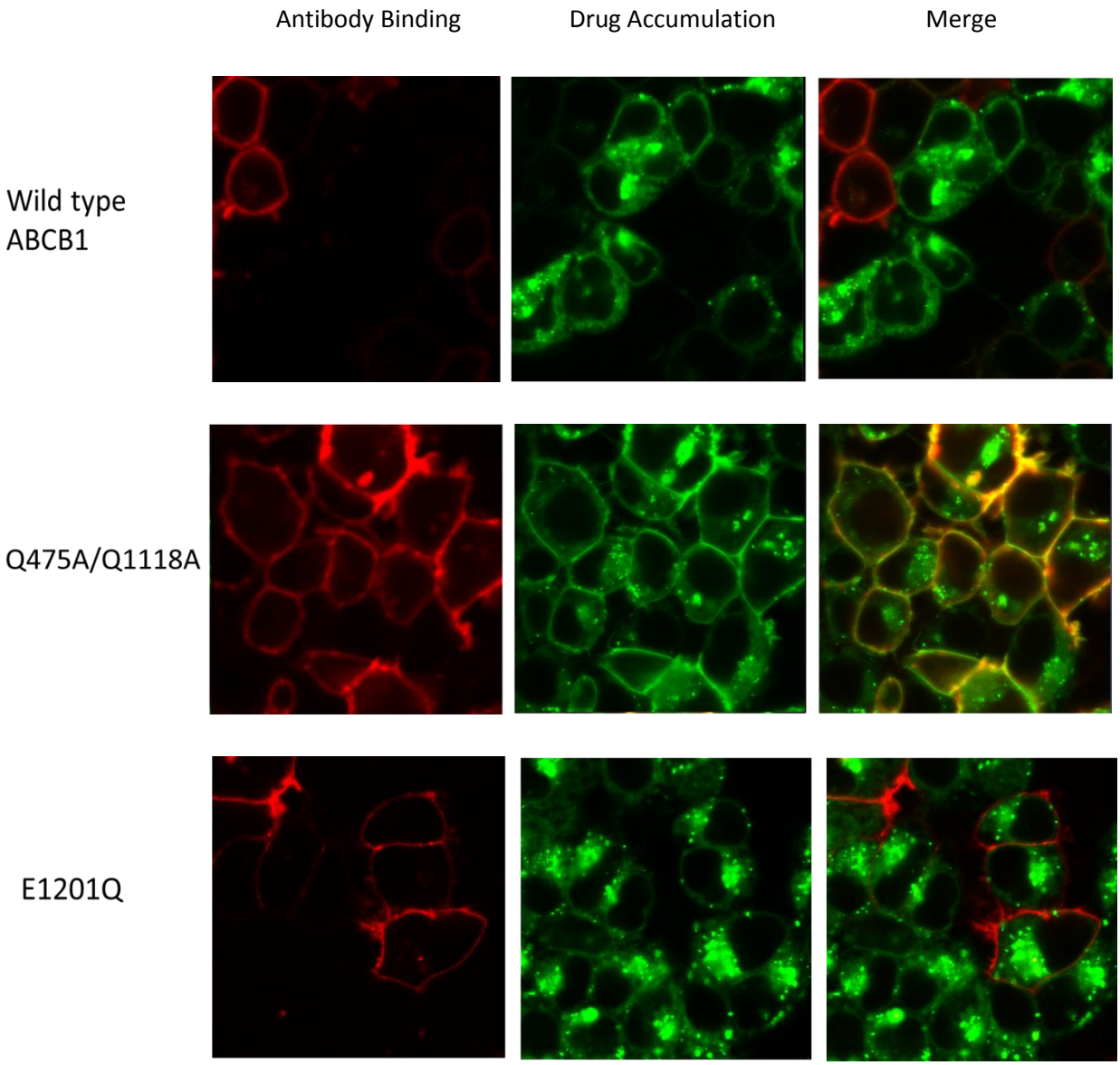

Figure 3.28: Transiently-transfected HEK293T cells were used to investigate the subcellular location of accumulated drug. The red-fluorescence reports ABCB1 antibody binding (4E3), and green fluorescence is BODIPY®FL-vinblastine accumulation. The right hand panel shows the merged image of red and green fluorescence. Wild type ABCB1 is highly active and exports BODIPY®FL-vinblastine out of the cell such that no drug accumulation can be seen in the cell or cell membrane. The Q475A/Q1118A double Q-loop mutant binds drug and the merged image shows drug accumulation in the plasma membrane overlapping with the bound antibody. In contrast, the Walker B mutant (E1201Q) looks similar to untransfected cells and has no detectable drug in the plasma membrane.

3.4. Discussion and Conclusions

The early structural data showed that the Q-loop motif glutamines (Q475 and Q1118A) were in close proximity to the putative attacking water molecule in the Rad50 and HisP crystal structures [63, 184]. Mg^{2+} was not present in the HisP structure, but water- 407 was thought to occupy the location of Mg^{2+}, and the Q-loop glutamine was in close proximity to this water molecule [63]. In the Rad50 structure, in which the non-hydrolyseable Mg^{2+}-AMP-PNP nucleotide analogue was co-crystallised, the Q-loop glutamine (Gln-140) co-ordinated both the Mg^{2+} and the putative attacking water molecule [184]. This led to the interpretation that the Q-loops might activate the attacking water molecule or have a role in the coordination of Mg^{+2}. The crystal structures focussed attention on the Q-loop motif which was subsequently analysed by biochemical studies after purification and reconstitution into proteoliposomes. Urbatsch *et al.* showed that the single Q-loop mutants of the mouse homologue of human ABCB1 lost nearly all of their ATPase activities *in vitro*. The residual activity was dependant on Mg^{2+} and inhibitable by vanadate [164]. However, the dramatic loss of ATPase activity in the single Q-loop mutants was contradicted later by ECAR measurements in live cells (Dr. Zolnerciks, see section 3.1.). The single Q-loop mutants retain the ability to hydrolyse ATP in live cells (up to 50% of the wild-type activity) but this is largely lost during purification, which is likely due to inactivation of the single Q-loop mutants during the purification process.

Subsequent analyses of ABCB1 and other ABC transporters has clearly identified that the Walker B glutamate is more important for ATP hydrolysis and most likely activates the attacking water for catalysis [185, 186], but this need not exclude a role for the Q-loop glutamine in the process.

The structural data suggest a potential role for the Q-loops in signal transduction between the ATP catalytic sites and ligand binding cavities. The Q-loop resides in close proximity to the intracellular coupling loops of the TMDs [57]. The second intracellular loop of both TMDs sits in a groove on the top surface of the juxtaposed NBD, with the Q-loop at the base of each groove. In the crystal structure of the *E. coli* vitamin B12 importer BtuCD, the Q-loop of BtuD is in contact with the cytoplasmic loop of BtuC which also suggests an interaction important for NBD:TMD communication in ABC importers [187].

The Q-loop also links the core and the α-helical subdomains of the NBDs and has been suggested to function as a flexible hinge to allosterically couple the two nucleotide binding pockets. The α-helical subdomains are suggested to rotate around the Q-loops to contact nucleotide that is bound by the core subdomain of the apposed NBD [60]. With the Q-loop serving as a hinge, any conformational change to bind ATP or release the products of ATP hydrolysis can theoretically be transmitted to the TMDs via the coupling helices. These mechanistic interpretations of X-ray crystallographic data fit well with the observed phenotype of the Q-loop mutants of ABCB1. If the double Q-loop mutant is unable to influence conformational change at the NBDs after drug binding then the mutant transporter will not be able to efflux drug, but the drug may remain bound to the TMDs in the plasma membrane. This is evident in the flow cytometry transport studies which show that this mutant is unable to efflux drug, and in the confocal microscopy data that localises

the additional drug accumulation to the plasma membrane in cells expressing this mutant. The inability of the double Q-loop mutant to change conformation is also supported by the high level of UIC2 binding, consistent with the transporter adopting the inward-open conformation. However, the single mutants retain transport function because the hypothesised conformational change induced by drug binding can still be transmitted to the NBDs via the remaining wild-type Q-loop.

My data also shows that different transport ligands interact with ABCB1 to stimulate the transport cycle in different ways. The drug binding sites are considered to be a property of the TMDs, yet single mutations in the Q-loops of the NBDs have distinct effects on the transport of different drugs. The Q-loop is a critical motif for function shown by the complete inactivity of the double Q-loop mutants (Q475A/Q1118A) for all drugs. However, there is redundancy in the mechanism for BODIPY® FL-verapamil with wild-type levels of efflux activity for the single Q-loop mutants, and partial but significant activity for the efflux of Rhodamine123 and BODIPY® FL-taxol. Most surprisingly, BODIPY® FL-vinblastine efflux activity is absent for single Q-loop mutants. The situation is further complicated when point mutations (Q132R and Q773R) are introduced into the TMDs to dissect the pseudo-symmetrical ligand binding cavities [163].

The Q132R and Q773R mutations separate pseudosymmetric drug binding sites for BODIPY® FL-verapamil, and in combination with the single Q-loop mutants, distinct inter-domain communication pathways were identified: the Q132-gated verapamil binding cavity communicates with both Q-loops but the Q773-gated verapamil binding cavity communicates primarily with the Q475 of the NBD1 Q-loop to transport the bound drug (Figure 3.29). This suggested that the NBD2 Q-loop mutant might short-circuit the transport

cycle when only the Q773-gated binding cavity is available to bind BODIPY® FL-verapamil (ensured by mutation of the Q132 residue to arginine). If the transport cycle can be short-circuited and only one molecule of ATP is hydrolysed, it was hypothesised that one of the Walker B motifs might no longer be necessary. Both single Walker B mutants were therefore introduced into the Q132R/Q1118A mutant. Transport assays of the new mutants showed that both Walker B motifs were necessary for wild-type levels of BODIPY® FL-verapamil transport activity. Mutation of the NBD1 Walker B catalytic glutamate completely inhibited BODIPY® FL-verapamil transport, but mutation of the NBD2 Walker B motif was not fully penetrant, and the Q132R/Q1118A/E1201Q retained a residual transport activity that was significantly different to either single Walker B mutant. This rescue of the NBD Walker B mutant phenotype, albeit subtly, might suggest that the Q132R/Q1118A mutant is capable of short-circuiting the ATP catalytic cycle and hydrolyses only one ATP to transport BODIPY® FL-verapamil. Mechanistically, this could be explained if the NBD2 Q-loop glutamine was required to co-ordinate the γ-phosphate in order to position the ATP for attack by the water activated by the Walker B glutamate. But why would full activity not be restored in the triple mutant? Hypothetically, this may be explained if the Walker B motif is also important for a conformational step post hydrolysis. Evidence for such a role for the Walker B motif may be found in the crystal structure of HlyB from *E. coli* solved with ADP bound, in which the Q-loop glutamine (Q550) forms a direct interaction with the peptide backbone of residue T633 in the presence of ADP. T633 is towards the carboxyl end of the Walker B motif suggesting a role for the Walker B motif, and a further role for the Q-loop, in the outward rotation of α-helical subdomain [61]. If the E1201Q mutant changes the conformation or positioning of the Walker B motif then the involvement of the latter in the outward rotation may be impaired and the

Q132R/Q1118A/E1201Q triple mutant might therefore struggle to complete the transport cycle even after hydrolysis of the (single) ATP.

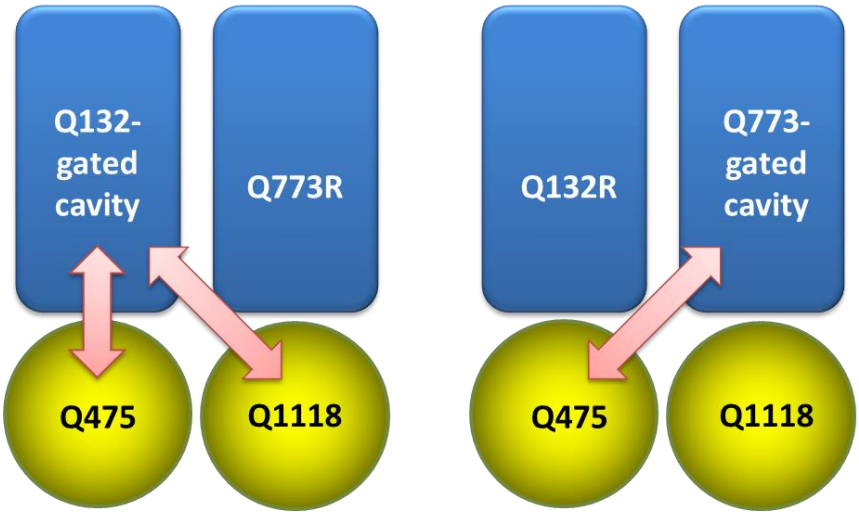

Figure 3.29: Communication paths during BODIPY® FL-verapamil transport.

Combining the Q132R ligand binding cavity mutant with each of the two NBD Q-loop mutants Q475A and Q1118A had little impact on the already impaired Rhodamine123 transport activity of each single Q-loop mutant. This is as expected because Rhodamine123 does not appear to be transported via the Q132 cavity. Combining the Q773R mutant with each of the Q-loop mutants further impaired the transport activity of the transporter (the transport activities of these mutants were not significantly different to the inactive Walker B mutants). The impact of the Q-loop mutations on the ability of the Q773R mutant to efflux Rhodamine123 was symmetrical, implying that Rhodamine123 by the Q773-lined cavity transduces energy through both Q-loops to engage the ATP catalytic cycle.

In conclusion, it was shown that different drugs trigger the transport cycle in different ways. Rhodamine123 transport via the Q773-lined cavity requires both Q-loops whereas BODIPY® FL-verapamil transport from the same cavity is dependent largely on the Q-loop of NBD1. In addition to these data, single Q-loop mutants can transport BODIPY® FL-verapamil, Rhodamine123 and BODIPY® FL-taxol, but cannot transport BODIPY® FL-vinblastine. It was also shown by flow cytometry and confocal microscopy, and also by the use of the conformation-specific antibody UIC2, that the double Q-loop mutant is trapped in the basal state which retains affinity for BODIPY® FL-verapamil and BODIPY® FL-vinblastine. In contrast, the single Walker B mutants are likely trapped in the ATP-bound state and do not bind drug. The Walker B mutants have previously been shown to be unable to hydrolyse ATP [185] and these mutants are therefore likely to be trapped in a state resembling the inwardly-closed ATP-bound conformation, and consequently should have a low-affinity for transport ligand entirely consistent with the microscopy data included herein.

Chapter Four

4. The Potential Role of ABCB1 in Alzheimer's Disease and the Potential Regulation of ABCB1 by Ubiquitination

4.1. Introduction

Alzheimer's disease is characterised by the accumulation of β-amyloid within the brain and one contributory factor for this is reduced clearance [188]. Transport of the β-amyloid peptide requires transporters and clearance across the blood-brain barrier from brain to blood is a two-step process. β-amyloid must first pass through the abluminal membrane of endothelial cells forming blood-brain barrier and then the luminal membrane. Low density lipoprotein receptor-related protein 1 (LRP1) has been suggested to be responsible for β-amyloid transport across the abluminal membrane [189]. In the luminal membrane, the transport of β-amyloid into blood has been suggested to be mediated by ABCB1 [190-192]. In a mouse model of Alzheimer's disease (the human amyloid precursor protein (hAPP)-overexpressing Tg2576 strain) the loss of mouse ABCB1 homologue was shown to correlate with accelerated accumulation of β-amyloid in the brain [193]. In the same study, it was also shown that inhibition of Abcb1 by PSC833 (a potent ABCB1 inhibitor) resulted in decreased transport of β-amyloid into the lumen of brain capillaries isolated from wild-type mice. The data from animal studies parallels data from human studies. Studies of Alzheimer's disease patients show decreased level of ABCB1 at the BBB suggesting a progressive loss and an inverse correlation between ABCB1 expression and deposition of β-amyloid in the brains of Alzheimer's disease patients [194, 195]. These findings suggest that reduced ABCB1 on luminal membranes of blood-brain barrier epithelial cells contributes to β-amyloid accumulation in the brain. Internalisation of proteins from the membrane is often regulated by ubiquitination and in the Linton Lab, it was shown by one of my colleagues that ABCB1 can be ubiquitinated by Nedd4-1 (Prof. Linton, personal

communication) (Figure 4.1) and another colleague has shown that expression of Nedd4-1 reduces surface expression of ABCB1 expressed stably in Flip-IN cells (Figure 4.2).

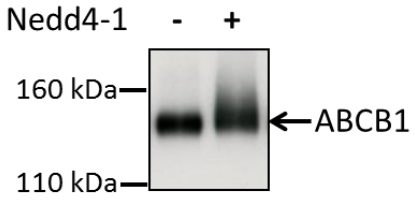

Figure 4.1: Wild-type ABCB1 purified from insect cells was ubiquitinated by Nedd4-1 *in vitro* and the ubiquitination status was investigated by SDS-PAGE and western blotting (Dr. Tasha Ritchie, Linton Group, personal communication). The left lane shows the purified untreated wild-type protein and the right lane represents the Nedd4-1 treated protein. The mobility shift between the two lanes suggests that ABCB1 can be ubiquitinated by Nedd4-1.

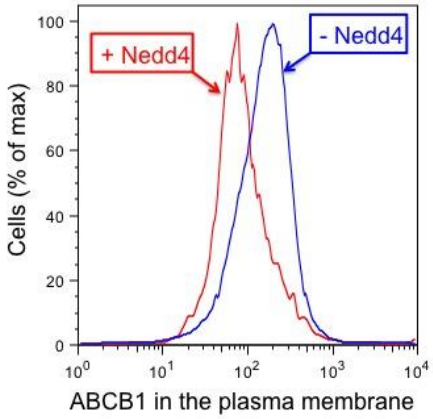

Figure 4.2: Histogram showing that Nedd4-1 expression in cells lowers ABCB1 density at the plasma membrane. Flip-in-ABCB1 cells stably expressing ABCB1 were transiently-transfected with pmCherry-Nedd4.1 or control plasmid. The level of ABCB1 at the plasma membrane was measured by flow cytometry after incubating the cells with saturating levels of anti-ABCB1 monoclonal antibody 4E3 and a red-fluorescent secondary (Linton Lab, unpublished data).

Herein, I extend these observations, and identify the residues ubiquitinated by Nedd4-1. This was achieved by purification of wild-type human ABCB1 and mass spectrometry after ubiquitination by Nedd4-1 *in vitro*. This required a multistep approach described in Figure 4.3.

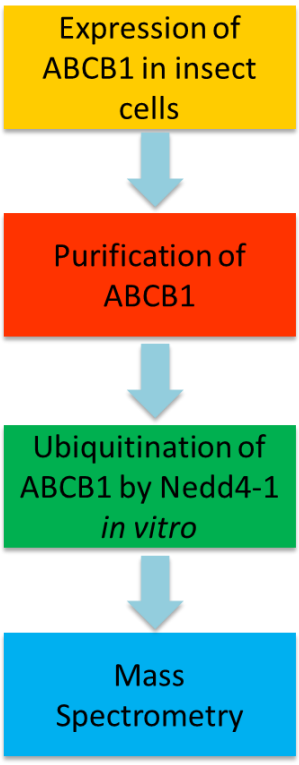

Figure 4.3: Multistep approach used in this study.

4.2. Ubiquitination

Ubiquitination is a post-translational modification which regulates several cellular functions. Although the first identified role of ubiquitination was to target proteins for degradation by the 26S proteasome, further roles in regulating many diverse cellular processes have been revealed. These processes include protein quality control, cell-cycle progression, membrane protein trafficking and control of protein subcellular localization, internalization of signal receptors, gene transcription and even in some cases prevention of protein degradation [54, 196-198]. Post-translational modification by ubiquitin can be formed in three ways; monoubiquitination, multi-monoubiquitination or polyubiquitination (Figure 4.4).

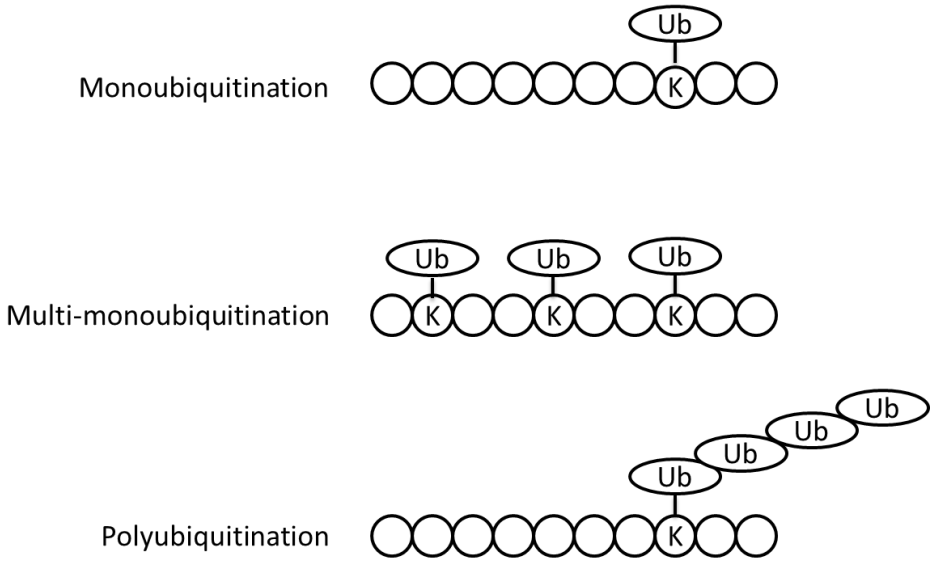

Figure 4.4: Ubiquitination modifications.

Ubiquitin is a 76 amino acid polypeptide which is most commonly attached covalently to target protein lysine residues. The sequential activation of three enzymes is required for ubiquitination: the ubiquitin-activating enzyme (E1), the ubiquitin-conjugating enzymes (E2s), and the ubiquitin ligases (E3s). In an ATP-dependent pathway, the E1 enzyme activates the C-terminus of ubiquitin which forms a thiol-ester bond between ubiquitin and the active site Cys residue of E1. The E2 enzyme carries the activated ubiquitin from the E1 enzyme to the E3 enzyme. The E3 enzyme recognizes the target substrate(s) and transfers the activated ubiquitin from the E2 enzyme to a lysine or, rarely, to a cysteine residue of the substrate [199], or to the growing end of a polyubiquitin chain on a substrate protein. The E3 ligase catalyses the formation of an isopeptide bond between the carboxyl group of glycine residue 76 of the ubiquitin and the ε -amino group of a lysine residue within the substrate [54] (Figure 4.5). All three steps are necessary for all ubiquitination reactions, whatever the fate of the substrate. Polyubiquitination studies showed that all seven lysine residues (K6, K11, K27, K29, K33, K48, K63) in the ubiquitin protein can be used for

polyubiquitin chain formation and that K63-linked chains can result in nonproteolytic outcomes such as trafficking or lysosomal degradation, whereas K48-linked polyubiquitination usually results in 26S proteasomal degradation [200]. Ubiquitination is a reversible process; the human genome encodes deubiquitinating enzymes which can cleave ubiquitin from its substrates [201].

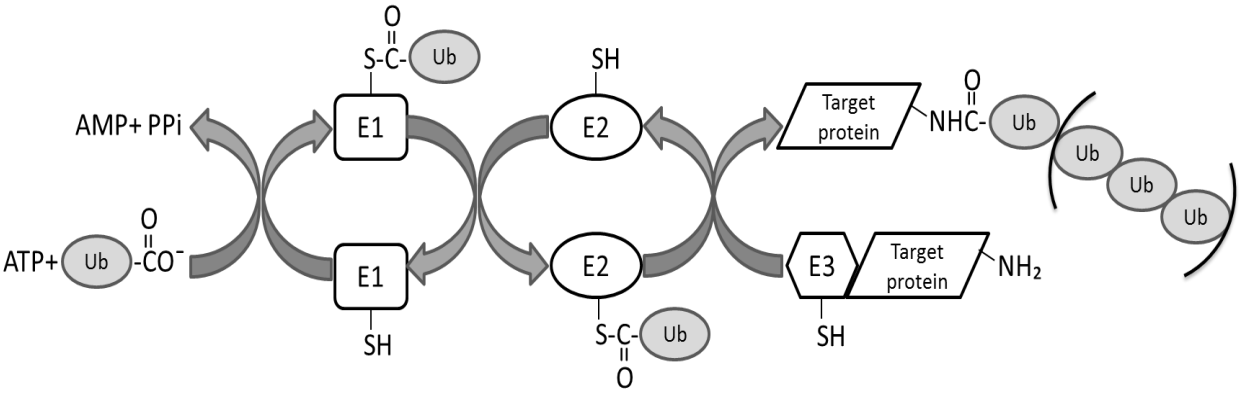

Figure 4.5: The ubiquitination cascade. Free ubiquitin (Ub) is activated by the ubiquitin-activating enzyme (E1), resulting in formation of a thioester bond between the C-terminal glycine of Ub and the active site cysteine residue of E1. Activated Ub is then transferred to the active site cysteine residue of the ubiquitin-conjugating enzyme (E2). Then, Ub is transferred from E2 to the ubiquitin ligase (E3) which is bound to the target protein, forming an isopeptide linkage between Ub and the ε-amino group of a lysine in the target protein.

4.3. The Human Nedd4 Family

There are two main classes of E3 enzymes; the RING (Really Interesting New Gene) finger and the HECT (Homologous to E6-AP Carboxy Terminus) domain E3s. The RING E3s mediate the E2-substrate interaction to promote ubiquitin transfer directly from E2s to substrates [202]. The HECT domain was first characterized in the human ubiquitin protein ligase E6-AP (E6-associated protein) [203] and, unlike RING fingers, HECT domains are always located C-terminally, and provide a catalytic contribution to transfer the ubiquitin to the substrate from a thiol-ester intermediate formed with a conserved cysteine residue within the E3 ligase [204].

Nedd4 (Neural precursor cell Expressed, Developmentally Down-regulated 4) is a HECT domain E3 ligase which was first described in 1992 in a screen for developmentally down-regulated genes in the early embryonic mouse central nervous system [205]. In the study by Kumar *et al*., ten cDNA clones were isolated and described as Nedd 1 to 10. Although the expression of *Nedd4* mRNA levels decrease gradually in adult central nervous system, it is expressed in almost all adult tissues.

In human, there are 9 distinct members of the Nedd4 family (Figure 4.6) [206]. The domain organization of all 9 members is similar, each contain a C2 domain, 2-4 WW domains, and a C-terminal HECT domain. The C2 domain was first described in classical protein kinase C isoforms as a Ca^{2+}-dependent phospholipid binding domain [207, 208]. This domain is involved in protein localization and trafficking and it has been shown that N-terminally deleted Nedd4 localizes to the nucleus whereas full-length Nedd4 localizes in the cytosolic periphery [209]. The WW domain is a small protein-protein interaction module (approximately 40 amino acids), named for the presence of two highly conserved tryptophan residues approximately 20-22 amino acids apart. [210]. The WW domains mediate substrate recognition and are classified based on their recognition sequences. Class I WW domains, which include the Nedd4 family WW domains, bind PxY motifs, Class II domains bind PPLP sequences, Class III domains bind [R]-R/K/x-PP or PP-R/x-[R] protein sequences and Class IV domains bind (phospho-S/T)P sequences [211].

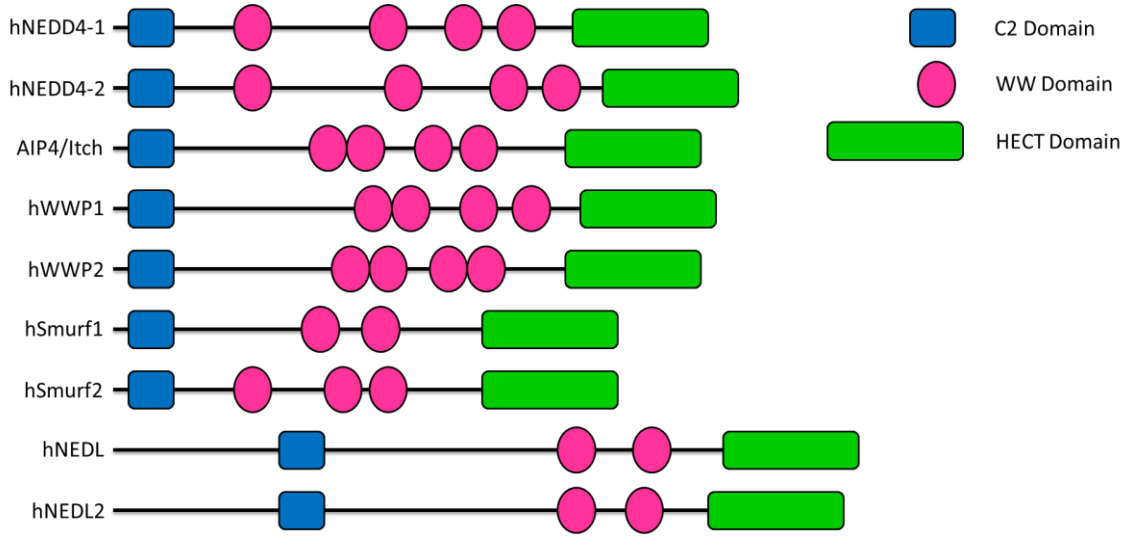

Figure 4.6: The human Nedd4 family. The C2 domain is represented by a blue box, the WW domain is depicted by pink circles and the HECT domain by a green bar. Diagrams are not to scale (modified from Ingham *et al.* [206]).

In the human genome, from the 9 distinct members of the Nedd4 proteins, Nedd4-1 and Nedd4-2 are the two most closely related. The phylogenetic analysis of the two proteins indicates that Nedd4-1 is the ancestral member of the family with a single homologue in *S. cerevisiae* whereas *D. melanogaster* has four members of the Nedd4 family but no orthologue of Nedd4-2 [212]. Nedd4-1 and Nedd4-2 share 64% identity and 74% similarity at the protein level and both have four WW domains that recognize the PY motif (PxY) [213]. While Nedd4-1 is ubiquitously expressed, Nedd4-2 expression is more restricted, being high in liver and kidney, and expressed to a lesser extent in heart, brain, and lung [214].

4.4. Expression of Recombinant Protein

To identify the ABCB1 residues ubiquitinated by Nedd4-1, required first the purification of ABCB1. Four different protein expression hosts are commonly used to express recombinant proteins: bacteria, yeast, insect cell or mammalian cell expression systems. To purify membrane proteins each has its own advantages and disadvantages.

Bacterial and yeast protein expression systems are easy to cultivate and quick to grow in large amounts and are relatively inexpensive. On the other hand, their cell walls need to be broken down either by lysozyme, a glycoside hydrolase or high-pressure homogenization or sonication. In addition, membrane protein post-translational modifications in bacteria differ from mammalian post-translational modifications which can lead to misfolding and degradation of the recombinant membrane protein. Another important difference is that the yeast cell membrane does not contain cholesterol but ergosterol and zymosterol which might affect insertion and localization of the membrane protein.

Insect and mammalian cell protein expression systems are more expensive to grow, and insect cells need to be infected with baculovirus which is also expensive and time-consuming to generate, but insect cells remain simpler to maintain as large-scale cultures than mammalian cells. Both insect and mammalian cells have complex post-translational modifications. Mammalian cells tend to glycosylate with complex N-glycans including mannose, N-acetyl glucosamine, galactose and, terminally, sialic acid, whereas insect cells glycosylate essentially with mannose [215]. Nevertheless, insect cells are arguably a more natural host than yeast for recombinant mammalian proteins. Although mammalian cell protein expression would be the most natural for ABCB1, the protein yield is often poor compared to insect cells and this is the reason why insect cell expression was chosen for this study. Once the membrane protein of interest is expressed and the cell membrane fraction has been collected (by homogenization and differential centrifugation), the protein needs to be solubilized from the membrane to enable purification. This is routinely achieved by the use of detergents and sonication.

4.5. Detergent Solubilisation of Membrane Proteins

Detergents are amphipathic molecules, consisting of a polar head group that determines the detergent's class and a nonpolar hydrophobic tail having aliphatic or aromatic character. The ionic character of the polar head group designates the detergent as either ionic (charged, either anionic or cationic), nonionic (uncharged) or zwitterionic (both positively and negatively charged groups but with a net charge of zero).

Membrane proteins have regions of high hydrophobicity which are embedded in the membrane under physiologic conditions and thus they have limited solubility in aqueous solutions. Because of this, membrane proteins need to be solubilised with detergents which break the membrane structure. Lipids are also included to mimic the physiologic environment of the protein and help maintain its stability [216]. The choice of the detergent is the crucial part of solubilisation; it must be strong enough to solubilise the membrane effectively, but gentle enough not to denature or unfold the protein. Within the available detergent range, zwitterionic or non-ionic detergents are the detergents of standard use for most membrane proteins because of their ability to retain the function of the protein [217].

The detergents exhibit unique properties in aqueous solutions such as forming thermodynamically stable, non-covalent aggregates called micelles when the detergent monomer concentration increases above a critical narrow-range concentration called the critical micellar concentration (CMC) [218]. Detergents solubilize membrane proteins by mimicking the natural lipid bilayer environment physiologically inhabited by the protein to

generate protein-detergent micelles [219]. The process involves several steps. Initially, the detergent monomers bind and disrupt the cell membrane and then solubilisation begins above the critical solubilisation concentration (CSC) at which very small membrane sheets or mixed detergent-lipid-protein micelles are formed. After reaching the CMC, the membrane is fully solubilized and detergent-lipid and detergent-protein micelles are formed [220].

4.6. Baculovirus Expression Systems

The Baculovirus expression system is a viral system which has been used to express heterologous genes from different sources in insect cells. The *Baculoviridae* is a family of occluded DNA viruses which are pathogenic, predominantly to holometabolous insects. They are enveloped, double-stranded DNA viruses with rod shaped nucleocapsids. Taxonomically, baculoviruses divide into three subgroups; A, B and C, depending on their virion deposition. Subgroup A can have many virions occluded within single intranuclear crystals called polyhedra and are therefore described as the nuclear polyhedrosis viruses (NPVs). NPVs are subdivided into two further classes depending on the extent of their nucleocapsids within the envelope; present as either single (SNPVs) or multiple (MNPVs). The most extensively studied baculovirus strain is the *Autographa californica* multiple nuclear polyhedrosis virus (AcMNPV). Subgroup B are the granulosis viruses (GVs) which have only one single virion within each polyhedron. Subgroup C is the nonoccluded baculoviruses (NOBs) which have no occlusion bodies surrounding the virions [221].

The polyhedra, which are also known as the occlusion bodies, are composed of 29 kDa polyhedrin proteins and are very stable to protect the virus outside the host. In the life cycle of NPVs, there are two virion phenotypes; the polyhedra-derived virus (PDV) (occluded virus) which is found within the polyhedra and budded virus (BV) (nonoccluded virus) which is found in the host cells [221]. Envelopes of PDVs are specialized for interaction with polyhedrin and for infection of the columnar epithelial cells of the insect midgut whereas BV envelopes are specialized for infection of the rest of the tissues in insect cell body. PDVs enter midgut epithelial cells by fusion whereas BVs enter cells by adsorptive endocytosis. Only the BV envelopes contain a glycoprotein called gp64 which is highly important for BV endocytosis and infectivity [222]. Infectivity of the BVs is much higher than the PDVs [223]. The BVs are therefore the virion of choice for *in vitro* experiments, and for safety reasons (to limit survival outside of the lab), the polyhedrin gene is typically replaced with the gene of interest. PDVs cannot therefore be formed by recombinant virus under tissue culture conditions.

4.6.1. The Baculoviral Genome

The replication cycle of baculoviruses is generally regulated at the transcriptional level. Baculoviral transcription is divided into three stages, called early, late and very late. 0-8 hours post infection is the early stage and is driven by cellular RNA polymerase II to produce enzymes that will support viral DNA replication. The start of viral DNA synthesis terminates the early stage and initiates the late stage which takes place between 8-18 hours post infection. In the late stage, genes encoding structural proteins of the BVs are expressed and BVs are assembled and released from the host cell during this time.

In the very late stage, although some BVs are produced, the pattern of transcription changes in favour of PDVs. Genes important in PDV assembly in occlusion bodies, such as P10 and polyhedrin, are expressed in the very late stage.

The two baculoviral genomes used for the work described herein are AcMNPVs, which have a circular, double-stranded, super-coiled DNA genome that encodes about 150 open reading frames (orfs) [224].

These expression systems have been engineered to differentiate the parental from the recombinant virus. The *E. coli lacZ* (β-galactosidase) gene has been inserted into the virus genome so the recombinant viral plaques could be distinguished by X-gal staining. Then a unique restriction endonuclease site (*Bsu*36I) was introduced at the polyhedrin locus (Ac8) to linearize the virus genome prior to insertion of the gene of interest via a transfer vector [225]. Later, the polyhedron gene was replaced by the *lacZ* gene that included a *Bsu*36I site to allow the selection of the clear plaques of recombinant virus. Following this, two *Bsu*36I sites were introduced, covering *lacZ* gene at the polyhedrin locus and a section of ORF1629 which is vital for virus replication [226]. This led to a very high efficiency of recombinant virus acquisition because after *Bsu*36I digest, non-recombinant virus loses the ability to replicate unless the ORF1629 is rescued by recombination with the transfer vector, which is also used to introduce the gene of interest (described below).

4.6.2. flashBAC

The *flash*BAC genome contains a bacterial artificial chromosome (BAC) at the polyhedrin gene locus, replacing the polyhedrin gene and lacks a section of the essential ORF1629. In addition, it also lacks the baculoviral chitinase gene (ORF121, Ac126) which is involved in liquefaction of insect tissues with the help of cathepsin, but is considered to limit the expression of recombinant secreted or membrane proteins because it competes for translation sites on the rough endoplasmic reticulum (ER). It is compatible with most of the baculovirus transfer vectors.

4.6.3. ProFold™-ER1

The ProFold™-ER1 genome contains the lacZ gene in place of the polyhedrin gene and it also lacks a section of the essential ORF1629. In addition to these, the ProFold™-ER1 genome encodes calreticulin (to aid protein folding in the ER and efficient trafficking to the Golgi), protein disulphide isomerase (which improves protein folding by the formation and breakage of disulphide bonds), and the *Aequorea victoria* green-fluorescent protein (GFP, for the monitoring of recombinant baculovirus infection). Simultaneous high level expression of four recombinant proteins was provided by localising these genes far away from each other in the baculovirus genome. The ProFold™-ER1 baculovirus expression system is compatible with most transfer vectors including BacPAK9 which can also be used with flashBAC system.

4.7. Mass Spectrometry

Mass Spectrometry is an analytical tool used for measuring the mass of a molecule by separation of its ions according to the mass/charge ratios (m/z). It was used in this study to identify Nedd4-1 ubiquitination sites on ABCB1 (the mass spectrometry was outsourced but the raw data was analysed by myself). Mass spectrometry is used in various applications such as pharmaceutical, clinical and environmental assays and also in biotechnology. In biotechnology, mass spectrometry can be used for amino acid sequencing, oligonucleotide sequencing or to investigate protein structure or post-translational modifications like glycosylation, phosphorylation and ubiquitination.

There are several different types of mass spectrometer available but the basic principal is always the same. Within a mass spectrometer, the sample molecules are ionized by an ionisation source to easily affect their deviation while passing through an electric or magnetic field. The ions are then accelerated to have the same kinetic energy and deflected by the analyser (electric or magnetic field) according to their masses. The lighter they are, the more they are deflected and the *vice versa* for heavier molecules. Other than mass, the charge of these ions is also important. The more charge, the more the ion is deflected. These factors are combined into mass/charge ratio (m/z) which is detected by a detector.

4.7.2. Linear Ion Trap Quadrupole with Orbitrap Mass Spectrometry

Linear Ion Trap Quadrupole (LTQ) Orbitrap Velos (Thermo Fisher Scientific, Germany) is a high resolution tandem mass spectrometer (MS/MS). The combination of a Linear Ion Trap Quadrupole (LTQ) Velos™ (dual-pressure ion trap assembly) and the Orbitrap™ allows fast isolation and high capture efficiency into the linear ion trap and high accuracy and resolution analysis in the Orbitrap.

A TriVersa Nanomate chip-based electrospray device (Advion, NY, USA) connected to the LTQ Orbitrap Velos is used to provide the electrospray ionisation (ESI). ESI is a soft ionisation method that produces multiply charged ions [227].

The LTQ can store, isolate, and fragment ions and later send them to the orbitrap for further analysis. The LTQ uses a collision induced dissociation (CID) technique in which a neutral gas (helium in this study) is used to fragment the ions. In this technique, the ions are accelerated to a high kinetic energy and then collisions occur between the ions and helium which result in an increase in internal energy of the ions and subsequent dissociation producing b and y ions. From the linear ion trap to the Orbitrap™, ions move through gas-free octapole into the gas-filled curved linear trap (C-Trap). The Orbitrap™ consists of an outer barrel-like electrode and an inner spindle-shaped central electrode that form an electrostatic field to trap ions in an orbit around the central electrode [228]. The outer electrode is split in half to detect the image current produced by axial oscillating ions. The detected image current is digitized and converted into frequency and then mass spectra by Fast Fourier Transformation (FFT). The instrument acquires the frequencies of these axial oscillations and therefore the mass-to-charge ratios of the ions (Figure 4.7).

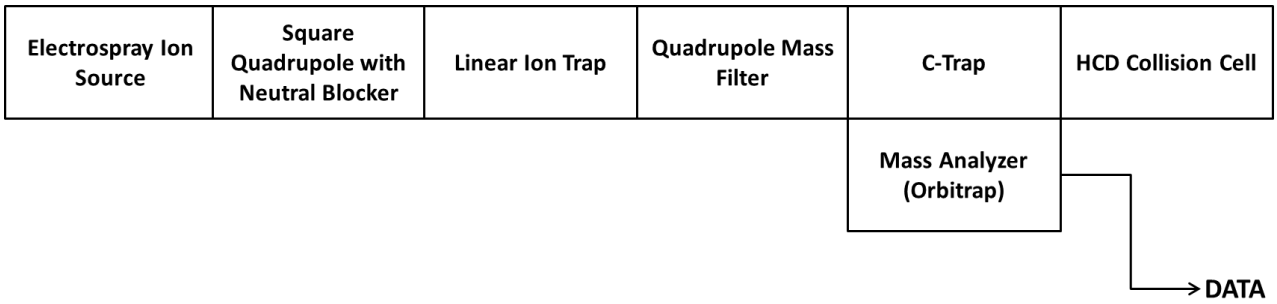

Figure 4.7: Schematic figure of LTQ Orbitrap XL™ (Thermo Fisher Scientific, Germany). Electrospray ionization introduces the sample to the square quadropole which filters the ions according to the mass/charge (m/z) ratio by an oscillating electrical field. The selected ions are fragmented in the collision chamber of LTQ linear ion trap where collision induced dissociation (CID) with helium was used to fragment ions. From the linear ion trap to the Orbitrap™, ions move into the gas-filled curved linear trap (C-Trap) to identify the m/z ratio of the fragments.

4.8. Aims

- To express recombinant ABCB1 and compare the protein yield from *flash*BAC and ProFold™-ER1.
- To purify recombinant human ABCB1.
- To identify the ABCB1 residues that are ubiquitinated by Nedd4-1.
- To identify putative binding site(s) for Nedd4-1 on ABCB1.

4.9. Results

4.9.1. Transfer vector generation, pBacPAK9

As described in section 2.8., the coding cDNA for wild-type ABCB1-12His was excised from the pCI-neo mammalian expression vector by *BstE*II and *Nhe*I digests (Figure 4.8). The 3.9 kb cDNA fragment was then ligated between the *BstE*II and *Nhe*I sites of the pBacPAK9 vector to generate pBacPAK9-ABCB1-12His (Figure 4.9). Putative clones were digested with *Bal*I and those matching the expected restriction digest profile were sequenced to confirm the veracity of BacPAK9 ABCB1-12His (Figure 4.10).

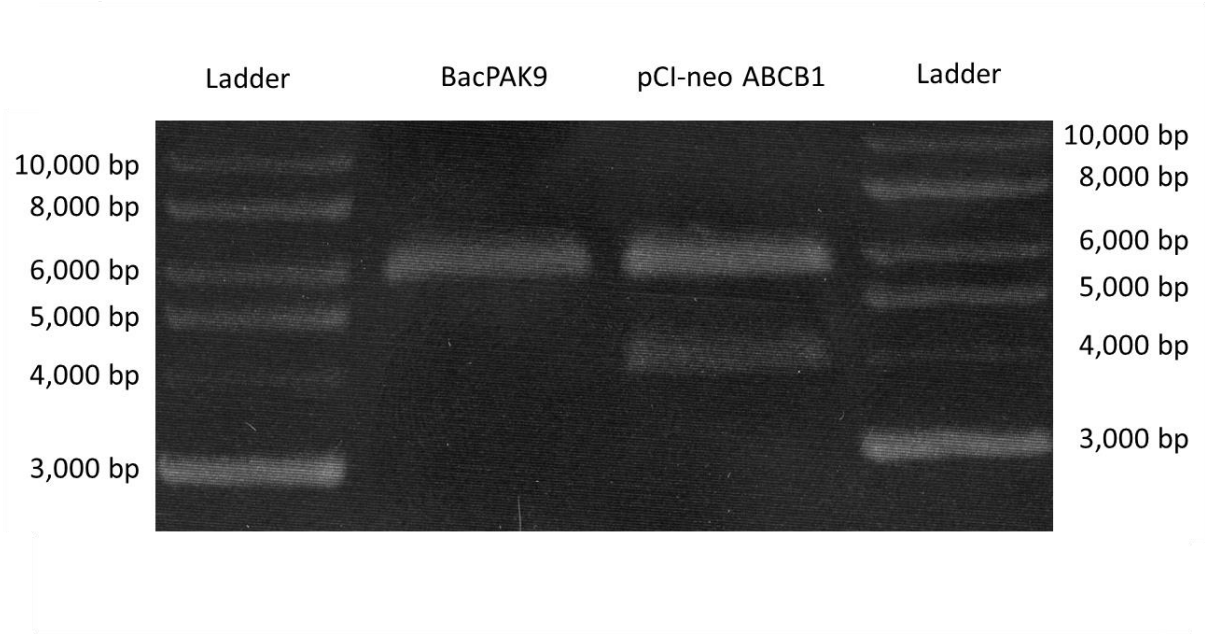

Figure 4.8: *Nhe*I and *BstE*II digest of pCI-neo ABCB1-12His. After *Nhe*I and *BstE*II digest, pCI-neo ABCB1-12 His should release two DNA fragments of 3888 and 5542 basepairs (bp). (Please see Figure 2.1 for the vector map of pCI-neo ABCB1-12His.)

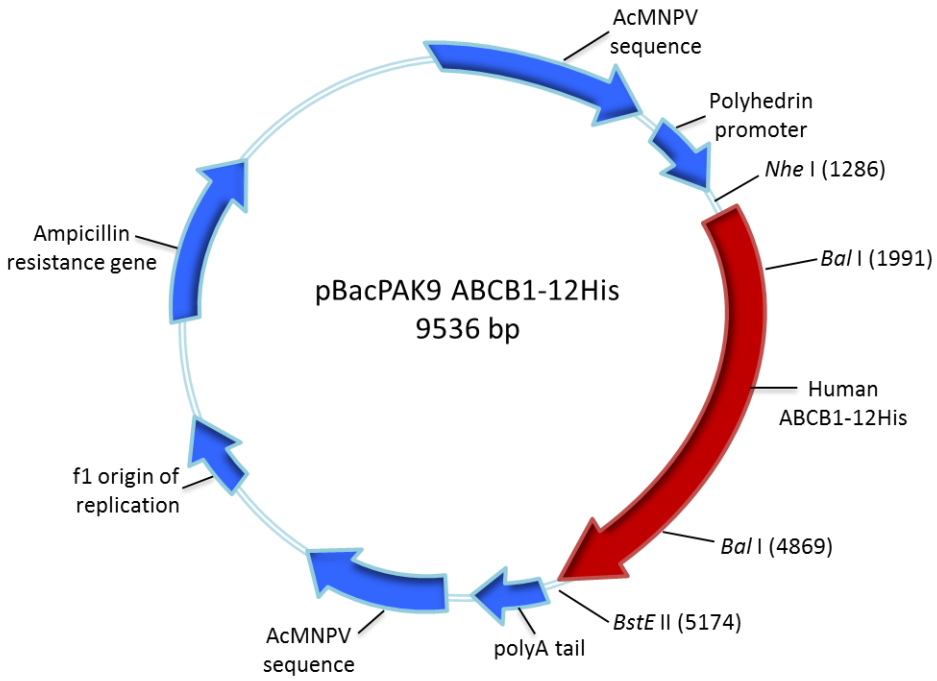

Figure 4.9: pBacPAK9 ABCB1-12His.

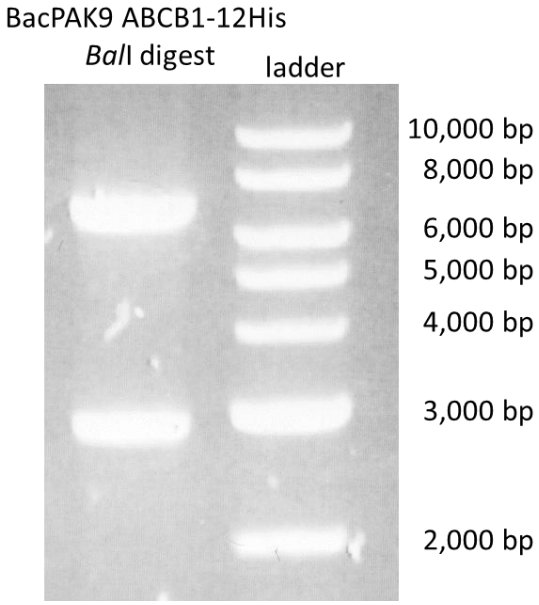

Figure 4.10: *Bal*I digest of BacPAK9 ABCB1-12His. The expected fragments should measure 6658 and 2878 basepairs (bp).

4.9.2. Generation of recombinant baculovirus

To generate a recombinant baculovirus, the linear baculoviral genomes (*flash*BAC and ProFold™-ER1) must recombine with the transfer vector (BacPAK9 ABCB1-12His) to reform ORF1629 that is vital for virus replication (see section 4.6.1.). This helps to ensure pure samples of recombinant baculovirus.

4.9.3. Amplification and titration of working stocks

As detailed in section 2.2. the rationale for baculoviral amplification is to infect insect cells with a low ratio of baculovirus to cell number (multiplicity of infection; MOI) to allow cell growth to continue while multiple cycles of viral infection and release occur. To determine the titre of the virus samples, plaque assays were performed as described in the materials and methods section (section 2.2.8.). Briefly, monolayers of Sf21 cells were infected with a series of dilutions of the baculovirus intermediate stock and overlayed with low melting point agarose, then incubated at 28°C for 3 days. After 3 days, the cells were stained with neutral red and as the infected dead cells do not internalise the dye, the dead cell populations were visualised as clear plaques in a red monolayer. After acquiring the virus titre, suspension cultures were infected at a low MOI of 0.1 (1 virus to 10 cells) to acquire the intermediate and working stocks.

Insect cells were then infected with incremental volumes of the baculoviral working stock to determine the optimal ratio for ABCB1 expression (Figure 4.11). Recombinant *flash*BAC or ProFold™-ER1 working stock baculoviruses engineered to express human ABCB1 were used to infect Sf21 cells at a density of $1x10^6$ cells in 35mm dishes to compare protein

expression levels. After 72 hours post infection, the insect cells were solubilised in equal volumes (500 µl) of 2% SDS lysis buffer. Equal volumes of the whole cell lysates were diluted with loading buffer (please see section 2.13.1.), the protein separated by SDS-PAGE and blotted onto nitrocellulose membrane. All immunoblots were probed with C219 anti-ABCB1 antibody (Cambridge Bioscience, UK). Infection with 150 µl of *flash*BAC and 20 µl of ProFold™-ER1 working stocks were found to give the highest levels of ABCB1 expression from $1x10^6$ cells.

A.

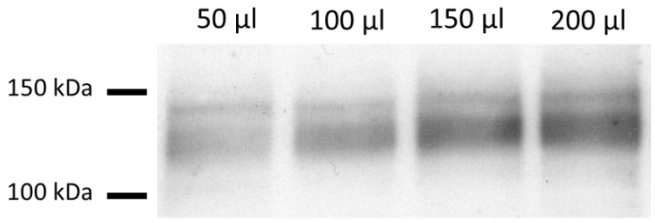

B.

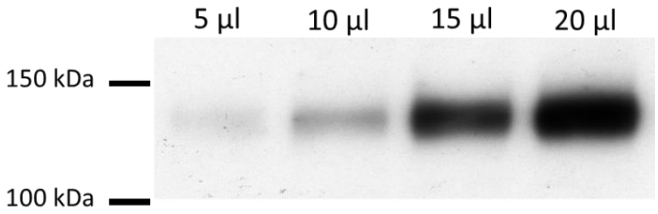

Figure 4.11: Titration of baculovirus working stocks by western blotting for ABCB1 expression. A. ABCB1 expression of *flash*BAC working stock baculovirus in incremental amounts B. ABCB1 expression of ProFold™-ER1 working stock baculovirus in incremental amounts. Microliters indicate the volume of virus added to $1x10^6$ Sf21 cells in Sf-900™ II SFM media. All the expression experiments were performed by seeding equal amounts of insect cells ($1x10^6$) in 35 mm dishes. After 72 hours post infection, the cells were lysed and equal volumes of each sample were loaded onto SDS-PAGE gels.

4.9.4. Time course for ABCB1 expression in insect cells

The optimal post-infection harvest time, to obtain the maximum recombinant protein yield, was determined by a time course assay. Sf21 cells were infected with *flash*BAC or ProFold™-ER1 virus in four different 35 mm dishes. The cells were harvested 24, 48, 72 and 96 hours post-infection (Figure 4.12).

A.

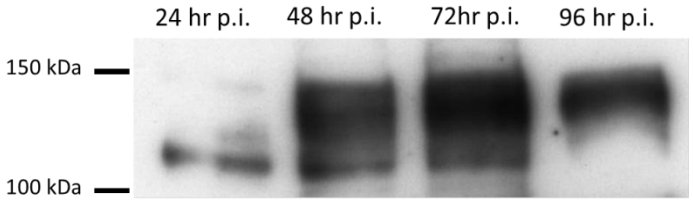

B.

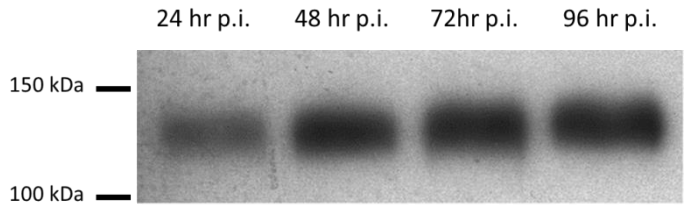

Figure 4.12: Time course for ABCB1 expression in Sf21 cells with *flash*BAC (A) and ProFold™-ER1 (B) baculoviruses. (p.i. indicates post infection). *flash*BAC baculovirus ABCB1 expression was highest at 72 hours post infection whereas ProFold™-ER1 baculovirus ABCB1 expression levels are similar at 48, 72 and 96 hours post infection.

4.9.5. Expression yield from ProFold™-ER1 is better than flashBAC

After determining the optimal virus titre and the harvest time to acquire the highest protein yield, the two recombinant baculoviruses (*flash*BAC and ProFold™-ER1) were compared with each other. $1x10^6$ Sf21 cells were seeded into 35 mm dishes and infected with *flash*BAC or ProFold™-ER1 virus. After 72 hours incubation, the monolayer cultures were harvested and ABCB1 was quantified by immunoblotting. ABCB1 expression was highest with ProFold™-ER1 virus compared to *flash*BAC virus (Figure 4.13). Two protein forms were visible in the immunoblots of *flash*BAC expressed ABCB1, the larger form migrating at 140 kDa likely corresponds to the mature ABCB1 and the smaller 90 kDa form was probably due to degradation. Only one single protein form migrating as a 140 kDa species consistent with mature full-length ABCB1 was observed with ProFold™-ER1 virus infection.

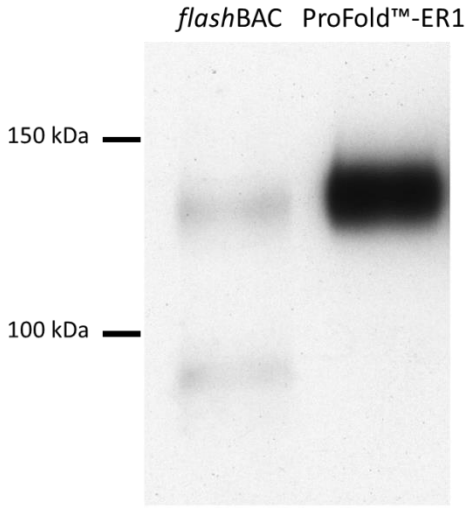

Figure 4.13: Comparison of ABCB1 expression from ProFold™-ER1 and *flash*BAC baculovirus. The same number of cells were infected under the same conditions. Whole cell lysates were prepared in equal volumes of 2% SDS and equivalent fractions were loaded onto the gel.

4.9.6. Expression in Sf21 Vs. Hi5 cells

ProFold™-ER1 virus was shown to give a higher yield of ABCB1 than *flash*BAC and before growing large scale cultures, the expression levels in Sf21 cells and Hi5 cells were analysed. The two insect cell lines ($1x10^6$ cells in 35 mm dishes or 100 ml suspension culture at a density of $1x10^6$ cells/ml) were infected with equal volumes of ProFold™-ER1 virus (20 µl virus per $1x10^6$ insect cells). After 72 hours, monolayers and suspension cultures were harvested and tested for ABCB1 expression by western analysis. Sf21 cells in Sf-900™ II SFM media generated significantly more ABCB1 compared to Hi5 cell in EX-CELL® 405 serum-free medium (Figure 4.14). ImageJ densitometry analysis (Rasband, W.S., ImageJ, U. S. National Institutes of Health, Bethesda, Maryland, USA, http://imagej.nih.gov/ij/, 1997-2014.) showed that Sf21 cell suspension or monolayer cultures express 2.4 times more ABCB1 than Hi5 cells.

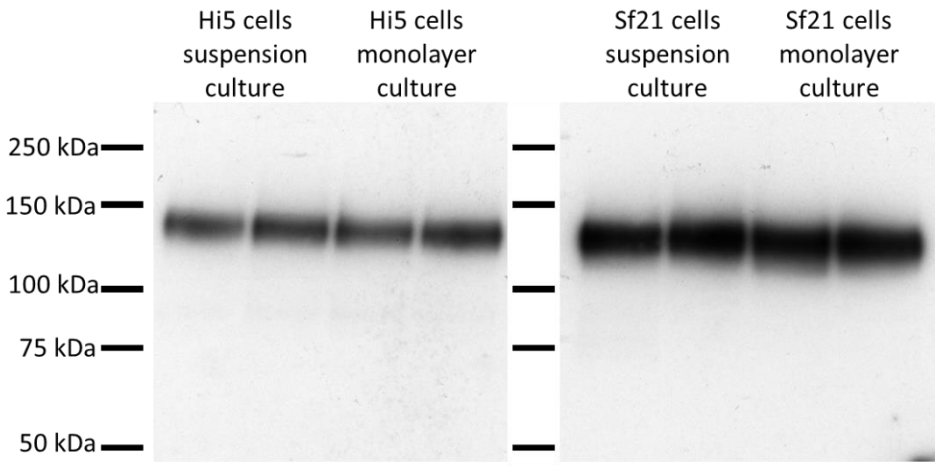

Figure 4.14: ProFold™-ER1 virus infection of suspension and monolayer cultures of Hi5 and Sf21 cells in duplicates which were run on the same gel.

4.9.7. Large scale ABCB1 expression from the ProFold™-ER1 baculovirus

Large scale infections of Sf21 cells in Sf-900™ II SFM media were performed in round bottom glass flasks shaking at 27°C. Suspension cultures of $2x10^6$ Sf21 cells/ ml in Sf-900™ II SFM media were infected with 20 µl virus/ $1x10^6$ cells and harvested 72 hours post-infection. Membrane fractions were prepared by mechanical homogenisation.

4.9.8. Purification of recombinant ABCB1 from Sf21 insect cells

4.9.8.a. Membrane fractionation

Insect cell suspension cultures were lysed by homogenisation using an Ultra-Turrax T25 homogeniser. Membrane fractions were obtained by a high speed centrifugation following a low speed centrifugation step to first remove unbroken cells and nuclei.

4.9.8.b. Quantification of total protein yield

The protein content of membrane fractions resuspended in 'resuspension buffer' was measured using bovine serum albumin (BSA) standards and spectrophotometry (see section 2.14.1.).

4.9.8.c. Solubilisation

n-dodecyl β-D-maltoside (DDM) is a water soluble, non-ionic detergent. It has been widely used with ABC proteins and in ABCB1 purification studies as a non-denaturing detergent. A recent study suggested that DDM is the most effective detergent in extracting ABCB1 from SF+ insect cells from a panel of 15 non-ionic detergents [229]. Previous studies have shown that ABCB1 is particularly sensitive to the removal of lipids during the purification process [230] and also to the level of cholesterol [231, 232]. The membrane preparations were therefore solubilised with a mixture of DDM and *E. coli* lipids, supplemented with 20% cholesterol. The solubilisation buffer also contained 20% (v/v) glycerol, which has been shown to act as an osmolyte protectant [233]. DDM at a concentration of 2% with 72 mg lipid (4:1 ratio of total *E. coli* lipid:cholesterol) was used to solubilise crude membrane preparations in a volume of 18 ml per 100mg protein. The membrane fractions were resuspended and solubilised by repeated syringing through a 25G needle at 4°C (on ice). The insoluble fraction was pelleted by high speed ultracentrifugation and the supernatant recovered as the solubilised protein fraction.

4.9.8.d. Nickel-NTA affinity chromatography

The recombinant ABCB1 includes a 12-His tag at its C-terminus. This was exploited to purify the recombinant protein by metal affinity chromatography. The polyhistidine tag will bind to divalent cations, in this case nickel, which is immobilised in a nitroloacetic acid (NTA) resin. This interaction binds and immobilizes the recombinant protein to the resin and can be eluted later with imidazole. Imidazole competes with the polyhistidine tag to bind to the

nickel. The solubilised membrane protein fraction was incubated with Ni-NTA resin (2 ml, 50% slurry per 15 ml soluble membrane protein) for over an hour at 4°C.

A low concentration of imidazole (10 mM) was used during the binding reaction to limit non-specific binding of other proteins and higher concentrations (40-500 mM) were used to wash the resin and extract the bound ABCB1.

Following incubation of the Ni-NTA resin with the solubilised protein, the resin was pelleted by slow speed centrifugation and the unbound material was decanted. The resin was then washed four times with 20 bed volumes of wash buffer containing incremental concentrations of imidazole (40 mM, 80 mM, 100 mM, 120 mM) to remove protein bound non-specifically. The remaining bound material that comprised ≥ 95% pure ABCB1-12 His was eluted with 500 mM imidazole (Figure 4.15).

Protein fractions and purified ABCB1 were TCA precipitated, resolubilised and separated by SDS-PAGE. The gel was stained with colloidal blue and visualised by ODYSSEY® (Figure 4.15). The yield of purified protein was quantified using BSA standards (Figure 4.16). From 100mg of total membrane protein 45 µg of ABCB1 was purified. The main losses were observed in the unbound flow through material and also in the third and the fourth washes (Figure 4.17).

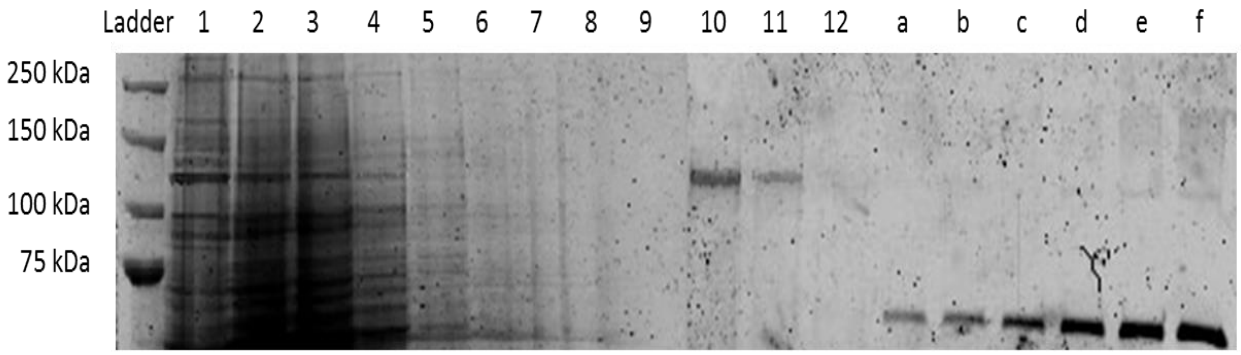

Figure 4.15: Polyacrylamide gel stained with colloidal blue and visualised by ODYSSEY®, showing the proteins from each fraction. Lane: 1, 30 µl crude membrane preparation (0.6 % of total volume); 2, 30 µl resuspended membrane preparation (0.15 % of total volume); 3, 30 µl solubilised membrane preparation (0.2 % of total volume); 4, 200 µl unbound Ni-NTA resin flow through (1.3 % of total volume); 5-8, 500 µl washes 1-4 (2.5 % of total volumes); 9, 500 µl elution 0 (buffer pH change; 2.5 % of total volume); 10-12, 30 µl elutions 1-3 (1.5 % of total volume); a-f increasing BSA concentrations (0.1 µg, 0.2 µg, 0.4 µg, 0.6 µg, 0.8 µg, 1 µg respectively).

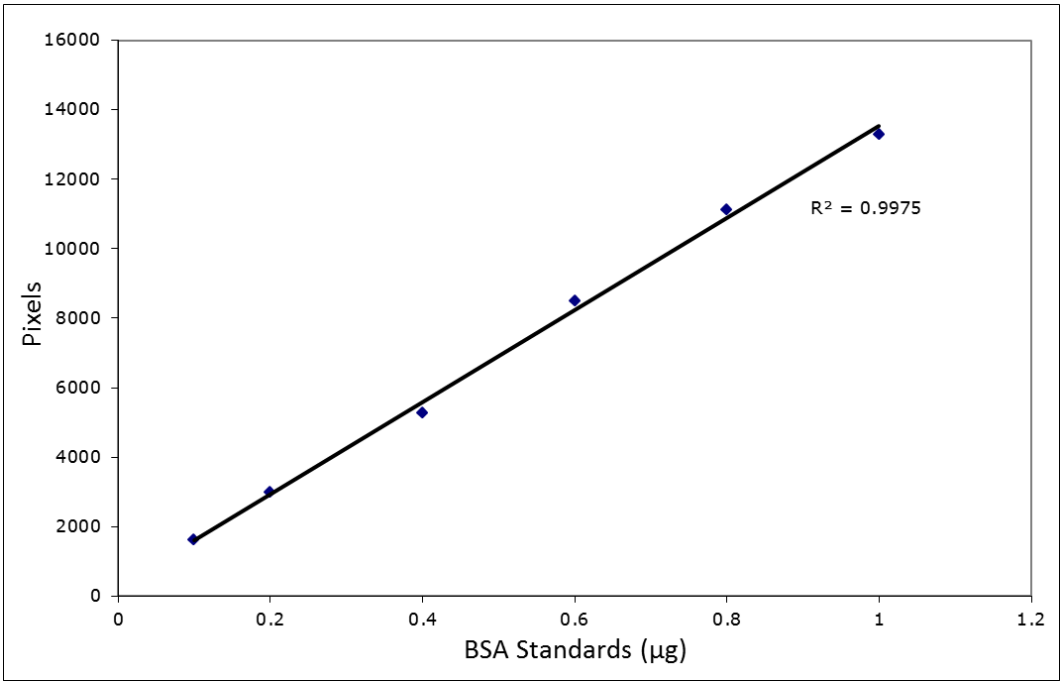

Figure 4.16: BSA standard curve for protein assay. Pixel values of 0-1 µg of BSA were measured by ImageJ densitometry (Rasband, W.S., ImageJ, U. S. National Institutes of Health, Bethesda, Maryland, USA, http://imagej.nih.gov/ij/, 1997-2014.) and compared with the purified wild-type ABCB1-12His. The first eluate has a concentration of 19 µg/ml protein and the second has a concentration of 3.5 µg/ml.

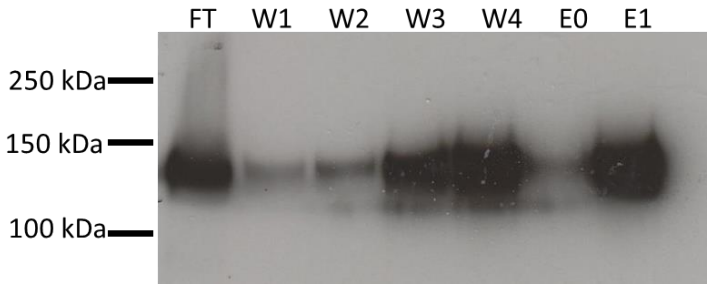

Figure 4.17: Protein losses during purification showed by SDS-PAGE. FT stands for flow through, W1 wash1, W2 wash2, W3 wash3, W4 wash4, E0 elution zero and E1 for first elution. 300 µl unbound Ni-NTA resin flow through (2 % of total volume); 500 µl washes 1-4 (2.5 % of total volumes); 500 µl elution 0 (2.5 % of total volume); 10 µl elution 1 (0.5 % of total volume). Major losses occurred during the third and the fourth washes and also in the unbound Ni-NTA resin flow through and an amount close to 20% of the purified ABCB1 in the first eluate was lost in each of these three steps.

4.9.8.e. Concentration of the purified ABCB1

The purified protein was concentrated using centrifugal filters and the imidazole concentration in the resulting sample was decreased by repeated dilution-concentration cycles and visualised by ODYSSEY® after SDS-PAGE and colloidal blue staining (Figure 4.18). 19 µg/ml purified ABCB1 (corresponding to the first eluate fraction in Figure 4.15) was concentrated 21 fold to 400µg/ml in a final volume of 25 µl (from 1 ml of eluate).

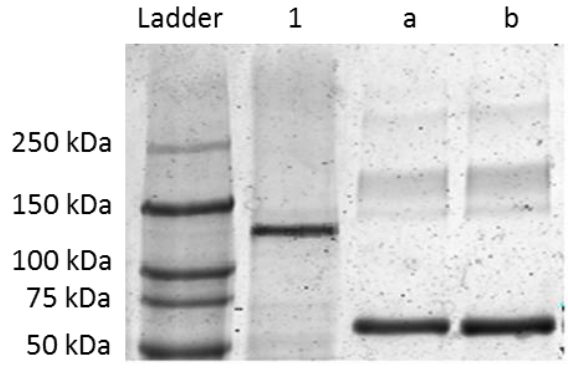

Figure 4.18: SDS PAGE of the concentrated ABCB1 sample. Lane: 1, 5 µl from concentrated ABCB1 (20 % of total); a, 2 µg of BSA; b, 2.5 µg of BSA.

4.9.9. *In vitro* Ubiquitination of ABCB1 by Nedd4-1

Ubiquitination of purified ABCB1 was performed *in vitro* by the addition of essential enzymes (E1 and E2), methylated ubiquitin (which cannot form polyubiquitin chains), and Nedd4-1 in the presence of ATP and $MgCl_2$ (Dr. Sullivan, personal communication). After the ubiquitination reaction, the samples were loaded onto an 8% Precise™ tris- glycine gel (Thermo Fisher Scientific, UK). The proteins were separated by electrophoresis and stained with colloidal blue. Protein migrating with a mobility of 140 kDa and above was excised from the gel and sent for mass spectrometry (Birmingham Science City Translational Medicine: Experimental Medicine Network of Excellence project).

4.9.10. Preparation of protein for mass spectrometry

Protein preparation and tandem mass spectrometry was carried out by Birmingham Science City Translational Medicine: Experimental Medicine Network of Excellence project.

Briefly, following excision from the tris-glycine gel, the protein was digested using trypsin, yielding peptide fragments of known size (Table 4.1). The tryptic fragments were dissolved in 0.1% formic acid and loaded onto the mass spectrometer.

	Sequence	Peptide Start	Peptide End
1	MDLEGDRNGGAKKK	1	15
2	DLEGDRNGGAKKKNFFK	2	19
3	NFFKLNNKSEK	15	26
4	LNNKSEKDK	19	28
5	KEKKPTVSVFSM	28	40
6	EKKPTVSVFSMFRYSNWLDK	29	49
7	YSNWLDKLYMVVGTLAAIIHGAGLPLMM	42	70
8	DLMSNITNRSDINDTGFFMNLEEDMTR	87	114
9	CLAAGRQIHK	137	147
10	KQFFHAIMR	149	158
11	QEIGWFDVHDVGELNTR	158	175
12	LTDDVSKINEGIGDKIGMFFQSM	175	198
13	INEGIGDKIGMFFQSMATFFTGFIVGFTR	182	211
14	FFTGFIVGFTRGWK	200	214
15	WAKILSSFTDKELLAYAK	232	250
16	ILSSFTDKELLAYAKAGAVAEE	235	257
17	ELLAYAKAGAVAEEV	243	258
18	AGAVAEEVLAAIR	250	263
19	TVIAFGGQKKELER	263	277
20	ELERYNKNLEEAKRIGIKK	273	292
21	QVLTVFFSVLIGAFSVGQASPSIEAFANAR	330	360
22	AFANARGAAYEIFKIIDNKPSIDSYSK	354	381

23	GAAYEIFKIIDNKPSIDSYSKSGHKPDNIK	360	390
24	IIDNKPSIDSYSK	368	381
25	GHKPDNIKGNLEFR	382	396
26	NVHFSYPSR	396	405
27	GLNLKVQSGQTVA	412	425
28	VQSGQTVALVGNSGCGK	417	434
29	STTVQLMQR	434	443
30	SGCGKSTTVQLMQRLYD	429	446
31	LYDPTEGMVSV	443	454
32	QLMQRLYDPTEGMVSVDGQDIR	438	460
33	EIIGVVSQEPVLFATTIAENIR	468	490
34	YGRENVTMDEIEKAVK	490	506
35	EANAYDFIMKLPHK	506	520
36	FDTLVGERGAQLSGGQKQRIAIAR	520	544
37	NPKILLLDE	548	557
38	EATSALDTESEAVVQVALDKARK	556	579
39	TTIVIAHRLSTV	581	593
40	NADVIAGFDDGVIVEKGNHDELMKEK	594	620
41	GIYFKLVTMQTAG	620	633
42	EVELENAADESK	634	646
43	SEIDALEMSSNDSR	646	660
44	SSLIRK	660	666
45	RSTRRSVRGSQAQDR	666	681

46	LSTKEALDESIPPVSFWRIMK	682	703
47	IIFSKIIGVFTRIDDPETK	730	749
48	IIGVFTR	735	742
49	IDDPETKRQ	742	751
50	QNSNLFSLLFLALGI	750	765
51	GIISFITFFLQGFTFGK	763	780
52	GKAGEILTKR	778	788
53	RLRYMVFR	787	795
54	SMLRQDVSWFDDPK	795	809
55	NTTGALTTR	809	818
56	LANDAAQVKGAIGS	818	832
57	LAVITQNIAN	833	843
58	VPIIAIAGVVEMKMLSGQALK	865	886
59	MKMLSGQALKDK	876	888
60	ELEGSGKI	889	897
61	IATEAIENFR	896	906
62	TVVSLTQEQK	906	916
63	FEHMYAQSLQVPYR	916	930
64	NSLRKAHIFGITFSFTQAMMYFSYA	930	955
65	GCFRFGAYLVAHK	955	968
66	LMSFEDVLLVFSAVVFG	968	985
67	AMAVGQVSSFAPDYAK	985	1001
68	AKISAAHIIMIIEKT	1001	1016

69	PDIPVLQGLSLEVKK	1048	1063
70	GQTLALVGSSGCGK	1064	1077
71	STVVQLLER	1077	1086
72	FYDPLAGK	1086	1094
73	KVLLDGKEIK	1093	1103
74	RLNVQWLR	1103	1111
75	AHLGIVSQEPILFDCSIAENIAYGDNSR	1111	1139
76	VVSQEEIVRAAKEANIHA	1139	1157
77	ESLPNKYSTK	1159	1169
78	VGDKGTQLSGGQKQR	1169	1184
79	QPHILLLDEATSALDTESEK	1193	1213
80	VVQEALDK	1213	1221
81	HRLSTIQNADLIVVFQNGRVK	1232	1253
82	EHGTHQQLLAQK	1253	1265
83	GIYFSMVSVQAGTKRQ	1265	1281
84	QGHHHHHHTGHHHHHH	1280	1296

Table 4.1: Complete tryptic digestion of wild-type ABCB1 results in 84 fragments. The five very high probability ubiquitinated lysines are highlighted in yellow (Fragments 19, 38, 46, 69). The three high probability ubiquitinated lysines are underlined and indicated in red letters (Fragment 59).

4.9.11. Analyses of Mass Spectrometry Data

The mass spectrometry results were obtained from Birmingham Science City Translational Medicine in the mgf file format. The SearchGUI programme was used for proteomics identification along with peptide-shaker to interpret the proteomics data. The mass spectrometry data identified trypsin-digest products that covered 88% of the ABCB1 protein sequence which also confirmed that purification was successful. Fragments covering the 70-87th, 138-148th, 214-232nd, 292-330th, 460-467th, 579-581th, 703-730th, 843-865th, 1017-1048th, 1185-1192nd and 1221-1233rd residues were therefore missing from the analysis (Figure 4.19). The analysis system was set to accept up to 2 missed trypsin cleavage sites and capture fragments with 2 to 4 precursor charges. Carboxymethylation of cysteine was allowed as a fixed modification because the mass spectrometer introduces this modification. Oxidation of methionine, phosphorylation and ubiquitination were set as variable modifications. Analysis of phosphate groups showed that previously described [44] serine residues within the linker region 661, 671, 675 and 683 were phosphorylated and, in addition, serine residue 658 was phosphorylated (Figure 4.20).

Five lysine residues (K271, K272, K575, K685, K1062) were identified as Nedd4-1 ubiquitinated with very high probability. These sites were not modified in the control sample to which methylated ubiquitin was not added (Figure 4.21). Three lysine residues were identified as ubiquitinated with high probability (K877, K885, K887). These residues were also observed as modified in the control sample but with very low probability (Figure 4.22). All three of these residues are located towards the cytosolic face of TMH10 in very close proximity to a PxY motif (residues 995-998) of ABCB1 (Figure 4.23). Lysine residues that were also ubiquitinated in the control sample, to which methylated ubiquitin was not

added were ignored. Insect cell ubiquitin ligases can also ubiquitinate the recombinant protein. A large number of lysines were found to be modified in the host cell (lysine residues 31, 48, 149, 242, 279, 285, 372, 380, 384, 389, 416, 502, 515, 519, 550, 609, 619, 624, 702, 779, 786, 808, 895, 915, 1002, 1014, 1061, 1093, 1102, 1220, 1264, 1278). For each site it was also possible to identify the equivalent fragment without ubiquitination in the untreated sample demonstrating that ubiquitination by insect cell ubiquitin ligases is not complete. However, this does suggest that the specific Nedd4-1 sites are underestimated.

Nedd4-1 is therefore capable of ubiquitinating more than one lysine residue of ABCB1 and because ABCB1 has only one PxY motif (PDY), it was hypothesized that this motif may be a potential binding site for Nedd4-1.

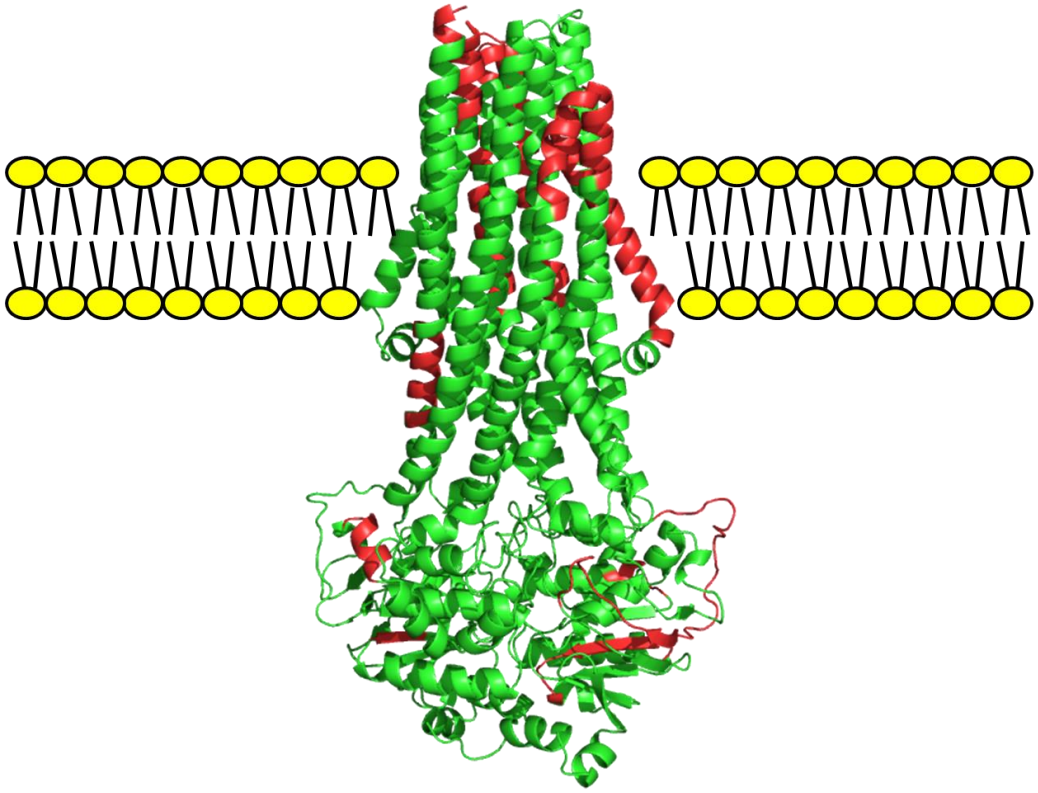

Figure 4.19: Cartoon of ABCB1 modelled on the structure of the homologous drug efflux pump Sav1866 from *S. aureus*. (pdb ID 2HYD) [234, 235]. Regions highlighted in red show the tryptic digest fragments that were not identified by mass spectrometry.

A.

B.

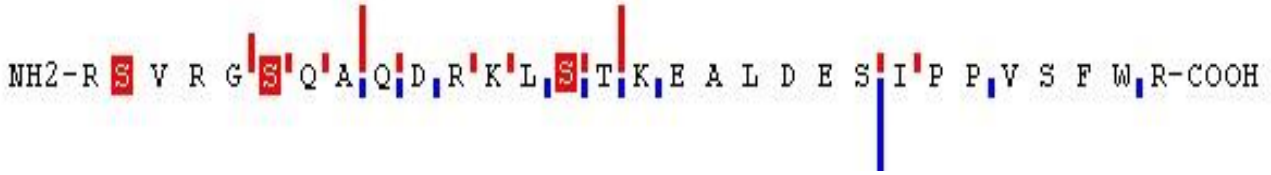

Figure 4.20: Phosphorylation of linker region. Examples of peptide fragments covering the linker region of ABCB1 (corresponding to tryptic digest fragment 43 to 46 shown in Table 4.1). Red lines indicate the y ions identified and blue lines indicate the b ions. Serines highlighted in red were found to be phosphorylated. (A) Residues 646 to 666, Ser 658 and Ser661 are phosphorylated. (B) Residues 670 to 699, serines 671, 675 and 683 were found to be phosphorylated.

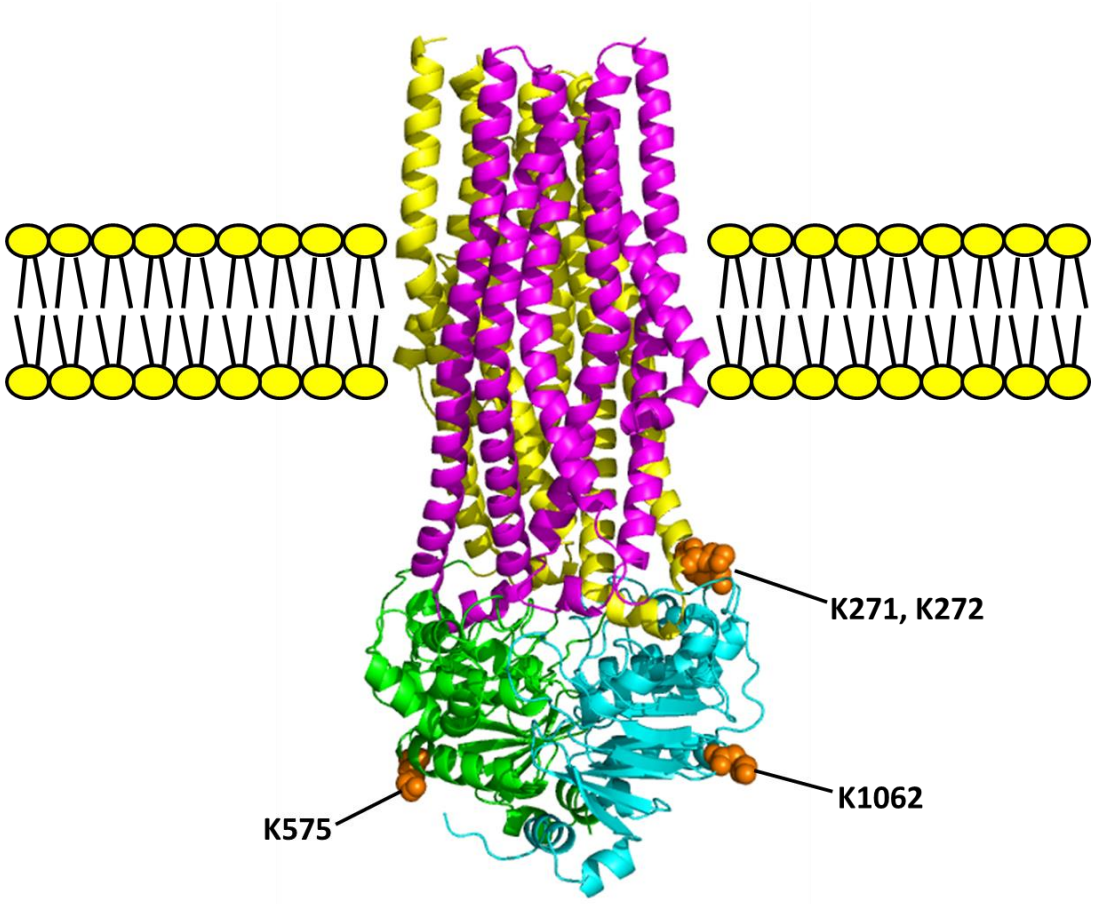

Figure 4.21: Very high probability Nedd4-1 ubiquitination sites on ABCB1. Cartoon model of ABCB1 as before (pdb ID 2HYD) [234, 235]. K271, K272 are located in the intracellular loop between TMH4 and TMH5, K575 is in NBD1 and K1062 is in NBD2. K685 cannot be shown because it is in the linker region separating the two halves of the transporter and is not present in Sav1866 (and was not resolved in Abcb1a). TMD1; yellow, TMD2; magenta, NBD1; green, NBD2; cyan. Homology model of ABCB1 [234, 235].

A.

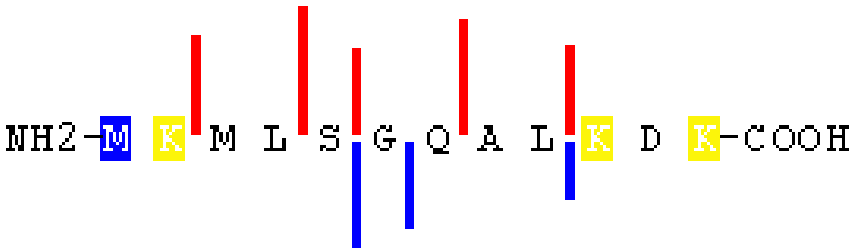

B.

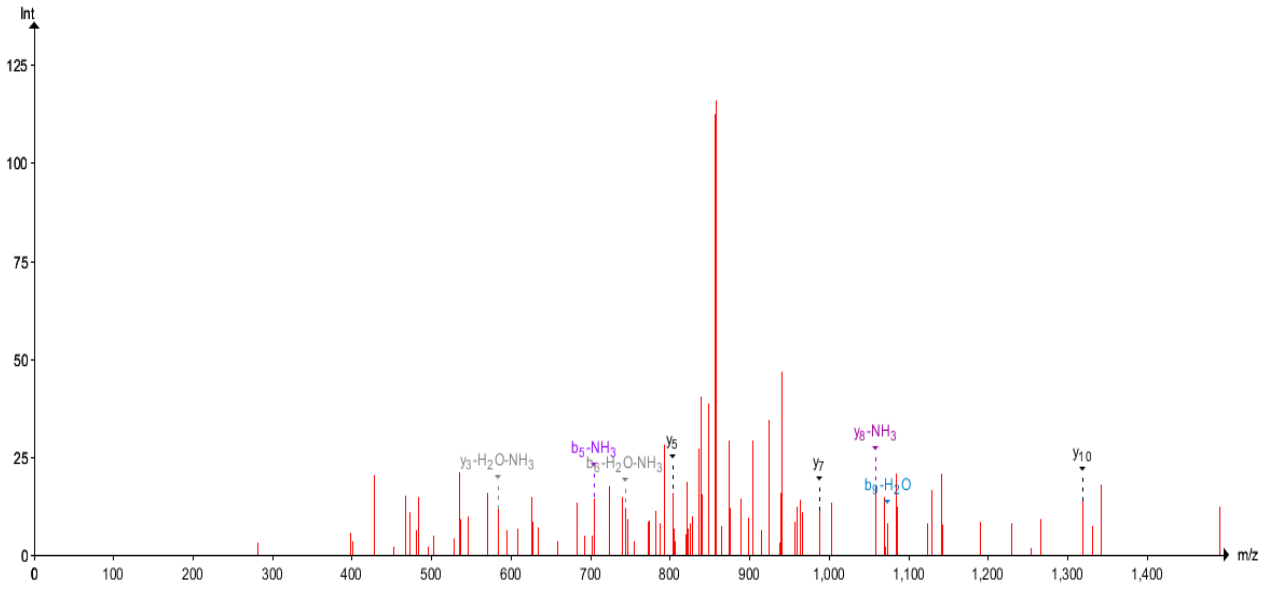

Figure 4.22: (A) Fragmentation of peptide extending intracellularly from TMH10 that contains three ubiquitinated lysines. Red lines indicate the y ions and blue lines indicate the b ions identified. The N-terminal methionine is oxidized and three lysines (Lys 877, 885 and 887) in this fragment are ubiquitinated. (B) Raw mass/charge spectra of the relevant peptide fragment

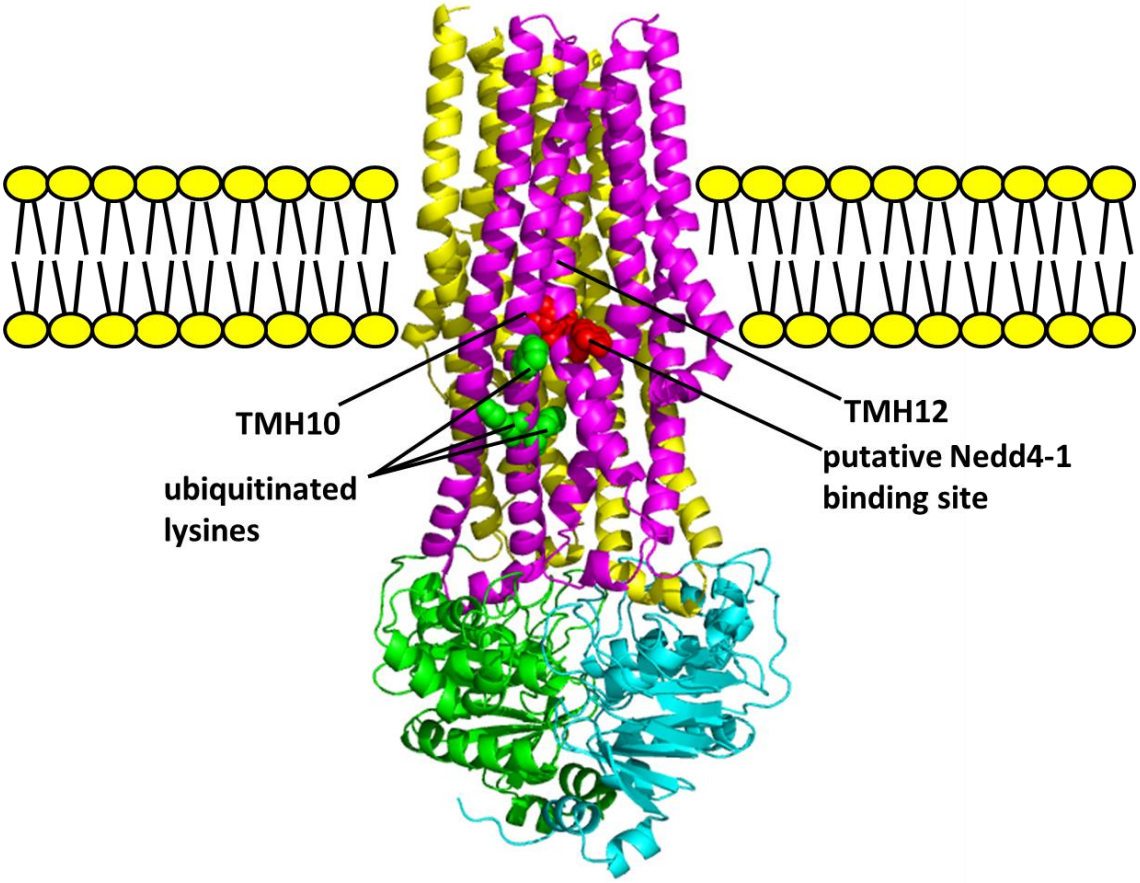

Figure 4.23: High probability Nedd4-1 ubiquitination sites preceding TMH10. The green spheres represent lysine residues that were ubiquitinated by Nedd4-1 and red spheres represent the PxY motif in ABCB1 that is hypothesized as a possible Nedd4-1 binding site (TMD1; yellow, TMD2; magenta, NBD1; green, NBD2; cyan). Homology model of ABCB1 (pdb ID 2HYD) [234, 235].

4.10. Discussion and Conclusions

In this chapter, it was shown that the ProFold™-ER1 baculovirus system results in improved ABCB1 expression in insect cells compared to *flash*BAC. One of the differences between ProFold™-ER1 and *flash*BAC is that the *flash*BAC genome does not include chitinase. In an infected insect, chitinase together with cathepsin facilitate host cuticle breakdown and tissue liquefaction at the very late stages of infection allowing the virus to be released to infect more hosts. Chitinase is known to target to the endoplasmic reticulum where it remains in paracrystalline form. This is considered to limit the function and the efficiency of the secretory pathway [236]. In insect cell culture conditions, chitinase is not necessary and its deletion should improve protein trafficking to the plasma membrane and secretion. However, in this study, it does not appear to be an important factor that limits the expression of ABCB1. Chitinase and cathepsin act together and it is possible that they are stored together in the endoplasmic reticulum. Deletion of the cathepsin gene in addition to chitinase deletion might be necessary to achieve improved membrane protein expression. Other differences between ProFold™-ER1 and *flash*BAC are that ProFold™-ER1 has been engineered to express protein disulphide isomerase and calreticulin. Protein disulphide isomerase is important in regulation of disulphide bridging between two cysteine residues. Calreticulin is an ER chaperone protein that improves the folding efficiency of membrane and secreted proteins. This is likely the key factor that provides a higher yield of ABCB1 expression in cells infected with ProFold™-ER1, because ABCB1 does not contain any disulphide bridges.

In this study, n-Dodecyl-β-D-maltoside (DDM), a water soluble, non-ionic detergent, was used to solubilise ABCB1 from insect cell membranes. DDM has been previously shown to be very effective for ABCB1 extraction from insect cells [229]. From 100 mg of total membrane protein, only 45 µg of ABCB1 was purified but at a high state of purity. A prior study by Kodan *et.al* which used SF+ insect cells to express ABCB1, reported maximal purification of 2.25 mg ABCB1 from 100 mg of crude membrane fraction by immobilized metal chelate affinity chromatography (IMAC) [229]. This yield, the best reported to date, is 75 fold higher than achieved in the current study. Kodan *et. al*, used a different baculovirus expression system (BD BaculoGold, Pharmingen, CA, USA) and expressed in SF+ cells that are engineered for maximal expression. In the current study, significant loss of protein was mainly observed in the flow through and the third and fourth washes suggesting either that insufficient Ni-NTA resin was used or that the 12 histidine carboxy-terminal tag was not intact. This could have been addressed by increasing the concentration of carboxy-peptidase inhibitors (the likely cause of tag loss without significant change to the apparent molecular weight of the protein). A combination of these factors likely contribute to the poor yield attained, however, sufficient ABCB1 was purified to allow ubiquitination and mass spectrometry including the appropriate controls. The purified ABCB1 was concentrated and the imidazole concentration reduced (by dilution and concentration cycles) to avoid inhibition of the Nedd4-1 ligase. Purified Nedd4-1 ligase was used to ubiquitinate ABCB1 and the products were separated by SDS-PAGE, stained with colloidal blue and excised from the gel for mass spectrometry. The mass spectrometry revealed the phosphorylation of serine residues within the linker region (Ser661, 671, 675, 683 as described previously [44], and also Ser658). The recognition of these sites by insect cell kinases suggests that the recombinant protein has adopted its native fold.

Analyses of the mass spectrometry data revealed five very high probability Nedd4-1 ubiquitination residues (K271, K272, K575, K685, K1062) that are all located on the exposed surface of cytosolic domains of ABCB1, suggesting that the protein is likely to be in its native fold and also that these residues could be ubiquitinated in cells under physiological conditions. Three high probability ubiquitination sites were also identified; lysines at positions 877, 885 and 887. These residues are located on the same planar surface in close proximity to the only PxY motif in ABCB1. It was hypothesized that this motif may be a binding site for Nedd4-1 allowing ubiquitination of the lysines in TMH10. It is debatable whether the high probability sites can be ubiquitinated from the same binding site. Some may have been modified during random collision with the ligase *in vitro*. However, these should still be considered putative Nedd-4-1 ubiquitination sites because Nedd4-1 is known to ubiquitinate target proteins that do not have a PxY motif, but with which it can interact via an adaptor protein to facilitate Nedd4-1 binding [237]. With potential future experiments, it may be possible to test directly the Nedd4-1 binding site and whether ubiquitination of ABCB1 effects protein levels at the plasma membrane and/or whether ubiquitination can inhibit protein function.

In conclusion, it was shown that Nedd4-1 is able to ubiquitinate ABCB1. Further analysis will be required to address the importance of this mechanism in regard to protein function and trafficking, and ultimately in the progression of Alzheimer's Disease by inhibition of β-amyloid export from neuronal tissue into blood vessels (please see General Discussion).

Chapter Five

5. ABCC1 and ABCC3 in Carcinogenesis

5.1. Introduction

Lysophosphatidylinositol (LPI) is a lysophospholipid which is mainly synthesized by the activation of cytosolic phospholipase A2 (PLA2). By catalysing the hydrolysis of phosphatidylinositol, PLA2 forms LPI and arachidonic acid. Arachidonic acid is converted into more complex eicosanoids and prostaglandins which are important in vasoconstriction and vasodilation. LPI was first accepted as only a modulator of ion channels and membrane curvature due its function in altering the mechanical properties of lipid bilayers [238]. However, the stimulatory effect of LPI on insulin release was later reported and oncogenic Ras activation resulting in LPI accumulation was shown later in 1988 [239-241]. In 2007, a G-protein coupled transmembrane receptor; GPR55 was identified as the receptor for LPI and it was shown that LPI induces a rapid phosphorylation of ERK and also causes Ca^{2+} mobilization in the cell [242]. LPI-induced intracellular calcium mobilisation was supported by other studies [243, 244] and the effect of LPI on cell proliferation and migration was also shown [241, 245-247]. LPI has been suggested to have a role in different signalling cascades such as phosphorylation of ERK1/2 [248], activation of Rho [244] and activation of various transcription factors such as; NFAT, CREB, NF-κB, ATF-2 [244, 248].

G protein-coupled receptors (GPCRs), or 7 transmembrane proteins, exert their functions by associating with a family of heterotrimeric proteins called G proteins (consisting of α, β, and γ subunits) that are capable of binding and hydrolysing guanosine triphosphate (GTP). After ligand binding, GPCRs undergo conformational changes that are mechanically transduced to the G proteins and activated G proteins can then positively or negatively modulate ion channels or second messengers. LPI binds to and activates GPR55 and simulation studies suggested that LPI adopts a tilted head orientation by inserting its fatty acid tail deep within TM helices 2, 3, 6, and 7 of the receptor [249].

A clinical study which compared plasma lysophospholipid levels in ovarian cancer patients and healthy controls has shown that LPI levels increase significantly in the first, second and third stages of ovarian cancer [250]. LPI has also been shown in prostate cancer cells to induce a calcium influx via TRPV2 channels which results in migration [246]. LPI was also shown to have a role in migration, orientation and polarization of human breast cancer cells via GPR55 activation [247]. These lines of evidence suggest that LPI has a role in carcinogenesis via GPR55 activation, however its pathway is still unclear. In 2011, Pineiro *et al*. suggested that LPI acts in an autocrine loop in which activation of GPR55 by LPI results in mobilisation of intracellular calcium, Akt activation and ERK1/2 phosphorylation inducing prostate and ovarian cell proliferation [110]. In the Pineiro *et al.* study, siRNA knock-down of GPR55 resulted in the complete loss of LPI activity in prostate and ovarian cancer cell lines showing that LPI is not a signalling molecule and its specific receptor is GPR55. One gap in the characterisation of this autocrine loop is definitive proof of how LPI is released from the cell. In the Pineiro *et al.* study, siRNA knock-down of the ABC transporter ABCC1 resulted in a significant decrease in LPI release to the culture media, pointing to the

importance of ABC transporters in this pathway (Figure 5.1). ABCC1 and ABCC3 have been shown to be up-regulated in prostate and ovary cancer patient samples and cell lines [251-253]. They have also been implicated as possible mediators of multidrug resistance but, as yet, there is little evidence for their clinical importance in this role.

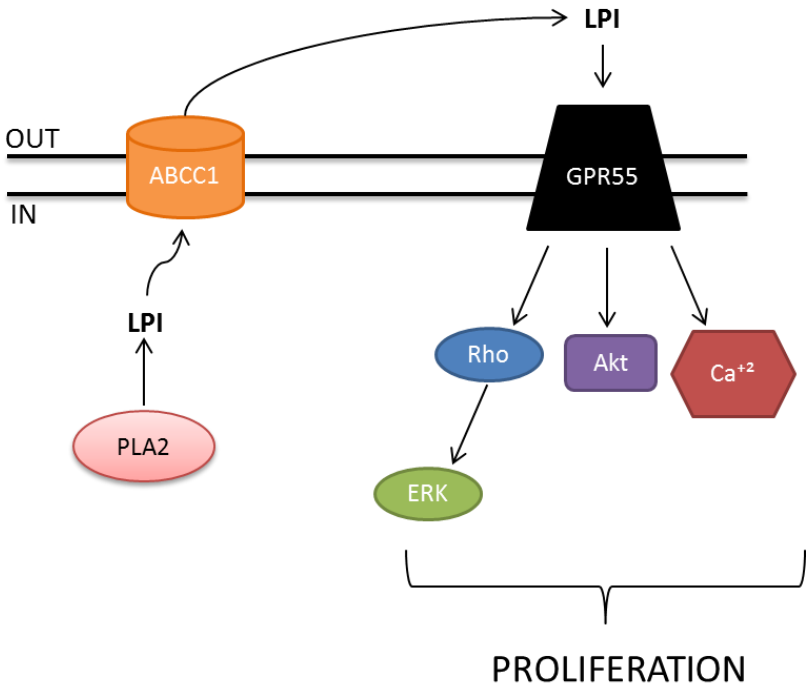

Figure 5.1: Suggested LPI autocrine loop in cancer cells (Figure modified from Pineiro *et al.* [110]).

5.2. Aim

- To test directly whether ABCC1 and/or ABCC3 transport LPI.

5.3. Results

5.3.1. Expression of functional ABCC1 and ABCC3 in HEK293T cells

In order to test the transport of new substrate it was first necessary to demonstrate expression of ABCC1 and ABCC3 in a naïve host cell and show that they are functional. Wild-type ABCC1 and ABCC3 encoded by recombinant pcDNA3.1 plasmids (kind gifts from Prof. Susan Cole [158, 159]) were transfected-transiently into HEK293T cells. ABCC1 and ABCC3 expression was demonstrated by western blot (Figure 5.2). Western blot shows that ABCC1 or ABCC3 are not expressed in naïve HEK293T cells. The molecular weights of ABCC1 and ABCC3 are similar and between 170 to 190 kDa, depending on the level of glycosylation. The same volumes of cell fractions were loaded into each well and probed with ABCC1 (QCRL1, Alexis) or ABCC3 (C-18, Santa Cruz) antibodies.

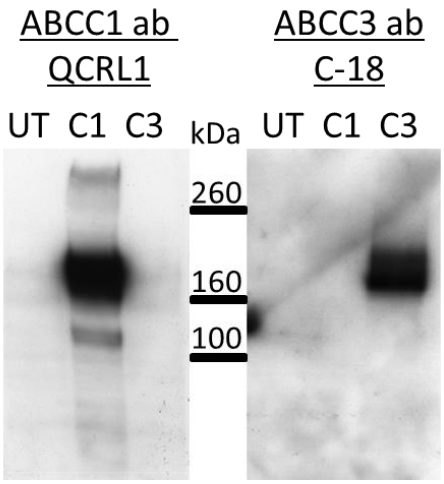

Figure 5.2: ABCC1 and ABCC3 expression in HEK293T cells. Left panel shows a western blot probed with ABCC1 antibody (ab; QCRL1, Alexis) and right panel shows a western blot probed with ABCC3 antibody (ab; C-18, Santa Cruz). UT indicates untransfected HEK293T cell lysate, C1 indicates whole cell lysate prepared from HEK293T cells transiently-transfected with *ABCC1* and C3 indicates whole cell lysate prepared from HEK293T cells transiently-transfected with *ABCC3*.

Both ABCC1 and ABCC3 are known to transport calcein-AM [254, 255] so calcein-AM was used as a control transport substrate to show the activity of the expressed wild-type proteins (Figure 5.3). End-point flow-cytometric transport assays were performed as explained in section 2.15. Both proteins are able to export calcein-AM from cells but with different efficiencies. The ABCC1 expressing HEK293T cells accumulate less calcein-AM than the ABCC3 expressing HEK293T cells most likely because ABCC1 is more efficient at exporting calcein-AM. The transiently-transfected HEK293T cell populations also show two peaks that differ in their abilities to export calcein-AM. These likely represent transfected and untransfected cells within same sample when cells are transfected with *ABCC1.* When transfected with *ABCC3* a single peak with a pronounced shoulder results from the overlap of two peaks very close to each other.

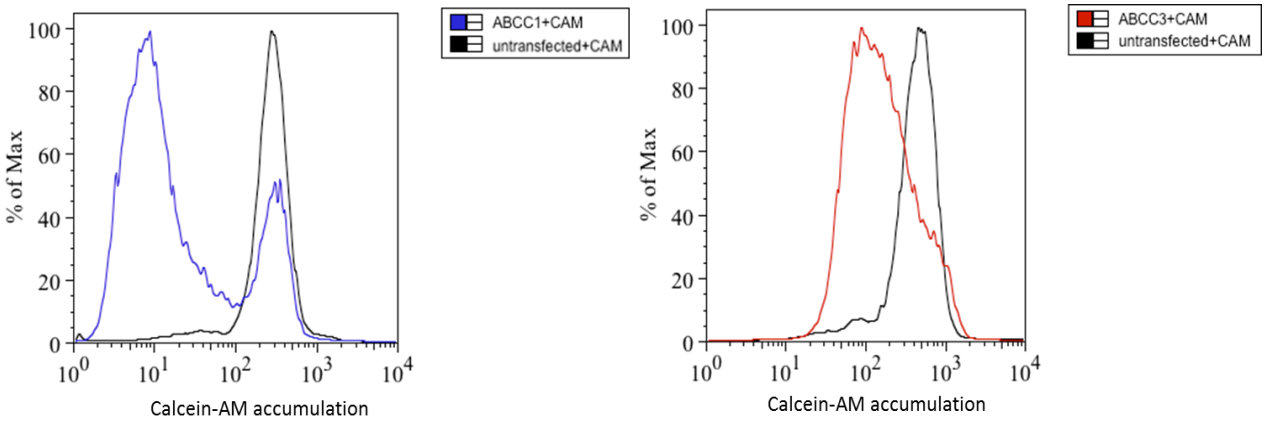

Figure 5.3: Both ABCC1 and ABCC3 are capable of calcein-AM transport. The left panel shows the calcein-AM accumulation in cells transiently-transfected with *ABCC1* (blue) and untransfected cells (black) and right panel shows the calcein-AM accumulation in cells transiently-transfected with *ABCC3* (red) and untransfected cells (black).

5.3.2. Transport of Tritiated Estradiol 17-β-D-glucuronide and LPI by ABCC1 and ABCC3

5.3.2.a. Membrane Vesicle Preparation

Human ABC transporters are all exporters and they transport their ligands actively from the cytosol to the outside across the cell membrane or into the organelles. Inside-out membrane vesicles in which the NBDs of the ABC transporter is on the outside of the vesicle and accessible to ATP in the reaction medium, can be used to measure transport of their ligands from the reaction medium into the vesicle lumen [24]. Membrane vesicles can be used to demonstrate transport of radio-labelled, fluorescent or non-labelled compounds. The transport ligand accumulated in the vesicle can be quantified directly by liquid scintillation counter, fluorescence plate reader or high-performance liquid chromatography (HPLC), respectively. This is a well-defined transport assay technique which allows direct evaluation of the ABC transporter activity in the presence or absence of ATP or specific inhibitors in the reaction medium and has been used previously to study the transport of estradiol-17β-glucuronide by ABCC1 [256]. To establish this technique in our lab, it was first necessary to express ABCC1 and ABCC3 in HEK293T cells and demonstrate that the transporters in the vesicle preparations were functional.

Untransfected HEK293T cells and HEK293T cells expressing ABCC1 and ABCC3 were homogenised with a glass-dounce homogeniser and membrane fractions were collected by high speed centrifugation after the unbroken cells and large organelles were discarded (detailed in section 2.13.3.). The membrane fractions were then syringed to, likely, produce a mixture of three forms; open lamellar membranes which did not form vesicles, right-side-out vesicles which will not have a role in the transport assay as the NBDs cannot access ATP in the medium and inside-out vesicles which should be capable of ATP-dependent radioactive ligand accumulation within the vesicles (Figure 5.4).

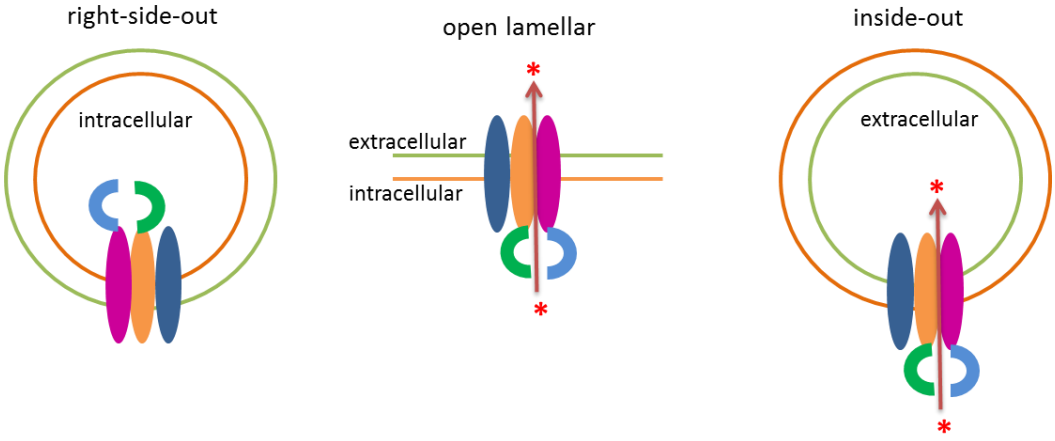

Figure 5.4: Cartoon showing the likely membrane forms after syringing. Left figure shows the right-side-out vesicles which do not contribute to radioactivity measurements as they cannot access ATP molecules. Middle figure shows the open lamellar form which cannot trap radioactive ligand. Right figure shows the inside-out membrane vesicles which will accumulate the radioactive ligand inside the vesicles. Blue oval shape, TMD0; orange oval shape, TMD1; purple oval shape, TMD2; green shape, NBD1; light blue shape, NBD2; arrow represents the direction of transport and red star represents ligand.

5.3.2.b. The Vesicles Contain Functional ABCC1 or ABCC3

Tritiated estradiol 17-β-D-glucuronide (^{3}H-E_2-17βDG) is a well-defined transport ligand of both ABCC1 and ABCC3 and has been used in membrane vesicle transport studies previously [155, 256]. The activities of the transporters in the membrane vesicles were therefore tested by the use of ^{3}H-E_2-17βDG as a control ligand. The transport assays were performed as described in section 2.17. Briefly, the membrane vesicles were loaded with ^{3}H-E_2-17βDG for 15 minutes at 37°C. The transport reaction was stopped immediately with a large volume of ice-cold transport buffer and trapped on filter discs by rapid filtration and washed 4 times with 3 ml transport buffer. First, ^{3}H-E_2-17βDG concentration was titrated to identify the optimum for measuring transport efficiency (Figure 5.5). The data show that ABCC1 was active in the vesicle preparation. 400 nM ^{3}H-E_2-17βDG was found to be the optimum concentration for detection of ^{3}H-E_2-17βDG accumulation in membrane vesicles prepared from ABCC1-expressing cells and easily distinguishable from untransfected cells. The concentration of 400 nM was also used by other research groups [256]. For later reference, 400 nM cold (non-radioactive) E_2-17βDG was used with 40 nCi ^{3}H-E_2-17βDG to ensure optimal transport efficiency but with less radioactive material used.

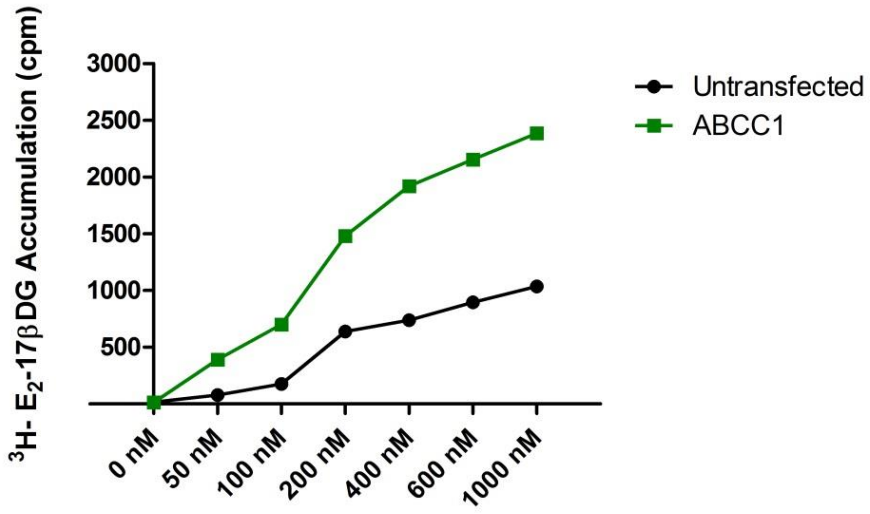

Figure 5.5: Titration of ^{3}H-E$_2$-17βDG concentration to reveal the optimum concentration for detection of ^{3}H-E$_2$-17βDG accumulation between membrane vesicles prepared from ABCC1-expressing and untransfected cells. Green line represents the ^{3}H-E$_2$-17βDG accumulation in membrane vesicles of ABCC1-expressing cells and black line represents the ^{3}H-E$_2$-17βDG accumulation in membrane vesicle of untransfected cells.

5.3.2.c. Transport of ^{3}H-E$_2$-17βDG is dependent on ATP

The ^{3}H-E2-17BDG transport data indicated that the membrane vesicles prepared from ABCC1 and ABCC3 expressing cells accumulated significantly more ^{3}H-E$_2$-17βDG than vesicles prepared from untransfected cells and that ABCC1 and ABCC3 are capable of ^{3}H-E$_2$-17βDG transport (Figure 5.6).

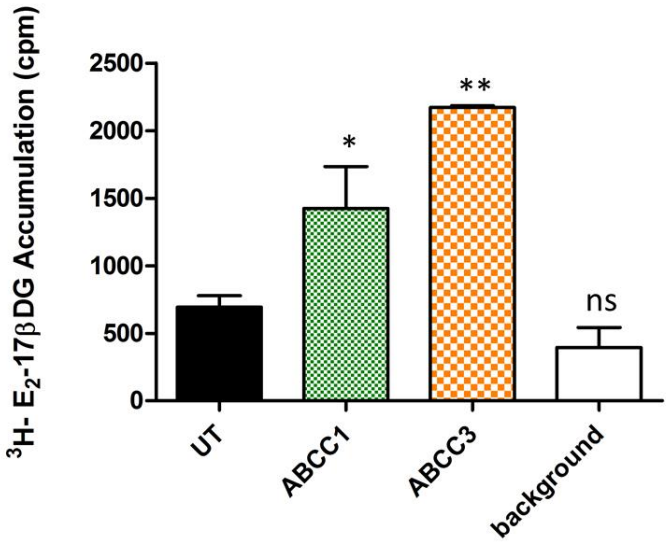

Figure 5.6: ^{3}H-E_2-17βDG accumulation in membrane vesicles prepared from ABCC1 or ABCC3 expressing cells and untransfected cells. UT represents vesicles prepared from untransfected cells, ABCC1 represents vesicles prepared from ABCC1 expressing cells and ABCC3 represents vesicles prepared from ABCC3 expressing cells. ^{3}H-E_2-17βDG accumulation in vesicles of transfected cells is significantly different to untransfected cells. p values calculated with respect to ^{3}H-E_2-17βDG accumulation in the membrane vesicles prepared from untransfected cells; ** p<0.01, * p<0.05, ns p>0.05.

To test whether the ^{3}H-E_2-17βDG accumulation in membrane vesicles prepared from ABCC1- and ABCC3-expressing cells is a result of primary active event, vanadate was used. Vanadate replaces the phosphate formed after ATP hydrolysis and inhibits ABC transporters by preventing completion of the ATP catalytic cycle which depends on sequential release of Pi and ADP. The data shows that transport activity obtained from membrane vesicles prepared from ABCC1 and ABCC3-expressing cells is an active event and can be inhibited by vanadate (Figure 5.7 and Figure 5.8).

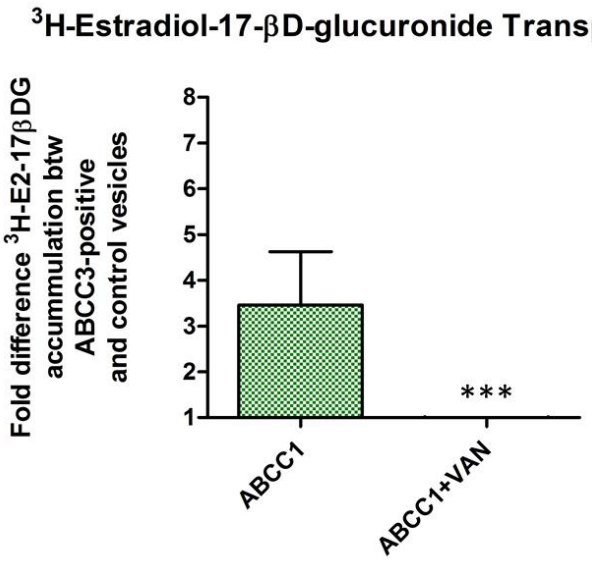

Figure 5.7: Fold difference ^{3}H-E_2-17βDG accumulation in membrane vesicles prepared from ABCC1-expressing cells and untransfected cells. The ^{3}H-E_2-17βDG transport activity of ABCC1 and inhibition of transport in the presence of 100 µM vanadate are shown. p values calculated with respect to fold difference ^{3}H-E_2-17βDG accumulation in the membrane vesicles prepared from ABCC1-expressing cells and untransfected cells; *** p<0.001.

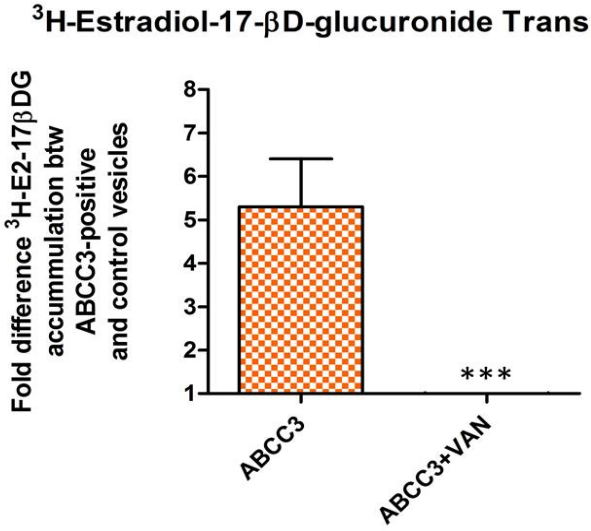

Figure 5.8: Fold difference ^{3}H-E_2-17βDG accumulation in membrane vesicles prepared from ABCC3-expressing cells and untransfected cells. The ^{3}H-E_2-17βDG transport activity of ABCC3 and inhibition of transport in the presence of 100 µM vanadate are shown. p values calculated with respect to fold difference ^{3}H-E_2-17βDG accumulation in the membrane vesicles prepared from ABCC3-expressing cells and untransfected cells; *** p<0.001.

5.3.2.d. Transport of Radiolabelled LPI

Tritiated LPI was prepared by Professor Falasca [241]. Briefly, prostate or ovary cancer cells (PC-3 and OVCAR3, respectively) were fed tritiated myo-inositol and ^{3}H-LPI released by the cells was extracted by acid medium extraction and isolated by thin layer chromatography [110]. The ovary and prostate cancer cells synthesize and release LPI endogenously which is non-radioactive and cannot be measured by scintillation counting. Cold LPI (non-radioactive) was added to provide the ligand concentration within 1500 nM to 2500 nM at which the reaction rate is quantifiable. The transport assays were performed as described above. Cellulose nitrate filter discs on which the membrane vesicles are trapped by rapid filtration were found to also bind a small but measurable amount of the 3H-LPI and this background radioactivity was substracted from the measured radioactivity. The membrane vesicles prepared from ABCC1 and ABCC3 expressing cells accumulated significantly more ^{3}H-LPI than vesicles of untransfected cells (Figure 5.9).

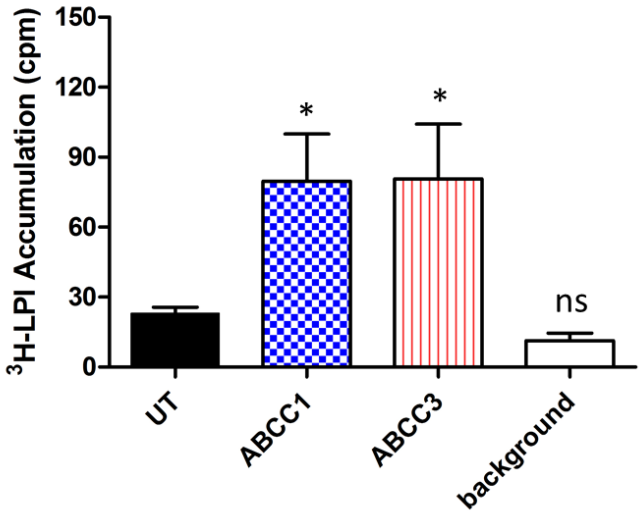

Figure 5.9: Radioactive LPI accumulation in membrane vesicles prepared from ABCC1 or ABCC3 expressing cells and untransfected cells. UT represents vesicles prepared from untransfected cells, ABCC1 represents vesicles prepared from ABCC1 expressing cells and ABCC3 represents vesicles prepared from ABCC3 expressing cells. ^{3}H-LPI accumulation in vesicles of transfected cells is significantly different to untransfected cells. p values calculated with respect to ^{3}H-LPI accumulation in the membrane vesicles prepared from untransfected cells; * $p<0.05$, ns $p>0.05$.

Vanadate was used to reveal if the ^{3}H-LPI accumulation in membrane vesicles prepared from ABCC1 or ABCC3 expressing cells was dependant on ATP hydrolysis (Figure 5.10 and Figure 5.11). Glutathione can also stimulate the transport of some ABCC1 ligands [144] and to test if LPI transport is dependent on co-transport of glutathione, 100 µM glutathione [257] was added to the reaction mixture (Figure 5.10). The data show that LPI transport of ABCC1 and ABCC3 is dependent on ATP and LPI transport of ABCC1 does not require glutathione.

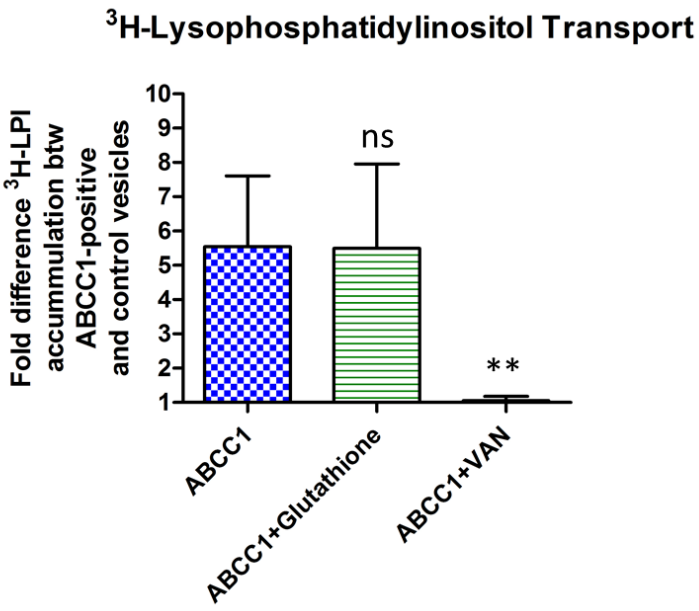

Figure 5.10: Fold difference ^{3}H-LPI accumulation in the vesicles prepared from ABCC1 expressing cells compared to untransfected cells. The LPI transport activity of ABCC1 in the presence or absence of 100 µM glutathione or 100 µM vanadate are shown. p values calculated with respect to fold difference LPI accumulation in the membrane vesicles prepared from ABCC1 expressing cells and untransfected cells; ** p<0.01, ns p>0.05.

As described above ABCC3 is also over-expressed in pancreatic cancer cell lines and clinical samples and could also potentially contribute to the secretion of the LPI. Its ability to transport LPI was therefore also tested. ABCC3 was found to transport LPI into inside-out vesicles. The level of accumulation was similar to that achieved by ABCC1 and the mechanism was also inhibited by vanadate (Figure 5.11).

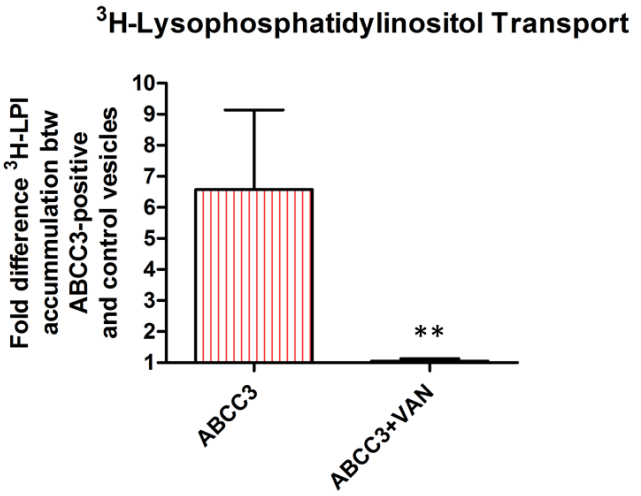

Figure 5.11: Fold difference ^{3}H-LPI accumulation in the vesicles prepared from ABCC3 expressing cells compared to untransfected cells. The LPI transport activity of ABCC3 in the presence or absence of 100 µM vanadate is shown. p values calculated with respect to fold difference LPI accumulation in the membrane vesicles prepared from ABCC3 expressing cells and untransfected cells; ** p<0.01.

5.3.2.e. Inhibition of ABCC3 and ABCC1 transport activity by drugs

MK-571 competitively inhibits the binding of leukotriene C4 (LTC4) to ABCC1 and is more specific for ABCC1 than vanadate [258]. MK-571 was therefore used as a further test that LPI transport in these vesicles was mediated by ABCC1. MK-571 at a concentration of 10 µM caused a statistically significant decrease in E_2-17βG transport. LPI transport was similarly affected (Figure 5.12).

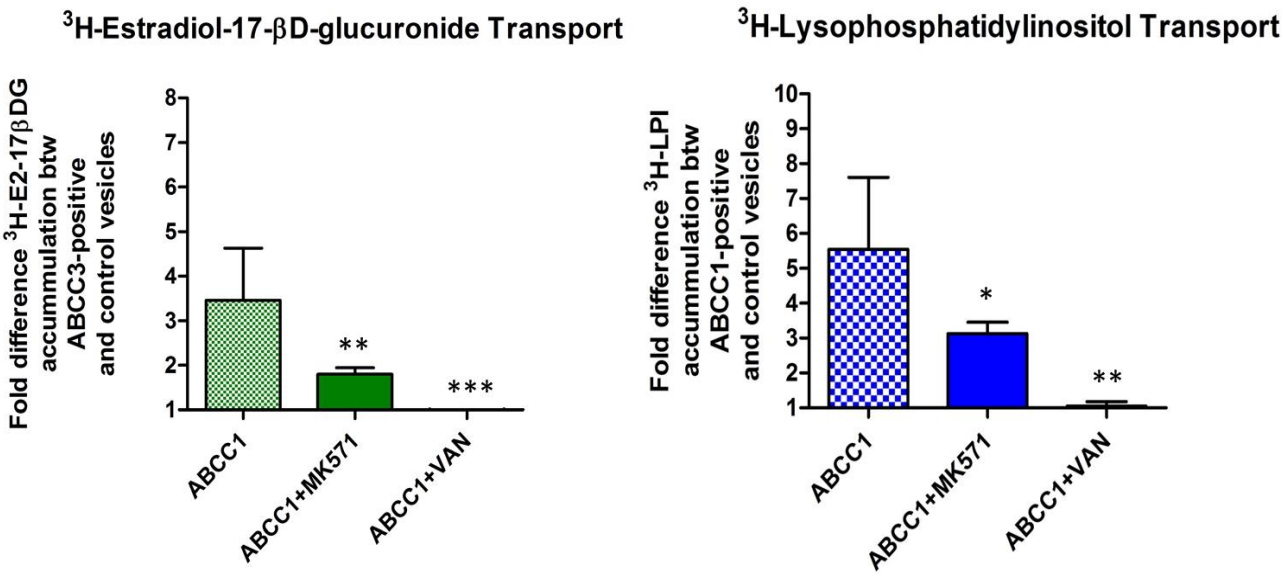

Figure 5.12: Fold difference E_2-17βDG and LPI accumulation in the vesicles prepared from ABCC1 expressing cells compared to untransfected cells and inhibition of transport by MK-571. Left figure indicates the E_2-17βDG transport activity of ABCC1 and inhibition of E_2-17βDG transport in the presence of 10 µM MK-571. Right figure indicates the LPI transport activity of ABCC1 in the presence of 10 µM MK-571 or 100 µM vanadate. p values calculated with respect to fold difference triated ligand accumulation in the vesicles prepared from ABCC1 expressing cells to untransfected cells; *** p<0.001, ** p<0.01, * p<0.05.

A study by Zhang *et al*., [154] identified taurocholate as a transport substrate of ABCC3 when used at a concentration of 30 µM. The same study also showed that, at 80 µM, taurocholate would behave as a competitive inhibitor for transport of E_2-17βDG [154]. To test whether taurocholate could also inhibit the transport of ^{3}H-E_2-17βDG and ^{3}H-LPI it was added to the vesicle preparations at a concentration of 100 µM prior to transport assays (Figure 5.13). Taurocholate was able to inhibit ^{3}H-E_2-17βDG transport of ABCC3 to a significant level but ^{3}H-LPI transport by ABCC3 was unaffected.

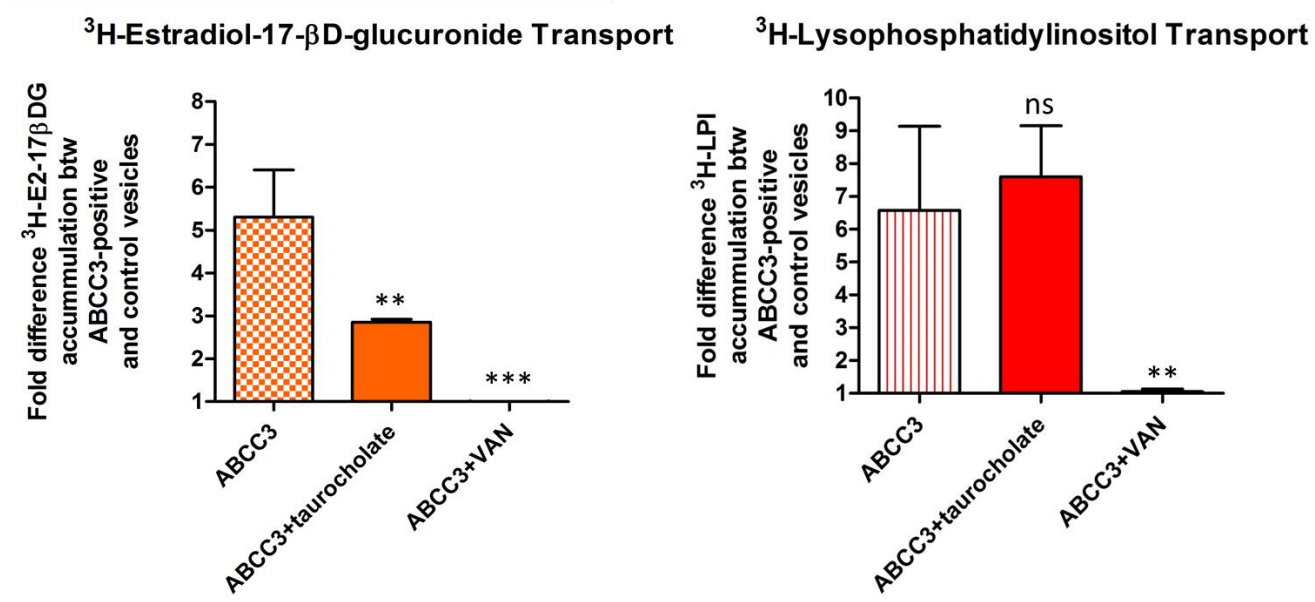

Figure 5.13: Fold difference E_2-17βDG and LPI accumulation in the vesicles prepared from ABCC3 expressing cells compared to untransfected cells and inhibition of transport by taurocholate. Left figure indicates the E_2-17βDG transport activity of ABCC3 and inhibition of E_2-17βDG transport in the presence of 100 µM taurocholate. Right figure indicates the LPI transport activity of ABCC3 in the presence of 100 µM taurocholate or 100 µM vanadate. Taurocholate at a concentration of 100 µM is not able to inhibit LPI transport of ABCC3. p values calculated with respect to fold difference in triated ligand accumulation in the vesicles prepared from ABCC3 expressing cells and untransfected cells; *** $p<0.001$, ** $p<0.01$, ns $p>0.05$.

5.4. Discussion and Conclusions

Prior to the discovery of a receptor specific for lysophosphatidylinositol (LPI), LPI was only considered as a byproduct of the arachidonic acid production pathway. After the LPI receptor, GPR55 was discovered, LPI and its potential functions in the cell attracted attention. It was shown that LPI can induce migration, proliferation and cell survival of ovary, prostate and breast cancer cell lines [246, 247, 250]. The Pineiro *et al.* study [110] also showed that siRNA knockdown of GPR55 results in growth restriction of ovary (OVCAR-3) and prostate (PC-3) cancer cell lines supporting that proliferation of cancer cells is dependent on the LPI autocrine loop. Specimens and plasma samples from ovarian cancer patients at different stages have shown that LPI concentration increases by the stage of the tumour except the last stage (stage 4) [250]. Pinero *et al*., also implicated ABCC1 as an efflux transporter for LPI because siRNA knockdown of human ABCC1 led to a significant decrease in LPI in the culture media of the PC-3 prostate cancer cell line. Although the siRNA knockdown studies performed by Prof. Falasca's group only targeted ABCC1 [110], ABCC3 is also over-expressed in pancreatic cancer cell lines and it shares a wide range of transport ligands with ABCC1 [127]. It was therefore important to test directly whether ABCC1 and ABCC3, which are up-regulated in many cancer lines and tumour samples, can transport LPI.

In this chapter, I have demonstrated that ABCC1 can transport LPI and this transport activity can be inhibited by both vanadate and the ABCC1 inhibitor MK-571 indicating the transport activity is specific to ABCC1. One limitation of this study was that the concentration and specific activity of the radioactive LPI was unknown. This prevented determination of the Km and Vmax of LPI transport by ABCC1 and ABCC3. A study by Sullivan *et al.* has shown that ABCC1 expression increases in patient specimens as the stage of prostate cancer progresses [251]. The study by Pineiro *et al.* and the results presented in this chapter indicate that increased expression of ABCC1 in prostate cancer cells can result in increased LPI secretion and cancer cell proliferation. Zalcberg *et al.* have also shown that ABCC1 is the predominant multidrug resistance protein in two prostate cancer cell lines; DU-145 and PC-3 [252] and Monet *et al.* have shown that LPI causes Ca^{2+} influx and stimulates migration of prostate cancer cell line PC-3 [246]. This relation of ABCC1 and ABCC3 over-expression, together with increased LPI secretion also appears to be true for ovarian cancer; LPI and *ABCC1* and *ABCC3* mRNA levels increase with an unfavourable clinical outcome [250, 253]. These results indicate that an inhibitor specific to ABCC1, which can be used *in vivo*, might increase the survival rate of prostate and ovary cancer patients. In this chapter, it was shown that MK-571 can inhibit ABCC1 transport of LPI. *In vivo* studies will be required to show LPI transport inhibition and direct effects of MK-571 on tumour proliferation and migration. It should be noted that MK-571 can also inhibit ABCC2 and it also induces LTD4-induced bronchoconstriction which might be an obstacle for its therapeutic use.

ABCC3 shares 58% amino acid identity with ABCC1 which makes it the closest relative of ABCC1. Other than the amino acid sequence identity, ABCC1 and ABCC3 share a wide variety of common ligands. The main difference between the two proteins is that glutathione can be transported or co-transported by ABCC1 and it can also stimulate the transport of several ABCC1 ligands. Glutathione is not transported by ABCC3 and does not influence the transport of other compounds by this transporter. Like ABCC1, ABCC3 is also highly expressed in several cancers such as pancreatic carcinoma [127]. As shown in the results section, LPI is also transported by ABCC3 and this transport is inhibited by vanadate. However, LPI transport by ABCC3 could not be inhibited by taurocholate. Taurocholate acts as a competitive inhibitor for E_2-17βDG transport but perhaps it does not affect the binding of LPI. It is also possible that the relative affinities of taurocholate and LPI for ABCC3 make taurocholate a poor inhibitor at 100 μM. Further elevation of the taurocholate concentration was considered but was not tested largely because, as a strong detergent, high concentrations are likely to affect the integrity of the vesicles. The high expression level of ABCC3 in pancreatic carcinoma specimens [127] and the demonstration that inhibition or siRNA knockdown of GPR55 results in reduced pancreatic cancer cell proliferation (Prof. Falasca, personal communication) suggests that the LPI autocrine loop also operates in pancreatic carcinoma. To elucidate this, a specific inhibitor of ABCC3 is required.

In conclusion, I have shown that ABCC1 and ABCC3 can both transport LPI, strengthening the argument that they are important in the LPI autocrine loop in cancer cells supporting a new role for an ABC transporter in cancer progression other than in chemotherapeutic drug resistance.

Chapter 6

6. General Discussion and Future Work

This thesis describes different aspects of the function and regulation of three related members of the ATP-binding cassette superfamily of proteins; ABCB1, ABCC1 and ABCC3. In chapters 3 and 4, the molecular mechanism of ABCB1 (specifically the importance of the Q-loop for interdomain communication) and its potential regulation by post-translational modification was investigated. In chapter 5, transport of lysophosphatidylinositol (a signalling molecule implicated in carcinogenesis) by ABCC1 and ABCC3 was tested. The data generated was discussed in each of results chapters. Here the data are summarised and the wider implications and potential future directions for the research are considered.

6.1. Interdomain Communication within ABCB1

As described in the introduction and chapter 3, the Q-loop motifs are located at the base of the grooves occupied by second ICLs of TMDs (ICL2 of the TMD1 and ICL4 of the TMD2). The Q-loop is also located between the core subdomain of the NBD, which facilitates nucleotide binding via the Walker-A and -B motifs, the A-loop, D-loop and H-loop and the α-helical subdomain which interacts via its ABC signature motif with the nucleotide bound by the core subdomain of the apposed NBD. During the transport cycle it is thought that this interaction requires the α-helical subdomain to rotate around the Q-loop to form the ATP sandwich dimer of NBDs. The Q-loop is therefore in a suitable position to facilitate conformational changes and transduce signals from the ligand binding sites to the NBDs. The role of the Q-loops for the mechanism of ABCB1 was therefore tested by mutagenesis and analysed by drug efflux assay.

The inactivity of the double Q-loop mutant supports the hypothesis that the Q-loops are critical for the transport cycle of ABCB1. It was also shown that double Q-loop mutant is trapped in a conformation consistent with the inwardly-open state which is reactive to the conformation-sensitive antibody UIC2. As the inward-open state has a high affinity for drugs, this provides additional binding sites in the plasma membrane for verapamil and vinblastine. In contrast, Walker-B mutants adopt an inwardly-closed conformation which lack affinity for drugs and UIC2. The functionality of the single Q-loop mutants (in contrast to the previously published data on equivalent mutants in related ABC transporters) allowed the communication pathway(s) linking the drug binding sites and the ATP catalytic cycle to be determined.

Identification of two ligand binding cavities and their separation by mutagenesis showed that different ligands have different tendencies to bind to these two cavities [163]. Introduction of these cavity mutations into the single Q-loop mutants, showed that the Q-loop glutamines were critical for communication between the drug binding cavities of the TMDs and the ATP catalytic cycle of the NBDs. Surprisingly, the signal transduction path was found to differ depending on the drug bound. BODIPY® FL-verapamil, BODIPY® FL-taxol and Rhodamine123 were found to be transported by single Q-loop mutants but BODIPY® FL-vinblastine was not. BODIPY® FL-verapamil transport by ABCB1 from the Q773-lined ligand binding cavity was also found to require only the NBD1 Q-loop glutamine. These results indicate that the signal communication pathway to perform a transport cycle varies for different ligands both with respect to the binding cavity used, and also the chemistry of ligand/binding site interaction which likely affects the trigger mechanism. The interaction of a ligand with the TMDs triggers conformational change that is transmitted through one or

both of the coupling helices via the Q-loops to facilitate the allosteric binding of two molecules of ATP and bring the two NBDs together.

These data position the Q-loop at the centre of the transport cycle where it controls the coupling of the aspect and affinity of the drug binding cavities to the ATP catalytic cycle. The side chain amide of the Q-loop glutamine may also be necessary to tether the bound ATP (via a hydrogen bond to the γ-phosphate) in order to allow hydrolytic attack by a water molecule activated by the Walker B glutamate. Evidence for this was found in the subtle but statistically-relevant rescue of BODIPY® FL-verapamil transport from the E1201Q Walker B mutant by the Q1118A Q-loop mutant.

6.1.1. Future Work

The experiments described in chapter 3 of this thesis have uncovered important information regarding the role of the Q-loop motif in the communication pathway between the NBDs and the TMDs of ABCB1. Dr. Zolnerciks has previously shown that the single ABC-signature mutant ABCB1 and the single D-loop mutant ABCB1 have wild-type levels of BODIPY® FL-taxol transport activity whereas double mutants of both motifs are inactive. The extracellular acidification rate (ECAR) data suggest that single ABC-signature or D-loop mutants cannot hydrolyse ATP *in vivo* and this suggests a mechanism in which ATP hydrolysis and transport function is uncoupled, although it is also theoretically possible that these mutants hydrolyse ATP constitutively (unpublished data, Prof. Linton Lab, personal communnication). However, Furman *et. al* has investigated the role of D-loop in Pdr5, a drug resistance gene from *S. cerevisiae*, and has suggested that NBD2 D-loop mutant has nearly wild-type levels of ATPase activity and has a level of transport activity [259]. They also showed that mutation of well-conserved Aspartate residue in the D-loop into

Asparagine or Glutamate has different consequences. During imazalil transport D1042E mutant has nearly wild-type levels of transport activity whereas D1042N mutant is dead and the transport activity of these two mutants differ depending on the transported ligand.

Separation of the two ligand binding cavities by mutagenesis could also enable investigation of the potential roles of the D-loop or ABC signature motif in the signal transduction pathway of ABCB1 and can help us to understand the mechanism of this uncoupling.

Single Q-loop mutations inhibit the export of BODIPY® FL-vinblastine but not BODIPY® FL-verapamil, BODIPY® FL-taxol or Rhodamine123. The mechanism for transport of BODIPY® FL-vinblastine must therefore be different to BODIPY® FL-verapamil and the other drugs used in this study. This is most likely due to the chemistry of the interaction of the drugs with the binding cavities and through that interaction their capacity to trigger formation of the inward closed conformation. It may only be possible to fully understand the differences if the transporter can be co-crystallised with these drugs in the binding cavities. However, the capacity of NBD mutations to change the apparent drug specificity of the transporter should be considered in future experiments particularly where the ATPase activity is characterised by stimulation *in vitro* and a different drug is used to measure binding or transport. The different mechanism underlying the BODIPY® FL-vinblastine transport can also be tested with single ABC-signature or D-loop motif mutants.

6.2. Post-translational Regulation of ABCB1 by Nedd4.1

All membrane proteins are likely recycled and as such are therefore regulated post-translationally. Ubiquitination by ubiquitin ligases commonly marks proteins for internalisation from the membrane from where they can be recycled back to the membrane or targeted for degradation. This can have pathological consequences and it has been hypothesised that loss of ABCB1 from the luminal membrane of the BBB can exacerbate Alzheimer's disease. Alzheimer's disease is characterised by the accumulation of a neurotoxic peptide, β-amyloid, in the brain and it has previously been shown that β-amyloid can be effluxed by ABCB1 across the luminal membrane of the endothelial cells of the BBB [190-192]. The loss of ABCB1 from the BBB has been observed in human patients with Alzheimer's disease and also in rodent models of the disease prompting the suggestion that ABCB1 may be targeted for internalisation from the lumenal membrane by ubiquitination. Prior studies in the Linton Lab had indicated that ABCB1 could be ubiquitinated by the ubiquitin ligase, Nedd4-1 *in vitro* (Prof. Linton; personal communication). In the current study, I extended the earlier work by purifying recombinant human ABCB1 from the membrane, incubating it with the ligase complex and identified the ubiquitinated residues by mass spectrometry. Five very high probability residues K271, K272, K576, K685, K1063 and also three high probability residues K877, K885 and K887 were identified as putative ubiquitination sites.

Nedd4 ubiquitin ligases commonly recognise PY motifs (PxY) on target proteins. ABCB1 has a PDY motif, residues 996-998 in the intracellular loop of TMH12 which, is very close to the

three Nedd4-1 ubiquitinated residues K877, K885 and K887 in the tertiary structure of the transporter.

6.2.1 Future Work

One aspect of the study that could be tested in the future is the hypothesis that the PDY motif is a Nedd4-1 binding site. This hypothesis could be tested in HEK293T cells following co-expression of a PDY motif point mutant ABCB1 with Nedd4-1 and comparison of the expression level of the mutant ABCB1 at the plasma membrane with a wild-type control in the presence and absence of Nedd4-1. This would probably be best achieved using stably transfected cells (that express a low but consistent level of wild-type or PDY mutant ABCB1) and introduction of Nedd4-1 and ubiquitin by transient transfection. This approach could be complemented by purification of the PDY motif mutant for *in vitro* studies, to test whether Nedd4-1 can still ubiquitinate the transporter. The mobility of the Nedd4-1 treated material on SDS-PAGE may give the first indications of whether the protein is ubiquitinated followed by mass spectrometry to confirm.

Other potential for future work is to test the relevance of ABCB1 ubiquitination in a more physiologically-relevant cell line. The human brain microvascular endothelial cell line hCMEC/D3 cells express ABCB1, ABCC4, ABCC5 and ABCG2 typical for brain endothelium, as observed in freshly isolated human brain microvessels. ABCC1 has also been detected in this cell line suggesting that *in vitro* culturing may induce non-physiological expression of this gene [260]. One recent study has used the hCMEC/D3 cell line to show β-amyloid efflux as a model of the blood-brain barrier and also compared β-amyloid clearance in human brain microvascular endothelium (hCMEC/D3) with mouse brain endothelial cell line (bEnd3) [261]. The hCMEC/D3 cell line could therefore be useful as a model of the blood-

brain barrier for potential future experiments of this study. In my study, Nedd4-1 was used as the ubiquitin ligase for ABCB1 ubiquitination but as described in chapter 4, the 'Human Nedd4 Family' consists of nine distinct members that all have similar domain organisation. hCMEC/D3 cells may help to discover which of the nine human Nedd4 ligases are expressed in human brain endothelial cells and which are elevated on challenge with β-amyloid. hCMEC/D3 cells could also be useful to test whether overexpression of the relevant Nedd4 can down-regulate ABCB1 at the plasma membrane and whether siRNA knockdown of the relevant Nedd4 ligase is able to prevent reduction of ABCB1 density at the plasma membrane. Beyond these potential future experiments, the regulation of the relevant Nedd4 could be studied and whether this regulatory network could be targeted in the future as a potential therapy for Alzheimer's Disease.

6.3. Lysophosphatidylinositol Autocrine Loop

A Lysophosphatidylinositol (LPI) autocrine loop has been recently been identified as an important signalling cascade in cancer cell proliferation and migration [241, 245-247]. This cascade uses GPR55 as the receptor for LPI. Once triggered, holo-GPR55 induces Akt and Rho activation, ERK phosphorylation and Ca^{2+} mobilization in the cell. The only gap in this cascade was definitive identification of the transporter which exports LPI from cells. siRNA knock down of ABCC1 inhibited proliferation in prostate cancer cells similar to the effect of GPR55 knock down and also resulted in a significant decrease in LPI release to the culture media [110]. The proliferative block could be rescued by the addition of exogenous LPI suggesting that ABCC1 was responsible for secretion of the LPI. ABCC3 is also often over-expressed in pancreatic cancer cell lines and it shares a wide range of transport ligands with ABCC1 [127]. Recently, siRNA knock-down of ABCC3 was also shown to result in down-regulation of proliferation in pancreatic cancer cell lines suggesting it may also be important in carcinogenesis (Prof Falasca, personal communication).

To confirm the role of ABCC1 and ABCC3 in LPI transport I expressed the transporters transiently in HEK293T cells and prepared inside-out vesicles. I have shown that tritiated-LPI is a transport substrate of both ABCC1 and ABCC3. The transport activity is inhibitable by vanadate, and ABCC1 transport of LPI can be inhibited by MK-571. These data support the conclusion ABCC1 and ABCC3 do indeed transport LPI and that they are likely to be important in various cancers, (in particular ABCC1 in prostate cancer and ABCC3 in pancreatic cancer, and both in ovarian carcinoma), for the LPI autocrine loop which promotes migration and proliferation (Figure 6.1)

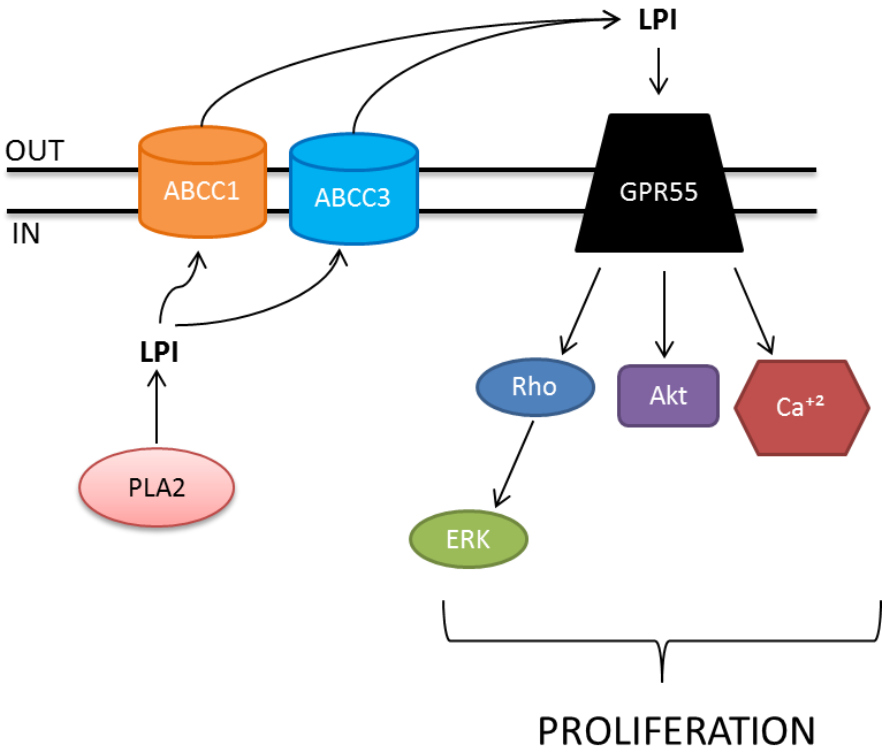

Figure 6.1: LPI autocrine loop in cancer cells. In this thesis, it was shown that ABCC1 and ABCC3 can both transport LPI.

.

6.3.1 Future Work

Translation of this knowledge into potential therapeutics should be the focus of the future work. Blockage of LPI release by ABCC1 and/or ABCC3 or blockage of GPR55 are potential targets for intervention and may result in therapeutic benefit. Putative drugs can be tested by vesicle transport assays and promising candidates can be tested on well-defined cell lines and animal models of cancer, before clinical trials in humans.

REFERENCES

1. Jardetzky, O., *Simple allosteric model for membrane pumps.* Nature, 1966. **211**(5052): p. 969-70.
2. Pedersen, P.L., *Transport ATPases into the year 2008: a brief overview related to types, structures, functions and roles in health and disease.* J Bioenerg Biomembr, 2007. **39**(5-6): p. 349-55.
3. Skou, J.C., *The influence of some cations on an adenosine triphosphatase from peripheral nerves.* Biochim Biophys Acta, 1957. **23**(2): p. 394-401.
4. Pedersen, P.L. and E. Carafoli, *Ion motive ATPases. I. Ubiquity, properties, and significance to cell function.* Trends Biochem Sci, 1987. **12**: p. 146-150.
5. Bublitz, M., J.P. Morth, and P. Nissen, *P-type ATPases at a glance.* J Cell Sci, 2011. **124**(Pt 15): p. 2515-9.
6. Capaldi, R.A. and R. Aggeler, *Mechanism of the F(1)F(0)-type ATP synthase, a biological rotary motor.* Trends Biochem Sci, 2002. **27**(3): p. 154-60.
7. Beyenbach, K.W. and H. Wieczorek, *The V-type H+ ATPase: molecular structure and function, physiological roles and regulation.* J Exp Biol, 2006. **209**(Pt 4): p. 577-89.
8. Higgins, C.F., *ABC transporters: from microorganisms to man.* Annu Rev Cell Biol, 1992. **8**: p. 67-113.
9. Berger, E.A. and L.A. Heppel, *A binding protein involved in the transport of cystine and diaminopimelic acid in Escherichia coli.* J Biol Chem, 1972. **247**(23): p. 7684-94.
10. Berger, E.A., *Different mechanisms of energy coupling for the active transport of proline and glutamine in Escherichia coli.* Proc Natl Acad Sci U S A, 1973. **70**(5): p. 1514-8.
11. Ross, J.I., et al., *Inducible erythromycin resistance in staphylococci is encoded by a member of the ATP-binding transport super-gene family.* Mol Microbiol, 1990. **4**(7): p. 1207-14.
12. Borst, P. and R.O. Elferink, *Mammalian ABC transporters in health and disease.* Annu Rev Biochem, 2002. **71**: p. 537-92.
13. Dean, M., A. Rzhetsky, and R. Allikmets, *The human ATP-binding cassette (ABC) transporter superfamily.* Genome Res, 2001. **11**(7): p. 1156-66.
14. Stieger, B. and C.F. Higgins, *Twenty years of ATP-binding cassette (ABC) transporters.* Pflugers Arch, 2007. **453**(5): p. 543.
15. Dano, K., *Active outward transport of daunomycin in resistant Ehrlich ascites tumor cells.* Biochim Biophys Acta, 1973. **323**(3): p. 466-83.
16. Juliano, R.L. and V. Ling, *A surface glycoprotein modulating drug permeability in Chinese hamster ovary cell mutants.* Biochim Biophys Acta, 1976. **455**(1): p. 152-62.
17. Cole, S.P., et al., *Overexpression of a transporter gene in a multidrug-resistant human lung cancer cell line.* Science, 1992. **258**(5088): p. 1650-4.
18. Mayer, R., et al., *Expression of the MRP gene-encoded conjugate export pump in liver and its selective absence from the canalicular membrane in transport-deficient mutant hepatocytes.* J Cell Biol, 1995. **131**(1): p. 137-50.
19. Kool, M., et al., *Analysis of expression of cMOAT (MRP2), MRP3, MRP4, and MRP5, homologues of the multidrug resistance-associated protein gene (MRP1), in human cancer cell lines.* Cancer Res, 1997. **57**(16): p. 3537-47.
20. Allikmets, R., et al., *Characterization of the human ABC superfamily: isolation and mapping of 21 new genes using the expressed sequence tags database.* Hum Mol Genet, 1996. **5**(10): p. 1649-55.
21. Doyle, L.A., et al., *A multidrug resistance transporter from human MCF-7 breast cancer cells.* Proc Natl Acad Sci U S A, 1998. **95**(26): p. 15665-70.
22. Roninson, I.B., et al., *Isolation of human mdr DNA sequences amplified in multidrug-resistant KB carcinoma cells.* Proc Natl Acad Sci U S A, 1986. **83**(12): p. 4538-42.

23. Ueda, K., et al., *The human multidrug resistance (mdr1) gene. cDNA cloning and transcription initiation.* J Biol Chem, 1987. **262**(2): p. 505-8.
24. Loe, D.W., et al., *Multidrug resistance protein (MRP)-mediated transport of leukotriene C4 and chemotherapeutic agents in membrane vesicles. Demonstration of glutathione-dependent vincristine transport.* J Biol Chem, 1996. **271**(16): p. 9675-82.
25. Leslie, E.M., R.G. Deeley, and S.P. Cole, *Multidrug resistance proteins: role of P-glycoprotein, MRP1, MRP2, and BCRP (ABCG2) in tissue defense.* Toxicol Appl Pharmacol, 2005. **204**(3): p. 216-37.
26. Taniguchi, K., et al., *A human canalicular multispecific organic anion transporter (cMOAT) gene is overexpressed in cisplatin-resistant human cancer cell lines with decreased drug accumulation.* Cancer Res, 1996. **56**(18): p. 4124-9.
27. Kool, M., et al., *MRP3, an organic anion transporter able to transport anti-cancer drugs.* Proc Natl Acad Sci U S A, 1999. **96**(12): p. 6914-9.
28. Schuetz, J.D., et al., *MRP4: A previously unidentified factor in resistance to nucleoside-based antiviral drugs.* Nat Med, 1999. **5**(9): p. 1048-51.
29. Wijnholds, J., et al., *Multidrug-resistance protein 5 is a multispecific organic anion transporter able to transport nucleotide analogs.* Proc Natl Acad Sci U S A, 2000. **97**(13): p. 7476-81.
30. Debenham, P.G., et al., *DNA-mediated transfer of multiple drug resistance and plasma membrane glycoprotein expression.* Mol Cell Biol, 1982. **2**(8): p. 881-9.
31. Nakayama, M., et al., *Hypomethylation status of CpG sites at the promoter region and overexpression of the human MDR1 gene in acute myeloid leukemias.* Blood, 1998. **92**(11): p. 4296-307.
32. Kantharidis, P., et al., *Altered methylation of the human MDR1 promoter is associated with acquired multidrug resistance.* Clin Cancer Res, 1997. **3**(11): p. 2025-32.
33. El-Osta, A., et al., *Precipitous release of methyl-CpG binding protein 2 and histone deacetylase 1 from the methylated human multidrug resistance gene (MDR1) on activation.* Mol Cell Biol, 2002. **22**(6): p. 1844-57.
34. Yague, E., et al., *P-glycoprotein (MDR1) expression in leukemic cells is regulated at two distinct steps, mRNA stabilization and translational initiation.* J Biol Chem, 2003. **278**(12): p. 10344-52.
35. Baker, E.K., et al., *Epigenetic changes to the MDR1 locus in response to chemotherapeutic drugs.* Oncogene, 2005. **24**(54): p. 8061-75.
36. Lehmann, J.M., et al., *The human orphan nuclear receptor PXR is activated by compounds that regulate CYP3A4 gene expression and cause drug interactions.* J Clin Invest, 1998. **102**(5): p. 1016-23.
37. Synold, T.W., I. Dussault, and B.M. Forman, *The orphan nuclear receptor SXR coordinately regulates drug metabolism and efflux.* Nat Med, 2001. **7**(5): p. 584-90.
38. Saeki, M., et al., *Identification of the functional vitamin D response elements in the human MDR1 gene.* Biochem Pharmacol, 2008. **76**(4): p. 531-42.
39. Hui, R.C., et al., *Doxorubicin activates FOXO3a to induce the expression of multidrug resistance gene ABCB1 (MDR1) in K562 leukemic cells.* Mol Cancer Ther, 2008. **7**(3): p. 670-8.
40. Mellquist, J.L., et al., *The amino acid following an asn-X-Ser/Thr sequon is an important determinant of N-linked core glycosylation efficiency.* Biochemistry, 1998. **37**(19): p. 6833-7.
41. Schinkel, A.H., et al., *N-glycosylation and deletion mutants of the human MDR1 P-glycoprotein.* J Biol Chem, 1993. **268**(10): p. 7474-81.
42. Gribar, J.J., et al., *Functional characterization of glycosylation-deficient human P-glycoprotein using a vaccinia virus expression system.* J Membr Biol, 2000. **173**(3): p. 203-14.
43. Zhang, Z., et al., *Regulation of the stability of P-glycoprotein by ubiquitination.* Mol Pharmacol, 2004. **66**(3): p. 395-403.
44. Chambers, T.C., et al., *Identification of specific sites in human P-glycoprotein phosphorylated by protein kinase C.* J Biol Chem, 1993. **268**(7): p. 4592-5.

45. Hrycyna, C.A., et al., *Structural flexibility of the linker region of human P-glycoprotein permits ATP hydrolysis and drug transport.* Biochemistry, 1998. **37**(39): p. 13660-73.
46. Chambers, T.C., et al., *Phosphorylation by protein kinase C and cyclic AMP-dependent protein kinase of synthetic peptides derived from the linker region of human P-glycoprotein.* Biochem J, 1994. **299 (Pt 1)**: p. 309-15.
47. Chambers, T.C., B. Zheng, and J.F. Kuo, *Regulation by phorbol ester and protein kinase C inhibitors, and by a protein phosphatase inhibitor (okadaic acid), of P-glycoprotein phosphorylation and relationship to drug accumulation in multidrug-resistant human KB cells.* Mol Pharmacol, 1992. **41**(6): p. 1008-15.
48. Ma, L.D., et al., *Analysis of P-glycoprotein phosphorylation in HL60 cells isolated for resistance to vincristine.* J Biol Chem, 1991. **266**(9): p. 5593-9.
49. Germann, U.A., et al., *Characterization of phosphorylation-defective mutants of human P-glycoprotein expressed in mammalian cells.* J Biol Chem, 1996. **271**(3): p. 1708-16.
50. Goodfellow, H.R., et al., *Protein kinase C-mediated phosphorylation does not regulate drug transport by the human multidrug resistance P-glycoprotein.* J Biol Chem, 1996. **271**(23): p. 13668-74.
51. Castro, A.F., et al., *Mechanism of inhibition of P-glycoprotein-mediated drug transport by protein kinase C blockers.* Biochem Pharmacol, 1999. **58**(11): p. 1723-33.
52. Muller, C., G. Laurent, and V. Ling, *P-glycoprotein stability is affected by serum deprivation and high cell density in multidrug-resistant cells.* J Cell Physiol, 1995. **163**(3): p. 538-44.
53. Goldstein, G., et al., *Isolation of a polypeptide that has lymphocyte-differentiating properties and is probably represented universally in living cells.* Proc Natl Acad Sci U S A, 1975. **72**(1): p. 11-5.
54. Hershko, A. and A. Ciechanover, *The ubiquitin system.* Annu Rev Biochem, 1998. **67**: p. 425-79.
55. Pickart, C.M. and M.J. Eddins, *Ubiquitin: structures, functions, mechanisms.* Biochim Biophys Acta, 2004. **1695**(1-3): p. 55-72.
56. Katayama, K., K. Noguchi, and Y. Sugimoto, *FBXO15 regulates P-glycoprotein/ABCB1 expression through the ubiquitin--proteasome pathway in cancer cells.* Cancer Sci, 2013. **104**(6): p. 694-702.
57. Dawson, R.J. and K.P. Locher, *Structure of a bacterial multidrug ABC transporter.* Nature, 2006. **443**(7108): p. 180-5.
58. Smith, P.C., et al., *ATP binding to the motor domain from an ABC transporter drives formation of a nucleotide sandwich dimer.* Mol Cell, 2002. **10**(1): p. 139-49.
59. Sauna, Z.E., et al., *Catalytic cycle of ATP hydrolysis by P-glycoprotein: evidence for formation of the E.S reaction intermediate with ATP-gamma-S, a nonhydrolyzable analogue of ATP.* Biochemistry, 2007. **46**(48): p. 13787-99.
60. Chen, J., et al., *A tweezers-like motion of the ATP-binding cassette dimer in an ABC transport cycle.* Mol Cell, 2003. **12**(3): p. 651-61.
61. Zaitseva, J., et al., *A structural analysis of asymmetry required for catalytic activity of an ABC-ATPase domain dimer.* EMBO J, 2006. **25**(14): p. 3432-43.
62. Kim, I.W., et al., *The conserved tyrosine residues 401 and 1044 in ATP sites of human P-glycoprotein are critical for ATP binding and hydrolysis: evidence for a conserved subdomain, the A-loop in the ATP-binding cassette.* Biochemistry, 2006. **45**(24): p. 7605-16.
63. Hung, L.W., et al., *Crystal structure of the ATP-binding subunit of an ABC transporter.* Nature, 1998. **396**(6712): p. 703-7.
64. Jones, P.M. and A.M. George, *Role of the D-loops in allosteric control of ATP hydrolysis in an ABC transporter.* J Phys Chem A, 2012. **116**(11): p. 3004-13.
65. Karpowich, N., et al., *Crystal structures of the MJ1267 ATP binding cassette reveal an induced-fit effect at the ATPase active site of an ABC transporter.* Structure, 2001. **9**(7): p. 571-86.

66. Yuan, Y.R., et al., *The crystal structure of the MJ0796 ATP-binding cassette. Implications for the structural consequences of ATP hydrolysis in the active site of an ABC transporter.* J Biol Chem, 2001. **276**(34): p. 32313-21.
67. Raviv, Y., et al., *Photosensitized labeling of a functional multidrug transporter in living drug-resistant tumor cells.* J Biol Chem, 1990. **265**(7): p. 3975-80.
68. Loo, T.W., M.C. Bartlett, and D.M. Clarke, *Simultaneous binding of two different drugs in the binding pocket of the human multidrug resistance P-glycoprotein.* J Biol Chem, 2003. **278**(41): p. 39706-10.
69. Chen, C.J., et al., *Internal duplication and homology with bacterial transport proteins in the mdr1 (P-glycoprotein) gene from multidrug-resistant human cells.* Cell, 1986. **47**(3): p. 381-9.
70. Aller, S.G., et al., *Structure of P-glycoprotein reveals a molecular basis for poly-specific drug binding.* Science, 2009. **323**(5922): p. 1718-22.
71. Shapiro, A.B. and V. Ling, *Positively cooperative sites for drug transport by P-glycoprotein with distinct drug specificities.* Eur J Biochem, 1997. **250**(1): p. 130-7.
72. Shapiro, A.B., et al., *Stimulation of P-glycoprotein-mediated drug transport by prazosin and progesterone. Evidence for a third drug-binding site.* Eur J Biochem, 1999. **259**(3): p. 841-50.
73. Kimura, Y., et al., *Cholesterol fill-in model: mechanism for substrate recognition by ABC proteins.* J Bioenerg Biomembr, 2007. **39**(5-6): p. 447-52.
74. Wise, J.G., *Catalytic Transitions in the Human MDR1 P-Glycoprotein Drug Binding Sites.* Biochemistry, 2012.
75. Becker, J.P., et al., *Molecular models of human P-glycoprotein in two different catalytic states.* BMC Struct Biol, 2009. **9**: p. 3.
76. Becker, J.P., et al., *Dynamics and structural changes induced by ATP binding in SAV1866, a bacterial ABC exporter.* J Phys Chem B, 2010. **114**(48): p. 15948-57.
77. Higgins, C.F. and K.J. Linton, *The ATP switch model for ABC transporters.* Nat Struct Mol Biol, 2004. **11**(10): p. 918-26.
78. Venter, H., et al., *An ABC transporter with a secondary-active multidrug translocator domain.* Nature, 2003. **426**(6968): p. 866-70.
79. Qu, Q., P.L. Russell, and F.J. Sharom, *Stoichiometry and affinity of nucleotide binding to P-glycoprotein during the catalytic cycle.* Biochemistry, 2003. **42**(4): p. 1170-7.
80. Martin, C., et al., *Drug binding sites on P-glycoprotein are altered by ATP binding prior to nucleotide hydrolysis.* Biochemistry, 2000. **39**(39): p. 11901-6.
81. Martin, C., C.F. Higgins, and R. Callaghan, *The vinblastine binding site adopts high- and low-affinity conformations during a transport cycle of P-glycoprotein.* Biochemistry, 2001. **40**(51): p. 15733-42.
82. Loo, T.W., M.C. Bartlett, and D.M. Clarke, *Nucleotide binding, ATP hydrolysis, and mutation of the catalytic carboxylates of human P-glycoprotein cause distinct conformational changes in the transmembrane segments.* Biochemistry, 2007. **46**(32): p. 9328-36.
83. Rosenberg, M.F., et al., *Three-dimensional structures of the mammalian multidrug resistance P-glycoprotein demonstrate major conformational changes in the transmembrane domains upon nucleotide binding.* J Biol Chem, 2003. **278**(10): p. 8294-9.
84. Rosenberg, M.F., et al., *Repacking of the transmembrane domains of P-glycoprotein during the transport ATPase cycle.* EMBO J, 2001. **20**(20): p. 5615-25.
85. Sonne, J., et al., *Simulation of the coupling between nucleotide binding and transmembrane domains in the ATP binding cassette transporter BtuCD.* Biophys J, 2007. **92**(8): p. 2727-34.
86. Urbatsch, I.L., et al., *P-glycoprotein catalytic mechanism: studies of the ADP-vanadate inhibited state.* J Biol Chem, 2003. **278**(25): p. 23171-9.
87. Senior, A.E., M.K. al-Shawi, and I.L. Urbatsch, *The catalytic cycle of P-glycoprotein.* FEBS Lett, 1995. **377**(3): p. 285-9.
88. Thiebaut, F., et al., *Cellular localization of the multidrug-resistance gene product P-glycoprotein in normal human tissues.* Proc Natl Acad Sci U S A, 1987. **84**(21): p. 7735-8.

89. Jodoin, J., et al., *P-glycoprotein in blood-brain barrier endothelial cells: interaction and oligomerization with caveolins.* J Neurochem, 2003. **87**(4): p. 1010-23.
90. Su, L., C.Y. Cheng, and D.D. Mruk, *Drug transporter, P-glycoprotein (MDR1), is an integrated component of the mammalian blood-testis barrier.* Int J Biochem Cell Biol, 2009. **41**(12): p. 2578-87.
91. Zhang, Z.J., et al., *Disruption of mdr1a p-glycoprotein gene results in dysfunction of blood-inner ear barrier in mice.* Brain Res, 2000. **852**(1): p. 116-26.
92. Ni, Z. and Q. Mao, *ATP-binding cassette efflux transporters in human placenta.* Curr Pharm Biotechnol, 2011. **12**(4): p. 674-85.
93. Higgins, C.F. and M.M. Gottesman, *Is the multidrug transporter a flippase?* Trends Biochem Sci, 1992. **17**(1): p. 18-21.
94. Litman, T., et al., *Competitive, non-competitive and cooperative interactions between substrates of P-glycoprotein as measured by its ATPase activity.* Biochim Biophys Acta, 1997. **1361**(2): p. 169-76.
95. Seelig, A. and E. Landwojtowicz, *Structure-activity relationship of P-glycoprotein substrates and modifiers.* Eur J Pharm Sci, 2000. **12**(1): p. 31-40.
96. Zhou, S.F., *Structure, function and regulation of P-glycoprotein and its clinical relevance in drug disposition.* Xenobiotica, 2008. **38**(7-8): p. 802-32.
97. Murakami, M. and I. Kudo, *Phospholipase A2.* J Biochem, 2002. **131**(3): p. 285-92.
98. Venable, M.E., et al., *Platelet-activating factor: a phospholipid autacoid with diverse actions.* J Lipid Res, 1993. **34**(5): p. 691-702.
99. Six, D.A. and E.A. Dennis, *The expanding superfamily of phospholipase A(2) enzymes: classification and characterization.* Biochim Biophys Acta, 2000. **1488**(1-2): p. 1-19.
100. Bernatchez, P.N., et al., *VEGF stimulation of endothelial cell PAF synthesis is mediated by group V 14 kDa secretory phospholipase A2.* Br J Pharmacol, 2001. **134**(1): p. 197-205.
101. McHowat, J., et al., *Endothelial cell PAF synthesis following thrombin stimulation utilizes Ca(2+)-independent phospholipase A(2).* Biochemistry, 2001. **40**(49): p. 14921-31.
102. Rubin, B.B., et al., *Cytosolic phospholipase A2-alpha is necessary for platelet-activating factor biosynthesis, efficient neutrophil-mediated bacterial killing, and the innate immune response to pulmonary infection: cPLA2-alpha does not regulate neutrophil NADPH oxidase activity.* J Biol Chem, 2005. **280**(9): p. 7519-29.
103. Ernest, S. and E. Bello-Reuss, *Secretion of platelet-activating factor is mediated by MDR1 P-glycoprotein in cultured human mesangial cells.* J Am Soc Nephrol, 1999. **10**(11): p. 2306-13.
104. Raggers, R.J., I. Vogels, and G. van Meer, *Multidrug-resistance P-glycoprotein (MDR1) secretes platelet-activating factor.* Biochem J, 2001. **357**(Pt 3): p. 859-65.
105. Aponte, M., et al., *Activation of platelet-activating factor receptor and pleiotropic effects on tyrosine phospho-EGFR/Src/FAK/paxillin in ovarian cancer.* Cancer Res, 2008. **68**(14): p. 5839-48.
106. Cellai, C., et al., *Growth inhibition and differentiation of human breast cancer cells by the PAFR antagonist WEB-2086.* Br J Cancer, 2006. **94**(11): p. 1637-42.
107. Biancone, L., et al., *Platelet-activating factor inactivation by local expression of platelet-activating factor acetyl-hydrolase modifies tumor vascularization and growth.* Clin Cancer Res, 2003. **9**(11): p. 4214-20.
108. Ferreira, M.A., et al., *Tumor growth, angiogenesis and inflammation in mice lacking receptors for platelet activating factor (PAF).* Life Sci, 2007. **81**(3): p. 210-7.
109. Sreevidya, C.S., et al., *Inhibition of photocarcinogenesis by platelet-activating factor or serotonin receptor antagonists.* Cancer Res, 2008. **68**(10): p. 3978-84.
110. Pineiro, R., T. Maffucci, and M. Falasca, *The putative cannabinoid receptor GPR55 defines a novel autocrine loop in cancer cell proliferation.* Oncogene, 2011. **30**(2): p. 142-52.
111. Ueda, K., et al., *Human P-glycoprotein transports cortisol, aldosterone, and dexamethasone, but not progesterone.* J Biol Chem, 1992. **267**(34): p. 24248-52.

112. Croop, J.M., et al., *The three mouse multidrug resistance (mdr) genes are expressed in a tissue-specific manner in normal mouse tissues.* Mol Cell Biol, 1989. **9**(3): p. 1346-50.
113. Schinkel, A.H., et al., *Normal viability and altered pharmacokinetics in mice lacking mdr1-type (drug-transporting) P-glycoproteins.* Proc Natl Acad Sci U S A, 1997. **94**(8): p. 4028-33.
114. Schoenfelder, Y., C. Hiemke, and U. Schmitt, *Behavioural consequences of p-glycoprotein deficiency in mice, with special focus on stress-related mechanisms.* J Neuroendocrinol, 2012. **24**(5): p. 809-17.
115. Schinkel, A.H., et al., *Disruption of the mouse mdr1a P-glycoprotein gene leads to a deficiency in the blood-brain barrier and to increased sensitivity to drugs.* Cell, 1994. **77**(4): p. 491-502.
116. Sun, M., et al., *Expression of the multidrug resistance P-glycoprotein, (ABCB1 glycoprotein) in the human placenta decreases with advancing gestation.* Placenta, 2006. **27**(6-7): p. 602-9.
117. Mathias, A.A., J. Hitti, and J.D. Unadkat, *P-glycoprotein and breast cancer resistance protein expression in human placentae of various gestational ages.* Am J Physiol Regul Integr Comp Physiol, 2005. **289**(4): p. R963-9.
118. Trock, B.J., F. Leonessa, and R. Clarke, *Multidrug resistance in breast cancer: a meta-analysis of MDR1/gp170 expression and its possible functional significance.* J Natl Cancer Inst, 1997. **89**(13): p. 917-31.
119. Baekelandt, M.M., et al., *P-glycoprotein expression is a marker for chemotherapy resistance and prognosis in advanced ovarian cancer.* Anticancer Res, 2000. **20**(2B): p. 1061-7.
120. Chan, H.S., et al., *Immunohistochemical detection of P-glycoprotein: prognostic correlation in soft tissue sarcoma of childhood.* J Clin Oncol, 1990. **8**(4): p. 689-704.
121. Leith, C.P., et al., *Frequency and clinical significance of the expression of the multidrug resistance proteins MDR1/P-glycoprotein, MRP1, and LRP in acute myeloid leukemia: a Southwest Oncology Group Study.* Blood, 1999. **94**(3): p. 1086-99.
122. Falasca, M. and K.J. Linton, *Investigational ABC transporter inhibitors.* Expert Opin Investig Drugs, 2012. **21**(5): p. 657-66.
123. Evers, R., et al., *Basolateral localization and export activity of the human multidrug resistance-associated protein in polarized pig kidney cells.* J Clin Invest, 1996. **97**(5): p. 1211-8.
124. Konig, J., et al., *Characterization of the human multidrug resistance protein isoform MRP3 localized to the basolateral hepatocyte membrane.* Hepatology, 1999. **29**(4): p. 1156-63.
125. Varadi, A., et al., *Membrane topology of the human multidrug resistance-associated protein (MRP) and its homologs.* Cytotechnology, 1998. **27**(1-3): p. 71-9.
126. Deeley, R.G. and S.P. Cole, *Substrate recognition and transport by multidrug resistance protein 1 (ABCC1).* FEBS Lett, 2006. **580**(4): p. 1103-11.
127. Konig, J., et al., *Expression and localization of human multidrug resistance protein (ABCC) family members in pancreatic carcinoma.* Int J Cancer, 2005. **115**(3): p. 359-67.
128. Steinbach, D., et al., *The multidrug resistance-associated protein 3 (MRP3) is associated with a poor outcome in childhood ALL and may account for the worse prognosis in male patients and T-cell immunophenotype.* Blood, 2003. **102**(13): p. 4493-8.
129. Deeley, R.G., C. Westlake, and S.P. Cole, *Transmembrane transport of endo- and xenobiotics by mammalian ATP-binding cassette multidrug resistance proteins.* Physiol Rev, 2006. **86**(3): p. 849-99.
130. Bakos, E. and L. Homolya, *Portrait of multifaceted transporter, the multidrug resistance-associated protein 1 (MRP1/ABCC1).* Pflugers Arch, 2007. **453**(5): p. 621-41.
131. Bakos, E., et al., *Membrane topology and glycosylation of the human multidrug resistance-associated protein.* J Biol Chem, 1996. **271**(21): p. 12322-6.
132. Muller, M., et al., *Evidence for the role of glycosylation in accessibility of the extracellular domains of human MRP1 (ABCC1).* Biochemistry, 2002. **41**(31): p. 10123-32.
133. Chen, Q., et al., *Cytoplasmic retraction of the amino terminus of human multidrug resistance protein 1.* Biochemistry, 2002. **41**(29): p. 9052-62.
134. Chou, P.Y. and G.D. Fasman, *Prediction of beta-turns.* Biophys J, 1979. **26**(3): p. 367-83.

135. Chen, Q., et al., *The amino terminus of the human multidrug resistance transporter ABCC1 has a U-shaped folding with a gating function.* J Biol Chem, 2006. **281**(41): p. 31152-63.
136. Rosenberg, M.F., et al., *The structure of the multidrug resistance protein 1 (MRP1/ABCC1). crystallization and single-particle analysis.* J Biol Chem, 2001. **276**(19): p. 16076-82.
137. Yang, Y., et al., *Regulation of function by dimerization through the amino-terminal membrane-spanning domain of human ABCC1/MRP1.* J Biol Chem, 2007. **282**(12): p. 8821-30.
138. Wijnholds, J., et al., *Increased sensitivity to anticancer drugs and decreased inflammatory response in mice lacking the multidrug resistance-associated protein.* Nat Med, 1997. **3**(11): p. 1275-9.
139. Robbiani, D.F., et al., *The leukotriene C(4) transporter MRP1 regulates CCL19 (MIP-3beta, ELC)-dependent mobilization of dendritic cells to lymph nodes.* Cell, 2000. **103**(5): p. 757-68.
140. Wijnholds, J., et al., *Multidrug resistance protein 1 protects the choroid plexus epithelium and contributes to the blood-cerebrospinal fluid barrier.* J Clin Invest, 2000. **105**(3): p. 279-85.
141. Rao, V.V., et al., *Choroid plexus epithelial expression of MDR1 P glycoprotein and multidrug resistance-associated protein contribute to the blood-cerebrospinal-fluid drug-permeability barrier.* Proc Natl Acad Sci U S A, 1999. **96**(7): p. 3900-5.
142. St-Pierre, M.V., et al., *Expression of members of the multidrug resistance protein family in human term placenta.* Am J Physiol Regul Integr Comp Physiol, 2000. **279**(4): p. R1495-503.
143. Saito, T., et al., *Expression of multidrug resistance protein 1 (MRP1) in the rat cochlea with special reference to the blood-inner ear barrier.* Brain Res, 2001. **895**(1-2): p. 253-7.
144. Cole, S.P. and R.G. Deeley, *Transport of glutathione and glutathione conjugates by MRP1.* Trends Pharmacol Sci, 2006. **27**(8): p. 438-46.
145. Lorico, A., et al., *Disruption of the murine MRP (multidrug resistance protein) gene leads to increased sensitivity to etoposide (VP-16) and increased levels of glutathione.* Cancer Res, 1997. **57**(23): p. 5238-42.
146. Kreisholt, J., et al., *Immunohistochemical detection of DNA topoisomerase IIalpha, P-glycoprotein and multidrug resistance protein (MRP) in small-cell and non-small-cell lung cancer.* Br J Cancer, 1998. **77**(9): p. 1469-73.
147. Filipits, M., et al., *Clinical role of multidrug resistance protein 1 expression in chemotherapy resistance in early-stage breast cancer: the Austrian Breast and Colorectal Cancer Study Group.* J Clin Oncol, 2005. **23**(6): p. 1161-8.
148. Grant, C.E., et al., *Structural determinants of substrate specificity differences between human multidrug resistance protein (MRP) 1 (ABCC1) and MRP3 (ABCC3).* Drug Metab Dispos, 2008. **36**(12): p. 2571-81.
149. Zelcer, N., et al., *Characterization of drug transport by the human multidrug resistance protein 3 (ABCC3).* J Biol Chem, 2001. **276**(49): p. 46400-7.
150. Hirohashi, T., et al., *Hepatic expression of multidrug resistance-associated protein-like proteins maintained in eisai hyperbilirubinemic rats.* Mol Pharmacol, 1998. **53**(6): p. 1068-75.
151. Ogawa, K., et al., *Characterization of inducible nature of MRP3 in rat liver.* Am J Physiol Gastrointest Liver Physiol, 2000. **278**(3): p. G438-46.
152. Hirohashi, T., et al., *ATP-dependent transport of bile salts by rat multidrug resistance-associated protein 3 (Mrp3).* J Biol Chem, 2000. **275**(4): p. 2905-10.
153. Zeng, H., et al., *Transport of methotrexate (MTX) and folates by multidrug resistance protein (MRP) 3 and MRP1: effect of polyglutamylation on MTX transport.* Cancer Res, 2001. **61**(19): p. 7225-32.
154. Zhang, D.W., et al., *Characterization of the role of polar amino acid residues within predicted transmembrane helix 17 in determining the substrate specificity of multidrug resistance protein 3.* Biochemistry, 2003. **42**(33): p. 9989-10000.
155. Zeng, H., et al., *Transport of amphipathic anions by human multidrug resistance protein 3.* Cancer Res, 2000. **60**(17): p. 4779-84.

156. Graham, F.L., et al., *Characteristics of a human cell line transformed by DNA from human adenovirus type 5.* J Gen Virol, 1977. **36**(1): p. 59-74.
157. Zolnerciks, J.K., C. Wooding, and K.J. Linton, *Evidence for a Sav1866-like architecture for the human multidrug transporter P-glycoprotein.* FASEB J, 2007. **21**(14): p. 3937-48.
158. Iram, S.H. and S.P. Cole, *Mutation of Glu521 or Glu535 in cytoplasmic loop 5 causes differential misfolding in multiple domains of multidrug and organic anion transporter MRP1 (ABCC1).* J Biol Chem, 2012. **287**(10): p. 7543-55.
159. Oleschuk, C.J., R.G. Deeley, and S.P. Cole, *Substitution of Trp1242 of TM17 alters substrate specificity of human multidrug resistance protein 3.* Am J Physiol Gastrointest Liver Physiol, 2003. **284**(2): p. G280-9.
160. Lowry, O.H., et al., *Protein measurement with the Folin phenol reagent.* J Biol Chem, 1951. **193**(1): p. 265-75.
161. Vaudel, M., et al., *SearchGUI: An open-source graphical user interface for simultaneous OMSSA and X!Tandem searches.* Proteomics, 2011. **11**(5): p. 996-9.
162. Barsnes, H., et al., *compomics-utilities: an open-source Java library for computational proteomics.* BMC Bioinformatics, 2011. **12**: p. 70.
163. Parveen, Z., et al., *Molecular dissection of dual pseudosymmetric solute translocation pathways in human P-glycoprotein.* Mol Pharmacol, 2011. **79**(3): p. 443-52.
164. Urbatsch, I.L., et al., *Investigation of the role of glutamine-471 and glutamine-1114 in the two catalytic sites of P-glycoprotein.* Biochemistry, 2000. **39**(39): p. 11921-7.
165. Van Veldhoven, P.P. and G.P. Mannaerts, *Inorganic and organic phosphate measurements in the nanomolar range.* Anal Biochem, 1987. **161**(1): p. 45-8.
166. Chifflet, S., et al., *A method for the determination of inorganic phosphate in the presence of labile organic phosphate and high concentrations of protein: application to lens ATPases.* Anal Biochem, 1988. **168**(1): p. 1-4.
167. Landwojtowicz, E., P. Nervi, and A. Seelig, *Real-time monitoring of P-glycoprotein activation in living cells.* Biochemistry, 2002. **41**(25): p. 8050-7.
168. Zolnerciks, J.K., et al., *The Q loops of the human multidrug resistance transporter ABCB1 are necessary to couple drug binding to the ATP catalytic cycle.* FASEB J, 2014.
169. Pitchford, S., *Ligand characterization using microphysiometry.* Curr Protoc Neurosci, 2001. **Chapter 7**: p. Unit7 8.
170. Buchman, A.R. and P. Berg, *Comparison of intron-dependent and intron-independent gene expression.* Mol Cell Biol, 1988. **8**(10): p. 4395-405.
171. Huang, M.T. and C.M. Gorman, *Intervening sequences increase efficiency of RNA 3' processing and accumulation of cytoplasmic RNA.* Nucleic Acids Res, 1990. **18**(4): p. 937-47.
172. Bernstein, P. and J. Ross, *Poly(A), poly(A) binding protein and the regulation of mRNA stability.* Trends Biochem Sci, 1989. **14**(9): p. 373-7.
173. Carswell, S. and J.C. Alwine, *Efficiency of utilization of the simian virus 40 late polyadenylation site: effects of upstream sequences.* Mol Cell Biol, 1989. **9**(10): p. 4248-58.
174. Boussif, O., et al., *A versatile vector for gene and oligonucleotide transfer into cells in culture and in vivo: polyethylenimine.* Proc Natl Acad Sci U S A, 1995. **92**(16): p. 7297-301.
175. Akinc, A., et al., *Exploring polyethylenimine-mediated DNA transfection and the proton sponge hypothesis.* J Gene Med, 2005. **7**(5): p. 657-63.
176. Muller, M.R., et al., *Simultaneous measurement of cellular P-glycoprotein content and function by multiparametric flow-cytometry.* Int J Clin Pharmacol Ther, 2000. **38**(4): p. 180-6.
177. Martin, C., et al., *Communication between multiple drug binding sites on P-glycoprotein.* Mol Pharmacol, 2000. **58**(3): p. 624-32.
178. Jones, P.M. and A.M. George, *Mechanism of ABC transporters: a molecular dynamics simulation of a well characterized nucleotide-binding subunit.* Proc Natl Acad Sci U S A, 2002. **99**(20): p. 12639-44.

179. Mechetner, E.B. and I.B. Roninson, *Efficient inhibition of P-glycoprotein-mediated multidrug resistance with a monoclonal antibody.* Proc Natl Acad Sci U S A, 1992. **89**(13): p. 5824-8.
180. Mechetner, E.B., et al., *P-glycoprotein function involves conformational transitions detectable by differential immunoreactivity.* Proc Natl Acad Sci U S A, 1997. **94**(24): p. 12908-13.
181. Muller, M., et al., *Altered drug-stimulated ATPase activity in mutants of the human multidrug resistance protein.* J Biol Chem, 1996. **271**(4): p. 1877-83.
182. Tombline, G., et al., *Combined mutation of catalytic glutamate residues in the two nucleotide binding domains of P-glycoprotein generates a conformation that binds ATP and ADP tightly.* J Biol Chem, 2004. **279**(30): p. 31212-20.
183. Minsky, M., *Memoir on inventing the confocal scanning microscope.* Scanning, 1988. **10**(4): p. 128-138.
184. Hopfner, K.P., et al., *Structural biology of Rad50 ATPase: ATP-driven conformational control in DNA double-strand break repair and the ABC-ATPase superfamily.* Cell, 2000. **101**(7): p. 789-800.
185. Sauna, Z.E., et al., *Importance of the conserved Walker B glutamate residues, 556 and 1201, for the completion of the catalytic cycle of ATP hydrolysis by human P-glycoprotein (ABCB1).* Biochemistry, 2002. **41**(47): p. 13989-4000.
186. Orelle, C., et al., *The conserved glutamate residue adjacent to the Walker-B motif is the catalytic base for ATP hydrolysis in the ATP-binding cassette transporter BmrA.* J Biol Chem, 2003. **278**(47): p. 47002-8.
187. Locher, K.P., A.T. Lee, and D.C. Rees, *The E. coli BtuCD structure: a framework for ABC transporter architecture and mechanism.* Science, 2002. **296**(5570): p. 1091-8.
188. Deane, R., Z. Wu, and B.V. Zlokovic, *RAGE (yin) versus LRP (yang) balance regulates alzheimer amyloid beta-peptide clearance through transport across the blood-brain barrier.* Stroke, 2004. **35**(11 Suppl 1): p. 2628-31.
189. Deane, R., et al., *LRP/amyloid beta-peptide interaction mediates differential brain efflux of Abeta isoforms.* Neuron, 2004. **43**(3): p. 333-44.
190. Kuhnke, D., et al., *MDR1-P-Glycoprotein (ABCB1) Mediates Transport of Alzheimer's amyloid-beta peptides--implications for the mechanisms of Abeta clearance at the blood-brain barrier.* Brain Pathol, 2007. **17**(4): p. 347-53.
191. Lam, F.C., et al., *beta-Amyloid efflux mediated by p-glycoprotein.* J Neurochem, 2001. **76**(4): p. 1121-8.
192. Cirrito, J.R., et al., *P-glycoprotein deficiency at the blood-brain barrier increases amyloid-beta deposition in an Alzheimer disease mouse model.* J Clin Invest, 2005. **115**(11): p. 3285-90.
193. Hartz, A.M., D.S. Miller, and B. Bauer, *Restoring blood-brain barrier P-glycoprotein reduces brain amyloid-beta in a mouse model of Alzheimer's disease.* Mol Pharmacol, 2010. **77**(5): p. 715-23.
194. Vogelgesang, S., et al., *Deposition of Alzheimer's beta-amyloid is inversely correlated with P-glycoprotein expression in the brains of elderly non-demented humans.* Pharmacogenetics, 2002. **12**(7): p. 535-41.
195. Jeynes, B. and J. Provias, *An investigation into the role of P-glycoprotein in Alzheimer's disease lesion pathogenesis.* Neurosci Lett, 2011. **487**(3): p. 389-93.
196. Pham, A.D. and F. Sauer, *Ubiquitin-activating/conjugating activity of TAFII250, a mediator of activation of gene expression in Drosophila.* Science, 2000. **289**(5488): p. 2357-60.
197. Shih, S.C., K.E. Sloper-Mould, and L. Hicke, *Monoubiquitin carries a novel internalization signal that is appended to activated receptors.* EMBO J, 2000. **19**(2): p. 187-98.
198. Hicke, L., *Gettin' down with ubiquitin: turning off cell-surface receptors, transporters and channels.* Trends Cell Biol, 1999. **9**(3): p. 107-12.
199. Cadwell, K. and L. Coscoy, *Ubiquitination on nonlysine residues by a viral E3 ubiquitin ligase.* Science, 2005. **309**(5731): p. 127-30.

200. Xu, P., et al., *Quantitative proteomics reveals the function of unconventional ubiquitin chains in proteasomal degradation.* Cell, 2009. **137**(1): p. 133-45.
201. Wilkinson, K.D., *Regulation of ubiquitin-dependent processes by deubiquitinating enzymes.* FASEB J, 1997. **11**(14): p. 1245-56.
202. Ozkan, E., H. Yu, and J. Deisenhofer, *Mechanistic insight into the allosteric activation of a ubiquitin-conjugating enzyme by RING-type ubiquitin ligases.* Proc Natl Acad Sci U S A, 2005. **102**(52): p. 18890-5.
203. Huibregtse, J.M., et al., *A family of proteins structurally and functionally related to the E6-AP ubiquitin-protein ligase.* Proc Natl Acad Sci U S A, 1995. **92**(7): p. 2563-7.
204. Rotin, D. and S. Kumar, *Physiological functions of the HECT family of ubiquitin ligases.* Nat Rev Mol Cell Biol, 2009. **10**(6): p. 398-409.
205. Kumar, S., Y. Tomooka, and M. Noda, *Identification of a set of genes with developmentally down-regulated expression in the mouse brain.* Biochem Biophys Res Commun, 1992. **185**(3): p. 1155-61.
206. Ingham, R.J., G. Gish, and T. Pawson, *The Nedd4 family of E3 ubiquitin ligases: functional diversity within a common modular architecture.* Oncogene, 2004. **23**(11): p. 1972-84.
207. Coussens, L., et al., *Multiple, distinct forms of bovine and human protein kinase C suggest diversity in cellular signaling pathways.* Science, 1986. **233**(4766): p. 859-66.
208. Knopf, J.L., et al., *Cloning and expression of multiple protein kinase C cDNAs.* Cell, 1986. **46**(4): p. 491-502.
209. Anan, T., et al., *Human ubiquitin-protein ligase Nedd4: expression, subcellular localization and selective interaction with ubiquitin-conjugating enzymes.* Genes Cells, 1998. **3**(11): p. 751-63.
210. Sudol, M., et al., *Characterization of a novel protein-binding module--the WW domain.* FEBS Lett, 1995. **369**(1): p. 67-71.
211. Sudol, M. and T. Hunter, *NeW wrinkles for an old domain.* Cell, 2000. **103**(7): p. 1001-4.
212. Yang, B. and S. Kumar, *Nedd4 and Nedd4-2: closely related ubiquitin-protein ligases with distinct physiological functions.* Cell Death Differ, 2010. **17**(1): p. 68-77.
213. Kamynina, E., C. Tauxe, and O. Staub, *Distinct characteristics of two human Nedd4 proteins with respect to epithelial Na(+) channel regulation.* Am J Physiol Renal Physiol, 2001. **281**(3): p. F469-77.
214. Kamynina, E., et al., *A novel mouse Nedd4 protein suppresses the activity of the epithelial Na+ channel.* FASEB J, 2001. **15**(1): p. 204-214.
215. Kost, T.A., J.P. Condreay, and D.L. Jarvis, *Baculovirus as versatile vectors for protein expression in insect and mammalian cells.* Nat Biotechnol, 2005. **23**(5): p. 567-75.
216. Schimerlik, M.I., *Overview of membrane protein solubilization.* Curr Protoc Neurosci, 2001. **Chapter 5**: p. Unit 5 9.
217. Seddon, A.M., P. Curnow, and P.J. Booth, *Membrane proteins, lipids and detergents: not just a soap opera.* Biochim Biophys Acta, 2004. **1666**(1-2): p. 105-17.
218. Tanford, C., *The hydrophobic effect and the organization of living matter.* Science, 1978. **200**(4345): p. 1012-8.
219. Raghuraman, H. and A. Chattopadhyay, *Effect of micellar charge on the conformation and dynamics of melittin.* Eur Biophys J, 2004. **33**(7): p. 611-22.
220. Kalipatnapu, S. and A. Chattopadhyay, *Membrane protein solubilization: recent advances and challenges in solubilization of serotonin1A receptors.* IUBMB Life, 2005. **57**(7): p. 505-12.
221. Blissard, G.W. and G.F. Rohrmann, *Baculovirus diversity and molecular biology.* Annu Rev Entomol, 1990. **35**: p. 127-55.
222. Blissard, G.W. and J.R. Wenz, *Baculovirus gp64 envelope glycoprotein is sufficient to mediate pH-dependent membrane fusion.* J Virol, 1992. **66**(11): p. 6829-35.
223. Volkman, L.E. and M.D. Summers, *Autographa californica nuclear polyhedrosis virus: comparative infectivity of the occluded, alkali-liberated, and nonoccluded forms.* J Invertebr Pathol, 1977. **30**(1): p. 102-3.

224. Ayres, M.D., et al., *The complete DNA sequence of Autographa californica nuclear polyhedrosis virus.* Virology, 1994. **202**(2): p. 586-605.
225. Kitts, P.A., M.D. Ayres, and R.D. Possee, *Linearization of baculovirus DNA enhances the recovery of recombinant virus expression vectors.* Nucleic Acids Res, 1990. **18**(19): p. 5667-72.
226. Kitts, P.A. and R.D. Possee, *A method for producing recombinant baculovirus expression vectors at high frequency.* Biotechniques, 1993. **14**(5): p. 810-7.
227. Fenn, J.B., et al., *Electrospray ionization for mass spectrometry of large biomolecules.* Science, 1989. **246**(4926): p. 64-71.
228. Makarov, A., *Electrostatic axially harmonic orbital trapping: a high-performance technique of mass analysis.* Anal Chem, 2000. **72**(6): p. 1156-62.
229. Kodan, A., et al., *Improved expression and purification of human multidrug resistance protein MDR1 from baculovirus-infected insect cells.* Protein Expr Purif, 2009. **66**(1): p. 7-14.
230. Callaghan, R., et al., *The functional purification of P-glycoprotein is dependent on maintenance of a lipid-protein interface.* Biochim Biophys Acta, 1997. **1328**(2): p. 109-24.
231. Rothnie, A., et al., *The importance of cholesterol in maintenance of P-glycoprotein activity and its membrane perturbing influence.* Eur Biophys J, 2001. **30**(6): p. 430-42.
232. Kimura, Y., et al., *Modulation of drug-stimulated ATPase activity of human MDR1/P-glycoprotein by cholesterol.* Biochem J, 2007. **401**(2): p. 597-605.
233. Maloney, P.C. and S.V. Ambudkar, *Functional reconstitution of prokaryote and eukaryote membrane proteins.* Arch Biochem Biophys, 1989. **269**(1): p. 1-10.
234. Dawson, R.J. and K.P. Locher, *Structure of the multidrug ABC transporter Sav1866 from Staphylococcus aureus in complex with AMP-PNP.* FEBS Lett, 2007. **581**(5): p. 935-8.
235. Stockner, T., et al., *Data-driven homology modelling of P-glycoprotein in the ATP-bound state indicates flexibility of the transmembrane domains.* FEBS J, 2009. **276**(4): p. 964-72.
236. Thomas, C.J., et al., *Localization of a baculovirus-induced chitinase in the insect cell endoplasmic reticulum.* J Virol, 1998. **72**(12): p. 10207-12.
237. Murillas, R., et al., *Identification of developmentally expressed proteins that functionally interact with Nedd4 ubiquitin ligase.* J Biol Chem, 2002. **277**(4): p. 2897-907.
238. Lundbaek, J.A. and O.S. Andersen, *Lysophospholipids modulate channel function by altering the mechanical properties of lipid bilayers.* J Gen Physiol, 1994. **104**(4): p. 645-73.
239. Metz, S.A., *Lysophosphatidylinositol, but not lysophosphatidic acid, stimulates insulin release. A possible role for phospholipase A2 but not de novo synthesis of lysophospholipid in pancreatic islet function.* Biochem Biophys Res Commun, 1986. **138**(2): p. 720-7.
240. Alonso, T., et al., *Malignant transformation by ras and other oncogenes produces common alterations in inositol phospholipid signaling pathways.* Proc Natl Acad Sci U S A, 1988. **85**(12): p. 4271-5.
241. Falasca, M. and D. Corda, *Elevated levels and mitogenic activity of lysophosphatidylinositol in k-ras-transformed epithelial cells.* Eur J Biochem, 1994. **221**(1): p. 383-9.
242. Oka, S., et al., *Identification of GPR55 as a lysophosphatidylinositol receptor.* Biochem Biophys Res Commun, 2007. **362**(4): p. 928-34.
243. Metz, S.A., *Mobilization of cellular Ca2+ by lysophospholipids in rat islets of Langerhans.* Biochim Biophys Acta, 1988. **968**(2): p. 239-52.
244. Oka, S., et al., *Lysophosphatidylinositol induces rapid phosphorylation of p38 mitogen-activated protein kinase and activating transcription factor 2 in HEK293 cells expressing GPR55 and IM-9 lymphoblastoid cells.* J Biochem, 2010. **147**(5): p. 671-8.
245. Falasca, M., et al., *Signalling pathways involved in the mitogenic action of lysophosphatidylinositol.* Oncogene, 1995. **10**(11): p. 2113-24.
246. Monet, M., et al., *Lysophospholipids stimulate prostate cancer cell migration via TRPV2 channel activation.* Biochim Biophys Acta, 2009. **1793**(3): p. 528-39.

247. Ford, L.A., et al., *A role for L-alpha-lysophosphatidylinositol and GPR55 in the modulation of migration, orientation and polarization of human breast cancer cells.* Br J Pharmacol, 2010. **160**(3): p. 762-71.
248. Oka, S., et al., *2-Arachidonoyl-sn-glycero-3-phosphoinositol: a possible natural ligand for GPR55.* J Biochem, 2009. **145**(1): p. 13-20.
249. Kotsikorou, E., et al., *Lipid bilayer molecular dynamics study of lipid-derived agonists of the putative cannabinoid receptor, GPR55.* Chem Phys Lipids, 2011. **164**(2): p. 131-43.
250. Sutphen, R., et al., *Lysophospholipids are potential biomarkers of ovarian cancer.* Cancer Epidemiol Biomarkers Prev, 2004. **13**(7): p. 1185-91.
251. Sullivan, G.F., et al., *The expression of drug resistance gene products during the progression of human prostate cancer.* Clin Cancer Res, 1998. **4**(6): p. 1393-403.
252. Zalcberg, J., et al., *MRP1 not MDR1 gene expression is the predominant mechanism of acquired multidrug resistance in two prostate carcinoma cell lines.* Prostate Cancer Prostatic Dis, 2000. **3**(2): p. 66-75.
253. Ohishi, Y., et al., *ATP-binding cassette superfamily transporter gene expression in human primary ovarian carcinoma.* Clin Cancer Res, 2002. **8**(12): p. 3767-75.
254. Robey, R.W., et al., *Inhibition of P-glycoprotein (ABCB1)- and multidrug resistance-associated protein 1 (ABCC1)-mediated transport by the orally administered inhibitor, CBT-1((R)).* Biochem Pharmacol, 2008. **75**(6): p. 1302-12.
255. Zaja, R., R.S. Klobucar, and T. Smital, *Detection and functional characterization of Pgp1 (ABCB1) and MRP3 (ABCC3) efflux transporters in the PLHC-1 fish hepatoma cell line.* Aquat Toxicol, 2007. **81**(4): p. 365-76.
256. Loe, D.W., et al., *ATP-dependent 17 beta-estradiol 17-(beta-D-glucuronide) transport by multidrug resistance protein (MRP). Inhibition by cholestatic steroids.* J Biol Chem, 1996. **271**(16): p. 9683-9.
257. Haimeur, A., R.G. Deeley, and S.P. Cole, *Charged amino acids in the sixth transmembrane helix of multidrug resistance protein 1 (MRP1/ABCC1) are critical determinants of transport activity.* J Biol Chem, 2002. **277**(44): p. 41326-33.
258. Leier, I., et al., *The MRP gene encodes an ATP-dependent export pump for leukotriene C4 and structurally related conjugates.* J Biol Chem, 1994. **269**(45): p. 27807-10.
259. Furman, C., et al., *The deviant ATP-binding site of the multidrug efflux pump Pdr5 plays an active role in the transport cycle.* J Biol Chem, 2013. **288**(42): p. 30420-31.
260. Weksler, B., I.A. Romero, and P.O. Couraud, *The hCMEC/D3 cell line as a model of the human blood brain barrier.* Fluids Barriers CNS, 2013. **10**(1): p. 16.
261. Qosa, H., et al., *Differences in amyloid-beta clearance across mouse and human blood-brain barrier models: kinetic analysis and mechanistic modeling.* Neuropharmacology, 2014. **79**: p. 668-78.